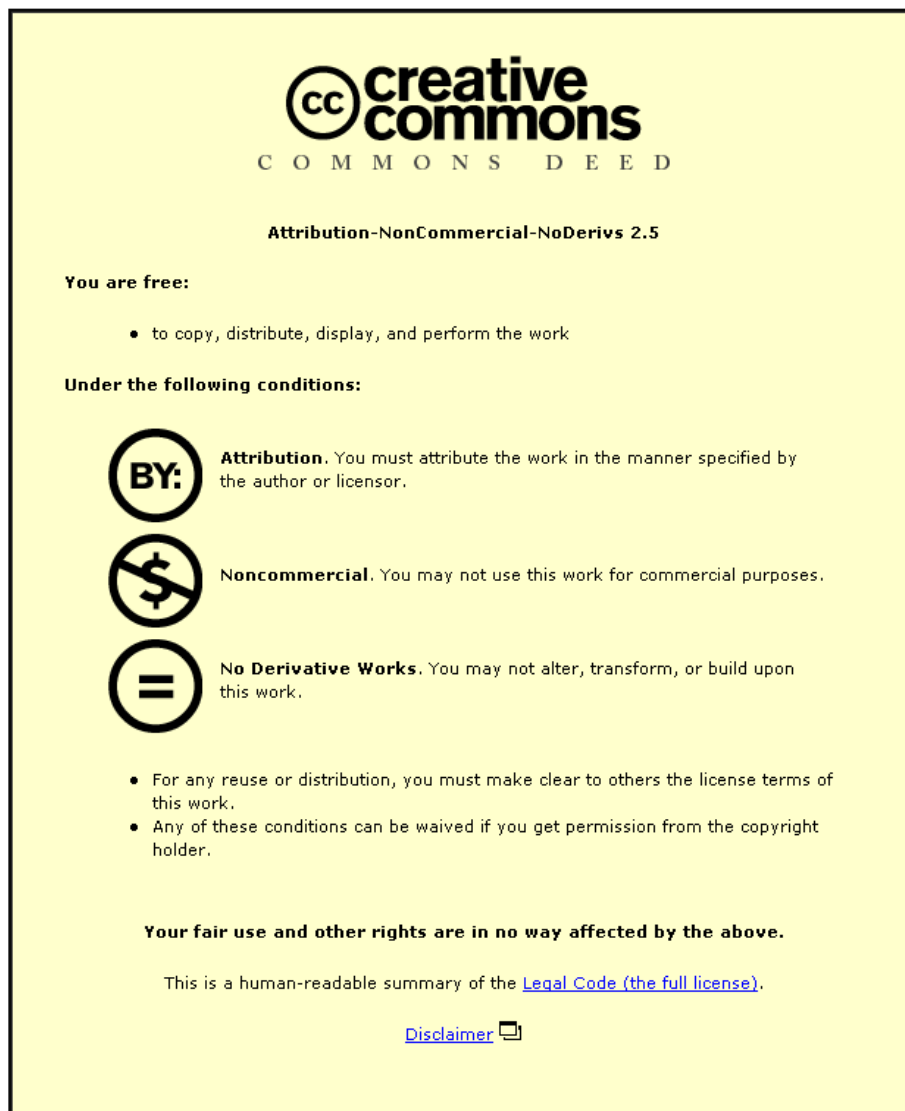


This item was submitted to Loughborough University as a PhD thesis by the author and is made available in the Institutional Repository (<https://dspace.lboro.ac.uk/>) under the following Creative Commons Licence conditions.



For the full text of this licence, please go to:
<http://creativecommons.org/licenses/by-nc-nd/2.5/>



Pilkington Library

Author/Filing Title SAMUELS, U

Accession/Copy No. 040152509

Vol. No. Class Mark:

<p>26 JUN 1998 (NO DISK) 4.9.01 LPS. (NO DISK).</p>	<p>LOAN COPY</p>	
---	------------------	--

ACCOMPANYING DISK HELD AT ISSUE DESK

0401525090



SERIAL LASER LITHOGRAPHY FOR
EFFICIENT MANUFACTURE OF
UNIVERSAL MICROSTRUCTURES

by

Dipl.-Ing. Uve Samuels, M.Phil.

A Doctoral Thesis

Submitted in the partial fulfilment of the requirements
for the award of
Doctor of Philosophy of the Loughborough University of Technology

March 1997

© Uve Samuels 1997

ACKNOWLEDGEMENTS

I would like to thank my supervisor Professor Dr. Rob Parkin for the continuous guidance throughout the project. Numerous fruitful discussions were the basis for the independent work in this project.

I would also like to thank Professor Dr. H. Kreitlow for his encouraging supervision of the theoretical investigations and experimental work as well as the financial support in the laboratories in the Institut für Lasertechnik Ostfriesland at the Fachhochschule Ostfriesland in Emden, Germany.

Futhermore, I would like to thank the members of the research team at the Fachhochschule Ostfriesland for the interest come into being of this work. In partcularly I would like to thank Mr. Dipl.-Ing. Jörn Miesner and Mr. Dipl.-Ing. Arno Hinrichs for the encouraging support of the experimental work, Mr. Arnold Terviel for the manufacture of the mechanical components and Dr. Steven Wright for the critical review of this report.

And finally, thanks to my parents and friends for tolerating my nocturnal habits throughout the research.

Uve Samuels

Loughborough / Emden, June 1997

ABSTRACT

SERIAL LASER LITHOGRAPHY FOR EFFICIENT MANUFACTURE OF UNIVERSAL MICROSTRUCTURES

By

Dipl.-Ing. U. Samuels, M.Phil.

The technique of microstructuring revolutionises all classical fields of engineering like electronics, optics and mechanics. In order to manufacture a microstructure in large quantities and at a reasonable price, master elements or masks will be formed that can be duplicated in a highly efficient process. Further development in technology leads, on the one hand, to further reduction of possible dimensions of structures down to the range of sub-nano technology and, on the other hand, to the development of more flexible systems in using more reasonably priced technologies for the structuring in the classical micrometre range, which in turn opens a much larger field of use.

This study examines the use of serial laser lithography for efficient manufacture of universal microstructures. To facilitate this, a laser beam writer or so-called Laser Pattern Generator (LPG) was developed and described here as well as in a previous work [Samu96a]. The laser beam writer uses a precise positioning system for the movement of a substrate for material processing using a focussed laser beam. This system permits the production of structures with dimensions down to 0.5 μm which can be used in several application fields. This was systematically analysed for optimisation of the production process. Based on the achieved results, a computer-aided simulation system for process parameter determination and optimisation was developed that may be used in order to minimise the experimental effort in LPG manufacturing. The total production process and the individual optimising steps are illustrated by the manufacture of different microstructures.

Because of the high reproducibility in manufacturing different structure types and, compared with other manufacturing methods, the low equipment and manufacturing effort, serial laser lithography is an efficient process for the microstructuring of universal microstructures down to the dimensions in the micrometre range.

 Loughborough University Library
Date Dec 97
Class
Acc No. 060152509

9 910098X

CONTENTS

	PAGE #
1 INTRODUCTION.....	1
2 MANUFACTURE OF MICROSTRUCTURES.....	3
2.1 Serial structuring systems.....	4
2.1.1 Electron beam scanner.....	5
2.1.2 Ion beam scanner.....	6
2.1.3 Laser beam scanner.....	7
2.1.4 Laser beam writer.....	8
2.2 Duplication of serially produced microstructures.....	8
2.2.1 Method of binary masks.....	9
2.2.2 Phase mask method.....	11
2.2.3 Binary raster scan method.....	12
2.2.4 Grey level mask method.....	13
2.2.5 Microgalvanic replication.....	14
2.3 Structuring of thin layers.....	14
2.3.1 Production of thin layers.....	14
2.3.2 Etching of thin layers.....	15
2.4 Comparison of the different manufacturing methods.....	16
3 APPLICATION OF MICROSTRUCTURES.....	17
3.1 Microoptics.....	17
3.1.1 Refractive microlens.....	17
3.1.2 Diffractive microlens.....	17
3.1.3 Structures of planar optical waveguides.....	18
3.2 Micromechanic.....	19
3.2.1 Acceleration sensor.....	19
3.2.2 Micro claw.....	19
3.3 Microelectronics.....	20
3.3.1 Transistor.....	20
3.3.2 Micro coil.....	21
3.4 Combination of micro components.....	21

4	DEVELOPMENT OF A SERIAL LASER LITHOGRAPHY SYSTEM.....	22
4.1	Hardware of the LPG.....	22
4.1.1	Optical system.....	23
4.1.1.1	Beam path of the exposure laser.....	23
4.1.1.2	Intensity closed-loop control system.....	26
4.1.1.3	Focal position closed-loop control system.....	32
4.1.2	Positioning system.....	36
4.1.2.1	Stages.....	37
4.1.2.2	Laser interferometer.....	38
4.1.2.3	Direct Axis Interface (DAI).....	38
4.1.3	Control system.....	39
4.1.3.1	Host computer.....	40
4.1.3.2	Control unit.....	40
4.2	Software of the LPG.....	42
4.2.1	System software.....	42
4.2.1.1	Axis control.....	42
4.2.1.2	Evaluation of the interferometer signal.....	43
4.2.1.3	DAI programming.....	44
4.2.1.4	Intensity control.....	45
4.2.1.5	Focal position control.....	49
4.2.2	Utility programs.....	49
4.2.2.1	Module test system.....	49
4.2.2.2	Laser stability.....	50
4.2.2.3	Positioning tracing.....	51
4.2.2.4	Positioning accuracy.....	51
4.2.2.5	Compensation program.....	52
4.2.3	Exposure programs.....	54
4.2.3.1	Macro programming.....	54
4.2.3.2	Pixel programming.....	59
4.2.3.3	Program generation.....	60
4.2.3.4	Realisation of a programming system.....	61
4.3	Characteristics of the LPG.....	62

5	STRATEGIES OF LPG OPERATION.....	64
5.1	Influence of the positioning system.....	64
5.1.1	Positioning method for the substrate.....	64
5.1.2	Pulse density modulation.....	65
5.2	Influence of the beam system.....	66
5.2.1	Shape and position of the gaussian beam.....	66
5.2.2	Pulse width modulation.....	66
5.3	Procedure for an efficient exposure.....	66
6	DETERMINATION OF PROCESS PARAMETERS FOR THE LPG.....	68
6.1	Resist structuring.....	68
6.1.1	Types of resist.....	68
6.1.2	Process steps.....	69
6.1.3	Mechanism of resist structuring.....	70
6.1.4	Shape and position of the Gaussian beam.....	71
6.2	Simulation.....	73
6.2.1	Principle of simulation.....	73
6.2.2	Simulation program <i>LASSI</i>	74
6.2.3	Simulation of selected structures.....	76
6.3	Use of simulation results.....	77
7	REALISATION OF SELECTED MICROSTRUCTURES.....	78
7.1	Binary.....	78
7.2	Multi-level.....	79
7.3	Continuous.....	80
7.4	Additional microelements.....	81
7.5	Results of the LPG microstructuring.....	85
8	DISCUSSION.....	86
9	CONCLUSION.....	89
	REFERENCES.....	90

APPENDICES

- A. LPG OVERVIEW DIAGRAMS
- B. RAYTRACING MODEL OF THE LPG
- C. CONTROLLER PARAMETER TABLE
- D. LPG CONTROL UNIT
- E. LPG SOFTWARE
- F. MECHANICAL SYSTEM OF THE LPG
- G. SIMULATION PROGRAM *LASSI*
- H. PUBLICATIONS

NOTATIONS/TERMINOLOGY

A	- Outer frame length
AOM	- Acousto optical modulator
A_p	- Coordinate starting point
a	- focus position, inner frame length
B_w	- Bandwidth
CP	- Continuous path
D	- Outer circle diameter
DAI	- Direct axis interface
DAQ	- Computer interface card
d	- Controller input value, inner circle diameter
E	- Exposure
E_p	- Coordinate end point
e	- Euler number
f	- focal length
f_g	- Cut off frequency
H	- Height
I	- Intensity
i	- Step variable for digital controller
\tilde{K}	- Auxillary parameter
K_D	- Derivative action parameter of the controller
K_I	- Integral action parameter of the controller
K_P	- Propotional action parameter of the controller
K_s	- Transfer factor
L	- Length
LPG	- Laser Pattern Generator
M	- Material constant (figure of merit)
m	- Matrix dimension
n	- Matrix dimension, mask number
P	- Power
P_A	- Point distance
PCX	- File format

PID	- Controller characteristic
PIO	- Parallel input output interface
PS	- File format
PtP	- Point to Point
P _Z	- Point number
RF	- Radio frequency
RS-232	- Serial computer interface
r	- Vector length
r ₁	- Etching rate for exposed resist
r ₂	- Etching rate for unexposed resist
T	- Time
T _A	- Sampling time
T _g	- Settling time
T _N	- Reset time
T _R	- Rise time
T _{RA}	- Time for one controller loop
TTL	- Transistor-Transistor Logic
T _t	- Dead time
T _U	- Transfer lag
T _V	- Derivative time
U	- Voltage
V	- Velocity
w ₀	- Beam waist
x	- Coordinate
x _d	- Controller input value (negative deviation)
y	- Coordinate, controller output value
Z	- Distance
Z _R	- Rayleigh length

α_0	- Exposure constant for positive resist
Δd	- Change of the resist layer thickness
ΔP	- Power derivation
Δr	- Etching rate difference r_1-r_2
ΔZ	- Focus position derivation
δ	- Mean-square deviation
Φ	- Accumulation
φ	- Angle
λ	- Wavelength
π	- 3.141592654...

LIST OF TABLES

TABLE	Description	PAGE #
1	Characteristics of the He-Cd laser	23
2	Characteristics of the microscope objective.....	24
3	Characteristics of the AOM	27
4	Characteristics of the photodetector.....	28
5	Characteristics of the linear axes	37
6	Characteristics of the rotation axis	37
7	Initialisation of the counting channels.....	43
8	Chip selection.....	44
9	Axis selection	45
10	Connections for the intensity controller.....	46
11	Connections for the focal position controller.....	49

LIST OF FIGURES

FIGURE	DESCRIPTION	PAGE #
1	Binary, staircase and continuous profile.....	3
2	Block diagram of microstructuring processes	4
3	Principle of an electron beam scanner/writer	6
4	Principle of a laser beam scanner	7
5	Principle of a laser beam writer.....	8
6	Principles of mask transfer	9
7	Process of mask generation	10
8	Sequence of operation in a multiple mask process.....	11
9	Comparison between a phase mask and a binary mask.....	12
10	Process principle of the binary raster scan method	13
11	Process principle of the grey level mask method	13
12	Wet a) and dry b) etching process	15
13	Refractive microlens.....	17
14	Fresnel zone plate	18
15	Structure of a planar optical waveguide	18
16	Principle of an acceleration sensor with piezoresistive signal generation.....	19
17	Construction principle of a micro claw	20
18	Construction principle of a transistor	21
19	Construction principle of a micro coil.....	21
20	Principle set-up of the Laser Pattern Generator.....	22
21	Beam path of the exposure laser.....	24
22	Gaussian beam transformation by a lens	24
23	Intensity closed-loop control system	26
24	Characteristic curve of the system to be controlled.....	28
25	Step response for the determination of the system parameter	29

26	Controlling characteristic of the intensity closed-loop control system	31
27	Controlling characteristic of the optimised closed-loop control system	32
28	Focal position closed-loop control system.....	33
29	Characteristic curve of the system to be controlled.....	33
30	Step response for the determination of the system parameter.....	34
31	Controlling characteristic of the focal position closed-loop control system	35
32	Controlling characteristic of the optimised closed-loop control system	36
33	Block diagram of the interferometer system	38
34	Principle of the Direct Axis Interface	39
35	Conversion of the sensor signal.....	46
36	Determination of the controller dead time	48
37	Modules used in the test system.....	50
38	Laser intensity as a function of time	50
39	st-diagram of the PM500	51
40	Gaussian curve for the PM500.....	52
41	Error curve of the positioning system.....	53
42	Minimised error curve.....	53
43	Definition of macros for annulus and frame.....	55
44	Line and annulus using the PtP - procedures	56
45	vt-diagram of the CP - procedure.....	57
46	Position and orientation of the structure.....	58
47	Matrix for pixel programming of a structure	59
48	Software concept for exposure programs.....	60

49	Structuring result of the LPG	62
50	Raster - and vector scanning method.....	65
51	Positive and negative resist.....	68
52	Cross-section of a Gaussian beam	72
53	Focal positions relatively located to the resist layer.....	73
54	Resist layer transfered to a matrix of n x m elements	74
55	Simulation series of various profiles	76
56	Cross section of the expected binary microstructure.....	79
57	Binary microstructure	79
58	Cross section of the expected multi level microstructure.....	80
59	Multi-level microstructure.....	80
60	Cross section of the expected continuous microstructure	81
61	Continuous microstructure	81
62	Binary ring structure with distortion.....	82
63	Continuous ring structure produced by post melting.....	82
64	Micro lens on the end of a fiber.....	83
65	Line disc (overview)	84
66	Line disc (detail).....	84

1 Introduction

Today microstructures have entered almost all areas of technology. It is standard to produce optical, mechanical and electronic elements in large quantities using the technique of microstructuring. Developments in industrial engineering have the aim to reduce structure sizes for increased integration density. In doing this not only precise images of existing elements were transformed from macro to micro-scale, but microstructures have also introduced completely new perspectives and application fields. The diffraction phenomenon shall be quoted, which has a strong effect when structure size reduces to the range of the wavelength of the used light and, therefore, it has been of little technical relevance before. Today, optical elements which benefit from the diffraction phenomenon and which are known as diffractive optical elements (DOE) are irreplaceable in the fields of medicine and spectroscopy. The success of microstructures in all application fields is well-founded in the fact that a flexible combination of only few standard components can be combined to manufacture complex systems [Menz93].

A great effort in research work was caused by numerous potential application fields and has improved the production methods of microstructuring. In most cases, the substrate cannot be structured directly, because the structure dimensions can not be achieved using *classical tools*. Therefore, the beam of a laser or an electron source acts as a tool and alters the characteristics of a polymer material (resist) which is sensitive to the radiation. In the next process step (development) the material is removed at the exposed locations. These technologies are well known as the lithographic process and permit structuring of the resist down to sub-micrometre ranges. The processing results and production costs vary due to the existing process variety. Resist structuring is followed by a process which manipulates the parts of the substrate that are not protected by the resist layer. This is done in a so-called batch process which affects the total substrate. For series production, the elements produced in this manner can be reproduced by a copying process in large quantities and at a reasonable price.

Further development of these technologies have the aim on the one hand to minimise possible structure sizes down to sub-nano technologies and on the other hand to develop systems which are as flexible as possible with reasonably priced technologies. In viewing the

efficiency of these processes, one has to consider the effort provided by machine and the production effort in time and material. Highly efficient technologies will result in wider application fields of microstructures, where a structuring in the classical micrometre range is applicable in most cases. Therefore, this study shall concentrate on the development of a process which permits the efficient manufacture of universal structures in the micrometre range.

In order to deliver a total overview on different manufacturing technologies, chapter 2 compares the existing serial production processes and illustrates the processing steps following the serial structuring.

Chapter 3 shows several microstructure applications in the field of microoptics, micromechanics, and microelectronics. This demonstrates the flexible use of the structuring methods and techniques for use in different fields.

Based on the results achieved in Chapters 2 & 3, a laser beam writer *or Laser Pattern Generator* (LPG) with its system components will be introduced in Chapter 4. It should be noted that this work builds upon an MPhil Thesis "Focal Position Controlled Processing Head for a Laser Pattern Generator (LPG) for Flexible Microstructuring" [Samu 96a], which should, for a full historical perspective, be read concurrently with this thesis.

Chapter 5 introduces different operation strategies of the laser beam writer which result from the mechanical and optical characteristics of the LPG. Reduction of processing time during the exposure is the main issue of these examinations.

Chapter 6 illustrates all technical steps for the resist structuring in their entirety. Starting with the theoretical examination of the process, a resulting computer simulation for the determination and optimisation of process parameters will be developed in order to reduce the experimental effort for LPG manufacturing.

The operation of the LPG to produce universal microstructures will be introduced in chapter 7.

In chapter 8, the discussion and in chapter 9 the conclusions of this work are presented.

2 MANUFACTURE OF MICROSTRUCTURES

The manufacturing process to be described is a technique for the structuring of appropriate materials (hereafter denoted substrate) in the required range. In most cases a direct structuring of these substrates by classical tools cannot be done with the required small detail dimensions. Therefore, additional process steps are introduced for which the substrate is covered with a special coating (resist). This resist can be exposed by particle- or laser radiation. In a following process step (development) this resist will be locally point-removed. At these locations, the substrate underneath is no longer protected by the resist and can be manipulated by a further process step, in the course of which the protected areas are not influenced. The resist structuring is an intermediate but crucial step in the total production process during which the resist profile, depending on its application (see chapter 3), can be of binary, staircase or continuous profile (see figure 1).

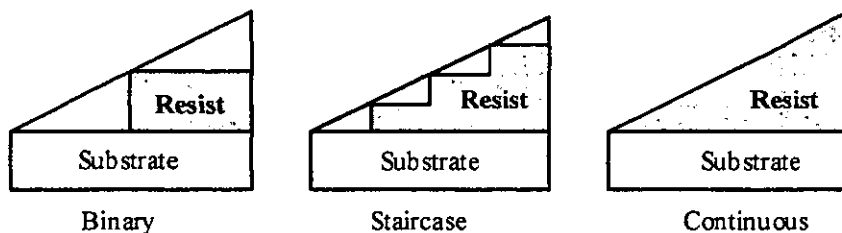


Fig. 1: Binary, staircase and continuous profile

All processes of resist structuring can be divided into two different categories: serial and parallel processes. Figure 2 illustrates the separation in a block diagram.

The pattern data are generated with a suitable CAD-program and saved in a file. A light - or particle beam writer will transfer these data either in original size to a resist covered substrate or as a reticle in magnified size to a radiation-sensitive material such as film. Further processing will reduce the structures on the reticle to the final size using a mask stepper. The pattern will be transferred to the resist covered substrate by appropriate mask projections such as contact -, proximity -, or projection procedures [Scha81a]. The writing is the serial process, while the use of masks is the parallel process.

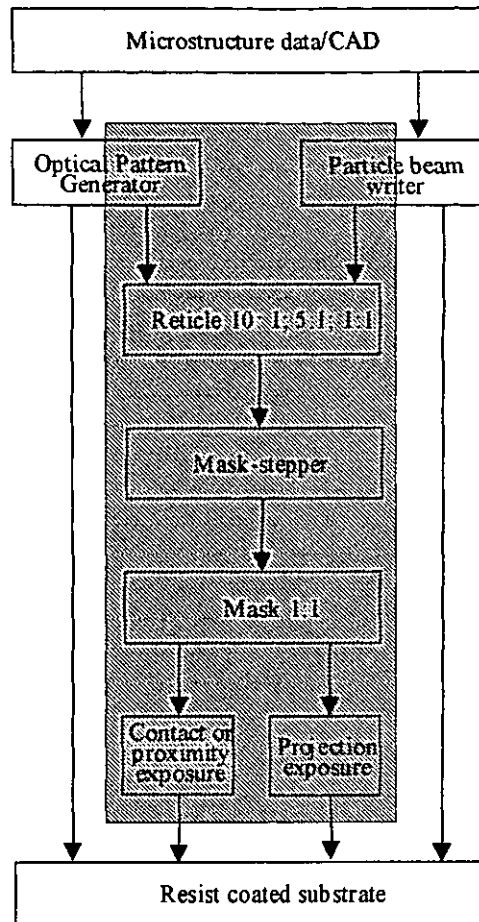


Fig. 2: Block diagram of microstructuring processes

In this chapter, four serial microstructuring devices will be introduced and the manufactureable structures as well as the required equipment - and process effort will be compared. Due to the relatively long manufacturing time, the serial process does not permit an economical series production. Therefore, this chapter also includes examinations of possible copying possibilities for different structures by efficient parallel processes.

2.1 Serial structuring systems

A serial process generates the required structure in guiding a light- (laser) [Golt90][Herz92][Jäge89] [Yata91] or corpuscular beam (electron or ion) [Aoya90][Arno85] [Frey92] over the surface of the material under treatment. During this process the intensity of the beams can be changed rapidly. The process control of the microstructuring devices will be done by a process control computer. Devices for serial processing can be divided into three groups:

- Writer

The object under treatment is moved underneath the focused beam by positioning units.

- Scanner

Deflection systems, i.e. mirrors steer the beam over the surface of the object.

- Combinations

A combination of above mentioned techniques can be combined in one equipment [Hase92].

Later in this chapter the different systems for serial microstructuring will be introduced.

2.1.1 Electron beam scanner

Electron beam lithography uses an electron beam to write the structure into a resist which is sensitive to electrons [Bauc91][Reim95]. This principle is related to the one used in the scanning electron microscope, where as the latter can be equipped with additional features for this task. One can find facilities using a Gaussian beam as well as facilities which shape the beam by placing a knife into the beam path [Menz 93].

The principle of an electron beam scanner/writer is illustrated in figure 3. Electrons are emitted from an electron source (helical filament) and accelerated and focused to a beam by an electric field. A magnetic field, positioned vertical to the beam path controls the deflection. In order to enlarge the writing range, an additional positioning unit can move the substrate. The smallest achievable structures lay in the range of nano-metres [Aoya90]. The effort in equipment engineering is relatively high because, for instance, the beam must be guided through a very high vacuum. Also the process costs are relatively high due the expensive electron resist and developer.

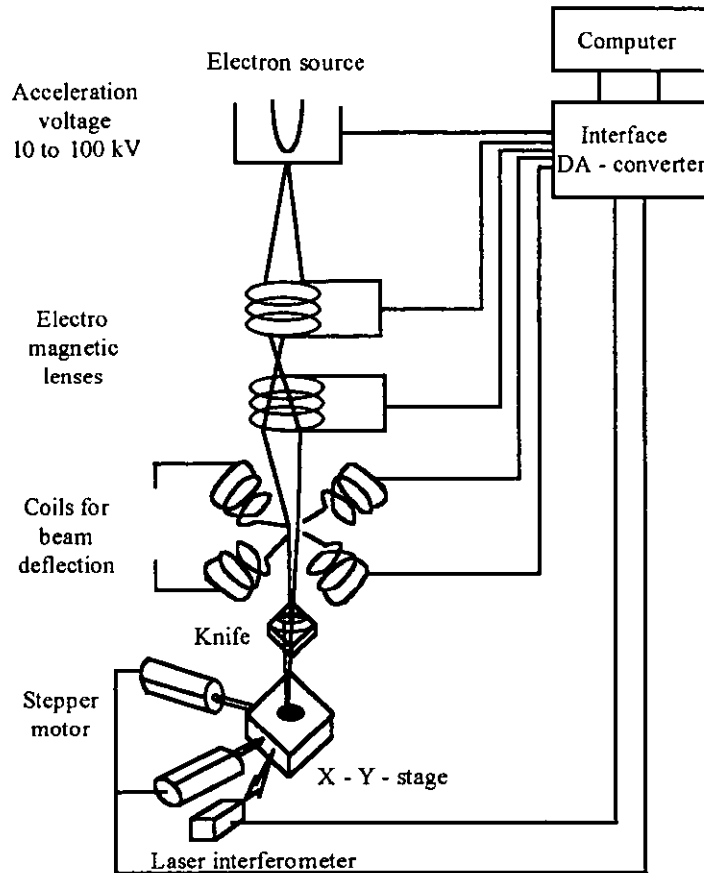


Fig. 3: Principle of an electron beam scanner/writer [Arno85]

2.1.2 Ion beam scanner

The principle and the setup is similar to that of an electron beam scanner, however because of the considerably higher mass of an ion the scattering in the resist is less than in electron beam lithography, which means there are almost no structural distortions caused by the proximity effect [Frey92][Mats91][Mack91][Smit91][Kube91]. With this system one can reach the highest structural resolutions going down into the range of 10nm, however with the drawback that this system needs the highest effort in equipment engineering. The ion resist and developer are the most expensive ones.

2.1.3 Laser beam scanner

The principle of a laser beam scanner is illustrated in figure 4. Mirror units (galvanometer) deflect the laser beam onto the substrate under exposure. The movement of the mirrors is controlled by very precise closed-loop control circuits. In order to avoid structural distortions, the necessary beam focusing is realised by a lens which is moved by a positioning system for dynamic focussing placed in front the deflection system or by a plane-field lens ($f-\Theta$ lens) placed behind the deflection system. The beam intensity will be matched to the necessary exposure via an acousto-optic modulator (AOM).

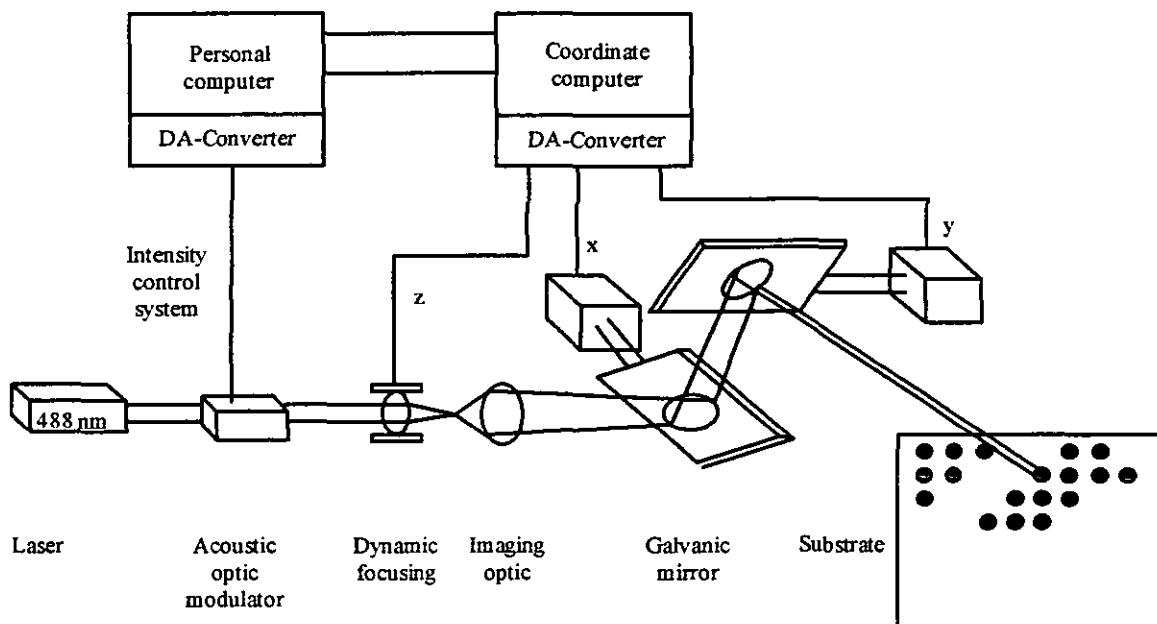


Fig. 4: Principle of a laser beam scanner [Jäge92]

The maximum writing velocity of this method is determined by the dynamic characteristic of the galvanometer mirror, while meaningful sizes of objects are limited by distortions of the structures caused by optical effects. Because focusing optics with large focal length have to be used, the minimum size of a structure lies in the range of 10-100 times of the wavelength of the laser used [Jäge92].

2.1.4 Laser beam writer

The principle set up of a laser beam writer [Fitz87][McWi83][Bern87][Burg88] is illustrated in figure 5. A positioning system is moving a resist coated substrate underneath the focused laser beam, while the intensity of the beam is matched to the necessary exposure by an acousto-optic modulator.

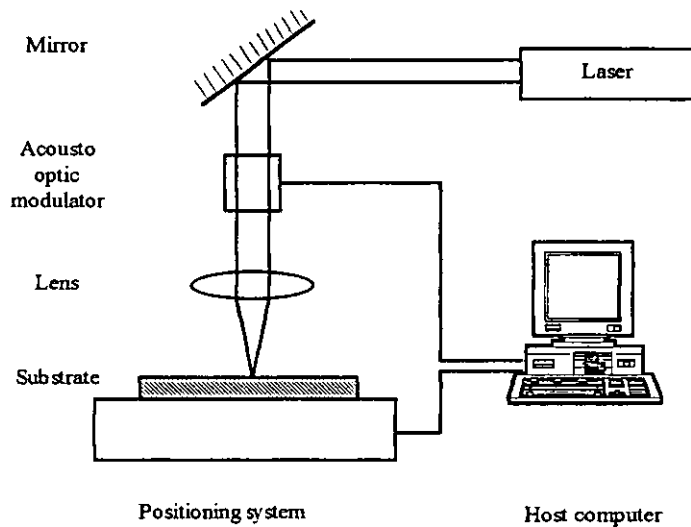


Fig. 5: Principle of a laser beam writer

Besides the required exposure time, the process time depends on the dynamic characteristic of the positioning system whereas the control range influences the maximum size of the object. The smallest step size of the positioning system and the focal point diameter determine the smallest size of a structure which can be produced. The smallest focal point possible lies in the range of the wavelength of the laser used. [Stre92].

2.2 Duplication of serially produced microstructures

As described in this chapter, in most cases the resist structuring is an intermediate step in the production process of a microstructure. The processing time of a serial process is relatively long, so that a process shall be introduced which leads to the required structure by using reasonably priced parallel duplication processes. The structures required for this will be produced by serial processes. In this chapter, different duplication processes will be

introduced and, in order to select the optimum manufacturing method, their structuring capacities will be compared.

2.2.1 Method of binary masks

Binary masks consist of a reflecting mask structure on a suitable substrate which is transparent to the used radiation. These structures can be copied at a reasonable price with one single parallel exposure of the total mask area. Figure 6 illustrates the methods which are in common use.

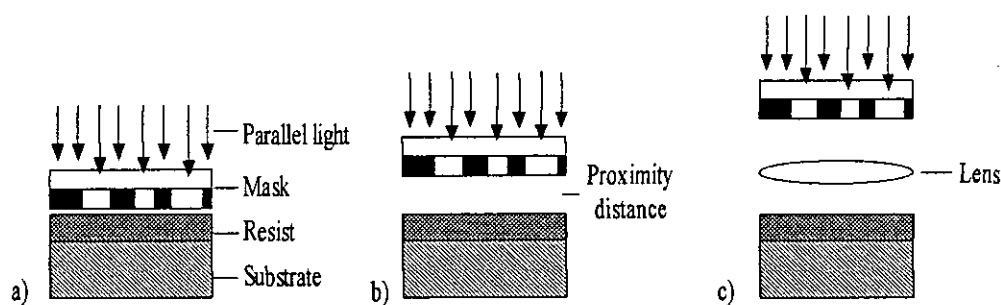


Fig. 6: Principles of mask transfer

In Figure 6a) the mask is in contact with the surface of the resist coated substrate while the exposure is performed. This method is called the contact method. The proximity method is shown in figure 6b) and maintains a small distance - proximity distance - between mask and substrate. The imaging method of figure 6c) transfers the mask structure to the substrate using a special imaging optic.

Depending upon the used method and depending upon the wavelength of the radiation, different minimum structure widths can be realised. With the contact method, the smallest structures can be achieved. The proximity method lies in the middle range and the largest structures are achieved with the imaging method. It is common to all methods that with decreasing wavelength smaller structures can be achieved. Different wavelengths require different substrates and structure materials for the construction of the mask. Whereas ultraviolet radiation requires a structure of chromium on glass substrate [d'Aur72], x-rays can only be used in conjunction with substrate films of boron nitrate or silicon with structures of gold [Tied95][Balla95]. The production of masks uses the method illustrated in figure 7.

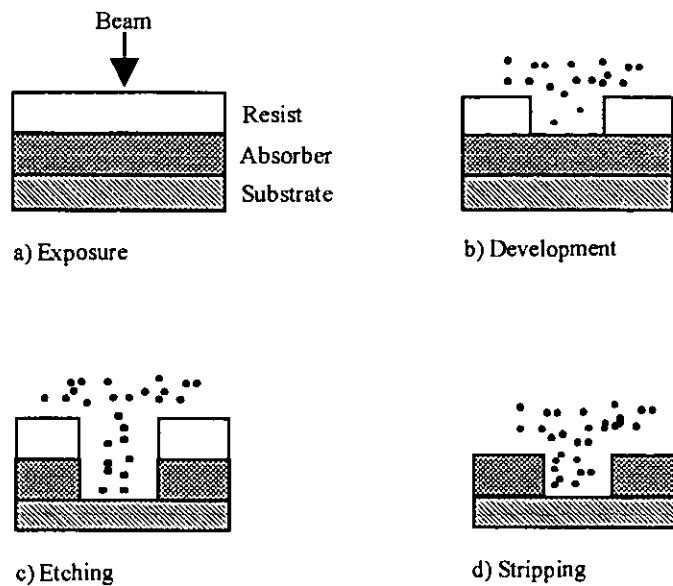


Fig. 7: Process of mask generation

The substrate that is transparent for the light source used is coated with an absorber layer which consists of a material impermeable to this radiation. On top of this layer the resist is applied, which in a first process step will be exposed by the serial structuring device (fig. 7a). In a second process step and using positive working material the resist is removed in the exposed areas while the unexposed areas remain as they are (fig. 7b). Those areas, which are then not protected by the resist will be removed by a wet chemical etching process (fig. 7c) and in a last process step the remaining resist will be removed (fig. 7d).

Masks generated according to the above process can be used in a single mask process for binary structures or in a multiple mask process for multi-level structuring, as shown in figure 8. In doing this, the masks will be exposed one after the other, where all subsequent exposure masks must be adjusted precisely to the first one. In a multi mask process n masks will result in 2^n levels [Dome91].

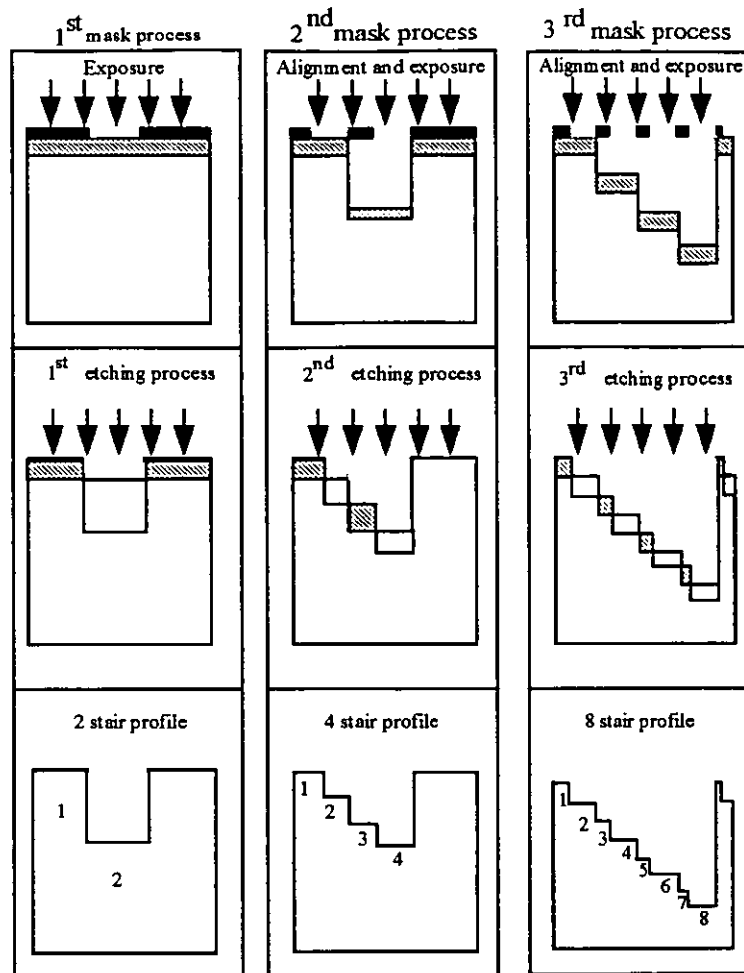


Fig. 8: Sequence of operation in a multiple mask process

2.2.2 Phase mask method

The newest development in the field of optical mask techniques are so-called phase masks. In doing this a pointwise influence of the phase proportions in the recticle plane improves the image contrast, resolution and focus depth. This method results in structures with a resolution down to $0.2\mu\text{m}$ [Nöls91][Leve83][Broc91].

Beside an absolutely opaque absorber pattern the phase masks have an additional pattern of a translucent layer which shifts the phase of the penetrating light wave. Selecting the correct thickness of the layer (phase shift by 180°) and the correct pattern of the phase shifting layer will result in destructive interferences between the gaps of the images so that smaller structures than those with binary masks can be transferred. Figure 9 illustrates the comparison of these two masks.

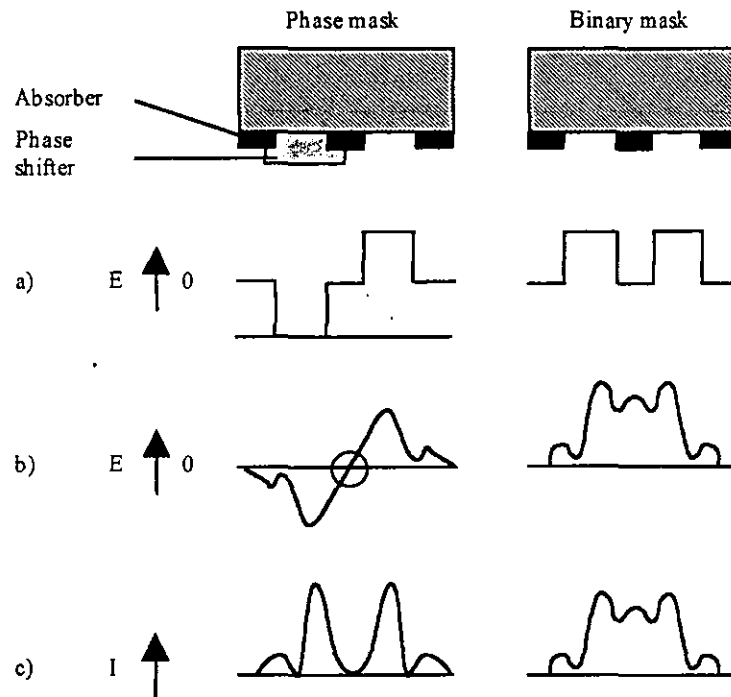


Fig. 9: Comparison between a phase mask and a binary mask

The direction of an electrical field E of each plane wave penetrating perpendicular through the mask (a) will be inverted by the phase shifter. After being imaged (b) this wave propagates further and, due to the destructive interference, improves the contrast of the image (c).

2.2.3 Binary raster scan method

By use of a binary mask structure, a multi-level or even a continuous resist structure can be achieved. As shown in figure 10, a special optic transfers the binary mask to the substrate. The lowpass characteristics of this optic causes a brightness distribution in the imaging plane which corresponds to an averaged transmission course of the mask. Compared with the previous described multiple mask process in this process the profile will be achieved with only one mask and with a single operating cycle which means that there is no difficult mask positioning required [Jäge92].

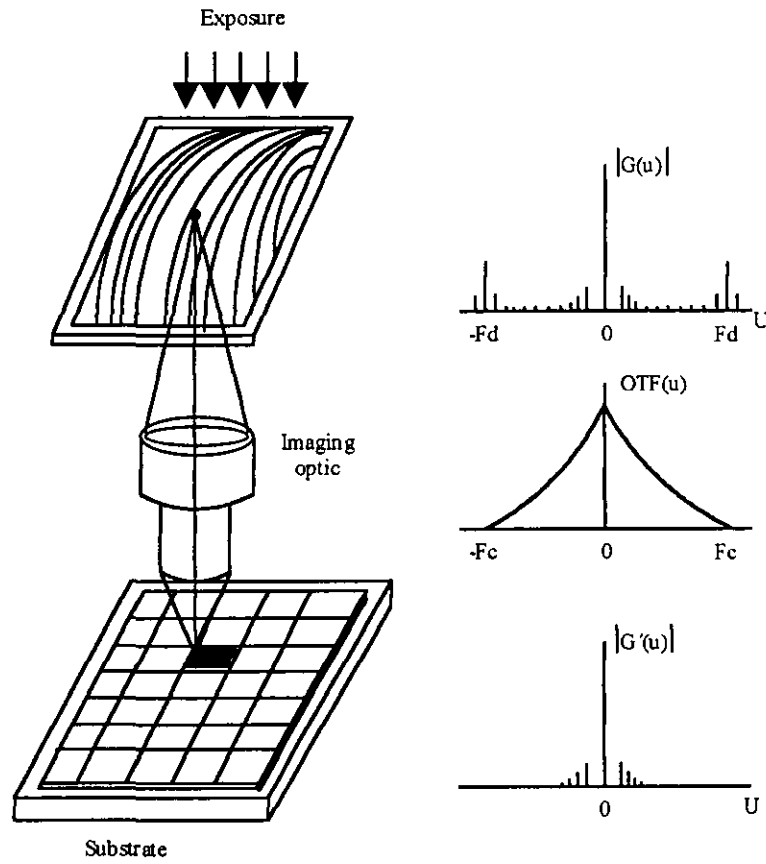


Fig. 10: Process principle of the binary raster scan method [Pole91]

2.2.4 Grey level mask method

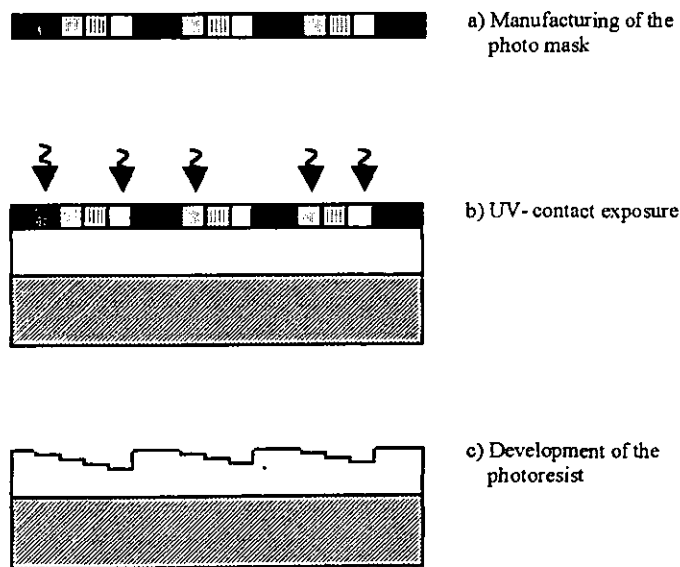


Fig. 11: Process principle of the grey level mask method [Ande90]

The grey level mask method is illustrated in figure 11. A photosensitive layer will be exposed in such a manner that a grey level is established, which is proportional to the illumination. The non-linear sensitivity of the photosensitive layer is the main disadvantage of this process. The mask produced in this way can be transferred to a binary, multi-level, or continuous height profile of the resist using the contact method and the resist height is a function of the grey level of the mask. This process also needs no difficult mask alignment.

2.2.5 Microgalvanic replication

Binary, multi-level, or continuously structured photoresist layers can be duplicated by microgalvanic replication. This will be done using the following method: The resist has insulating characteristics and, therefore, the surface must be coated with a conducting layer, which can be vapor-deposited or sputtered silver or copper. The conducting layer will be bonded and used as a cathode in an acid copper electrolyte. The anode consists of phosphatised copper. The electrolytically separated copper layer amplifies the metallization. In this manner, a mechanically stable unit is achieved, which can be used as a stamp and transferred into polymethylmethacrylate: PMMA many times. In turn, one of these replications may again be galvanically coated and utilised as another stamp. [Budz95][Lens92b].

2.3 Structuring of thin layers

Constructing working structures on a production scale in microelectronics, micromechanics and microoptics requires thin layers of different materials. These layers take over either the required function (such as printed wires) or serve as auxiliary layer (such as an isolator). First, these layers are applied to the substrate and afterwards, according to their functions, they are subject to pointwise structuring by appropriate etching processes.

2.3.1 Production of thin layers

The required characteristics of layers are very different; however, in general no inhomogeneity is allowed because the smallest amount of another substance could jeopardise useability. Also, these thin layers must have a very good adhesion to the substrate. For this

reason these layers are applied to the substrate by means of a high or a very high vacuum. In doing this, the materials to be applied (e.g. chromium, aluminium, quartz) are vaporised or atomised by ion bombardment and precipitate on the substrate, so that the required layers grow on the surface of the substrate in atomic layers [Razo95][Mura95][Anap95]. Besides this the growth of thin layers on a substrate originated by chemical reactions in a vacuum is also a well known method[Band95].

2.3.2 Etching of thin layers

Thin layers are structured according to their function using etching process techniques. This is done in so-called batch-processes exposing the total surface (very often of several substrates) either to an etching liquid, called wet etching process [Cram91][Camo95] or using the dry etching process by radiating particles using a beam with large cross section [Wolf96][Colli96][Korz93][Lo93]. Figure 12 shows the principle of both processes.

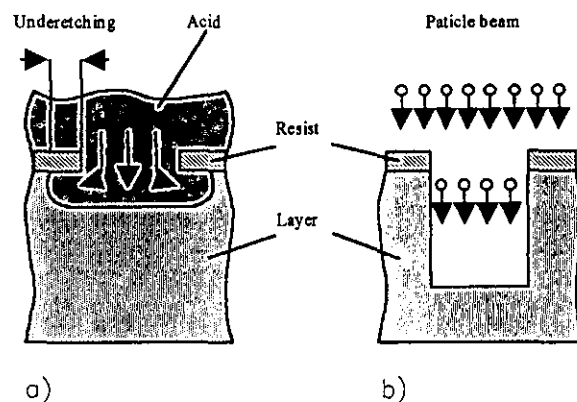


Fig. 12: Wet a) and dry b) etching process

In order to apply this processing step only to certain areas of the substrate, all other areas are covered with a resist layer which first has been subject to a lithographic structuring. In the past, wet etching has been the preferred process. An extraordinary selectivity with respect to different materials was its major advantage. With a few exceptions, these etching processes are isotropic which means that the etching velocity is independent of the direction. This results in a loss of material because at the sides of the substrate the material beneath the resist will also be taken away (see figure 12). In practice this results in structures with an aspect-ratio (ratio of structure height to minimum lateral distance) of less than 1. The under etching also leads to structures of less steep sides.

Because of this crucial disadvantage in certain applications, the dry etching process may be preferred which embodies an anisotropic etching response and allows structuring of steep skirts by using particle beams.

2.4 Comparison of the different manufacturing methods

The serial production process is capable of the direct production of binary, multi-level, or continuous structures. Because of the serial process, this technology is very time consuming and cannot therefore be the basis for mass production. However, this technique is absolutely necessary for the production of masks. For this purpose one can find corpuscular writers on the market, whereas laser beam exposure units at this stage can only be found in laboratories. In most application fields, structuring in micrometre range is required and this can be done at a reasonable price using laser beam devices. The laser beam writer compared to the laser beam scanner normally needs longer writing time but has the advantage of 10 to 100 times better resolution.

The propagation of the structures by parallel mask processes can be realised by the described standard procedures, whereby the selection of the mask type depends on the desired profile shape. Also the thin layer generation and manipulation by etching processes are well known processes. Industries offer complete systems for these techniques or the procedure itself as a service in a job shop. Therefore, the mask generation is the most time and money consuming task in the microstructuring process. If one can keep these costs down, microstructures can successfully capture further application fields.

3 APPLICATION OF MICROSTRUCTURES

This chapter presents selected examples of microstructures in different fields of engineering techniques. The components can be single [Liu95] layer or more complex multilayer based [Kette94], where the manufacturing techniques described in chapter 2 are used for the manipulation of different materials.

3.1 Microoptics

Optical components which guide, shape, and image a light beam have not only been taken from macro and miniaturised into micro-scale, but also completely new components have been developed by use of microstructuring techniques.

3.1.1 Refractive microlens

The principle of a refractive lens as well a refractive microlens shapes the beam by means of different optical paths. This can either be done by manipulating the refractive index [Ecke95] or the lens shape.

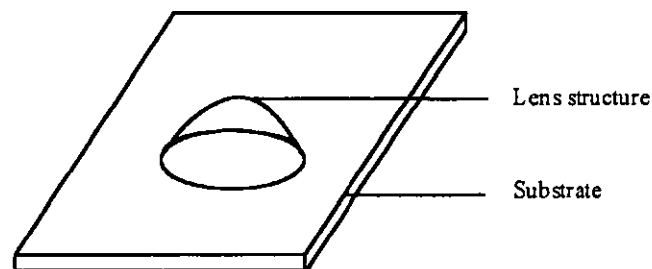


Fig. 13: Refractive microlens

Figure 13 illustrates the structure of a refractive microlens which is placed on a planar transparent substrate material. The shape and material of the lens have to be chosen so that it meets the desired optical characteristics [Nuss95][Früh95].

3.1.2 Diffractive microlens

Diffractive optics influences the light beam by means of diffraction. This diffraction is more pronounced at small dimensions of the structure. The Fresnel zone plate is a well known representative of this type of optical element [Swan89][Sasi93].

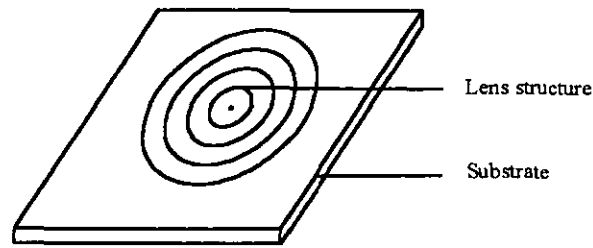


Fig. 14: Fresnel zone plate

The binary ring structure illustrated in figure 14 has the same function as the refractive lens. There is an opaque structure on a transparent substrate material, which focuses the incident radiation to one single spot. The radius of the rings for the required optical characteristic can be analytically determined [Cox90].

3.1.3 Structure of planar optical waveguides

If different domains of a transparent material (e.g. glass or PMMA) have different refraction indices, an optical waveguide structure can be constructed in a planar substrate on the basis of total internal reflection [Walk93][Find85][Bähr95][Ecke95].

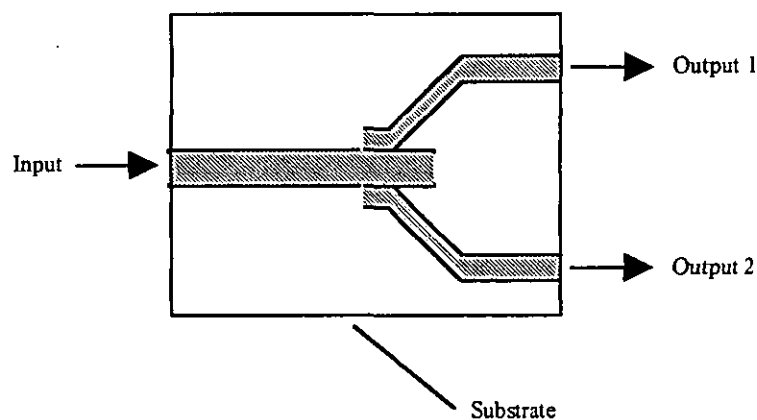


Fig. 15: Structure of a planar optical waveguide

The structure shown in figure 3 has the function of a fibre coupler. The radiation coupled into the input channel will be linked into the two output channels.

3.2 Micromechanic

There are passive and active micromechanic components. Among the latter one can distinguish between sensors and actuators. While sensors are already introduced into a broad range of application fields the development of actuators is still in the initial phase. The lifetime of the actuators developed so far is limited due to wear and tear [Burb91] [Fan95].

3.2.1 Acceleration sensor

A principle very often used in measuring acceleration is the principle of cantilever deflection. A known mass, which hangs on an elastic cantilever is accelerated so that the cantilever is exposed to an elastic distortion. This distortion can be measured either on a piezoresistive basis - with piezo elements integrated into the cantilever - or on a capacitive basis - by measuring the capacity of the system based on the cantilever and a fixed capacity plate. The essential parameters describing such a sensor are the natural frequency and sensitivity [Seid92].

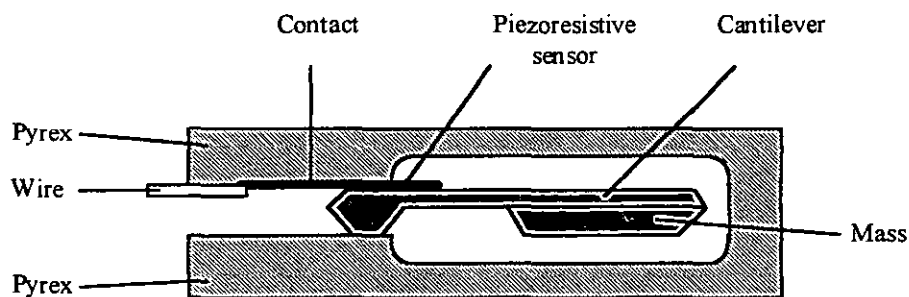


Fig. 16: Principle of an acceleration sensor with piezoresistive signal generation [Roy179]

Figure 16 illustrates the outline of a piezoresistive acceleration sensor, which consists of two treated pyrex-disks with a Si-disk placed between them acting as the cantilever.

3.2.2 Micro claw

The micro claw is one of the few actuators which nowadays can be produced with a long lifetime. This device experiences no friction forces since only an elastic distortion of a silicon deflection cantilever, caused by electrostatic forces, is used [Menz93][Walk90]. The principle of the system is shown in figure 17.

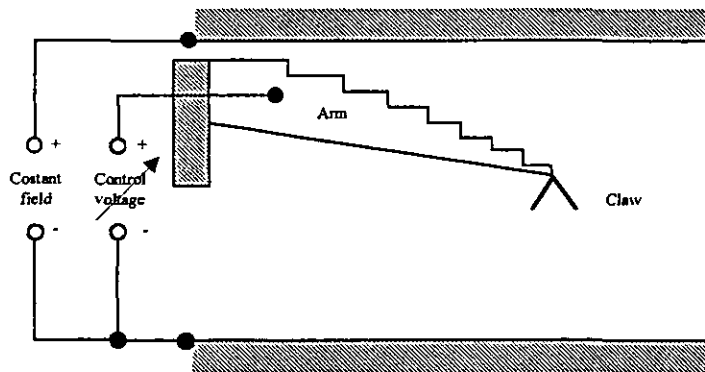


Fig. 17: Construction principle of a micro claw

By applying a control voltage to the conducting carrier arm of the claw, which is placed in a constant electric field, the resulting position of the claw is a function of the control voltage. In this way an object lying below the claw can be held.

3.3 Microelectronics

Microelectronics provides a variety of different components and component systems, which have found an enormous range of applications. Microelectronics can be seen as the initial application field of microstructuring techniques.

3.3.1 Transistor

The combination of two pn-transitions to a transistor is the well known representative of microelectronics components[Wang95]. Its development has led to numerous further innovations, whereas the combination of several transistors has resulted in very complex systems. The possibilities of combinations have been enhanced by the further increases of integration density.

In order to develop two pn-transitions into both sides of the doped starting material (silicon or germanium) a foreign atom pill (e.g. As) will be introduced, as can be seen in figure 18. By applying the required operating voltage a controllable switch and amplifier has been established [Chan95].

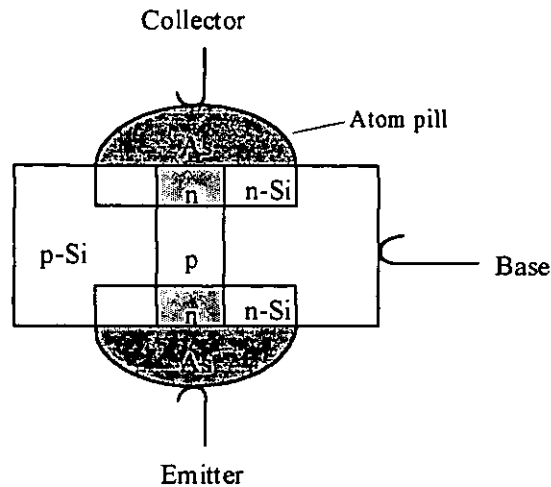


Fig. 18: Construction principle of a transistor

3.3.2 Micro coil

Structure height and the use of metals with low electrical resistance (copper) are the basis of micro coils with high current load capacity. In order to avoid a short-circuit, the metallic coil is positioned on an isolated substrate, as shown in Figure 19.

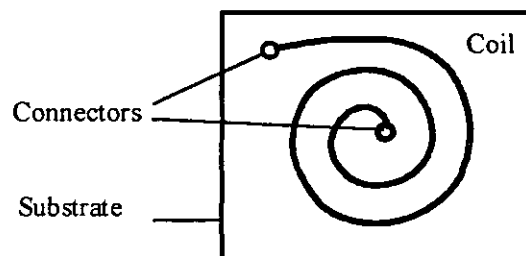


Fig. 19: Construction principle of a micro coil [Menz93]

3.4 Combination of micro components

All previously shown application examples are of technologically secondary interest, when one merely tries to transfer conventional components or component groups onto a reduced scale. Considering microelectronics, it is obvious that alone the production of discrete transistors as small and cheaply as possible only would not have led to the enormous success. Combining numerous components to component groups and to systems has tremendously increased the ability of microelectronics and underpinned their unprecedented success. Similar reasons are valid for all types of microstructures: the intelligent combination of a group of microcomponents leads to systems of high performance and applicability.

4 DEVELOPMENT OF A SERIAL LASER LITHOGRAPHY SYSTEM

In this chapter a Laser Pattern Generator (LPG) designed, constructed and tested in the Institut für Lasertechnik Ostfriesland at the Fachhochschule Ostfriesland (FHO) will be introduced.

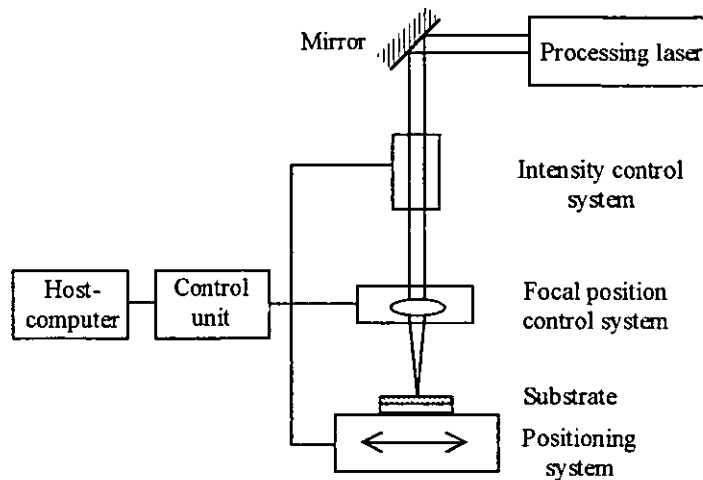


Fig. 20: Principle set-up of the Laser Pattern Generator

According to figure 20, the intensity of the laser beam is monitored by a closed-loop control circuit and focused by a position controlled processing head. A positioning system moves the substrate to be exposed under the laser focus. The total process is controlled by an electronic control unit in combination with a host computer. A survey plan and a block diagram of the LPG is shown in Appendix A.

4.1 Hardware of the LPG

The hardware of the system consists of three functional groups:

- The optical system for the exposure
- The positioning system for the movement of the substrate.
- The control unit for the co-ordination of all LPG actions.

All functional groups will be described in detail in this chapter.

4.1.1 Optical system

The beam source of the optical system is a He-Cd laser whose intensity is controlled to the required level by a closed-loop control system. A second closed-loop control system cares for the correct focal position of the laser beam during the exposure.

4.1.1.1 Beam path of the exposure laser

Table 1 shows the characteristics of the He-Cd laser from Omnichrome used for the exposure.

Model	4074-P-43
Laser-mode	TEM ₀₀
Beam output semi-diameter	0.5 mm
Waist position	5 mm behind the output window
Wavelength	441.6 nm
Rayleigh length	1.82 m
Polarisation	linear (1:500)
Divergence angle	0.57 mrad (full angle)
Power	43 mW

Table 1: Characteristics of the He-Cd laser

The output wavelength of the exposure laser lies within the sensitive wavelength range of typical photo resist and the intensity of the beam also permits a successful resist structuring. The output beam is focused by a microscope objective from Newport with a short focal length keeping the focus spot radius in the range of one micrometre required for the micro structuring.

Type	M-60X
Focal length	2.9 mm
Clear aperture	5 mm
Numerical aperture	0.85
Working distance	0.3 mm

Table 2: Characteristics of the microscope objective

The beam path of the optical system is shown in figure 21.

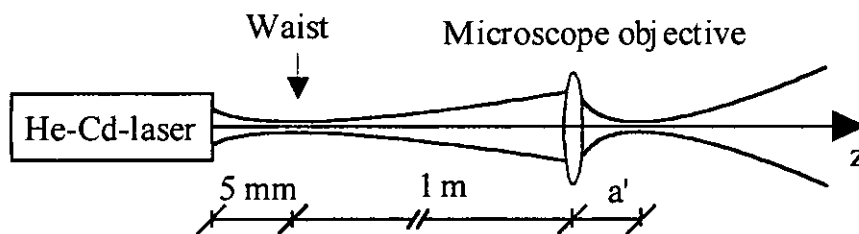


Fig. 21: Beam path of the exposure laser

For further examination of the beam geometry of the exposure laser the Gaussian beam transformation as sketched in figure 22 will be investigated.

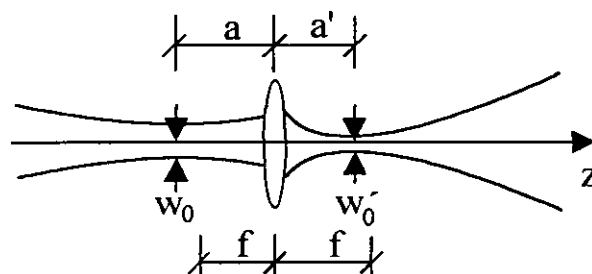


Fig. 22: Gaussian beam transformation by a lens

Starting point is the beam waist with the radius w_0 at a distance, a , to the lens. The beam transformation of the lens with a focal length f results in a new waist with the radius w_0' in

the distance a' to the lens. Both parameters w_0' and a' can be determined using following equations [Eich91] where equation (1) describes the position of the new beam waist

$$a' = -f + \frac{f^2(f - a)}{(f - a) + Z_R} \quad (1)$$

and equation (2) describes the radius of the beam

$$w_0' = \frac{fw_0}{\sqrt{(a - f)^2 + Z_R}} \quad (2)$$

with

$$Z_R = \frac{\pi w_0^2}{\lambda} \quad (3)$$

λ being the wavelength of the laser and Z_R the Rayleigh length. This parameter describes the distance between the position of the beam waist and the position where the cross-section of the beam has doubled and, therefore, this parameter describes the beam divergence.

According to equation (2) the focal radius and, therefore, also the focal spot will yield a minimum when the input Rayleigh length is as large as possible and for this in accordance to equation (3) the input waist of the beam is as large as possible as well. The maximum diameter of the input beam is limited by the aperture of the lens. Equation (2) also proves that a focal spot as small as possible is yielded when the distance, a , between laser output and microscope objective is as large as possible. Beam diffraction limits minimum focal spot diameter in the range of the wavelength of the laser.

In order to avoid further beam forming components, the required beam radius of $w_0' = 0.7\mu\text{m}$ was established in determining the distance a between laser and used microscope objective by equation (2):

$$a = 1.05\text{m}$$

with equation (1) the position of the focal point results in

$$a' = 2,903\text{mm}$$

The Rayleigh length Z_R will be determined using equation (3) and results in

$$Z_R = 3.5\mu\text{m}$$

These results were confirmed with the ray tracing program *Zemax* (see Appendix B).

4.1.1.2 Intensity closed-loop control system

To control the laser intensity during the exposure, a closed-loop control system shown in figure 23 was developed. The purpose of this circuit is on the one hand to avoid influences to the exposure result due to laser intensity instabilities and on the other hand to achieve different exposure results by adjustable laser intensities.

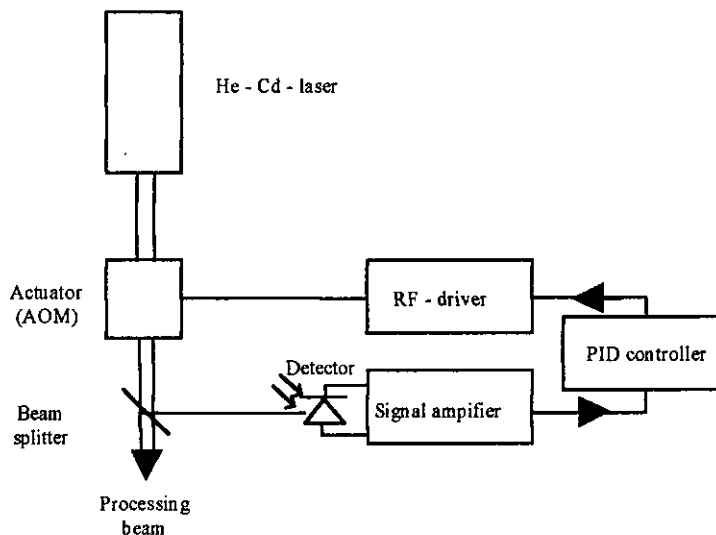


Fig. 23: Intensity closed-loop control system

The beam of the He-Cd exposure laser passes an actuator (acousto-optic modulator, AOM) driven by a RF source in order to adjust the intensity of the exposure beam. After beam splitting, one part of the beam is used for the exposure while the other part is registered by a detector. The output of the detector is fed to a process control computer (see chapter 4.1.3.1) with a software controller (see chapter 4.2.1.4) and which in term is coupling the controller output value via the RF driver again to the AOM.

The acousto-optic modulator (AOM) or Bragg-Cell establishes several orders of diffraction of the beam by interaction between the laser beam and a grating, where the intensity in the different diffraction orders depends on the grating profile. This grating is generated by a sound signal coupled into a crystal resulting in periodic density changes in the crystal, which represent the grating [Leka86]. Table 3 lists the characteristics of the AOM from Brimrose.

AOM Type	BRI FQM-8-2
Driver Type	BRI FFA -88
Wavelength	200 - 4500 nm
Center frequency	80 MHz
Active aperture	1.0 mm
Diffraction efficiency	> 70%
Optical transmission	> 95%
Wavefront distortion	$\lambda/10$
Diffraction angle	0.2 ° (at 280 nm)

Table 3: Characteristics of the AOM

The intensity of the first diffraction order (DO) I_1 used for the exposure can be described by the following equation [Naum92]:

$$I_1 = I \sin^2 \left[\frac{\pi}{\lambda_0} \left[\frac{M_2 P_{AL} L}{2H} \right]^{1/2} \right] \quad (4)$$

- I_1 : Intensity of the first diffraction order
- I : Intensity of the incoming beam
- P_{AL} : Acoustic power
- H : Height of the sound field
- L : Distance of light within the sound field
- λ_0 : Wavelength
- M_2 : Modulus (figure of merit)

By using the first diffraction order, the laser intensity needed for exposure can be adjusted continuously by changing the acoustic power P_{AL} . The acoustic power can be varied by an

analogue control voltage applied to the RF driver. A beam splitter divides the output intensity of the used diffraction order in a proportion of 1:1, one part being used for the exposure. The second portion is detected by an optoelectronic detector based on a PIN-photodiode in combination with an integrated transimpedance amplifier. The characteristics of the detector from Burr&Brown is listed in table 4.

Type	OPT 201
Photo area	2.29 x 2.29 mm
Sensitivity	0.1 A/W ($\lambda=44$ nm)
Bandwidth	4.4 kHz

Table 4: Characteristics of the photodetector

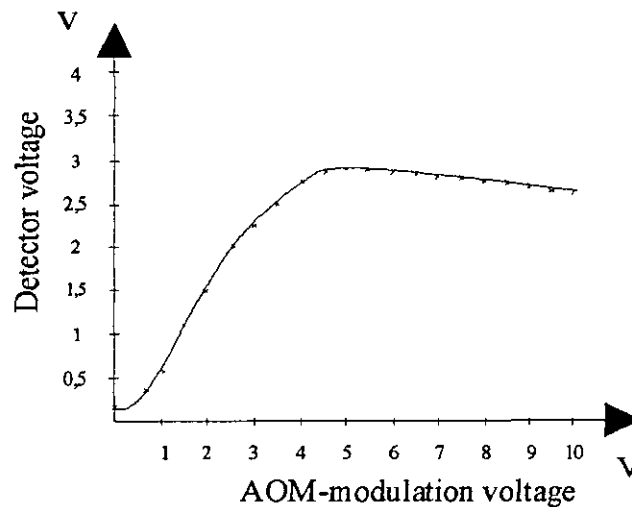


Fig. 24: Characteristic curve of the system to be controlled

The characteristic curve in figure 24 describes the operating characteristic of the above described system. An AOM modulation voltage on the x axis in the range of 1V to 3V will cause an approximately linear response of the detector voltage on the y axis in a range of 0.7V to 2.4V. This corresponds to an intensity range of 5mW to 25mW in which the intensity can be adjusted with an accuracy of $\Delta P = \pm 80\mu\text{W}$. This linear range is chosen for controlling because the non-linear part of the operating characteristics will support the oscillating susceptibility of the control system.

For the selection and parametrisation of an optimum controller the dynamic characteristics of this system has been determined by the investigation of the step response. A signal generator has been used to deliver an input step to the analogue modulation input port of the AOM driver while the output signal of the photodetector has been recorded.

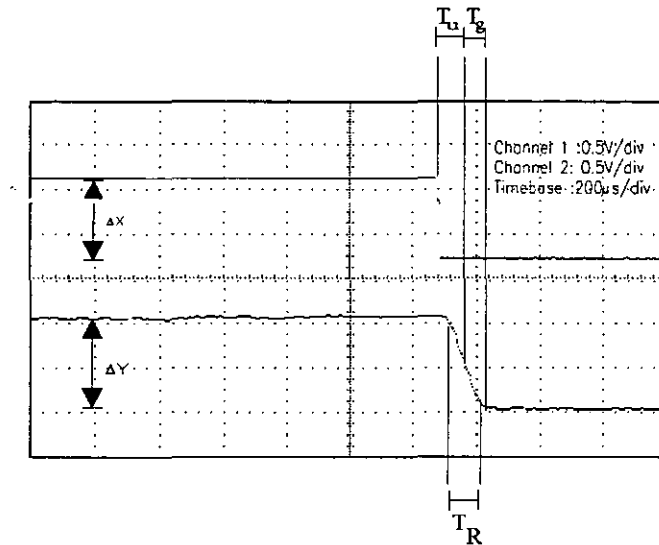


Fig. 25: Step response for the determination of the system parameter

Figure 25 illustrates the negative input step of -0.9V in the upper part of the figure and in the lower part the output signal step of -1.2V as a result of the input signal. The s-shaped response is characteristic of a delayed controlled system of higher order. The cut-off frequency f_g of the system is approximately determined by following equation:

$$f_g T_R \approx 0.35 \quad (5)$$

f_g represents the bandwidth (B_w) and T_R the rise time which is required to increase or decrease the value from 10% to 90% of the response signal. Figure 25 shows, the rise time $T_R = 80\mu\text{s}$ describing a bandwidth and thereby a cut-off frequency of $f_g \approx 4.4\text{kHz}$. This cut off frequency coincidence with the data of the manufacturer of the detector (see table 4), so that the detector is limiting the dynamic characteristics of the system to be controlled.

After the description and the determination of the characteristic of the system to be controlled, the selection of an optimum controller type with optimised controller parameters has to be performed. The selection of the controller type is not critical in comparison to the selection of the controller parameters. In closed loop system applications with controlled systems having a dead time or transfer lag, the controller parameter have to be adjusted correctly because they influence the stability of the system enormously [Reut90]. A smooth control response for the exposure process is desirable and leads to the design of a PI-controller whose operation characteristic is a compromise between a reasonable disturbance response to eliminate power fluctuations and a reasonable control response for the following controlling. The method of the inflection tangent [Chie52] graphically determines controller parameter from the step response of the system to be controlled of higher order (see figure 25).

- T_u : Transfer lag
- T_g : Settling time
- K_s : Transfer factor

The transfer factor K_s results from the changes of the output variable ΔY divided by the changes of the input variable ΔX . From figure 25 one gets the following values:

$$\begin{aligned} T_u &= 80\mu\text{s} \\ T_g &= 50\mu\text{s} \\ K_s &= 1.35 \end{aligned}$$

The experimentally determined dead time $T_t = 7\text{ms}$ of the digital controller (see chapter 4.2.1.4) is much greater than the acousto-optical transfer lag and is the dominating contribution to the feedback lag.

In order to determine the controller parameter the rules from Chien, Hrones, Rewick [Chie52] require the determination of the following auxiliary variable:

$$\widetilde{K} = \frac{T_g}{T_u K_s} = \frac{50 \cdot 10^{-6}}{7 \cdot 10^{-3} \cdot 1.35} = 0.005 \quad (6)$$

With this auxiliary variable, the controller parameter for the selected controller with the desired characteristics can be taken from a table (see Appendix C). The PI-controller with reasonable disturbance - and following controlling characteristic requires the following controller parameter:

$$K_P = 0.34K_{.0.6K} - > 0.003$$

$$T_N = 1.2T_g, 4T_U = 60\mu s, .28ms - > 500\mu s$$

With these parameters, the controlling characteristic was determined. For this reason figure 26 shows in the lower part the controller output value as a result of a step of the set point shown in the upper part. An overshooting of the signal can clearly be identified. The rise time after which the controlled variable adopts the desired value for the first time is $T_R = 40ms$ and the settling time after which the controlled output variable stays within a tolerable range is $T_g = 80ms$.

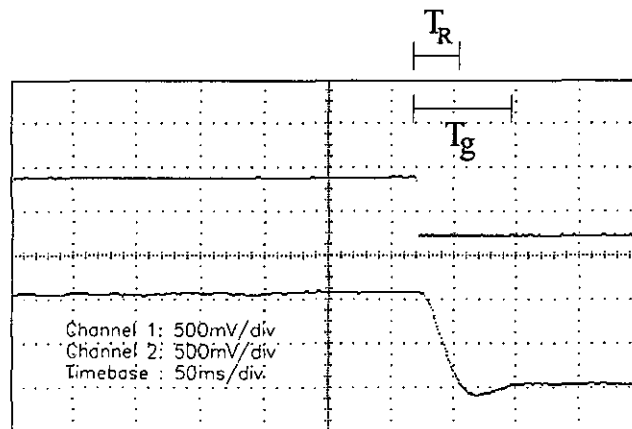


Fig. 26: Controlling characteristic of the intensity closed-loop control system

The experimental optimisation of above theoretically determined starting values of the controller parameter establishes the control characteristic shown in figure 27.

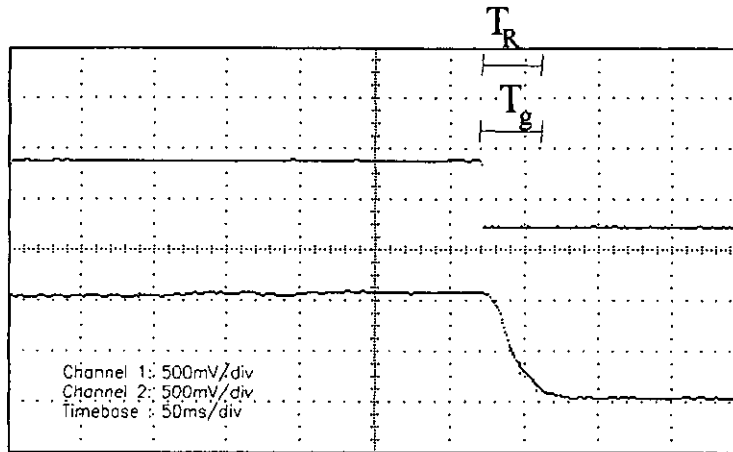


Fig. 27: Controlling characteristic of the optimised closed-loop control system

As figure 27 shows, a stabilised control loop response can be established. The rise time is $T_R = 50$ ms and the settling time is $T_g = 50$ ms. The noise of $U_R = \pm 17$ mV superimposing the output signal limits the accuracy to $\Delta P = \pm 200\mu$ W. Both the velocity and the accuracy permits a successful operation of the intensity controlling in the LPG.

The following variables were determined as optimum controller parameters:

$$K_p = 0.004$$

$$T_N = 1.1\text{ms}$$

4.1.1.3 Focal position closed-loop control system

As discussed in chapter 4.1.1.1, the processing beam has a Rayleigh length of $Z_R = 3.5\mu$ m. Because of the strong influence of the focal position on the exposure result the development of a position controlled processing head became necessary [Samu96a]. This on the one hand shall prevent changes of the focal position during the exposure on uneven surfaces and on the other hand shall allow different focal positions for the exposure in order to realise different exposure results. Figure 28 illustrates a block diagram of a position controlled processing head.

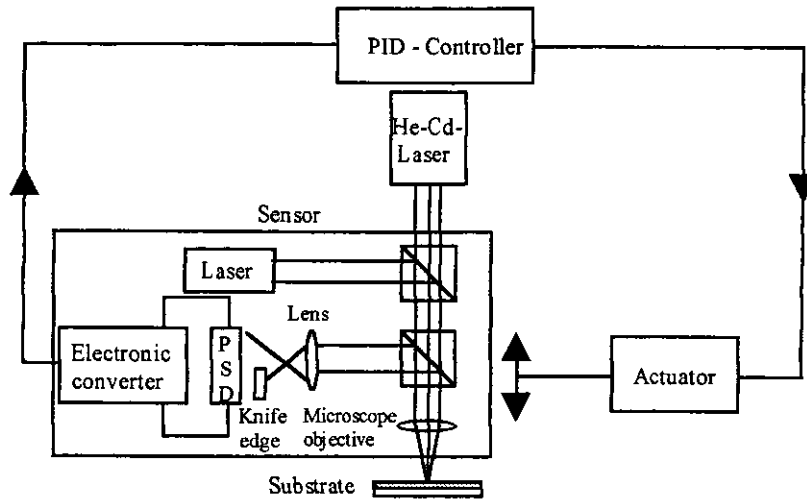


Fig. 28: Focal position closed-loop control system

The microscope objective, used for the beam focusing of the exposure laser is coupled to a distance measuring system. In order to control the focal position, this system is mounted to an actuator (piezo translator). The actual distance between microscope and substrate surface is registered using a modified autofocus principle. This will be done by superimposing the exposure beam with a second beam from a semiconductor laser and focusing the second beam to the substrate surface by the same microscope objective. The reflection of this measuring laser beam from the resist surface is decoupled from the main beam by introducing a beam splitter cube. Then the beam is manipulated by a lens and a knife edge (Foucault's cutting principle) and registered by a position sensitive detector (PSD) the two output signals of which are combined by transformation electronics and thus generate the distance signal.

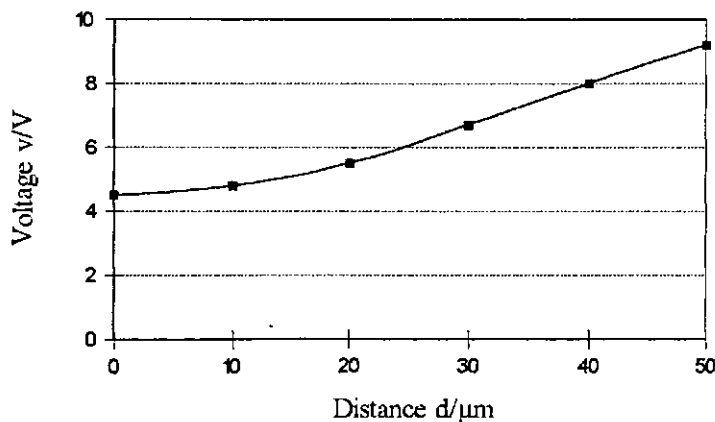


Fig. 29: Characteristic curve of the system to be controlled

Figure 29 shows the sensor signal as a function of the distance between measured surface and focus position. One can see on the x axis an optimised linear measuring range of $30\mu\text{m}$ between the distances from $20\mu\text{m}$ to $50\mu\text{m}$ which result in a signal on the y axis between 5.7V and 9.1V

In order to determine the dynamic characteristic of the system, the step response is investigated. This was established by applying a signal generator to the drive electronics of the piezo translator and recording the sensor signal.

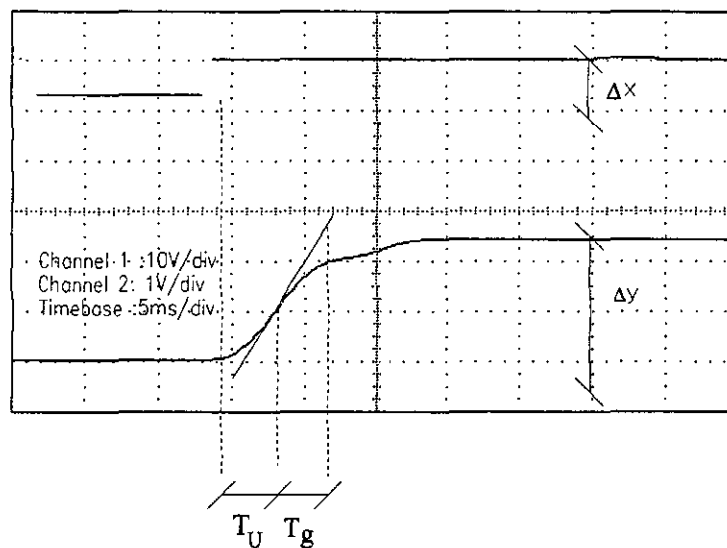


Fig. 30: Step response for the determination of the system parameter

Figure 30 shows the input step of 7.6V in the upper part of the figure and the response of 2.6V amplitude with a s-shaped characteristic in the lower part. For a rise time of $T_R = 8\text{ms}$, the bandwidth in accordance with equation (5) and, therefore, the cut-off frequency can be determined as $f_g \approx 43\text{Hz}$. This frequency matches the cut-off frequency of the piezo translator [Samu96a] which limits the dynamic characteristics of the system.

According to Chien, Hrones, Reswick the parameters of the system to be controlled will have the following values:

$$T_u = 4 \text{ ms}$$

$$T_g = 4 \text{ ms}$$

$$K_s = 0.345$$

Also in this case one has to add the additional dead time $T_t = 7$ ms of the digital controller to the total delay time and equation (6) will lead to the following auxiliary variable:

$$\tilde{K} = 1.1$$

Also for this system a PI-controller shall be realised which compromises between reasonable disturbance and following characteristic. The table in Appendix C delivers the following values:

$$K_p = 0.34K \dots 0.6K \rightarrow 0.5$$

$$T_N = 1.2T_g \dots 4T_U = 4.8\text{ms} \dots 44\text{ms} \rightarrow 30\text{ms}$$

The theoretically determined controller parameter leads to the characteristic of the closed-loop control system shown in figure 31.

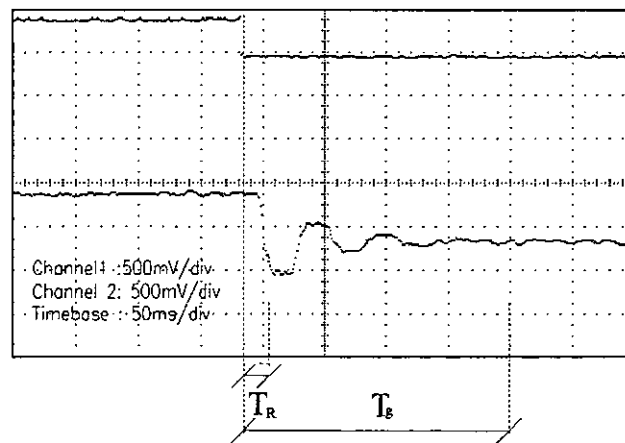


Fig. 31: Controlling characteristic of the focal position closed-loop control system

Figure 31 shows in the lower part the controller output value a result of a set point step shown in the upper part. An oscillation of the signal can clearly be identified. The rise time amounts to $T_R = 20\text{ms}$ and the settling time to $T_g = 175$ ms. Starting with this response of the system an experimental optimisation was executed and the result is shown in figure 32.

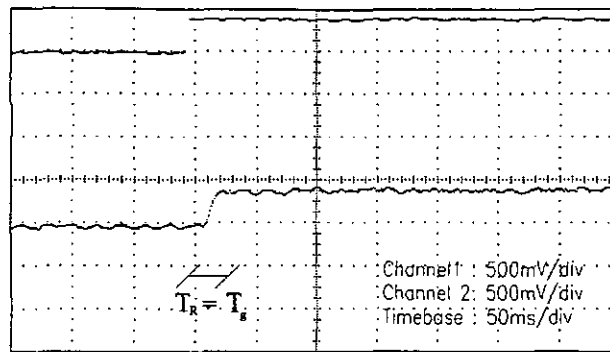


Fig. 32: Controlling characteristic of the optimised closed-loop control system

As figure 32 shows, a stabilised control loop response can be established. The controlling signal is superimposed with a noise of $U_R = \pm 60\text{mV}$ which permits a focal position accuracy of $\Delta Z = \pm 0.52\mu\text{m}$. The settling time equals the rise time and amounts to $T_g = T_R = 30\text{ms}$. The velocity as well as the accuracy permit a successful operation of the focal position closed-loop control system in the LPG.

The following optimised controller parameters were established:

$$K_p = 0.35$$

$$T_N = 7\text{ms}$$

4.1.2 Positioning system

The positioning system moves the substrate under the focused laser beam and, therefore, as the dynamic system component, it has a crucial influence on the process time of the LPG. The control range of the positioning system determines the maximum size of the object, while the positioning accuracy is responsible for the distortion of the object. In this chapter the stages, the laser interferometer which is needed for the survey of the axis, and the Direct Axis Interface (DAI) which is used to synchronise the movements of the substrate with external events will be introduced.

4.1.2.1 Stages

The positioning system used is the PM500 from Newport, whose controller monitors two crossed linear axes and a rotation axis mounted on the linear stage. This permits movements in cartesian coordinates using the two linear axes and in polar coordinates combining a linear and the rotation stage. The layout of this system permits the rotary axis to be adjusted relative to the optical exposure axis [Mils95] useful to realise rotationally symmetric structures with different diameters. The characteristics of the linear axes are listed in table 5 and those of the rotation axis in table 6.

Resolution	25 nm
Travel range	1" (= 25.4 mm)
Speed	0.01 μ /s - 50 mm/s
Acceleration/Deceleration	0 - 2500 mm/s ²

Table 5: Characteristics of the linear axes

Resolution	1/1000° (= 1 count)
Smallest step size	3/1000°
Travel range	no limitation
Radial runout	1.6 μ m
Speed	0- 10°/s

Table 6: Characteristics of the rotation axis

The controller monitors the position and velocity of the axes by internal control loops and places decision feedback on actions of the axes to the host computer. The data exchange takes place through a serial RS232 port. More specific instructions on this system can be found in the handbook [Newp93] and other publications [Humm95][Laas94].

4.1.2.2 Laser interferometer

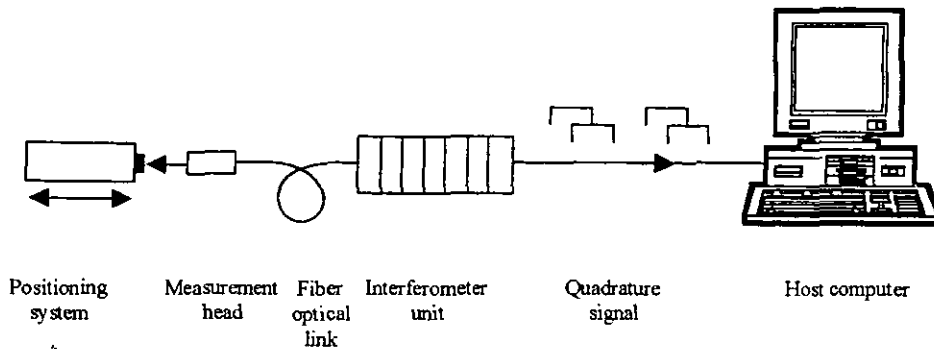


Fig. 33: Block diagram of the interferometer system [Grüb92]

Figure 33 illustrates the block diagram of the interferometer system. The beam of a stabilised semiconductor laser exits the interferometer unit and is routed to the measuring head through a flexible fibre optical link. In the measuring head, the measurement beam is decoupled. Opposite the measuring head, the measuring mirror is mounted which moves with the linear axes and by this enables recording of the movement of the axis. The light reflected by the mirror is coupled into the measuring head and transmitted to the interferometer unit. After signal conditioning, the incremental position information being quadrature signals with a measurement resolution of 16.25nm are transmitted to the host computer through a TTL port. A 24-bit counter card in the host computer registers these signals (see chapter 4.2.1.2).

4.1.2.3 Direct Axis Interface (DAI)

This option for the PM500 system generates, for every 250nm movement of the linear axes, a TTL pulse which enables the synchronisation of external events such as switching the laser beam at defined positions. Figure 34 illustrates an example in the vx-diagram. When the stage has travelled the distance x_1 the laser shall be switched on and stay on until position x_2 . This unit thus enables exposures of exactly the same length which can be repeated with the same accuracy and permits homogeneous exposures during axis movements. Also, an exposure during acceleration or deceleration can be avoided. The evaluation of the DAI pulses is done by a DAI unit which is integrated in the control unit of the LPG (see chapter 4.1.3.2).

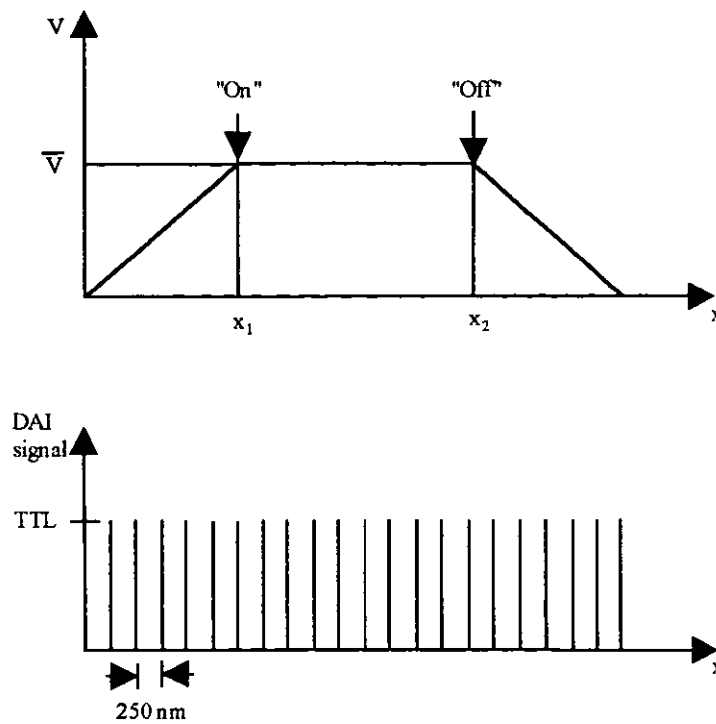


Fig. 34: Principle of the Direct Axis Interface

4.1.3 Control system

The successful operation of the LPG requires the co-ordination and synchronisation of all actions of the above described system components. For this, the host computer was equipped with special interface cards and connected to a control unit. The system has the following functions:

- Operation flow and process control
- Visualisation of the process status
- Visualisation of all control parameters
- Information of the user
- Alarm output to the user
- Safety monitoring and system shutdown
- Printout of the process protocol
- LPG adjustment

4.1.3.1 Host computer

The host computer is an IBM compatible personal computer based on an 80386 -33 processor from Intel. A hard disk is used for saving programs and data and a floppy disk drive can be used for data exchange. In addition to the serial interfaces used for the PM500 controller and mouse and a parallel interface for the printer, the host computer is equipped with three additional interfaces:

- A 12 bit A/D and D/A converter DAQ-1212A from Physik Instrumente (PI) transmits the analogue signals of all control circuit inputs and outputs from and to the host computer. This card further provides 8 TTL input and output lines. Layout and set up of this card are explained in the appropriate manual [Phys92].
- A 48 channel PIO card for the output of TTL signals used for the control of the DAI unit. Layout and set up of this card are explained in the appropriate manual [Conr92].
- A card with 3 channels with 24-bit counter is used for the evaluation of the quadrature signals from the laser interferometer. Layout and set up of this card are explained in the appropriate manual [Kolt93].

4.1.3.2 Control unit

User intervention for system setting before and during exposure can be done through a control unit where all process parameters can be controlled and adjusted. This control unit realises the connections between the host computer and components close to the process events. It is constructed from several discrete boards (see Appendix D1) which are interconnected through a bus system. The software of the host computer constantly analyses all actions of the control unit and supports the following units:

- DAQ unit: All input and output channels of the DAQ card are at disposal for the connection of external components so that monitoring signals can be realised through appropriate connectors (see Appendix D2).

- Power supply I: Voltages of -12V and -15V are generated. The voltages $\pm 15V$ are supplied to the front plate. The signal amplifier and AOM protector are supplied by this unit (see Appendix D3).
- Power supply II: Voltages of +12V and +15V are generated. The voltages $\pm 12V$ are supplied to the front plate. The photo detector I + II and the piezo driver are supplied by this unit (see Appendix D4).
- PIO unit: All 48 TTL channels of the PIO card are accessible for the connections of external components for monitoring the signal status (see Appendix D5).
- Signal amplifier: Supplies the autofocus sensor (PSD electronics) and permits electronic adjustments of the sensor. The add-on of the sensor signal to the host computer can be interrupted (see Appendix D6).
- Piezo driver: The mode of operation (auto/man) of the piezo control system and the manual control signal can be adjusted. It also supplies the piezo driver with the operating voltage (see Appendix D7).
- Power supply III: This unit generates a voltage of +5V which is supplied to the front plate. The AOM protector and the DAI Unit are supplied by this unit (see Appendix D8).
- AOM protector: This unit monitors the flow and temperature of cooling water and in case of an alarm cuts off the AOM power supply (see Appendix D9).
- DAI Unit: This unit counts the DAI pulses of the selected axis of the positioning system and compares the pulses with two stored counter values in order to switch the laser on and off with high position accuracy. Furthermore, the mode of operation of the AOM can be selected (auto/man) and the control signal can be adjusted manually (see Appendix D10 and D11).

- Photo detector I: Supplies the detector OPT201 and delivers the sensor signal to the host computer (see Appendix D12).
- Photo detector II: Supplies the detector OPT201 and delivers the sensor signal to the host computer (see Appendix D13).

4.2 Software of the LPG

The system software which supports all actions of the LPG components has to be combined to one program in order to control the desired task of the LPG. These tasks allow on the one hand to analyse and to configure system characteristics or system status of the LPG (utility programs) or on the other hand to control the exposure (exposure programs) with the LPG. The system requirements for the software are described in Appendix E1.

4.2.1 System software

All hardware components of the system are supported by software modules which are mainly assigned to the following tasks:

- Initialising the interface to the hardware component
- Communication with the hardware component

4.2.1.1 Axis control

For controlling the axes, the PM 500 controller is linked to the host computer via a serial RS-232 interface. The initialisation of the interfaces is followed by the predifinitions of the movement parameters for all PM500 axes (see handbook):

- Velocity
- Acceleration
- Deceleration

All movements of the stage can be monitored by status signal of the axis transferred to the host computer. The software for the axis control is documented in Appendix E2.

4.2.1.2 Evaluation of the interferometer signal

The LPG host computer incorporates a counter card for the evaluation of the interferometer signals. Two of three incremental counters, with 24 bit depth, register the quadrature signals of the interferometer units. Prior to the measurements, the channels are initialised through an 8255 I/O module. The 8255 is equipped with four registers namely port A, B, and C as well as a control port. The control port switches all channels of the 8255 to the output and enables three initialising channels M0, M1, and M2 of the counter card to be set to Mode 5 according to table 7. These allows a quadruple evaluation and directional detection of counting pulses from the two channels used for the evaluation of the interferometer signals. This kind of evaluation results in a measurement resolution of 16.25nm of the interferometer system.

Mode	M2	M1	M0	Description
0	0	0	0	Up/down counter determine only from direction discriminator
1	0	0	1	Counting of single pulses with direction detection for U/D
2	0	1	0	Inverse counting of mode 1
3	0	1	1	Double evaluation of pulses with direction detection for U/D
4	1	0	0	Inverse counting of mode 3
5	1	0	1	Quadruple evaluation of pulses with direction detection for U/D
6	1	1	0	Pulse counter: Phi0 is gate signal Phi90=high is UP/ low for DOWN counter counts synchronous to clock
7	1	1	1	Frequency counter: Phi0 is frequency input (TTL) Phi90 is interval gate counting synchronous to Phi0

Table 7: Initialisation of the counting channels

For determining the actual counter value, all three registers of the particular counter will be read-out. Because 8 bit registers are used their single values have to be converted to a 24 Bit value. This results in a total counter value of:

$$\text{counter} = 256 * 256 * \text{Higher Byte} \\ + 256 * \text{Medium Byte} \\ + \text{Lower Byte}$$

Afterwards, the multiplication of the counter value with the resolution of the interferometer delivers the distance change:

$$\text{Distance change} = \text{counter value} \cdot \text{resolution of the interferometer}$$

As the difference to a previously determined distance a displacement of the axis can be determined.

The software for the evaluation of the interferometer signal is documented in Appendix E3.

4.2.1.3 DAI programming

During a linear axis movement the DAI of the PM500 controller generates every 250nm a pulse to one of the two outputs, depending on the direction of the movement (see 4.1.2.3). These pulses are registered by the DAI unit (see 4.1.3.2) and compared with two counter values which describe the switch-on and switch-off point of the laser (see figure 25). These counter values are stored in a 24 bit register that are loaded through the PIO card. The PIO card has 48 TTL outputs which are programmed through two 8255 modules. Port A of the first 8255 is selected as the data port for all information transmissions to the DAI unit while port B serves as the control port. The first four bits of port B control the 74LS138 encoder on the DAI card (see Appendix D10 and D11) which selects the different counter IC's on the DAI card according to table 8.

Bit 0	Bit 1	Bit 2	IC-No.
1	1	1	Not used
0	1	1	Not used
1	0	1	6
0	0	1	5
1	1	0	4
0	1	0	3
1	0	0	2
0	0	0	1

Table 8: Chip selection

Through these lines the discrete counters can be selected and loaded with the signals from the data bus, in which bit 3 is the enabling bit of the encoder. A pulse on the line transfers the signals from the data port into the counter. According to table 9 bits 5,6 and 7 permit the selection of an axis which DAI pulses shall be counted.

Bit 5	Bit 6	Bit 7	Axis
1	1	1	Initial position
1	1	0	Initial position
1	0	1	Initial position
1	0	0	Initial position
0	1	1	x-
0	1	0	x+
0	0	1	y-
0	0	0	y+

Table 9: Axis selection

When at first the counters have been loaded with the corresponding values and an axis has been selected, the DAI generates counting pulses during an axis movement. The pulses are registered and evaluated by the programmed DAI unit.

The software for the DAI programming is documented in Appendix E4.

4.2.1.4 Intensity control

The intensity of the exposure laser is controlled through a software controller in the host computer of the LPG. For the input of the detector signal and the output of the signal to the AOM, a 12 bit DAQ card (see chapter 3:1.3.1) with A/D and D/A converter is introduced with the following connections.

A/D - converter	D/A - converter
Channel 7 (OPT-201)	Channel 6 (AOM)

Table 10: Connections for the intensity controller

The DAQ card digitises the voltage signal from the photo diode OPT-201 and feeds it to a software controlled signal standardisation. The input voltage range as a function of the laser power is internally assigned to a virtual input voltage range of -5V to +5V, which corresponds to a laser power of 5mW to 25mW.

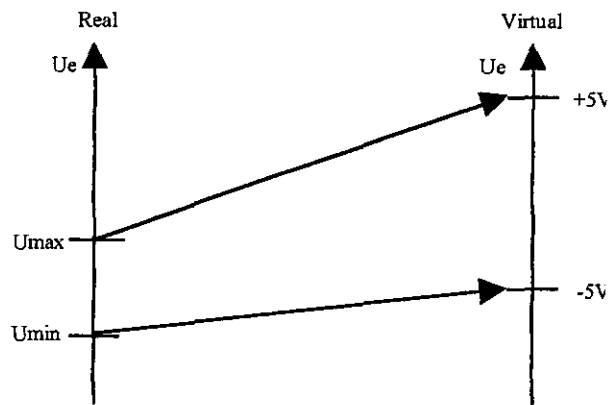


Fig. 35: Conversion of the input signal

The set point for the laser power is fed together with the converted actual value to a control algorithm which calculates the controller output value. The host computer simulates the function of an electronic controller in a numerical manner. An ideal PID controller can be described by the following equation [Bühl95]:

$$y(t) = K_p \left[x_d(t) + \frac{1}{T_N} \int x_d(t) dt + T_V \frac{dx_d(t)}{dt} \right] \quad (7)$$

with:

- $y(t)$: Output value of the controller
- x_d : Negative deviation
- K_p : Proportional action parameter of the controller
- T_N : Reset time
- T_V : Derivative time

The differential and integral part of equation (7) must be approximated for the digital controller [Sont91]:

$$\frac{dx_d(t)}{dt} \Rightarrow \frac{x_d(k) - x_d(k-1)}{T_A} \quad (8)$$

$$\frac{1}{T_N} \int x_d(t) dt \Rightarrow \frac{T_A}{T_N} \sum_{i=0}^{k-1} x_d(i) \quad (9)$$

T_A represents the sampling time and k the sample number. With the help of this approximation and the conversion to a voltage output signal, the output of the controller can be described as follows:

$$U(k) = K_p \left[x_d(k) + \frac{T_A}{T_N} \sum_{i=0}^{k-1} x_d(i) + \frac{T_V}{T_A} (x_d(k) - x_d(k-1)) \right] \quad (10)$$

The result of equation (10) must be added to the set point, before the output can be given to the actuator.

A fast and stable control characteristic is achieved by a small as possible but in every case constant dead time T_t of the controller. The dead time of a digital controller must be taken into account when designing a controller. This dead time is composed by the time for one pass through the control algorithm T_{RA} and the sampling time T_A [Bühl95].

$$T_t = T_{RA} + \frac{T_A}{2} \quad (11)$$

In order to determine the dead time of the controller, the control program was modified to allow monitoring the beginning and end of the controlling process with an oscilloscope connected to the output port of the control system. To do this, the program reads the sensor signal and stores it as the current set point. After that, a voltage is given to the output port to which the controller output is connected. This voltage is 0.5V higher than the output voltage read by the controller. Then the controller starts its work by measuring the control variable.

Because the controller is not able to detect a deviation of the set point and the actual value of the controlled parameter, the initial voltage level returns after one control pass. This cycle is followed by another one with an output voltage which is reduced by 0.5V in comparison to the original value. Figure 36 illustrates the examined signal form of the controller variable measured at the output port of the open closed-loop control system.

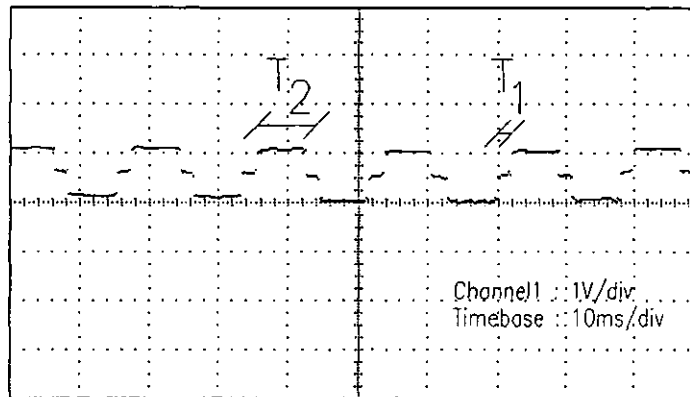


Fig. 36: Determination of the controller dead time

The time duration $T_1 = 2\text{ms}$ shown in figure 36 is required for the measuring and saving of the actual control variable as the current set point as well as calculating and output of a voltage increased or reduced by 0.5V to the analogue output port.

The signal with a time duration of $T_2 = 6\text{ms}$ shown in figure 36 is required for measuring the control variable, subsequent comparison between set point and actual value, saving of the negative deviation as well as one controller loop and the output of the calculated controller output voltage.

The difference $T_2 - T_1$ represents approximately one pass of the control algorithm T_{RA} , while the sampling time T_A of a discrete controller is determined by T_2 . The dead time T_t of the controller therefore amounts to:

$$T_t = \frac{T_A}{2} + T_{RA} = \frac{6\text{ms}}{2} + 4\text{ms} = 7\text{ms} \quad (12)$$

The software for the intensity control system is documented in Appendix E5.

4.2.1.5 Focal position control

The function of the focal position control program is identical to the function of the intensity control program. The software controller is connected to the following ports of the DAQ card:

A/D - converter	D/A - converter
Channel 8 (AFS)	Channel 7 (Piezo-Driver)

Table 11: Connections for the focal position controller

The software for the focal position control system is documented in Appendix E6.

4.2.2 Utility programs

Five different utility programs permit testing and optimisation of the LPG to the LPG user before starting the exposure. The utilities employ the modules introduced in chapter 3.2.1.

4.2.2.1 Module test system

All the software modules which are described in chapter 3.2.1 are combined to a module test system shown in figure 37.

With this program the following functions can be accomplished:

- All functions of all hardware components of the system can be tested
- The parametrisation can be accomplished

The software for the module test system is documented in Appendix E7.

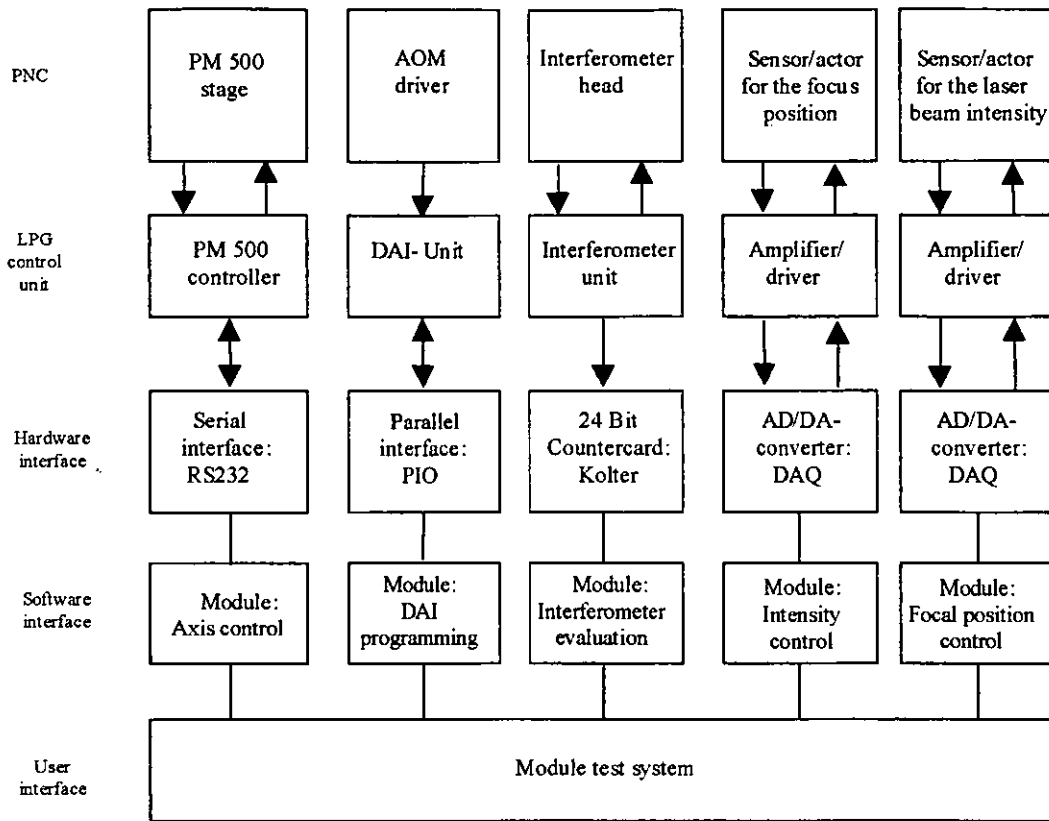


Fig. 37: Modules used in the test system

4.2.2.2 Laser stability

Considering the time consuming exposure of a microstructure, the stability of the laser is of high interest. The stability determination was done over an interval of one hour.

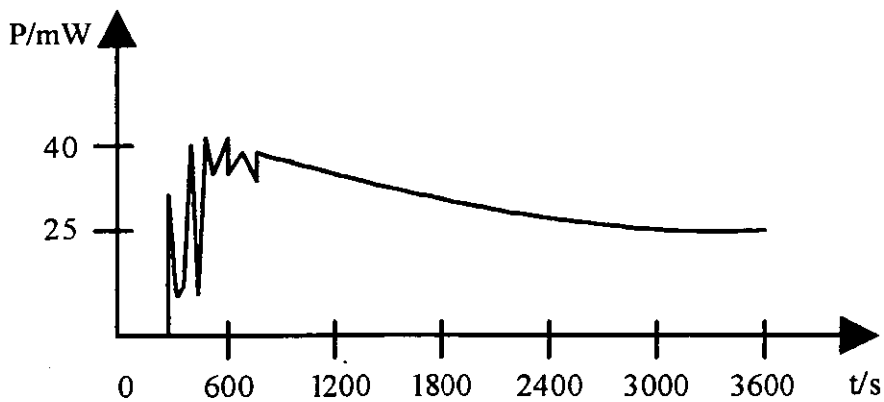


Fig. 38: Laser intensity as a function of time

The curve in figure 38 clearly shows, the start-up transients of the He-Cd laser are not finalised before one hour has passed. This means that, on the one hand, during the transient period the exposure must be controlled by the intensity control system or on the other hand the transient period must be allowed to pass before starting serious work. The software for the determination of the laser stability is documented in Appendix E8.

4.2.2.3 Positioning tracing

In order to determine the working characteristic for the positioning system, the stage is displaced by a certain distance, whereas the position of the axis is recorded by the laser interferometer data from which are recorded by the host computer and saved in a file. These data can be used for the visualisation of the positioning characteristic of the stage. Figure 39 shows, the displacement of $3437\mu\text{m}$ requires a time of 643ms . The movement is performed with a s-shaped characteristic indicating no movement with constant speed.

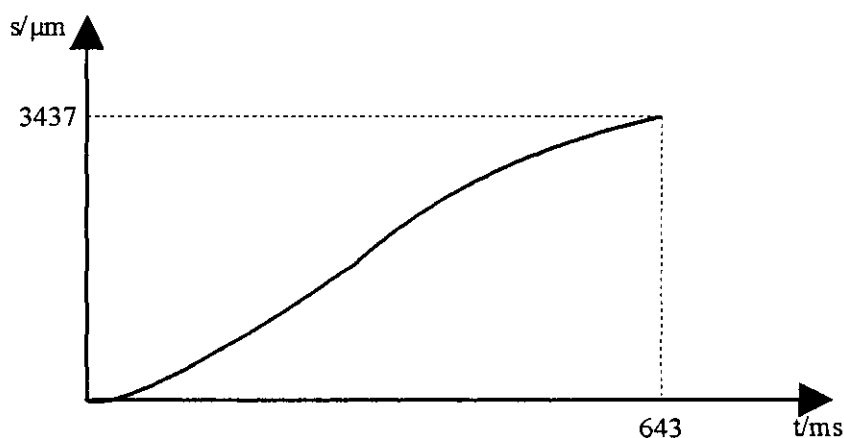


Fig. 39: st-diagram of the PM500

The stage parameter has to be tuned to the specific axis load and desired movement, so that this tool can be used to determine and optimise the movement of the axis for LPG applications. The software for the positioning tracing is documented in Appendix E9.

4.2.2.4 Positioning accuracy

After the initialisation of the motion parameter, the stage is placed to a defined initial position. After reaching this position the stage starts moving along half of a selected distance

in positive direction and back to the initial position which normally never will be met exactly at the same point. Moving and returning in negative direction will also result in a deviation. This operation will be repeated many times. The reached positions determined by the interferometer and the associated ideal positions are recorded into a file and then evaluated.

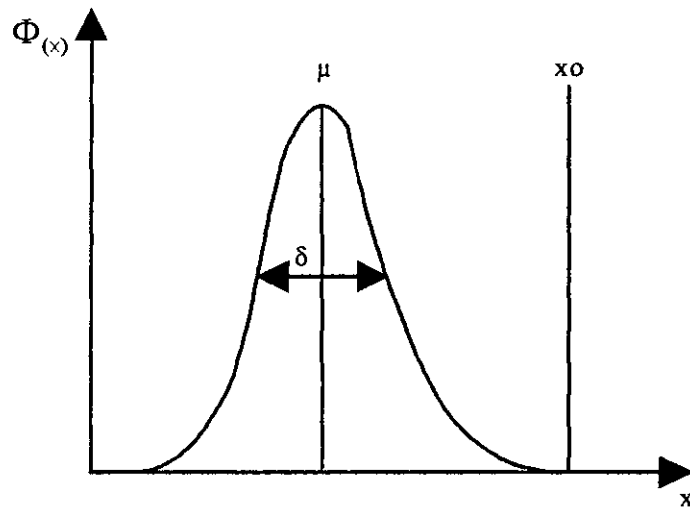


Fig. 40: Gaussian curve for the PM500

Figure 40 illustrates the accumulation distribution $\Phi(x)$ of an approached position. These values satisfy the normal distribution. The width of the distribution described by the standard deviation δ characterises the precision and the distance between the distribution maximum μ and the ideal position x_0 describes the motion accuracy of the stage system. This information can be used to determine the movement finalisation and to optimise it by tuning the axis parameter in accordance to the specific axis load and desired movement. The software for the determination of the positioning is documented in Appendix E10.

4.2.2.5 Compensation program

In order to determine and correct systematic positioning errors of the positioning system a compensation program was developed. The program LMS2.pas determines the positioning characteristic of the stage with the interferometer. The data are saved into a file. The curve in figure 41 illustrates the error as a difference of nominal and actual value being a function of the nominal value.

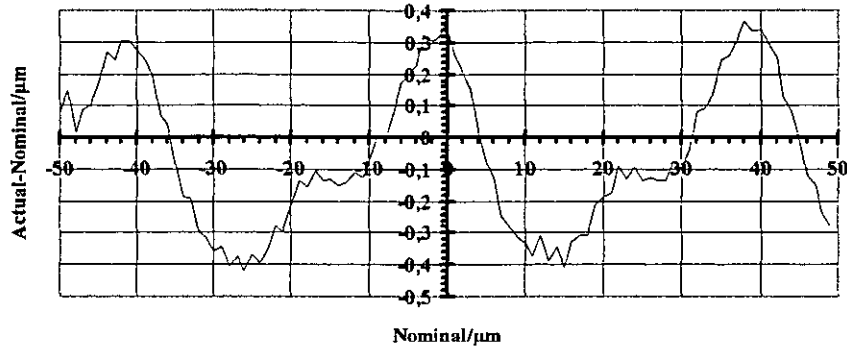


Fig. 41: Error curve of the positioning system

As can be seen from figure 41, the error is of periodic nature and can therefore be corrected. This will be realised in transferring one period of the curve into a program, which calculates by Fourier analysis corresponding Fourier elements and saves them into a file. For a stated step width or resolution and the number of elements to be calculated a look up table can be established, which can be used as a correction module by influencing the controller commands by a correction coefficient. This results in a improved positioning characteristic of the stage.

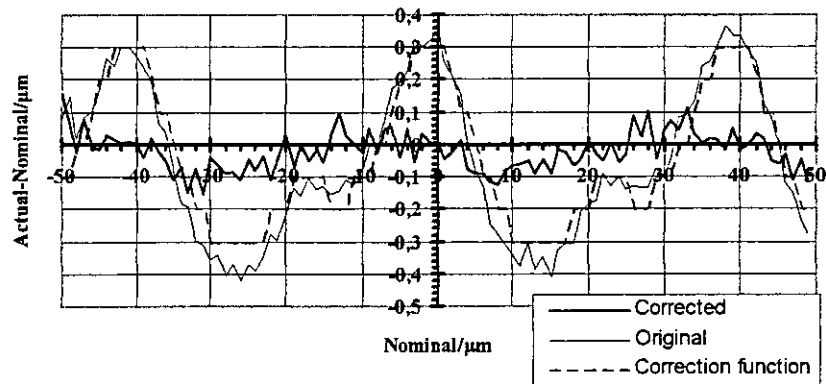


Fig. 42: Minimised error curve

Figure 42 shows the measured positioning of the axis, the calculated correction function and the the minimised error curve of the positioning system. It can be seen that the positioning error of the PM500 is reduced by one fourth of the initial value, that means from 800nm down to 200nm. The software for the error compensation is documented in Appendix E11.

4.2.3 Exposure programs

The exposure of microstructures requires the synchronisation of all actions of the LPG components. For this reason, the program modules which support the hardware components must be combined with the data of the desired structure. In order to avoid time and effort consuming system programming for each new structure, standard procedures for the program development are desired. For this reason, different procedures are compared and evaluated for different application cases.

4.2.3.1 Macro programming

For the description of the structure using macro programming, so called standard elements are defined. These elements will be combined in order to describe the total structure to be realised. The standard elements are designed as macros which are specified by parameters for the special application. The macros are saved in a batch file so that the total structure can be realised by the successive exposure of all macros in a batch file.

An enormous number of different macros are required for the realisation of most complex structures. But also with only a few flexible macros, several different structures can be realised. Figure 43 illustrates the macros for a frame and an annulus, whereas for different exposure strategies the macros are illustrated both for point to point - (PtP) and continuous path - (CP) procedure.

For the PtP - macros the structure is composed from discrete exposure points. For this reason not only geometry parameter, laser intensity, focal position, and exposure time but also point-to-point or spot distance must be stated.

For the CP - macros the exposure is done while the axes are moving. For this reason, not only geometry, focal position, intensity, and line distance but also velocity of the axes must be stated.

	PtP - Exposure	Geometry parameter	CP - Exposure
Frame		<p>A: Outer horizontal frame length a: Inner horizontal frame length B: Outer vertical frame length b: Inner vertical frame length x,y: Center position φ: Orientation</p>	
Annulus		<p>D: Outer diameter d: Inner diameter x, y: Center coordinate</p>	
Exposure parameter	<p>Spot distance Intensity Exposure time Focus position</p>		<p>Line distance Velocity Focus position Intensity</p>

Fig. 43: Definition of macros for annulus and frame

From these two basic elements, a large number of other elements can be derived considering different special cases. The frame can be modified to a rectangle by omitting the inner boundaries ($a=b=0$). Introducing the extension of only one dot (PtP- procedure) or one dash (CP-procedure) in one dimension, the element can be modified to a line and introducing the extension of only one pixel or one line in both dimensions the element can be modified to a dot. By omitting the inner boundary ($d=0$) the annulus can be modified to a disc. An annulus with inner and outer boundary being of the same diameter is modified to a circle with a line width of one dot or one line. Reducing the radius of inner and outer boundaries to zero the annulus will be modified to a dot.

For all macros, a homogenous exposure over the total surface of the element is required, which means for both procedures, PtP and CP, special precautions have to be taken.

Considering the PtP procedure, it is improbable that the length 'l' of a straight line or an annulus is an integral number of the required dot distance, so that the first and last point of exposure coincident with the beginning and ending of the line and the annulus will indicate a transient error at the joint (see figure 44).

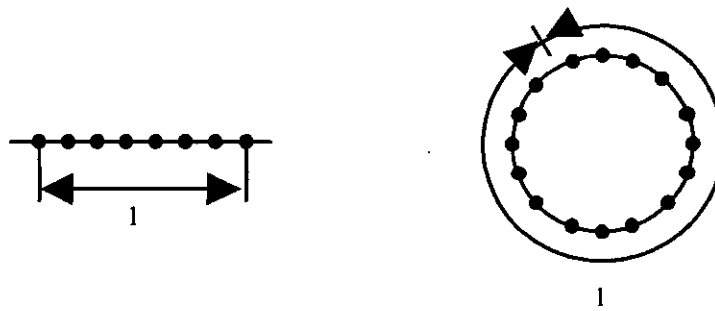


Fig. 44: Line and annulus using the PtP - procedures

Therefore, all exposure points must be distributed on a line in that way, that for a defined dot distance the transient error or starting and ending error is as small as possible. Therefore, the distance of the first exposure position to the beginning of the line is calculated using equation (13):

$$A_p = (1 - P_Z \cdot P_A) / 2 \quad (13)$$

The distance between the last exposure point and beginning of the line is calculated using equation (14):

$$E_p = A_p + P_Z \cdot P_A \quad (14)$$

The number of dot is defined by equation (15):

$$P_Z = (1 / P_A) \text{ DIV } 1 \quad (15)$$

with:

- l : length of the line or circle
- P_A : dot distance
- P_Z : number of dots
- A_p : position of the starting dot
- E_p : position of the final dot

Normally, this results in a shortening of the line length or a gap for an annulus structure, however the dot distance is steady throughout the total structure with exactly the prescribed value which has advantages for the determination of the exposure parameter. Other transient

procedures can settle above errors, however the dot distance will change and result in changing exposure results.

Operating with CP exposure, it is very important not to start the exposure before the axis has reached the required exposure velocity. For this reason, the DAI and the DAI unit were introduced. They can switch on the laser when the acceleration phase is finished and switch off the laser before the deceleration phase starts. In this case, the axis needs a time lead and time-lag which depends on the required velocity, acceleration and deceleration. This additional distance is already included in figure 45 illustrating the vt-diagram with the laser switching points.

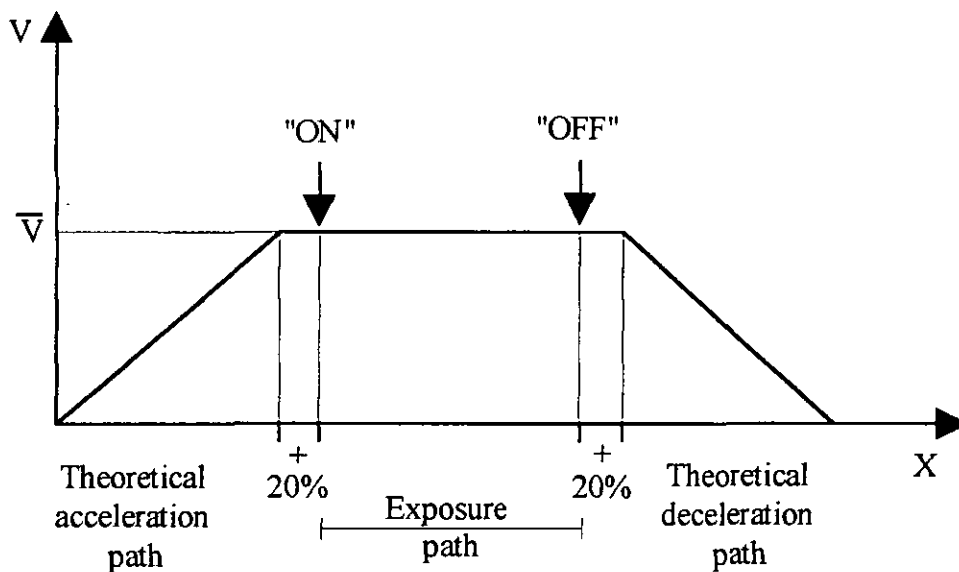


Fig. 45: vt-diagram of the CP - procedure

The theoretically determined time lead and time-lag is increased by a safety margin of 20% and is also added to the exposure distance. By this it will be ensured that acceleration and deceleration phase are faded out so that a homogenous exposure takes place during the movement of the axis.

The position of the macros is described by absolute coordinates related to the zero position of the machine while the orientation of the macros is set by angle φ relative to the directions of the linear stages. The macros are layed down in a batch file and form the structure which will be approached and exposed one after the other. The movement within a macro is performed

by relative motion commands. Prior to the exposure of a frame, the substrate will be aligned by the rotation axis so that the frame boundaries are parallel with the axes of the positioning system. This results in more precise and efficient motions on the linear axes without any conversion. For the determination of the substrate rotation, figure 46 shows the position and the orientation of a frame on a substrate. The centre of the frame is described by the coordinates x and y . The necessary rotation of the object, which is required for the alignment of the substrate corresponds to the angle α .

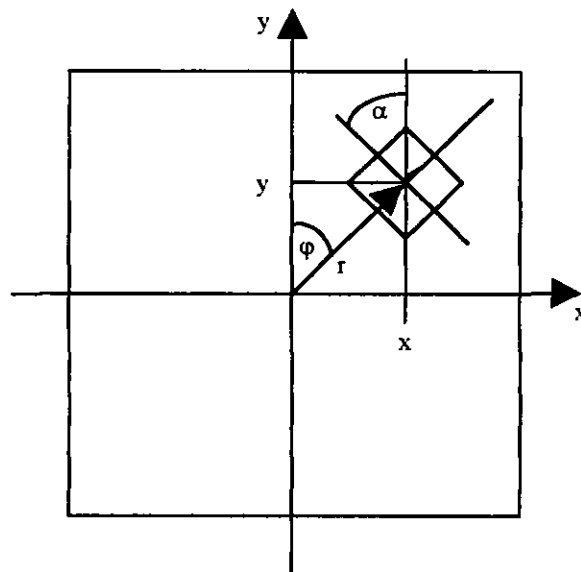


Fig. 46: Position and orientation of the structure

Using the PtP procedure, the exposure of a frame is done on a meandering path in course of which, and for efficiency reasons, only points are approached which will be exposed. The circle motion is done for highest precision combining motions of the linear axis. The axes are controlled by standard parameters.

Exposing a frame with the CP procedure also requires motion in a meandering path, while the circle motion for the exposure of an annulus must be executed by the rotation axis.

4.2.3.2 Pixel programming

Pixel programming describes the total structure by means of an $n \times m$ matrix in which each discrete element contains the required process parameters. With decreasing size of the elements, the ideal structure is approached with higher accuracy, but time expenditure for realisation increases.

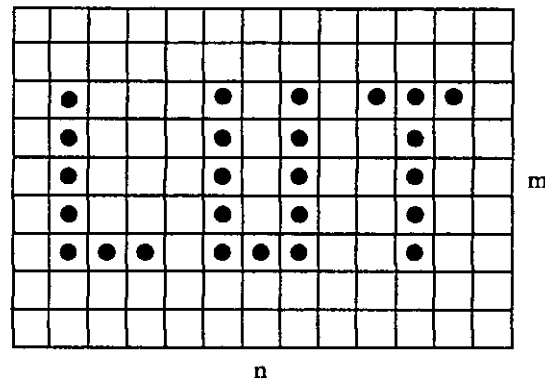


Fig. 47: Matrix for pixel programming of a structure

The simplest case is of binary nature. In this case, the value of a matrix element indicates whether it will be exposed or not (see figure 47). It is also possible to assign each discrete element its own focal position, intensity and exposure time. But this will result in increased data required to describe the structure. For this reason, as many global parameters as possible are introduced to describe all elements. All global parameter are stored in the header of a pixel file which can be the beginning part of the file. The dot distance of the individual exposures and the number of elements in different directions (dimension of the matrix) can also be stored in the header. The global parameters are followed by coded information describing the exposure.

For example, using a binary structure the element '1' indicates an exposure at this location while '0' indicates this location has to be omitted from an exposure. In this manner always eight elements which are next to each other can be assigned to be eight bits and combined to one byte the value of which is described in decimals. The value 255 indicates that all eight elements have to be exposed. These blocks will be combined to one line and in turn lines will make up the total structure. Also in this case the most efficient exposure is done in a meandering shape and only the elements to be exposed are approached.

4.2.3.3 Program generation

As illustrated in figure 48, the generation of exposure programs using macro - or pixel programming can be done by either using an editor or a CAD system.

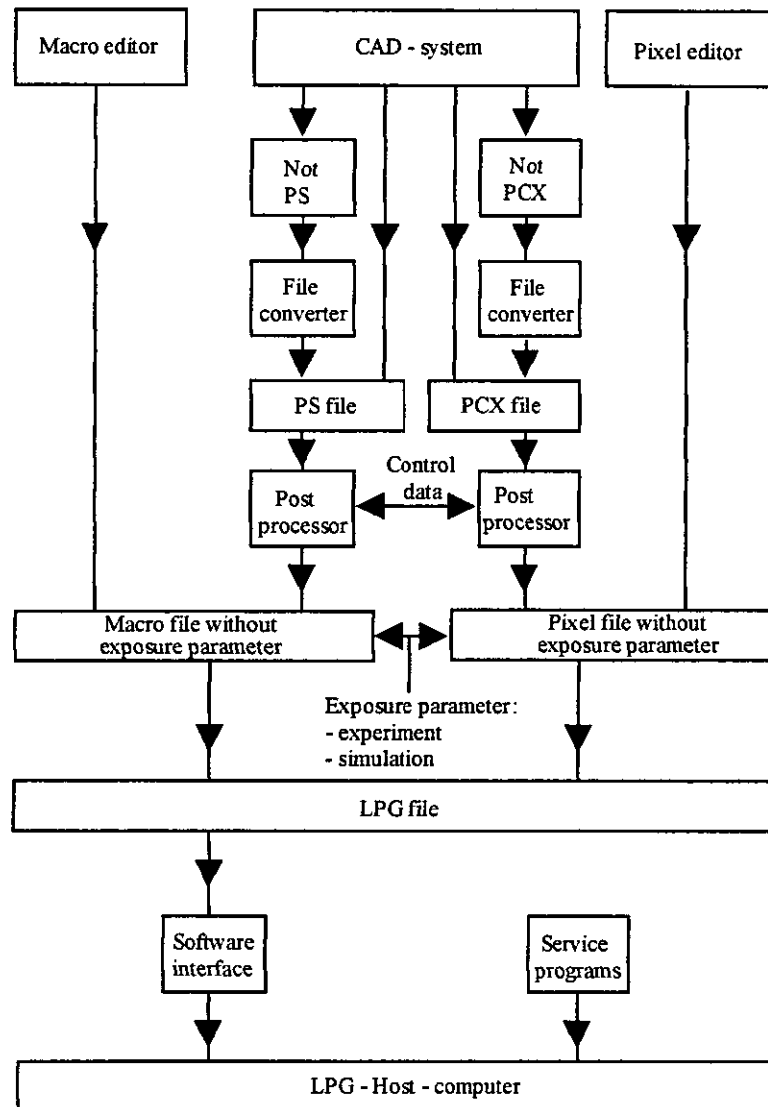


Fig. 48: Software concept for exposure programs

An editor can be used to establish an exposure file in accordance with the predefinitions of chapters 4.2.3.1 and 4.2.3.2. The generated file will be complemented with the exposure parameters determined by experiments or simulations. The executable LPG file can be downloaded to the LPG through a software interface.

For the CAD design of the macro structures, the vector orientated postscript (PS) format suggests itself for use as the optimum output format of the CAD system, while pixel structures can better be described using the pixel oriented PCX format. In case these formats are not the output format of the CAD-system, a file converter must convert the CAD output files into the desired file format. Finally the available postscript or PCX file is converted into a macro - or pixel file by a post processor. The post processor translates the original file into the format required by the LPG. The conversion will be specified by the following control data:

- Which CAD output file shall be converted
- Which format shall be assigned to the file
- Which corrections the files are subject to (filter setting)
- Which procedure (PtP or CP) will be used to generate the macro file
- Which dot - or line distance shall be implemented

By combining these files and the exposure parameter, an executeable LPG file is available which can also be downloaded to the LPG using the software interface and is combined with other LPG modules in order to assist the LPG hardware in process control and process monitoring. Prior to exposure, utility programs will assist in setting up the hardware of the LPG.

4.2.3.4 Realisation of a programming system

If a new design of different microstructures is often required the relatively high effort in developing a CAD design system is reasonable, but programming with an editor is also a reliable tool, although an extensive familiarisation time is needed because of the abstract representation mode. In this study, an editor is put into practice for macro programming of annuluses using the PtP procedure, which permits the generation of numerous rotationally symmetric structures. The software for the exposure is documented in Appendix E12.

4.3 Characteristics of the LPG

The described LPG components have been separately designed, constructed, tested and optimised and then matched to each other for the total system. This ensures the correct interaction of all components. The examination of the structuring characteristics was realised by exposing a photoresist layer which afterwards was developed and photographed through a microscope.

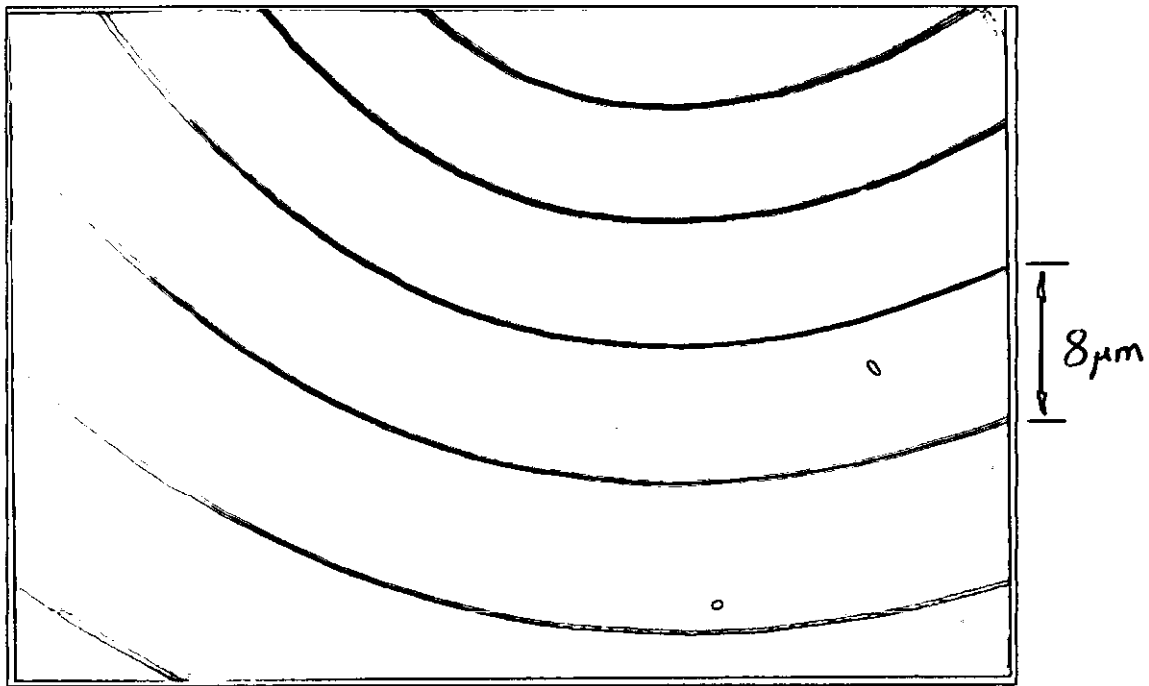


Fig. 49: Structuring result of the LPG

Figure 49 illustrates a section of a ring structure which was generated with the LPG. The exposure was performed during the substrate rotation by means of the rotation axis. The result can be reproduced and the structure evaluation proves the minimal structure width of $0.5\mu\text{m}$. The lines have a separation of $8\mu\text{m}$.

The assessment of the price-performance payoff shall in this place be accomplished by estimating the total costs of the LPG and which results in summing up the costs of every system component and neglecting the development time.

Number	Description	Price/1000Pounds
2	Interferometer	14.0
1	AOM	6.0
1	Positioning system	52.0
1	Autofocus sensor	1.3
1	Host computer	1.0
1	DAQ card	0.6
1	PIO card	0.1
1	Counter card	0.1
1	Control unit	0.7
1	He-Cd laser	14.0
	Total price	89.8

The total price is in the range of commercial electron beam writers. However the LPG is no low cost development, but for experimental purposes, incorporating as many degrees of freedom and system options as possible. Further development will result in system changes which will reduce the price very drastically (see discussion).

The technical realisation of the LPG is illustrated in Appendix F.

5 STRATEGIES OF LPG OPERATION

The positioning system and the beam system of the LPG both influence the exposure duration and, therefore, the efficiency of the structuring so that they are investigated in this chapter. Due to the serial structuring process, the exposure duration can extend to hours so it is subject of this investigation to find some selection rules for strategies of operations for this systems used in a specific application.

5.1 Influence of the positioning system

The positioning system moves the substrate, which is subject to exposure beneath the focused laser beam. The travelling range of the stage influences the maximum size of the object while the accuracy of the position unit essentially influences the structure accuracy of the resulting exposure. Besides these static parameters, the dynamic parameters velocity, acceleration, and deceleration are of crucial importance for exposure duration, or better, the efficiency of the exposure. The movements for an exposure shall be kept as short as possible and shall be as small as possible, however all movements also shall be as fast as possible in order to obtain a short exposure duration.

5.1.1 Positioning method for the substrate

For the beam exposures at relatively short exposure durations, two different strategies can be followed:

- Raster scanning method
- Vector scanning method

Using raster scanning method sketched in figure 41a), a controlled guidance on the total surface of the substrate beneath the laser beam takes place. The laser beam is switched on at the positions to be exposed and remains switched off at all other positions. The vector scanning method sketched in figure 41b) utilises the fact that in most structures large parts of the surface are not to be exposed. Instead of moving the total surface beneath the laser only the areas to be exposed are selected. Naturally, the laser beam remains switched off while jumping from one area to the next.

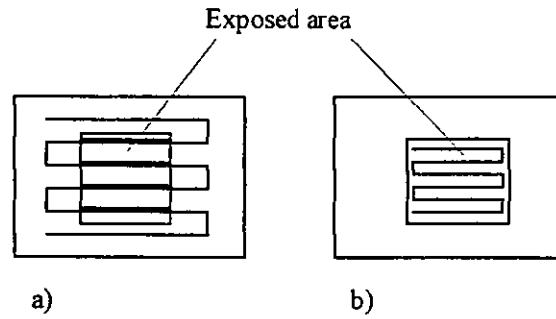


Fig. 50: Raster - and vector scanning methods

For time saving reasons, both methods use meandering motion while executing PtP - or CP - exposure. The disadvantage of PtP - exposure is long processing times due to necessary acceleration and deceleration manoeuvres for each discrete exposure dot, while the advantage emerges from the fact that there are no special requirements on motion accuracy aspects (acceleration, slow down, velocity), but positioning accuracy and keeping the exact position during exposure duration has a large impact. The CP - exposure not only sets requirements on the positioning accuracy of the system but also on the motion parameters which is a fact of the influence of these parameters on the exposure result. In order to obtain a reproducible exposure result the precise control of these parameters is required. Considering the deceleration and acceleration phase, the process control is of relatively high effort. Therefore, and to stay within the range of practical operations, exposures are of practical relevance during motions with constant velocity. Moving along the linear axis or the circle motion of only one axis is required, but in doing this deviating structures have to be treated using interpolation methods which normally will create a relatively high programming and controlling effort.

5.1.2 Pulse density modulation

In order to generate a special profile at a selected position of the substrate, the exposure using the PtP or CP procedure are combined. Also influencing the structure by the distance of the individual exposure dots (PtP procedure) or exposure lines (CP procedure) has also a crucial influence to the processing time. In case of a steady removal over a large surface range larger exposure spots can minimise the number of substrate movements. Therefore, when working with optimised beam geometry, the required structure has to be obtained in selecting the greatest distance possible between dots or lines.

5.2 Influence of the beam system

The Gaussian laser beam is used for exposure, where the exposure result is caused by the geometry of the beam and focal position in relation to the resist surface. Different combinations of exposures with variations of these parameters may result in equal structures, that the influence of the beam on the efficiency of the exposure needs to be examined.

5.2.1 Shape and position of the Gaussian beam

For the correct manufacture of the structure, the focus point has to be much smaller than the smallest structure. Considering structures of larger sizes, a focal position which is above or below the resist surface might be useful. In doing this, an exposure with a larger beam cross-section can be achieved which results in less exposure steps considering the same area.

5.2.2 Pulse width modulation

The diameter and the penetration depth of a Gaussian beam into the photo resist is determined by the product of intensity and exposure duration (pulse width). Large pulse widths can combine separately located exposure dots to a resulting total structure. In the PtP procedure, the exposure duration is the switch on time of the laser while in the CP procedure, the velocity of the substrate motion is the influencing factor. To be efficient, the exposure duration should be kept as short as possible which results in a pulse width adjustment mainly controlled by the intensity.

5.3 Procedure for an efficient exposure

In order to reach a flexible and efficient exposure of universal microstructures, all geometric data of the required structure must be transferred into the previously mentioned process parameters of the system and transmitted to the LPG. All parameters have been introduced and discussed and now some practical selection rules for combinations to be implemented into special applications as suitable as possible shall be illustrated.

If possible very complex geometries should be represented by a combination of macros (see chapter 3.2.3.1) and which should be combined using a vector scanning method. Large quantities of objects should be exposed in accordance with the CP procedure resulting in an exposure duration which is as short as possible. The increased effort in process controls is caused by monitoring dynamic motion parameters and taking into account the deceleration - and acceleration response. Smaller quantities should be accomplished in using a more simplified control in accordance with the PtP procedure. There should be no difference if a macro editor or a graphic programming system is used to develop the program.

Line and dot distance depends on the focal geometry and focal position. Selecting the line and dot distance as large as possible results in a decrease of exposure steps and in turn increases the efficiency. The set up of the other required exposure parameters:

- Focal position
- Exposure

must be matched for a desired profile. In order to minimise the experimental effort a computer simulation for LPG structuring was developed (see next chapter). For the theoretical parameter determination the efficiency criteria must also be taken into account.

If the required structures cannot be realised by combining objects, the structure must be described using pixel format. Also, the exposure parameter for this method shall be found by assistance of the simulation model.

6 DETERMINATION OF PROCESS PARAMETERS FOR THE LPG

In determining the process parameters for LPG microstructuring, all variables influencing the structuring result have to be investigated. The exposure and development result of the Gaussian beam structuring will be investigated in detail using a computer simulation.

6.1 Resist structuring

The resist is applied to the substrate and exposed to laser radiation in order to change the layer characteristics. Afterwards the processed resist is removed in a chemical process. All process steps [Step82][Bart77][Gamb91][Lens92a][Scha81b] which are applied to the resist will be described in the following paragraphs and also the physical mechanism of exposure and development will be theoretically examined.

6.1.1 Types of resist

Organic and inorganic resist types have been developed. All of these developments consist of four basic components, which are: resin, which is the layer building part, a light sensitive component, which absorbs radiation and by this modifies the reaction against the solubility of the lacquer. Supplements which stabilise certain variables of the lacquer and a solvent which keeps the other components liquid while in storage and during the process of coating.

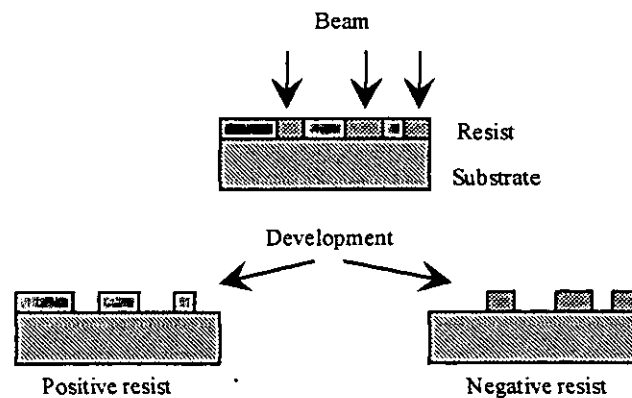


Fig. 51: Positive and negative resist

One has to distinguish between two different types of resist: positive and negative resist (see figure 51). The illuminated areas of a positive resist will be removed in the developing solvent whereas in case of a negative resist, the unexposed areas will be removed. One benefits from a positive resist where only small resist areas must be removed, i.e. a high covering ratio is required.

The different resists vary in operational use with respect to their sensitivity and resolution, which means the selection of the correct resist depends on the special application, the beam source in use, and the required resolution.

6.1.2 Process steps

The coating of lacquer is a physical process which transfers solid constituents of lacquer which is dissolved in a solvent into a coat due to the evaporation effect of the solvent. This coating takes place prior to exposure and development and is of very great importance to the reproducibility of the processing result. For this reason also this process will be described in detail and together with all the other process steps.

Pretreatments of the substrate

The pretreatment is a necessary process prior to coating and covers preparation of the surface to receive the lacquer which means the surface has to be planar, clean and of excellent binding potential for the resist. Degreasing and tempering - drying of the substrate with temperatures above 100°C - are parts of the pretreatment and if necessary to put on an adhesive flat coat.

Coating of lacquer

The spin coating results in a uniformly thick resist layer over the total surface of the substrate. A centrifuge spins the substrate and the resulting centrifugal force will spin-dry the redundant lacquer from the border of the substrate. The thickness of the lacquer is essentially a function of the angular velocity, the amount of lacquer, and its viscosity. Another method of coating is to spray on the resist using air or nitrogen pressure.

Tempering of the lacquer

Tempering of the lacquer is a heat treatment of the coating. In order to improve certain coat - and boundary surface characteristics and the reproducibility of the total lithographic process. The treatment normally will be done before exposure.

Exposure

Considering positive resist, the radiant exposure will destroy the homogeneous structure of complex systems of molecular chains. In case of a negative resist, single molecules which are not coupled to each other are forced to build complex structures.

Development

Contrary to the meaning of this concept in photography, developing of lacquer coating means removing certain areas in order to obtain the desired structure.

Batch process

This is to be understood every physical and chemical process which is addressed to the total surface of the substrate but delivers varying results which depend from the local thickness of the resist.

Stripping

After having finished all operations, physical or chemical stripping methods will remove all remaining resist structures.

The generation of complex systems uses multi-layer constructions which repeatedly run through each of the above mentioned sequence of operations until all layers are structured.

6.1.3 Mechanism of resist structuring

The characteristics of the photo resist will be described by changes of thickness of the resist Δd resulting from an exposure with an exposure E :

$$\Delta d = f (E) \quad (16)$$

Earlier studies [Bart77] have proven, the removal can be described approximately by the following equation:

$$\Delta d \approx \Delta r T \alpha_0 E + r_2 T \quad (17)$$

with:

Δd	: Changes of resist thickness
$\Delta r = r_1 - r_2$: Difference of etching rates between exposed and unexposed molecules
r_1	: Etching rate of exposed molecules
r_2	: Etching rate of unexposed molecules
T	: Development duration
α_0	: Exposure constant for positive resist
$E = I \cdot t$: Exposure (Intensity • time)

Changes in the dissolving velocity of the lacquer due to exposure is proportional to the intensity I and the exposure duration t . Consequently, the reciprocity theorem is valid which means, a lower beam intensity can be compensated by introducing longer exposure duration and vice versa.

The exposure of the resist coating varies in different areas. The etching process affects the total surface of the resist profile constantly. Considering positive resist, unexposed areas will be removed more slowly than exposed areas, which means different development duration (etching duration) will result in different profiles.

6.1.4 Shape and position of the Gaussian beam

The intensity distribution over the cross-section of a Gaussian profile is determined by equation (18) [Eich91].

$$I_r = I_0 e^{-2\frac{r^2}{w^2}} = \frac{2P}{\pi w^2} e^{-2\frac{r^2}{w^2}} \quad (18)$$

with:

I_r	: Intensity at radius r
I_0	: Output intensity
P	: Power
w	: Gaussian beam radius
r	: Radius

A cross-section of the profile is illustrated in figure 52.

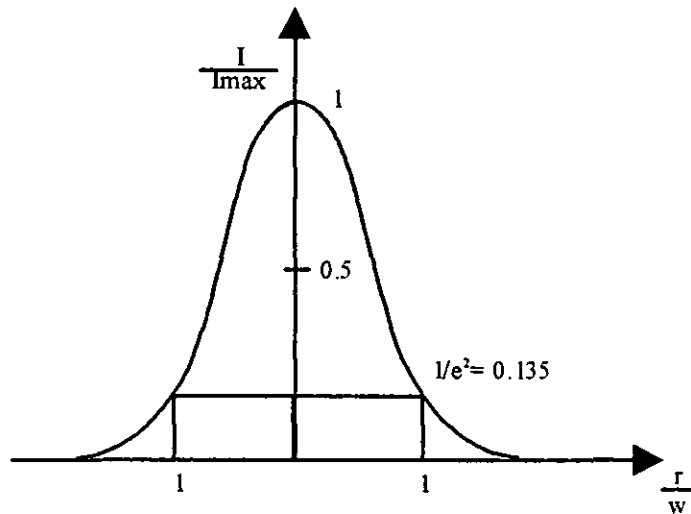


Fig. 52: Cross-section of a Gaussian beam

In case of a Gaussian beam, the diameter value is arbitrary because there are no borders. In order to define a beam parameter, the range where the intensity has been reduced to $1/e^2$ of the output intensity is considered to be the diameter (see chapter 3.1.1.1). The diameter of the beam as a function of the coordinate in the direction of beam propagation is described by equation (19) [Eich91].

$$w_{(z)}^2 = w_0^2 \left[1 + \left(\frac{\lambda z}{\pi w_0^2} \right)^2 \right] \quad (19)$$

with:

- $w_{(z)}$: Diameter of Gaussian beam in depth z
- w_0 : Minimum diameter
- λ : Wavelength of laser
- z : Coordinate in direction of propagation

Because of the relatively small focal spot w_0 , it was necessary to develop a focal position controlled processing head. It is therefore possible to control the focus point precisely to different focal positions during the exposure.

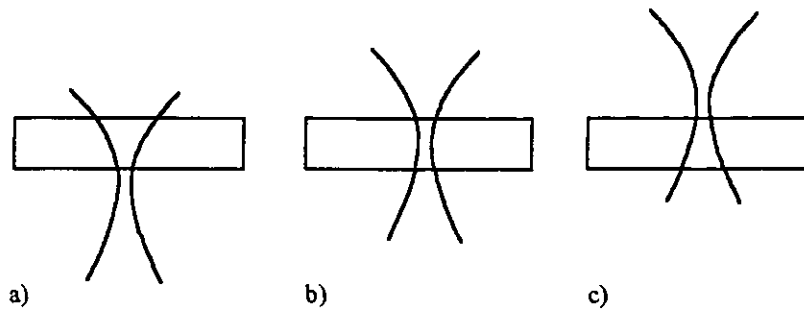


Fig. 53: Focal positions relatively located to the resist layer

Different focal positions not only permit an exposure with various beam diameters but also varying beam propagation within the resist. The exposures illustrated in figure 53 result from this fact. In case 53a the focal position is above the resist and results in a convergent wave front and in case 53c to a divergent wave front which is caused by a focal position beneath the resist. In case 53b, the focal position lies within the resist which results in both a convergent and a divergent wave front in the resist.

6.2 Simulation

In order to minimise the experimental effort in determining all process parameters for the LPG exposure, a simulation program was developed to determine the result of the resist exposure and resist development and to illustrate the results on the screen of the computer. With the assistance of the simulation, the producibility of a special structure can be demonstrated and all necessary parameter can be determined.

6.2.1 Principle of simulation

The simulation illustrates the results of all structuring process steps independent of whether PtP exposures of discrete dots or CP exposures of exposure lines. The individual exposures will be described by:

- Location
- Beam intensity
- Relative focal position
- Focal spot diameter
- Wavelength

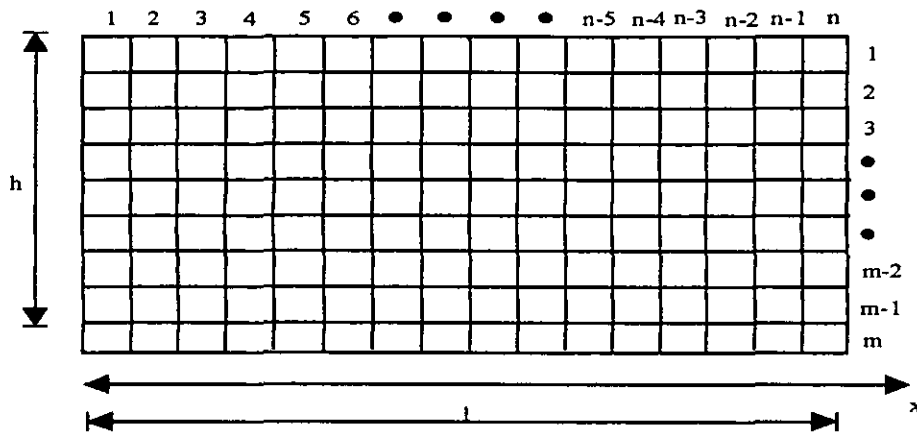


Fig. 54: Resist layer transferred to a matrix of $n \times m$ elements

The first step in simulation is the calculation of the exposure in a matrix of $n \cdot m$ elements which represents the resist layer and which is illustrated in figure 54. In each of the elements of the matrix, the beam intensity is summed up for all single exposures. The beam propagation is calculated in accordance with equation (19) and the intensity is determined by equation (18). Thereby it is assumed only a small portion of the incoming beam is absorbed by the resist and the total intensity remains constant while passing through the resist.

The second step in simulation calculates the resist structuring following equation (17) which will be rearranged to write $T = f(E, \alpha_0, r_1, r_2, \Delta d)$. This permits determination of the time for each individual matrix element after which this surface element has been removed. Because α_0 , r_1 , r_2 and Δd are constant, the time T only depends on the exposure E . Adding the times of all elements laying on top of the one under consideration, one will find the time needed to remove this element from the resist.

6.2.2 Simulation program *LASSI*

Working with the simulation program *LASSI* (*L*aser *S*tructuring *S*imulation) starts with the input of all exposure parameters. With the assistance of an editor, a table with all parameters for all required exposures will be generated. The first line will consist of global parameters like wavelength and focal spot diameter introduced in μm . Each following line describes a specific exposure by the following parameters:

location; focal position; exposure

Location: Entered in μm and representing the distance from a starting point arbitrarily selected. Only positive values are allowed for this value because the first exposure point is set to the left side of the simulation matrix and all further exposures proceed to the right side.

Focal position: Also entered in μm . It represents the distance of the focal position relative to the resist surface. Negative values represent a focal position above the resist surface and positive values represent a focal position beneath the resist surface.

Exposure: The exposure is entered in mJ. In the cases of both PtP and CP exposure the value represents the influence of the intensity; provided that, considering the PtP exposure the exposure time is constant, and considering the CP exposure the substrate motion is of constant velocity.

This file describing the exposure in this manner is downloaded into the simulation program which calculates exposure for the individual matrix elements and illustrates the result on the screen represented by varying blue colours which will deliver an impression of the exposure distribution over the total resist.

In the second simulation step, the structure is being developed. This will be realised by transferring the exposure matrix and introducing all development constants. Using the program parameter r_1/r_2 (see equation 17) it is possible to simulate both positive and negative resist.

The software is documented in Appendix G.

6.2.3 Simulation of selected structures

In order to demonstrate the flexibility in profile generation using laser lithography and to demonstrate the usability of *LASSI* all binary, multi-level, and continuous profiles are simulated.

Figure 55 illustrates the cross-section of a rotational-symmetric structure which is used in various applications. In microoptic the structure can have the function of a lens, in micromechanics the function of a membrane, or in microelectronics the function of a capacitor. The left profile border lies in the centre of the structure illustrating the profile as a function of the radius.

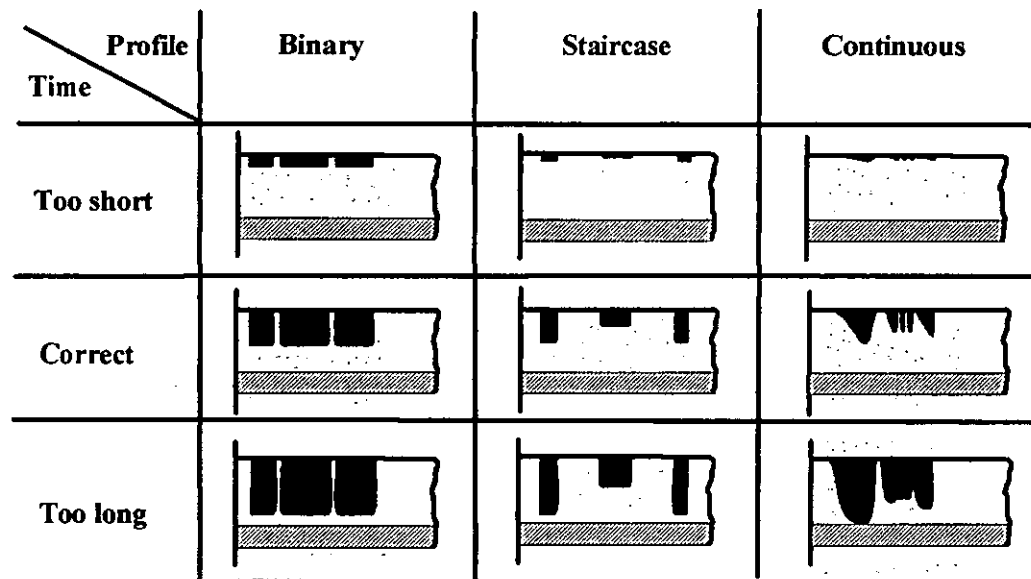


Fig. 55: Simulation series of various profiles

The left column illustrates the simulation of a binary profile. Starting from the top and going down, the exposure time is increasing while the illumination conditions stay constant. While in the upper and lower part of the figure the structure is not or too much pronounced which corresponds to a development time that is too short or too long. The profile in the centre of the figure corresponds to the required profile. The columns in the centre and to the right illustrates the same behaviour for a multi-level and a continuous structure. For all structures the number of required exposures was minimised by adaptation of all remaining parameters.

6.3 Use of simulation results

With the assistance of simulation, the producibility in principle of a structure using serial laser lithography can be determined. Because the process parameters are affected by different influences caused by parameter fluctuations like, for instance, ageing of the resist, it is difficult to determine their exact process parameter values. However one can find starting values of high quality which can be used to start LPG exposure and can be optimised by experimental means, thus simulation reduces the effort.

The exposure of a required structure can be achieved by more than one solution, so it is necessary to select a solution which on the one hand permits an exposure as fast as possible in order to stay reasonably priced and which on the other hand will result in stable results and high reproducibility although parameters are fluctuating slightly.

7 Realisation of selected microstructures

With the help of selected microstructures, flexible structuring of the serial laser lithography using the LPG will be demonstrated in this chapter.

The realisation starts with the preparation of the required substrates. 2" x 2" planar substrates from Struers were selected to be the substrate. The glasses were put into a beaker which was filled with acetone and cleaned in an ultrasonic bath for 1 minute. After rinsing with distilled water, the glasses were dried for about 2 hours in a special ultra cleaning oven at a temperature of 105°C. Next the glasses were transferred into a yellow light laboratory and coated with a resist layer having a thickness of about 1.7µm to 1.9µm. Using a resist spinner at a rotational speed of 3000 revolutions per minute and 20ml of photo resist of type Shipley S1818 ensured a layer of almost constant thickness. Prior to usage, the coated substrates were dried thoroughly for about 40 minutes at a temperature of 65°C and afterwards cooled carefully. As known from personal experience the substrate can be stored at room temperature and light-tight for about one week without adverse effect.

The exposure programs were developed with the help of the macro editor. The annuli were realised using the PtP procedure. Starting values are exposure parameters for a binary, multi-level, and continuous annulus structure which were determined with the help of simulation and optimised by changing pulse width by laser intensity variation and development duration. With all exposures, the focal position was directly located at the surface of the resist. The development was established at a temperature of 22°C and using developer Shipley Microposit 303 which was mixed with distilled water in a ratio of 1:9.

7.1 Binary

Figure 56 illustrates the cross section of the expected and figure 57 a photo of the generated binary microstructure. In all exposures the intensity was kept at steady value which results in a closed and evenly removed ring structure with an outer diameter of 200µm.

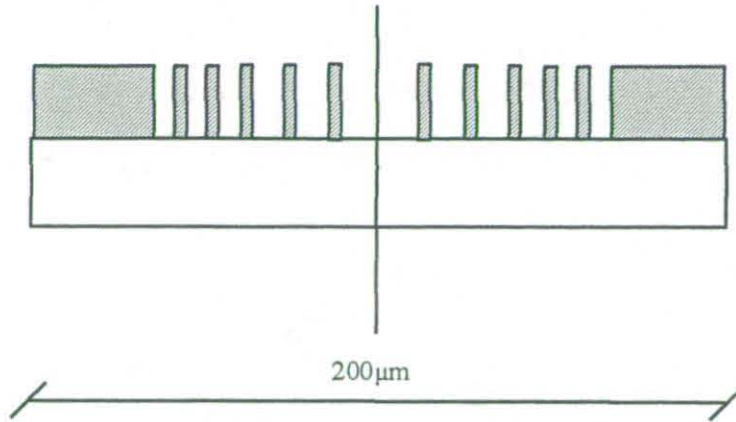


Fig:56: Cross section of the expected binary microstructure



Fig. 57: Binary microstructure

7.2 Multi-level

Figure 58 shows the cross section of the expected multi level structure. The multi-level structure of figure 59 was generated by selecting different intensities for zones located at different depths. Besides the total exposure of two zones, a level in between was also exposed which results in a three-level profile with an outer diameter of 200 μm.

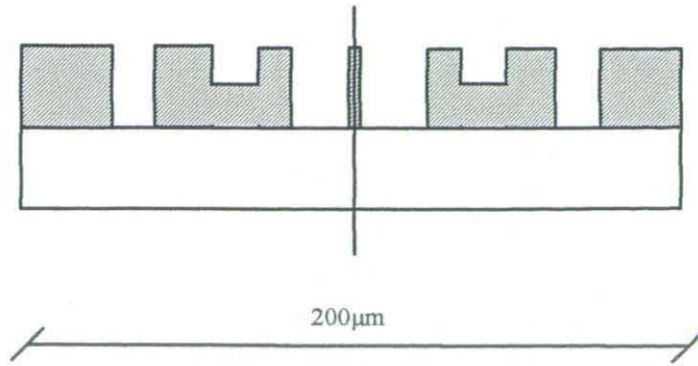


Fig. 58: Cross section of the expected multi level microstructure

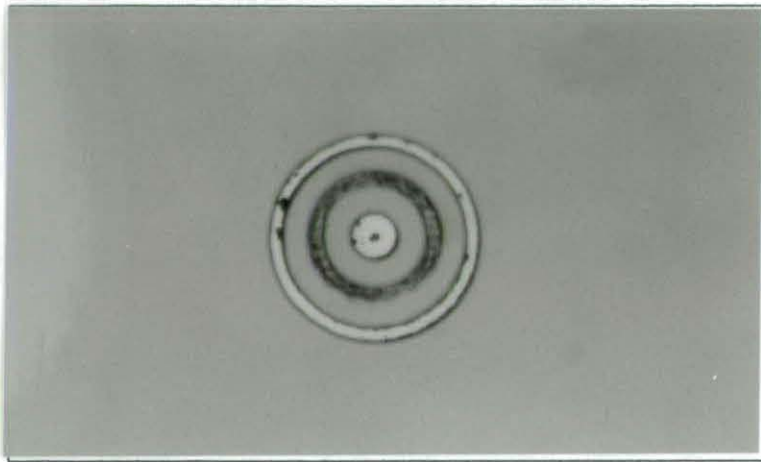


Fig. 59: Multi-level microstructure

7.3 Continuous

Figure 60 illustrates the expected cross section and figure 61 a photo of the generated continuous structure which results from individual exposures with varying intensity; the intensity being a function of the radius. One can clearly see continuous profile and a diameter of 80 μm.

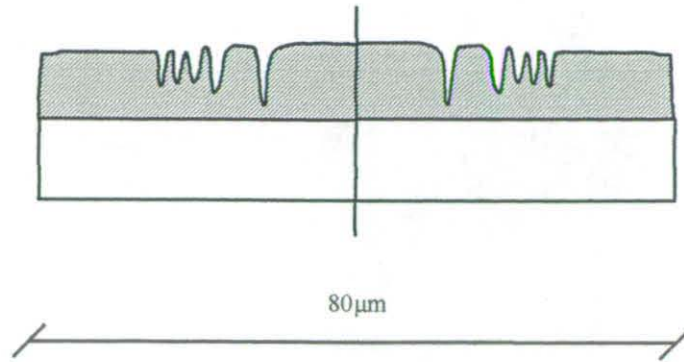


Fig. 60: Cross section of the expected continuous microstructure

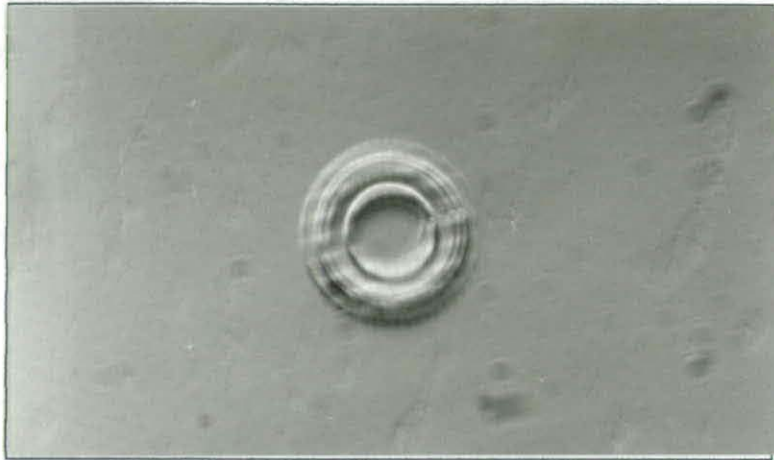


Fig. 61: Continuous microstructure

7.4 Additional microelements

The structures shown in figure 57,59 and 61 are realised by a movement of the linear axes during the exposure. These have the advantage that the concentric ring structure has a minimum distortion. The ring structure shown in figure 562 was realised by use of the rotary table. The lines have a width of $2\mu\text{m}$. It can be seen that the ring structure has a pronounced triangular distortion in the centre of the structure influenced by the radial runout of the rotary axis.

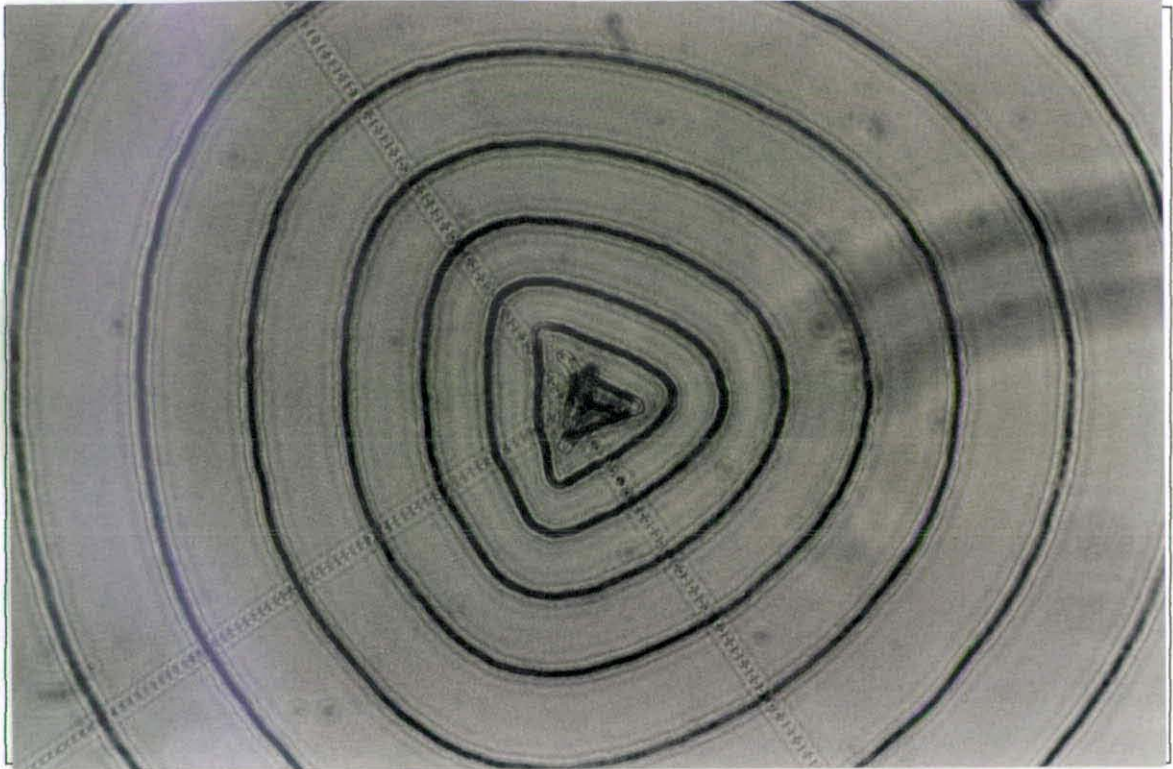


Fig. 62: Binary ring structure with distortion



Fig. 63: Continuous ring structure produced by post melting

The continuous profile ring structure shown in figure 63 has been realised by a post melting process where a binary ring structure was put into an oven.

Figure 64 shows the end of a glass fiber with a diameter of $200\mu\text{m}$. The end of the fiber was resist coated and the ring structure was achieved by transferring a previously generated ring structure to the fiber using a lens system.

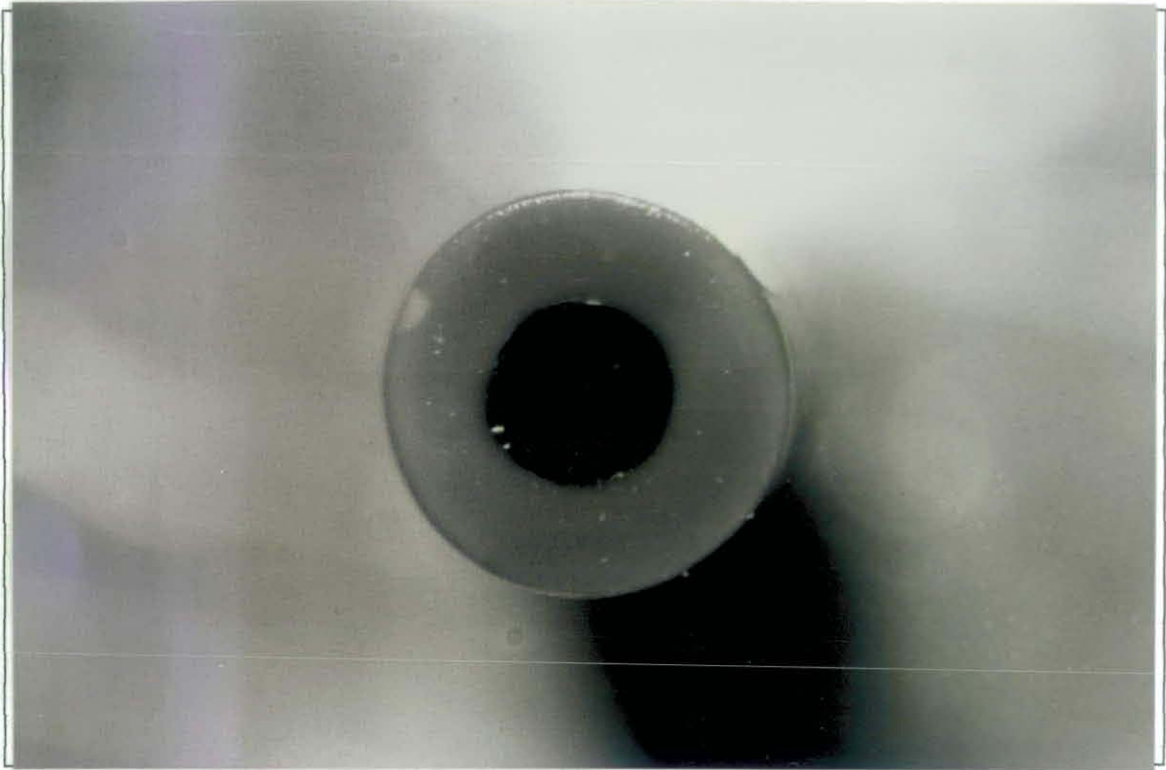


Fig. 64: Micro lens on the end of a fiber

Figure 65 and figure 66 show a segment of a line disk with $1\mu\text{m}$ wide lines. These lines represent a position information, so that this microstructure can be used as a position encoder.

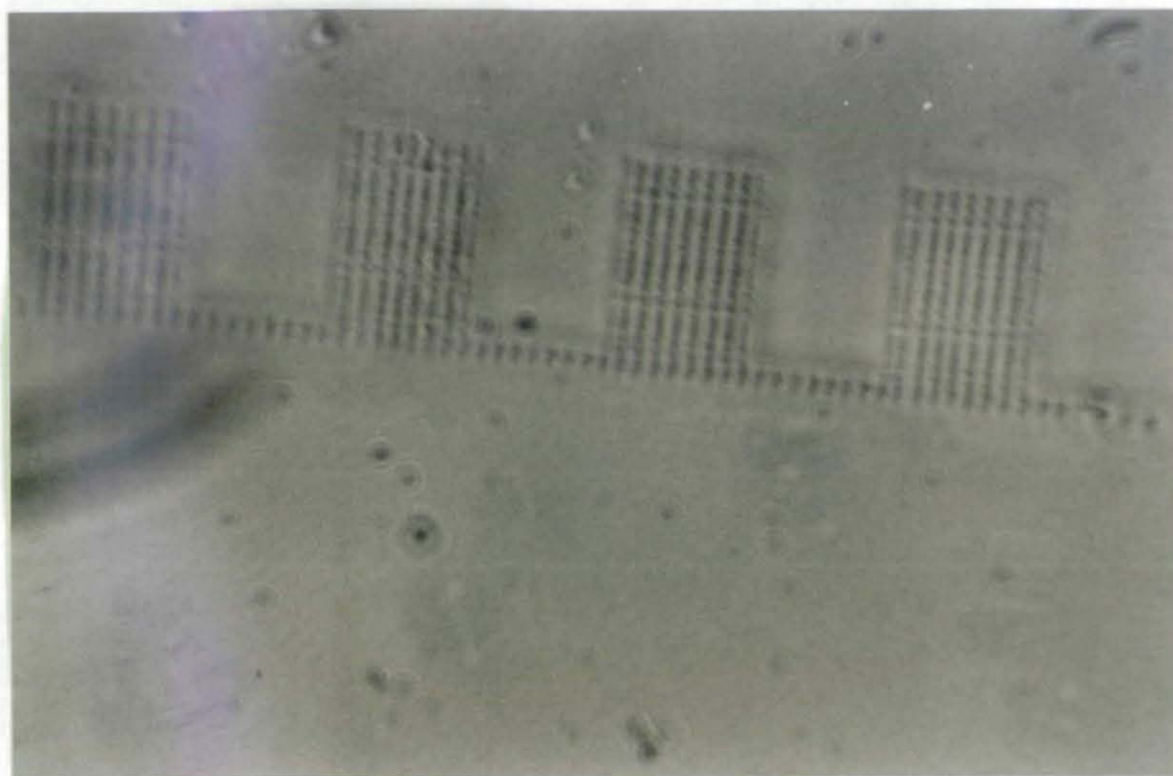


Fig. 65: Line disc (Overview)

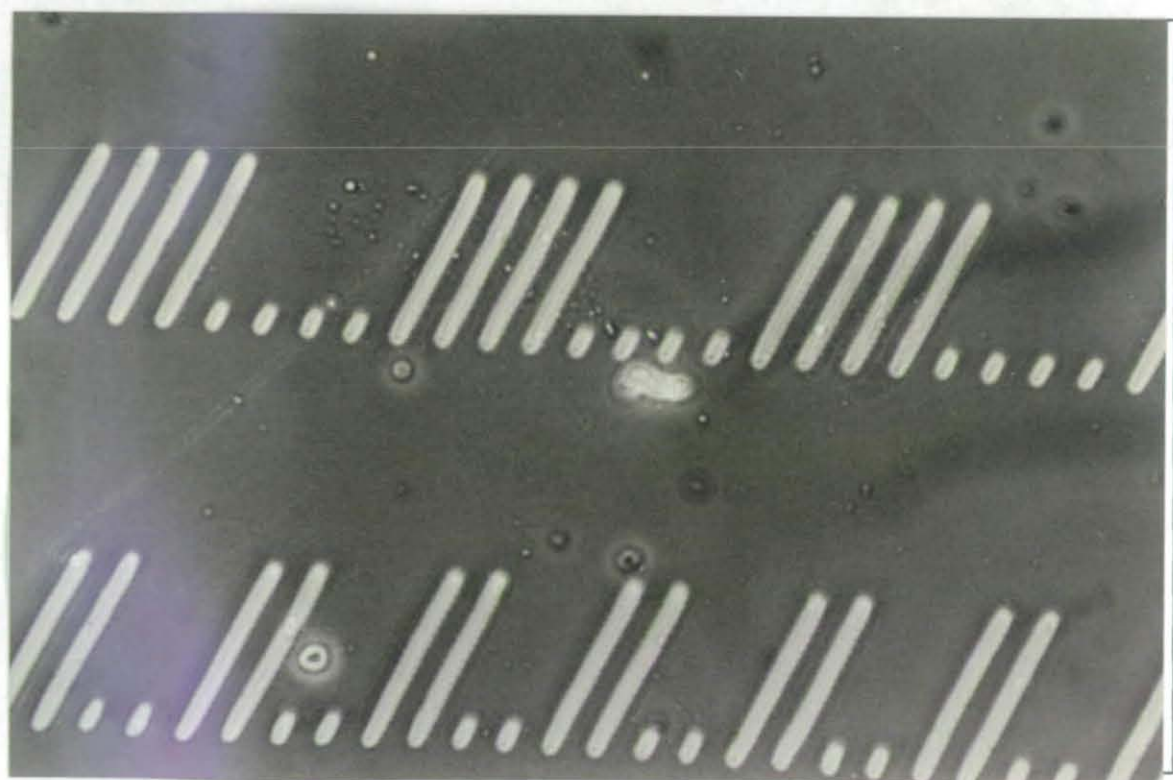


Fig. 66: Line disc (detail)

7.5 Results of the LPG microstructuring

After theoretical examinations of microstructuring using serial laser lithography, also the successful operation of the LPG in generating binary, multi-level, and continuous microstructures was demonstrated by several elements shown in this chapter. The determination of process parameters started using theoretically determined starting values, keeping the experimental effort directed to the optimisation of the parameters.

8 DISCUSSION

The beginning of a prototype generation or series production of microstructures starts with the generation of a resist structure which either is the required structure itself or an auxiliary element that can be transferred to this structure in a second process step by using different techniques. These elements are generated using resist structures that will be achieved using a serial writer. In comparing various production processes, the characteristics of all used serial writers were illustrated followed by the examination of serial resist structuring in later process steps. The results of these examinations clearly indicate, there are numerous applications in the area of micro structuring in the range of micrometres, but there are no structuring units used which are advantageously suitable in this field of application. The available structuring units like electron beam - or ion beam devices are over dimensioned and their acquisition costs are relatively high. This and in conjunction with the associated high process costs has complicated a broader acceptance. On the other hand, the units using laser lithography have been used on a casual basis because the efficiency of this production process was not high enough. However serial laser lithography has the potential to close this gap and for this reason a Laser Pattern Generator was developed in this study and a method of efficient microstructuring by means of serial laser lithography was introduced.

The Laser Pattern Generator was constructed without being optimised for a special application, but covering a wide range of operation and having a purpose of gaining experience in various applications and to monitor and change all process parameters. The beam path of the He-Cd laser was designed to cover a minimum focal spot in the range of $1\mu\text{m}$. The theoretical examination of the beam path proved the Rayleigh length $Z_R = 3.5\mu\text{m}$ which in term requires the development of a focal position controlled processing head. This system is the key component of the LPG development. The optimisation [Samu96a] and further operation [Samu95][Samu96b] [Samu96c] of this component was the subject of previous studies. The intensity of the exposure laser is controlled with the help of a second closed-loop control system which permits an accuracy of $\Delta P = \pm 200\mu\text{W}$. The AOM used in the environment has a broad bandwidth which results in a relatively high price. A semiconductor laser, meanwhile operating in the range of blue wavelengths would simplify the intensity control by simple current modulation and omitting the use of an AOM and in turn also omitting cooling and control circuits. This new laser also would contribute to a longer

lifetime and smaller dimensions of the LPG. The positioning of the substrate under the exposure laser is established by a support with two crossed linear axes and a rotational axis. With this support the positioning can be done in Cartesian as well as in polar coordinates which demonstrate particular advantages depending on the application. In order to reduce costs for most of the applications, one could omit a control range of this dimension. The monitoring of the axes using a laser interferometer with a resolution of 16.25nm cannot be avoided for the development of a prototype. Once the survey has been finished and the control errors in controlling the axes have been taken into consideration this feature can be omitted. The Direct Axis Interface (DAI) permits synchronisation between exposure and axis motion. In applications which are using PtP procedure also this option can also be omitted; however in other fields of application the option is irreplaceable which makes the question of its necessity in the system very much dependent on the special application of the LPG. The control unit and the host computer enable the set up and the process control of the LPG. The software is of modular type and the modules which are supporting the above mentioned hardware with the LPG can be combined to the LPG program for structuring. Five utility programs enable the monitoring of the individual components and the total installation. Special programming techniques (Labview or HPVEE) [Hels95] make the reproduction of functions of the control unit on the host computer possible. For all interfaces special drivers would have been mandatory. This would lead to a much higher information integration in a system and on the other hand would reduce the system price especially for future developments. The generation of exposure programs is performed by a macro editor which permits, with only a small number of macros, numerous different microstructures. Extending these macros with additional standard components would extend the operation field of the LPG. A programming as efficient as possible can only be reached by introducing a graphical programming platform. With a modified control program, the total LPG system cannot only be used for microstructuring, but also as a measurement and inspection system. In doing this, the positioning system moves the object under measurement beneath the autofocus sensor, while the distance to the surface will be measured and stored. Positioning the autofocus sensor over a wider range requires an extended control range and enabling the investigation of topologies of different objects.

In order to increase the efficiency of microstructuring using the LPG, various operational strategies have been developed. The differences in using raster scanning method or vector scanning method for exposure were discussed and the advantages of the more efficient vector scanning were outlined. The operation of the positioning system for the exposure of stationary substrate (PtP exposure) as well as the exposure of substrate in motion were discussed. Besides the process variables which are determined by the positioning also the influence of the focal position on the efficiency of the process was illustrated. As a rule, exposures should be done with distance between dots and lines which is as large as possible. This minimises time consuming substrate positioning. A focal position above or below the substrate will result in a larger spot diameter which in term reduces the number of individual exposures. In order to establish the required structuring the process variable intensity should be varied whereas, and this just for efficiency reasons, the intensity and not the duration should be influenced. Selection of the best substrate positioning in both methods raster scanning or vector scanning more or less depends on the required structure, whereas the vector scanning proves to be more efficient. Discussing the question of CP or PtP exposure one has to conclude, also this depends on the required structure. However the process of CP exposure should be faster than the process of PtP exposure. Whether a macro editor or a graphic editor is used, the programming effort is of the same magnitude.

In order to determine an optimal process control, the total manufacture process was split up into process steps and the most crucial process steps, which are resist exposure and resist development, were put into a computer simulation. This computer simulation not only enabled the determination of the general producibility of a structure but also the determination of starting values for the actual production process using the LPG. This reduces the production effort. The successful operation of the simulation was proven with representative micro structures of binary, multi-level, and continuous profile.

The resulting process parameters were used as starting values for the exposure and were experimentally optimised for use in the LPG. The reproducibility of all process parameters by optimising the interaction of all system components also led to a high reproducibility of laser lithography using the LPG.

9 CONCLUSION

Many areas require the production of micro structures with detailed dimensions in the range of micrometre, and for the time being a common process which characterises itself through small system efforts and low process costs is not available.

For this reason, an environment for microstructuring by serial laser lithography was developed. The structuring is established by introducing a focused He-Cd laser beam, underneath which the substrate to be exposed is positioned with very high accuracy while all process parameters necessary for the required reproducibility of the production result are monitored through a control unit and a host computer. In conjunction with a computer-aided simulation system, exposure and development parameters can be determined and provided to support the experimental process parameter optimisation. The operation of different application strategies of the system results in an exposure which is of high efficiency for a particular/specific application. The successful operation of serial laser lithography for efficient production of universal microstructures was proven for binary, multi-level, and continuous structures.

Compared to other production processes, relatively low equipment and production effort enables laser lithography for structures in micrometre range to have the potential for closing an existing production gap.

References

- [Anap95] Anapol, M., et.al., Ultralightweight silicon carbide infrared cryogenic telescope, Proceedings of SPIE, Vol. 2543, pp. 219-228, 1995
- [Ande90] Anderson, H., et.al., Single photomask multilevel kinoforms in quartz and photoresist: manufacture and evaluation, applied optics, Vol. 29, No. 28, pp.4259-4267, (1990)
- [Aoya90] Aoyama S., Horie, N. Yamashita, T., Micro Fresnel Lens Fabricated by Electron-Beam Lithography, Proc. SPIE, vol.1211, pp. 175-183, (1990)
- [Arno85] Arnold, S., Electron beam fabrication of computer generated holograms, Optical Engineering, Vol. 24(5), pp. 803-807, (1985)
- [Balla95] Ballandras, S., et.al., Deep etch x-ray lithography using silicon-gold masks fabricated by deep etch UV lithography and electroforming, Journal of Micromechanics and Microengineering, Vol. 5, No. 3, pp. 203-208, 1995
- [Band95] Bandyopadhyay, S., et. al., Optical, electronic, magnetic, and superconducting properties of quasi-periodic quantum dot arrays synthesized by a novel electrochemical technique, Proceedings of SPIE, Vol. 2397, pp. 12-30, 1995
- [Bart77] Bartolini, R.A., Holographic Recording Materials (edited by Smith, H.M.), Topics in Applied Physics, Vol. 20, Springer Verlag, pp. 209-227, (1977)
- [Bauc95] Bauch, L., et.al., Low voltage electron-beam lithography linked to photolithography, Proceedings of SPIE, Vol. 2437, pp. 402-411, 1995
- [Bähr95] Bähr, J., et. al., Herstellung von diffractiven Phasenelementen durch Ionenaustausch in Glas, Proceedings of „Jahrestagung der Deutschen Gesellschaft für angewandte Optik (DGaO), 6.-10. June 1995, Binz auf Rügen, Germany, 1995
- [Bern87] Bernhard, A.F., et.al., Laser microfabrication technology and its application to high speed interconnection of gate arrays, In Photon, Vol. 75, Materials Res. Soc. Proc., Pittsburg
- [Broc91] Brock, P.J., et.al., Fabrication of Grooved Glass Substrates by Phase Mask Lithography, SPIE, Vol. 1463, pp. 87-100, (1991)
- [Budz95] Budzinski, Ch., Tiziani, H.J., radiant resistant diffractive optics generated by micro electroforming, Laser und Optoelektronik, 27(1)/1995
- [Burb91] Burbaum, C., et. al., Sensors and Materials, 3, 2, pp. 75, 1991
- [Burg88] Burggraaf, P., Laser based pattern generator, Semiconductor international, pp. 116-121, 1988

- [Bühl95] Bühler, E., Script zur Vorlesung Regelungstechnik, FB E+I Fachhochschule Ostfriesland, 1995
- [Camo95] Camon, H., et.al., Atomic scale simulation of silicon etched in aqueous KOH solution, Sensors and Actuators, A, Physical, Vol. 46-47, pp. 27-29, 1995
- [Chan95] Chang, Y.S., et.al., Role of the bipolar transistor on the hot-carrier-degradation of SOI MOSFETs, IEEE International SOI Conference, ISBN 0-7803-2548-6, pp. 86-87, 1995
- [Chie52] Chien, K.L., Hrones, J.A., Rewick, J.B., On the Automatic Control of Generalized Pasive Systems, Trans of the ASME 74 (1952)
- [Colli96] Collison, W.Z., Kushner, M.J., Conceptual design of advanced inductively coupled plasma etching tools using computer modeling, IEEE Transactions on Plasma Science, Vol. 24, No. 1, pp. 135-136, 1996
- [Conr92] Conrad electronic, Data sheet PIO card
- [Cox90] Cox, J.A., et. al., Diffraction efficiency of binary optical elements, Computer and optical formed holographic optics, Proceedings of SPIE, Vol. 1211, pp. 116-124, 1990
- [Cram91] Cramer, L., et.al., Interface analysis during etchback of silicon oxide, Journal of Physics: Condensed Matter, Vol. 3, No. A, pp. 77-83, 1991
- [d'Aur72] d'Auria, L., Huignard, J.P., Roy, A.M., Spitz, E., Photolithographic fabrication of thin film lenses, Optics Communications, Vol. 5(4), pp. 232-235, (1972)
- [Done91] Domes, M.P., Dowling, R.J., McKee, P., Wood, D., Efficient optical elements generate intensity weight spot arrays; design and fabrication, Applied Optics 91, Vol. 30, No. 19
- [Ecke95] Eckert, W., et. al., Planare 3D-Mikrointegration refraktiver optischer Systeme mit ionenausgetauschten Mikrolinsen, Proceedings of „Jahrestagung der Deutschen Gesellschaft für angewandte Optik (DGaO), 6.-10. June 1995, Binz auf Rügen, Germany, 1995
- [Eich91] Eichler, J., Eichler, H.-J., Laser, Springer Verlag, Berlin (1991)
- [Fan95] Fan, L.S., et. al., Integrated multilayer high aspect ratio milliactuators, Sensors and Actuators, A, Physical, Vol. 48, No. 3, pp. 221-227, 1995
- [Find85] Findalky, Glas waveguides by ion exchange: a review, Opt.Eng., Vol.24, No.2, p244, (1985)
- [Fitz87] Fitzgibbons, E.T., et. al., A direct write laser pattern generator for rapid semiconductor device customization, In Proceedings of Laser in Microlithography, Vol. 774, SPIE, pp. 82- 87, 1987

- [Frey92] Frey, H., Ionenstrahlgestützte Halbleitertechnologie, VDI-Verlag, Düsseldorf, (1992)
- [Fröh95] Fröhlich, T, et. al., Perfect Shuffle Permutationselemente, Proceedings of „Jahrestagung der Deutschen Gesellschaft für angewandte Optik (DGaO), 6.-10. June 1995, Binz auf Rügen, Germany, 1995
- [Gamb91] Gambog, W., et.al., Holographic transmission elements using improved photopolymer films, SPIE Vol.1555, pp. 256-267, (1991)
- [Golt90] Goltsos, W., Liu, S., Polar Coordinate Laser Writer for Binary Optics Fabrication, Proc. SPIE, vol.1211, pp.137-149,(1990)
- [Grüb92] Grüber, H., et. al., Laserinterferometrie: Flexibel durch LWL Strahlführung, F&M, Jahrgang 98, Oktober 1992, Carl Hanser Verlag
- [Hase92] Haselbeck, S, et. al., Synthetic phase holograms written by laser lithography, Proc. SPIE, vol. 1718, pp. 117-128, (1992)
- [Hels95] Helsel, R., Graphische Programmierumgebung für Test- und Meßtechnik, Prentice Hall Verlag, 1995
- [Herz92] Herzig, H.P., Dändliker, R., Design and fabrication of diffractive optical elements for beam shaping and imaging, Proc. SPIE, vol. 1718, pp. 130-137, (1992)
- [Humm95] Hummelt, G., Hochpräzises Positionieren für die Mikrofertigung, F&M, Jahrgang 103, September 1995, Carl Hanser Verlag
- [Jäge89] Jäger, E., Hoßfeld, J., Tang, Q., Tschudi, T., Design of a laser scanner for kinoform fabrication. Proc. SPIE, vol. 1136, pp.228-235, (1989)
- [Jäge92] Jäger, E., Computergenerierte Holografisch Optische Elemente, Ph.D. Thesis, Tschudi, T., Lauterborn, W., Universität Darmstadt, (1992)
- [Kette94] Ketterson, J.B., et.al., Applications for superconductor/insulator multilayers, Proceedings of SPIE, Vol. 2157, pp. 274-284, 1994
- [Kolt93] Kolter elektronik, Manual: 24 bit counter card
- [Korz93] Korzec, D., Capacitance coupled high-frequency ion source with radial exciting electrodes for reactive ion beam etching, Ph.D Thesis, Fortschrittsberichte VDI, Reihe 8, No. 160, pp. 1-200, 1993
- [Kube91] Kubena, R.L., et. al., A low magnification focused ion beam system with 8nm spot size, Journal of vacuum science and technology, Part B, Vol. 9, No. 6, pp. 3079-3083, 1991
- [Laas94] Laas, F., Optische Bauteile positionieren, F&M, Jahrgang 102, März 1994, Carl Hanser Verlag

- [Leka86] Lekavich, J., Basis of acousto optic devices, *Laser & Applications*, April 1986, pp. 59-64
- [Lens92a] Lensch, G., Kreitlow, H., Lippert, P., Budzinski, Ch., Interferometrische Herstellung von tiefen diffraktiven Strukturen in Fotoresist, Jahrestagung der DGaO, Friedrichsroda, Germany, 1992
- [Lens92b] Lensch, G., Lippert, P., Kreitlow, H., Budzinski, Ch., Optimized Replication of Interferometrically Generated Deep Diffraction Structures by Embossing into Thermoplastics, SPIE No. 1780-27, (1992)
- [Leve82] Levenson, M. D., et. al., IEEE, ED29, pp.1828, 1982
- [Liu95] Liu, W., et.al., Reducing intergranular magnetic coupling by incorporating carbon into Co/Pd multilayers, in series: *Materials Res. Soc. Symp. Proc.*, Vol. 384, pp. 189-194, 1995
- [Lo93] Lo, T.C., et.al., Anisotropic etching of deep trench for silicon monolithic microwave integrated circuit, *Electronics Letters*, Vol. 29, No. 25, pp. 2202-2203, 1993
- [Mack91] Mackenzie, R.A.D., Developments and trends in the technology of focused ion beams, *Journal of vacuum science and technology, Part B*, Vol. 9, No. 5, pp. 2561-2565, 1991
- [Mats91] Matsui, S., et. al., high resolution focused ion beam lithography, *Journal of Vacuum Science and Technology, Part B*, Vol. 9, No. 5, pp. 2622-2632, 1991
- [McWi83] McWilliams, B.M., et. al., Wafer scale laser pantography: Fabrication of n-MOS transistors and small scale IC's by direct write laser induced pyrolytic reactions, *Appl. Phys Lett* 43, pp. 946-948, 1983
- [Menz93] Menz, W., Bley, P., *Mikrosystemtechnik für Ingenieure*, VCH Verlag, Weinheim, (1993)
- [Mils95] Milster, T., Technique for aligning optical and mechanical axes based on a rotating linear grating, *Optical engineering*, October 1995, Vol. 34(No. 10), pp. 2840-2845
- [More88] Moreau, W.M., *Semiconductor lithography*, Plenum Press, New York, 1988
- [Mura95] Muralt, P., et.al., Fabrication and characterization of PZT thin films for micromotors, *Transducer 95, Foundation for sensor and actuator technology*, Vol. 1, pp. 397-400, ISBN 91-630-3473-5, 1995
- [Naum92] Naumann, H., Schröder, G., *Bauelemente der Optik*, Carl Hanser Verlag, München, (1992)
- [Newp93] Newport, Manual: PM500

- [Nöls91] Nölscher, C, VDI-Berichte 935, VDI-Verlag, Düsseldorf, pp. 61, 1991
- [Nuss95] Nussbaum, Ph., et. al., Mikrolinsen-Arrays für Mikrolithographie und optische Mikrosysteme, Proceedings of „Jahrestagung der Deutschen Gesellschaft für angewandte Optik (DGaO), 6.-10. June 1995, Binz auf Rügen, Germany, 1995
- [Pole91] Poleshuk, A.G., Fabrication of phase structures with continuous and multilevel profile for diffractive optics, SPIE, Vol. 1574, 89-100, (1991)
- [Phys92] Physik instrumente, Manual: DAQ-1212A
- [Razo95] Razo. J., A comparison of semiconductor technologies used in display fabrication, Proceedings of SPIE, Vol. 2462, pp. 48-56, 1995
- [Reim95] Reimer, K., et. al., Minireticle for electron-beam lithography, VDI Berichte, Vol. 1243, ISBN 3-18-091243-x, pp. 97-112, 1995
- [Reut90] Reuter, M., Regelungstechnik für Ingenieure, Vieweg Verlag, Braunschweig 1990
- [Royl79] Roylance, L.M., et. al., IEEE Trans. Electron Devices, ED-26, S.1911 pp, 1979
- [Samu95] Samuels, U., Parkin, R., Kreitlow, H., Automated surface measurement via laser tomography, IEE, innovations in manufacturing control through mechatronics, Newport (GB), Gwent, 22. Nov. 1995, Digest 95/214, ISSN 0963-3308, pp. P6.1-P6.2
- [Samu96a] Samuels, U., Focal position controlled processing head for a laser pattern generator (LPG) for flexible microstructuring, Mphil Thesis, Loughborough University of Technology, January 1996
- [Samu96b] Samuels, U., Parkin, R., Kreitlow, H., Automated surface measurement via laser profiling, Submitted for publication in control theory and applications
- [Samu96c] Samuels, U., Kreitlow, H., Parkin, R., Optimised autofocus sensor for flexible distance and profile measurement without moving sensor parts, Proceedings of „Vision and control aspects of mechatronics, Ed. R.M. Parkin, M. Lima, T.G. King, Guimaraes, Portugal, 6-21 September 1996, ISBN 972-8063-07-5, pp. 211-216
- [Sasi93] Sasin, J.M., et. al., Staicase lens: a binary and diffractive field curvature corrector, Applied optics, Vol. 32, No. 1, 1993
- [Scha81a] Schade, K., Halbleitertechnologie, Band I, VEB-Verlag Technik, Berlin
- [Scha81b] Schade, K., Halbleitertechnologie, Band II, VEB-Verlag Technik, Berlin
- [Seid92] Seidel, H., Tech Digest, Transducer '87, Tokyo, Japan, p120-125, 1987

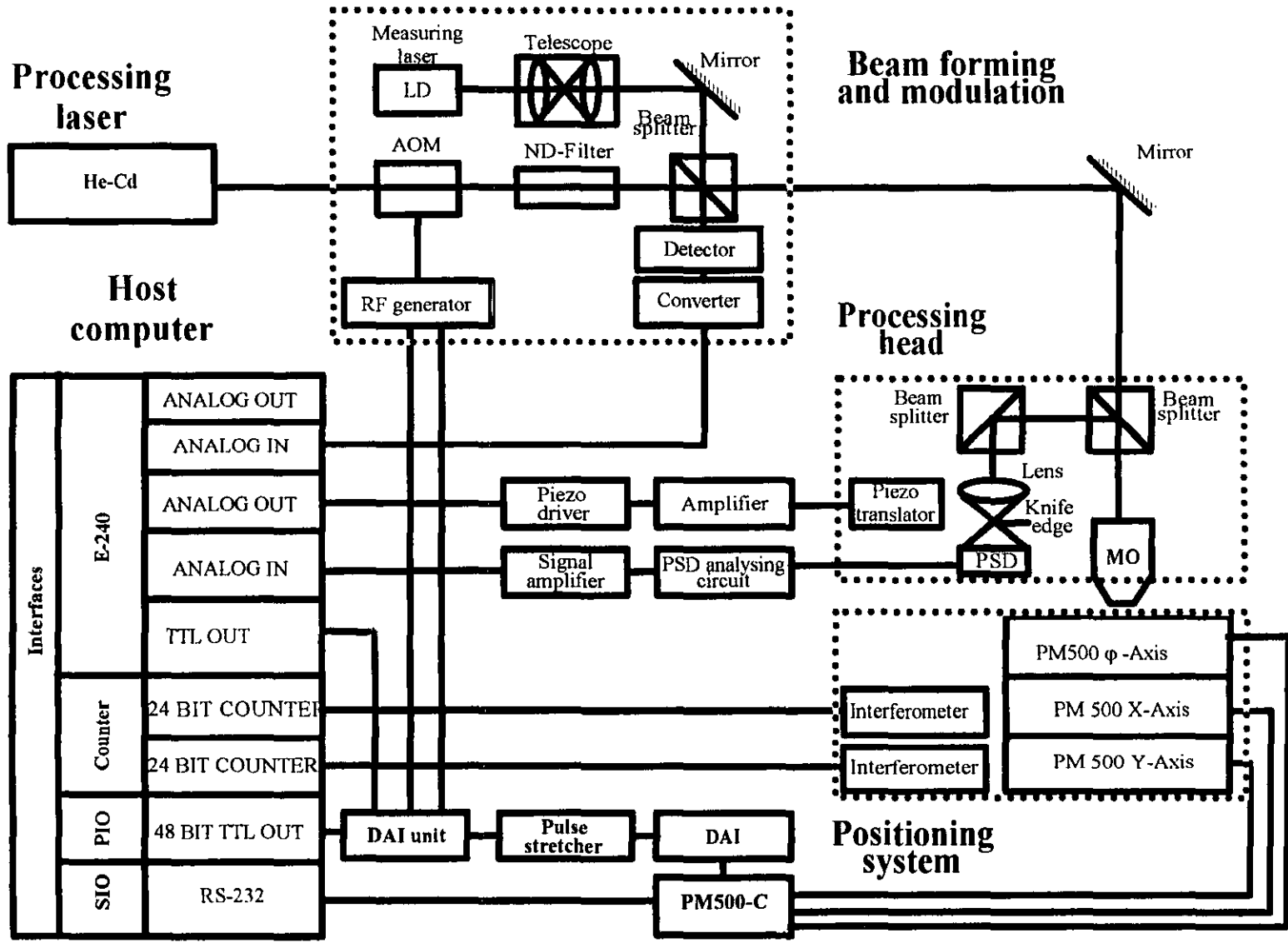
- [Smit91] Smith, H.I., et.al., A new approach to high fidelity e-beam and ion-beam lithography based on a in situ global-fiducial grid, Journal of vacuum science and technology, Part B, Vol. 9, No. 6, pp. 2992-2995, 1991
- [Sont91] Sontheim, B., Graf, G., Analoge und digitale Regelkreise auf dem PC simuliert, Elektronik 22/1991
- [Step82] Steppan, H., Buhr, G., Vollmann, H., The resist Technique - A Chemical Contribution to Electronics, Angew. Chem. Int. Ed. Engl., 21 (1982)
- [Stre92] Streibl, N., et. al., Laser Beam Writing of Computer generated Diffractive Optical Components, Proc. SPIE, vol. 1732, pp. 67-74, (1992)
- [Swan89] Swanson, G., et. al., Diffractive optical elements for use in infrared system, Optical engineering, Vol. 28, No. 6, 1989
- [Tied95] Tiedeken, S., Entwicklungen zur Herstellung von Mikrooptiken durch Laserbelichtung und Maskenverfahren, Final year project at Fachhochschule Ostfriesland, Supervisor: Prof. Dr. H. Kreitlow, Emden, Germany, (1995)
- [Walk90] Walker, J.A., Gabriel, K.J., Proceedings of Sensors and Actuators, 1990
- [Walk93] Walker, S.J., Design and fabrication of high efficiency beam splitters and beam deflectors for integrated planar micro-optic systems, Applied Optics, Vol. 32, No. 14, pp.2494-2501, (1993)
- [Wang95] Wang, J.S., et. al., Process design for manufacturability of GaAs MESFET integrated circuits using statistical experimental design techniques, Proceedings of SPIE, Vol. 2635, pp. 204-213, 1995
- [Wolf96] Wolf, R., Helbig, R., Reactive ion etching of 6H-SiC in SF₆O₂ and CF₄O₂ with N₂ additive for device fabrication, Journal of the Electrochemical society, Vol. 143, No. 3, pp. 1037-1042, 1996
- [Yata91] Yatagai, T., et. al., CAD system for CGHs and laser beam lithography, Proc. SPIE, vol. 1555, pp. 8-12, (1991)

APPENDICES

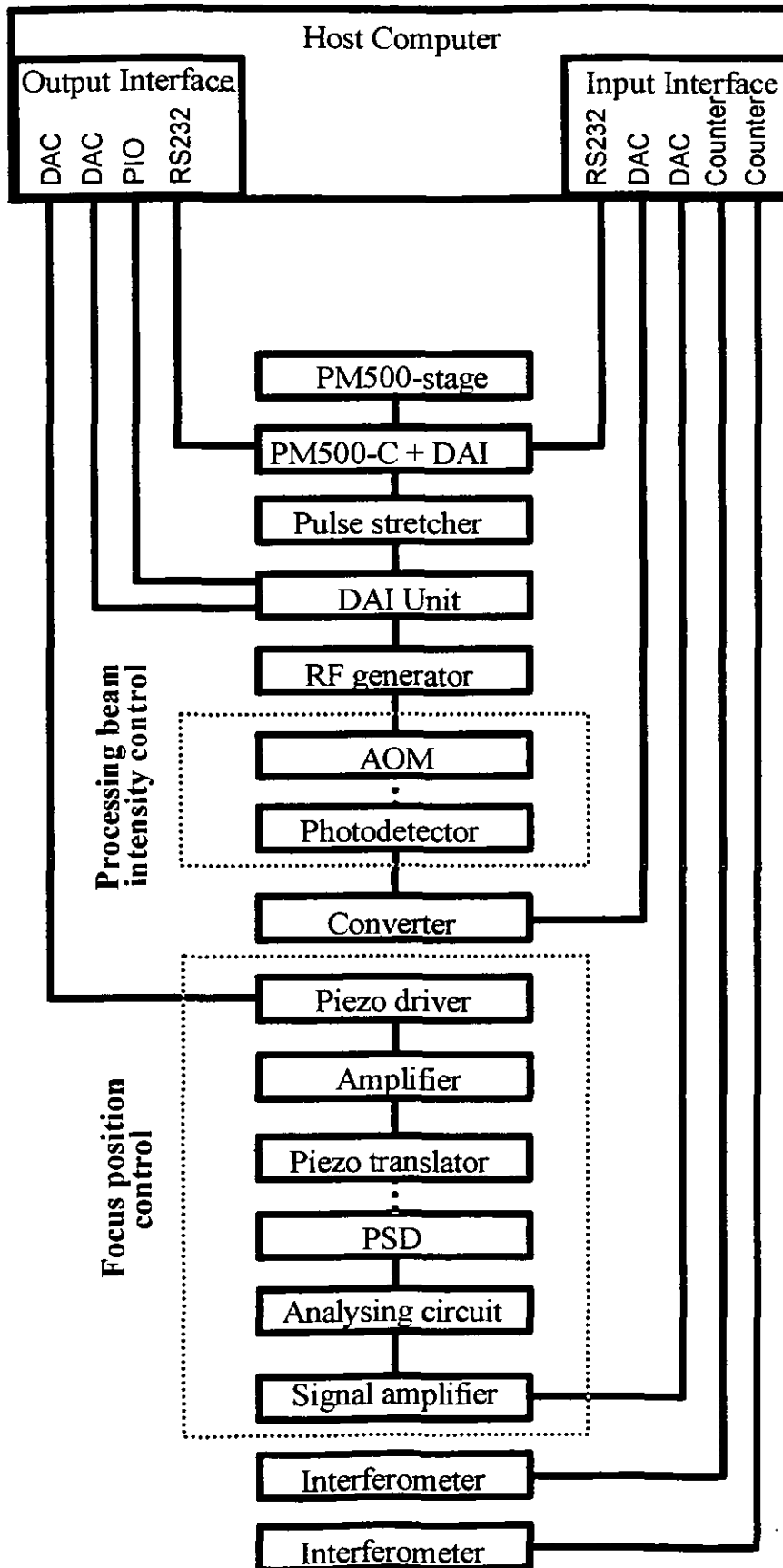
	Page #
A. LPG OVERVIEW DIAGRAMS.....	A1-A2
B. RAYTRACING MODEL OF THE LPG	B1-B4
C. CONTROLLER PARAMETER TABLE.....	C1
D. LPG CONTROL UNIT	D1-D118
E. LPG SOFTWARE	E1-E51
F. MECHANICAL SYSTEM OF THE LPG.....	F1-F21
G. SIMULATION PROGRAM <i>LASSI</i>	G1-G6
H. PUBLICATIONS.....	H1-H59

A. LPG OVERVIEW DIAGRAMS

CONTENTS	PAGE #
1. Overview	A1
2. Block diagram	A2



BLOCK DIAGRAM



B. RAYTRACING MODEL OF THE LPG

CONTENTS	PAGE #
1. Surface data summary	B1
2. General lens data	B1
3. 2D layout	B2
4. Through focus spot diagram	B3
5. Gaussian beam parameter	B4

1. Surface data summary

SURFACE DATA SUMMARY:

Surf	Type	Radius	Thickness	Glass	Diameter	Conic
OBJ	STANDARD	Infinity	Infinity		0	0
STO	STANDARD	Infinity	1005		5.4	0
2	STANDARD	3.9995	1.5	SF6	5.4	0
3	STANDARD	-8.00001	0.5	BK7	5.4	0
4	STANDARD	-99.9996	0.5999		5.4	0
5	STANDARD	5	1.9999	SF6	5.4	0
6	STANDARD	-5.9999	0.3	BK7	5.4	0
7	STANDARD	-100.0012	0.4108434		5.4	0
IMA	STANDARD	Infinity	0		5.4	0

2. General lens data

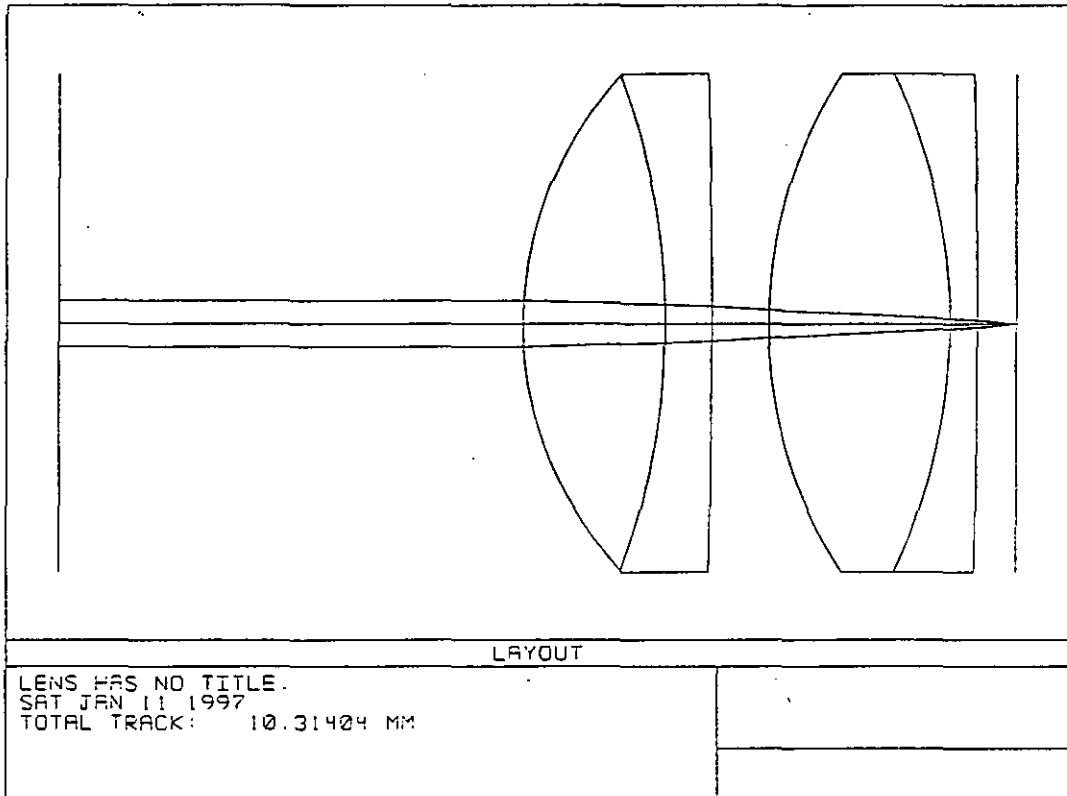
GENERAL LENS DATA:

Title : LENS HAS NO TITLE.
 Surfaces : 8
 Stop : 1
 System Aperture : Entrance Pupil Diameter
 Ray aiming : Off
 Gaussian Factor : 1.000000
 Eff. Focal Len. : 2.76415
 Total Track : 1010.31
 Image Space F/# : 5.5283
 Working F/# : 5.52512
 Obj. Space N.A. : 2.5e-011
 Stop Radius : 0.25
 Parax. Ima. Hgt. : 0
 Parax. Mag. : 0
 Entr. Pup. Dia. : 0.5
 Entr. Pup. Pos. : 0
 Exit Pupil Dia. : 0.00137721
 Exit Pupil Pos. : 0.011005
 Maximum Field : 0
 Primary Wave : 0.441600
 Lens Units : Millimeters
 Angular Mag. : 0

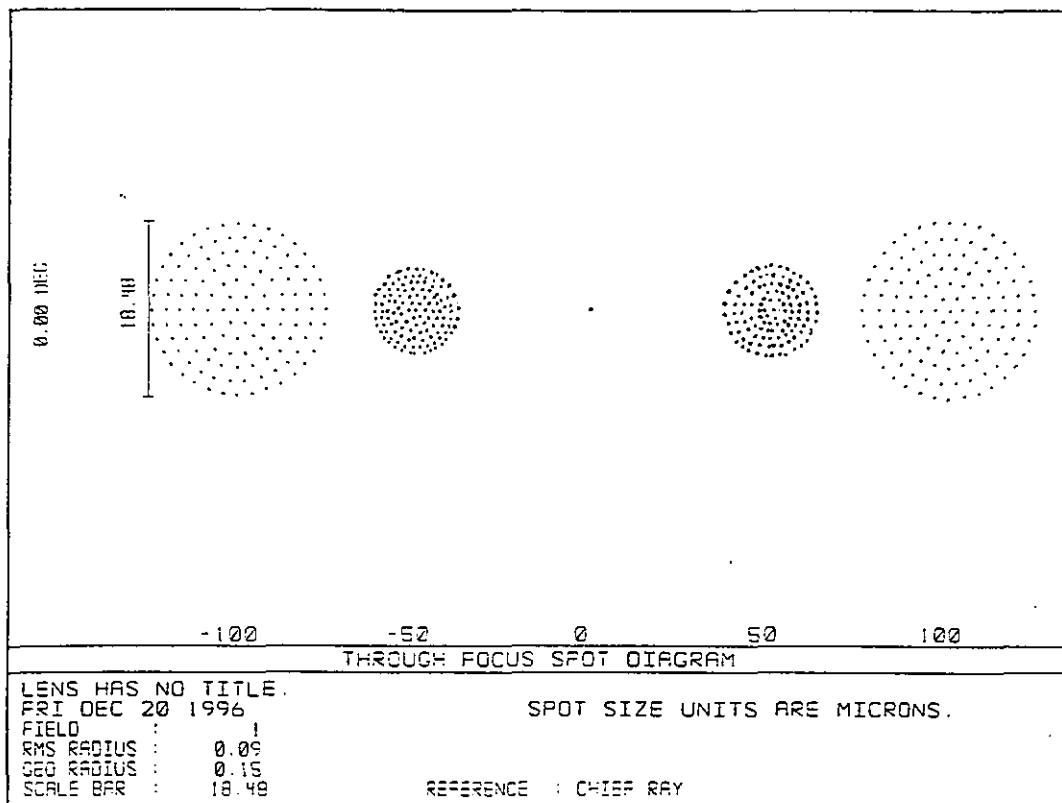
Fields : 1
 Field 1 : 0.00 deg weight: 1.000000

Wavelengths : 1
 Wavelength 1 : 0.441600 microns 1.000000 weight

3. 2D layout



4. Through focus spot diagram



5. Gaussian beam parameters

Gaussian Beam Parameters

LENS HAS NO TITLE.

Fri Dec 20 1996

Data for 0.4416 microns.

Units for waist, size, and waist-z distance are Millimeters.

Units for divergence semi-angle are radians.

Sur	Waist	Size	Waist Z	Divergence
OBJ	5.62263E+006	2.50000E-001	1.00000E+010	5.62263E-004
STO	2.50000E-001	2.50000E-001	0.00000E+000	5.62263E-004
2	6.17907E-001	1.08174E-003	-8.77049E+000	1.29220E-001
3	5.12228E-001	9.35087E-004	-5.20022E+000	1.49206E-001
4	4.62977E-001	9.20177E-004	-3.03076E+000	1.51588E-001
5	3.71337E-001	6.52364E-004	-3.17860E+000	2.12227E-001
6	1.37702E-001	6.30972E-004	-9.43305E-001	2.19197E-001
7	9.39094E-002	6.29576E-004	-4.20599E-001	2.19668E-001
IMA	2.26730E-003	6.29576E-004	-9.75560E-003	2.19668E-001

C. CONTROLLER PARAMETER TABLE

CONTENTS	PAGE #
1. Table from Chien, Hrones, Reswick	C1

Table from Chien, Hrones, Reswik [Chie52]

Recommended values for optimum controller adjustment				
Controller type	oscillating (short setting time)		creeping (without overshooting)	
	good disturbance behaviour at the input of the system to be controlled	good follow up characteristic	good disturbance behaviour at the input of the system to be controlled	good follow up characteristic
P	$K_p = 0.7 \hat{K}$	$K_p = 0.7 \hat{K}$	$K_p = 0.3 \hat{K}$	$K_p = 0.3 \hat{K}$
PI	$K_p = 0.7 \hat{K}$ $T_n = 2.3 T_u$	$K_p = 0.6 \hat{K}$ $T_n = T_g$	$K_p = 0.6 \hat{K}$ $T_n = 4 T_u$	$K_p = 0.34 \hat{K}$ $T_n = 1.2 T_g$
PID	$K_p = 1.2 \hat{K}$ $T_n = 2 T_u$ $T_v = 0.42 T_u$	$K_p = 0.95 \hat{K}$ $T_n = 1.35 T_g$ $T_v = 0.47 T_u$	$K_p = 0.95 \hat{K}$ $T_n = 2.4 T_u$ $T_v = 0.42 T_u$	$K_p = 0.6 \hat{K}$ $T_n = T_g$ $T_v = 0.5 T_u$

D. LPG CONTROL UNIT

CONTENTS	PAGE #
1. General system	D1-D4
2. DAQ Unit	D5-D20
3. Power supply I	D21-D26
4. Power supply II	D27-D32
5. PIO Unit	D33-D48
6. Signal amplifier	D49-D58
7. Piezo driver	D59-D66
8. Power supply III	D67-D72
9. AOM protector	D73-D80
10. DAI Unit	D81-D96
11. Pulse strecher	D97-D104
12. Photo detector I	D105-D110
13. Photo detector II	D111-D118

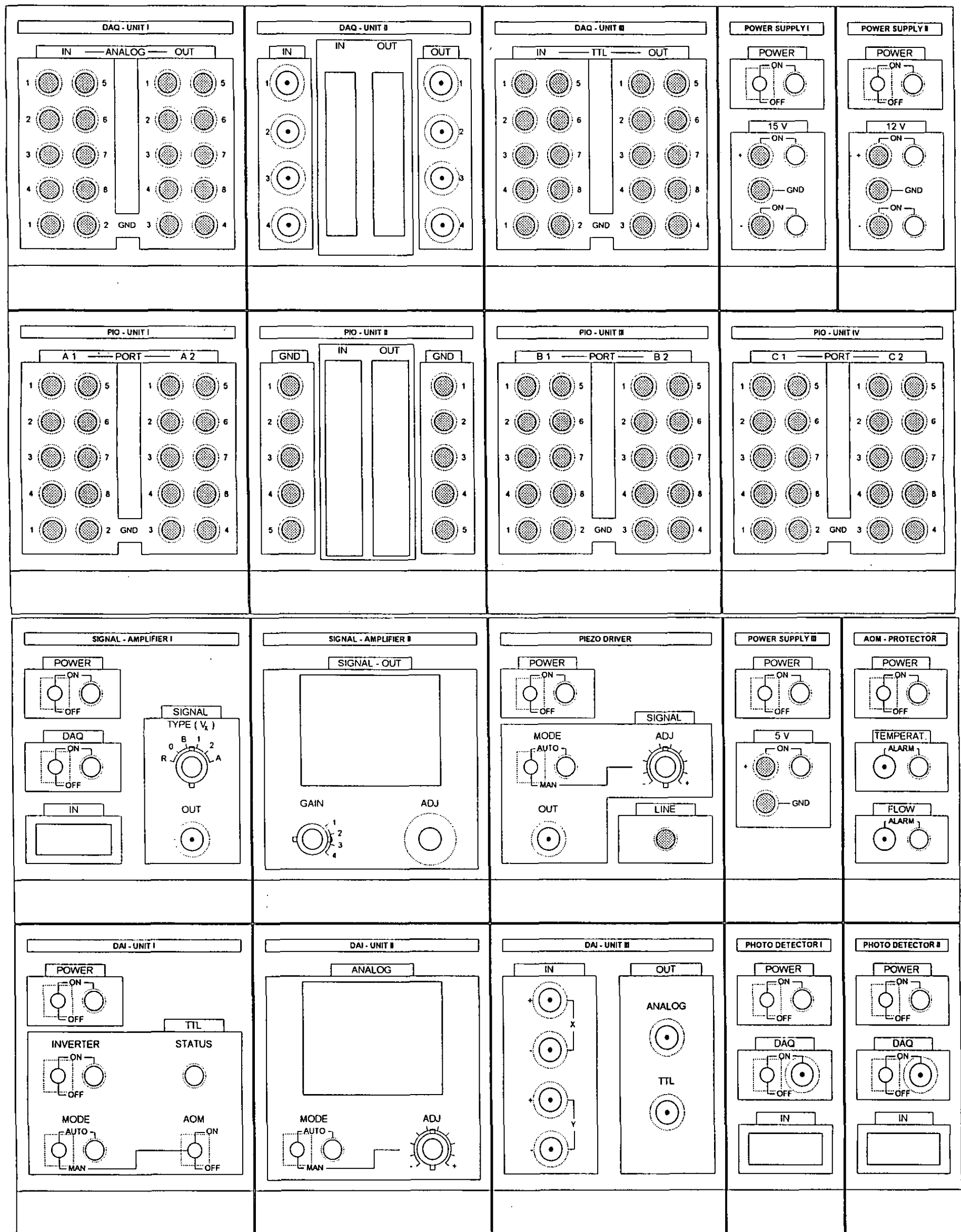
D.1 General system

CONTENTS	PAGE #
1. Frontplate overview	D2
2. Frontplate marking	D3
3. Photograph	D4

D.1.1 Frontplate overview



D.1.2 Frontplate marking



D.1.3 Photograph

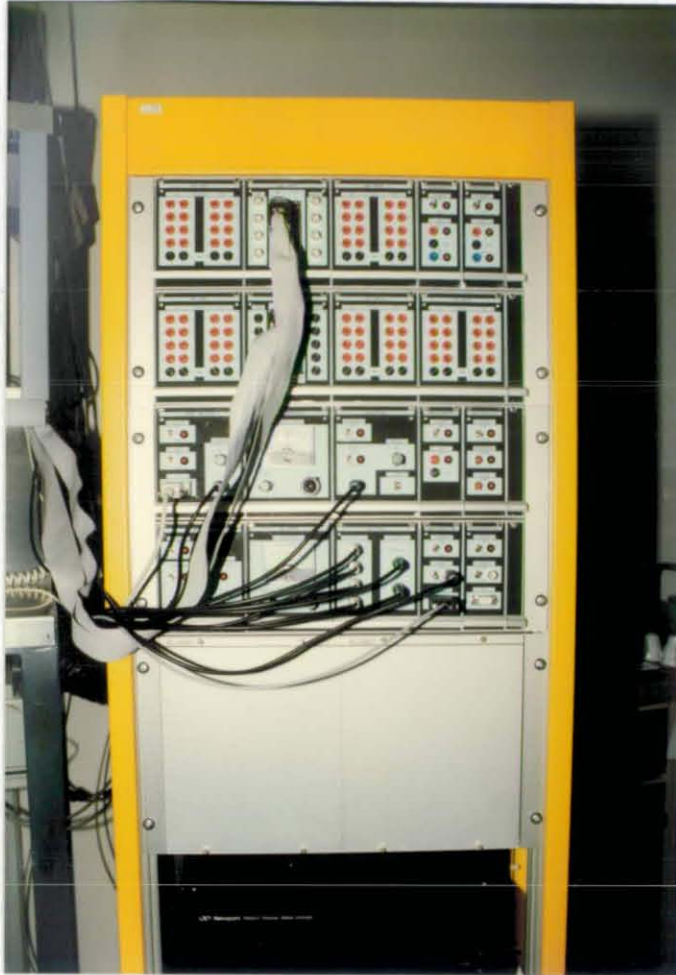
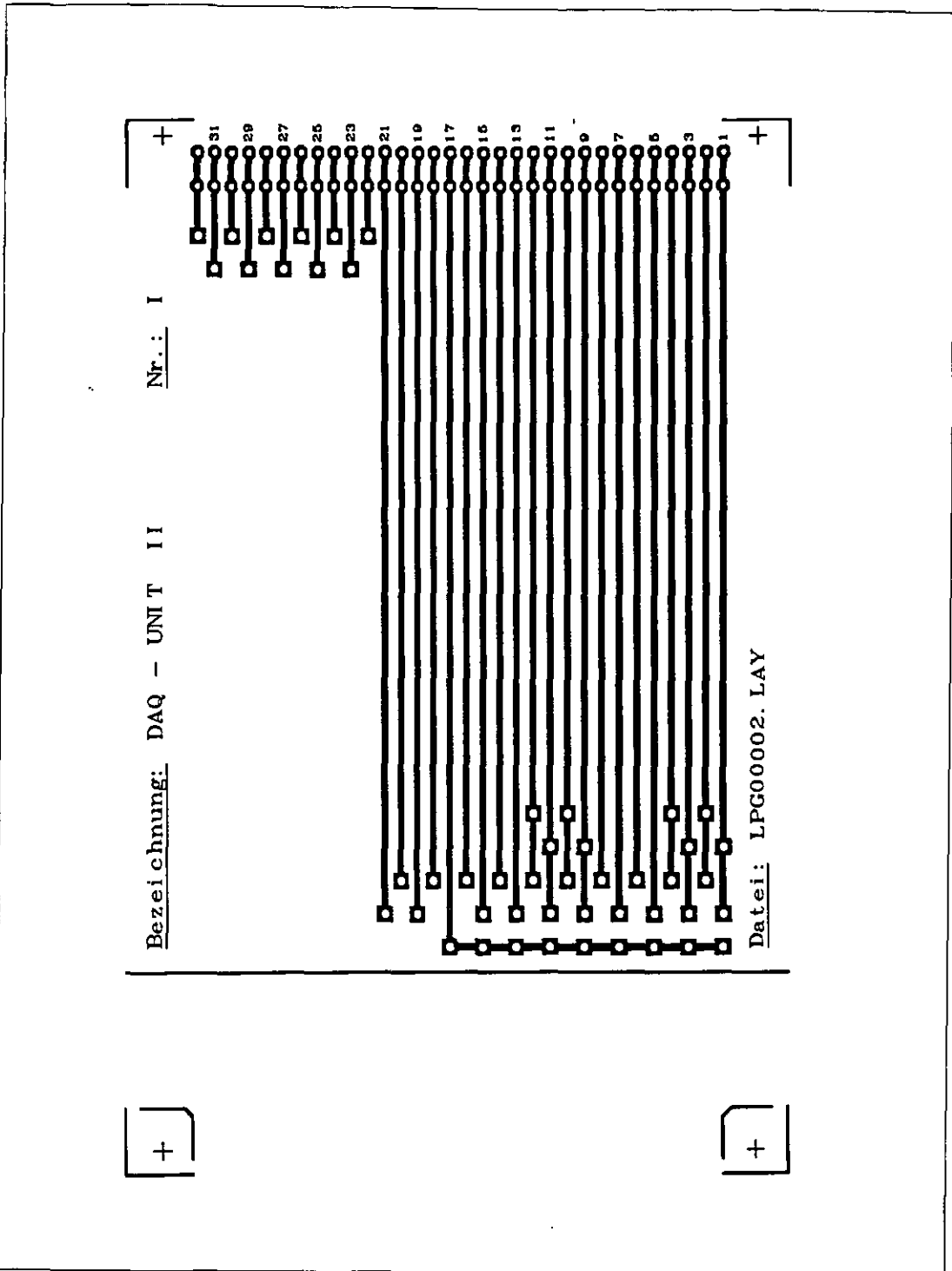


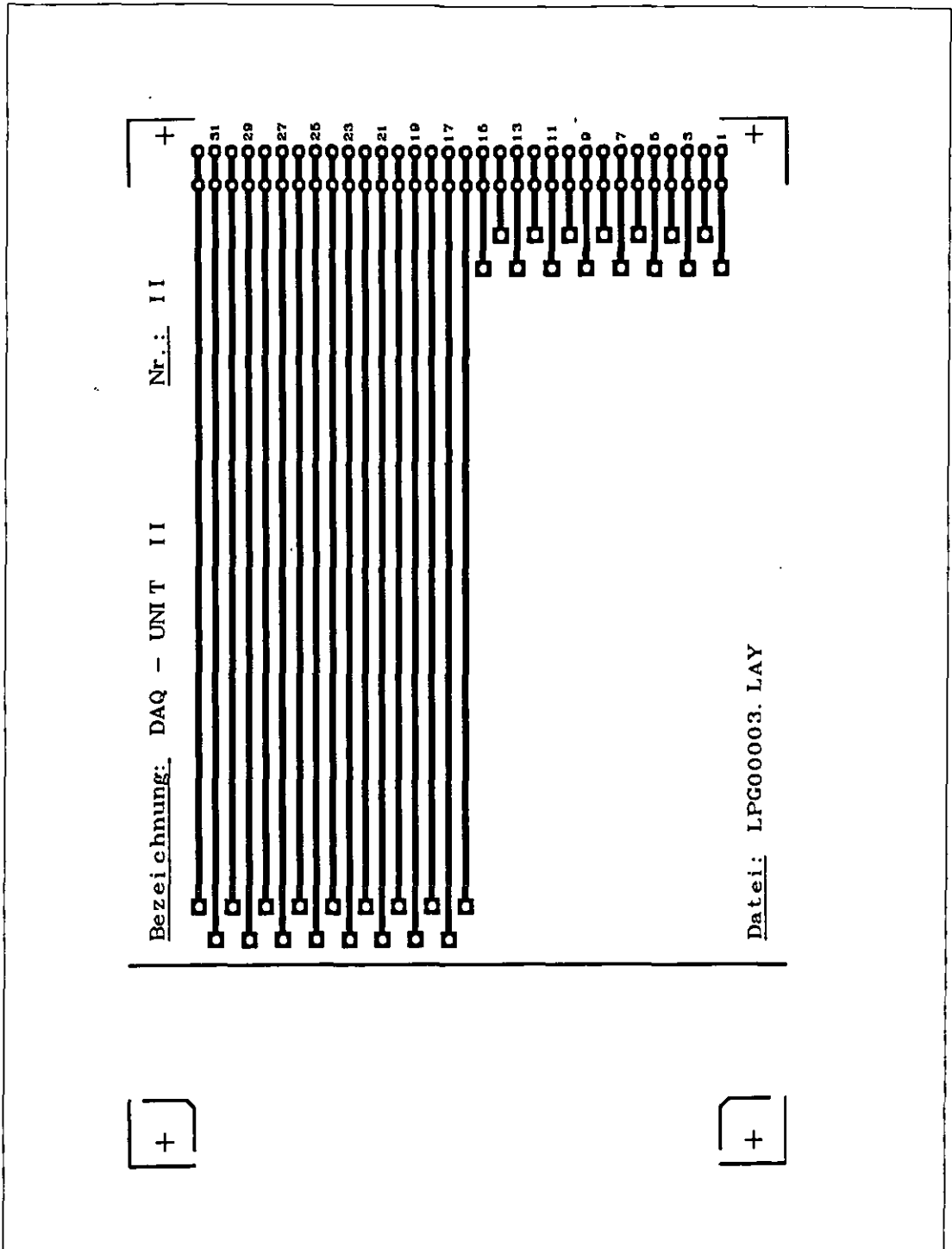
Photo D1: LPG control unit

D.2 DAQ Unit

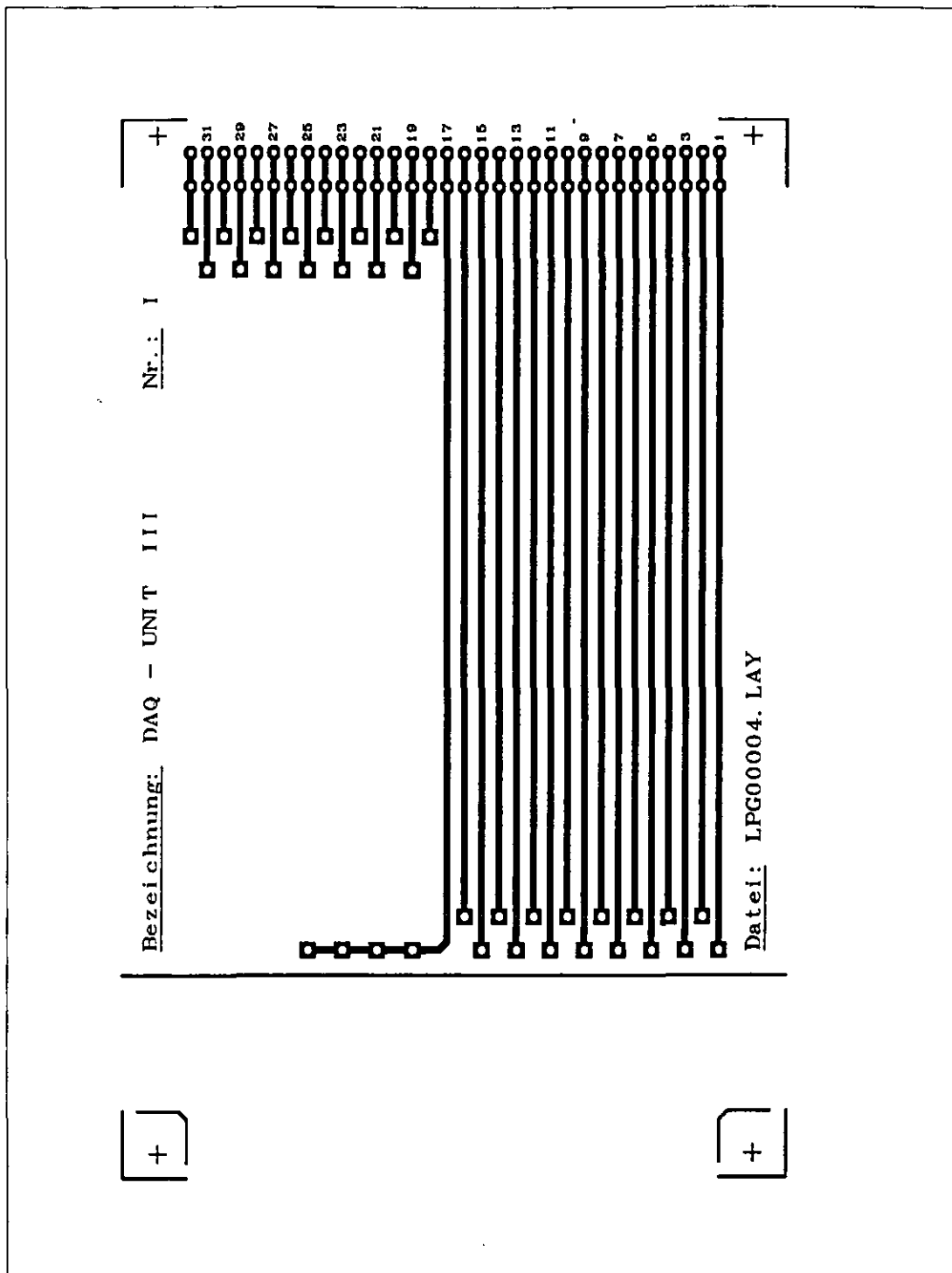
CONTENTS	PAGE #
1. PCB layout module I	D6
2. PCB layout module II/I	D7
3. PCB layout module II/II	D8
4. PCB layout module III/I	D9
5. PCB layout module III/II	D10
6. Bus port module I	D11
7. Bus port module II/I	D12
8. Bus port module II/II	D13
9. Bus port module III/I	D14
10. Bus port module III/II	D15
11. Pin connection of the input terminal	D16
12. Table of interconnections	D17
13. Photographs	D18-D20



Part-No.:	Title: PCB of the DAQ Unit module II/I
Scale:	
Material:	
Date: October 1996	FHO-Fachhochschule Ostfriesland -Institut für Lasertechnik Ostfriesland -
ENGR: Dipl.-Ing. U. Samuels	



Part-No.:	Title: PCB of the DAQ Unit module II/II
Scale:	
Material:	
Date: October 1996	FHO-Fachhochschule Ostfriesland -Institut für Lasertechnik Ostfriesland -
ENGR: Dipl.-Ing. U. Samuels	

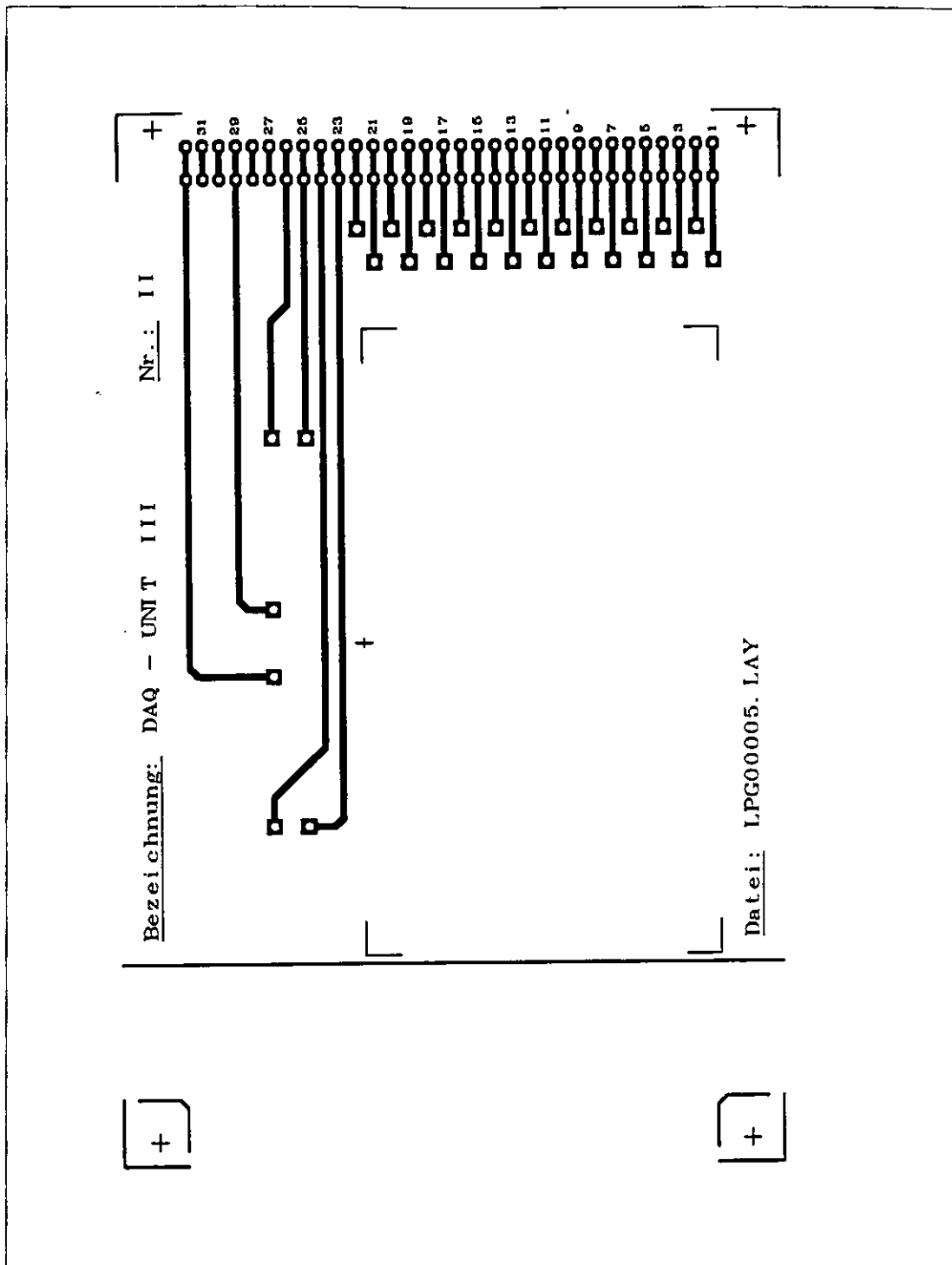


Nr.: I

Bezeichnung: DAQ - UNIT III

Detail: LPG00004. LAY

Part-No.:	Title: PCB of the DAQ Unit module III/I
Scale:	
Material:	
Date: October 1996	FHO-Fachhochschule Ostfriesland -Institut für Lasertechnik Ostfriesland -
ENGR: Dipl.-Ing. U. Samuels	



Part-No.:	Title: PCB of the DAQ Unit module III/II
Scale:	
Material:	
Date: October 1996	FHO-Fachhochschule Ostfriesland -Institut für Lasertechnik Ostfriesland -
ENGR: Dipl.-Ing. U. Samuels	

D.2.6 Bus port module I

Pin #	Description	DAQ - UNIT II, No.: I
1	Analog IN - Nr.: 1	Pin#: 1
2	Analog IN - Nr.: 2	Pin#: 2
3	Analog IN - Nr.: 3	Pin#: 3
4	Analog IN - Nr.: 4	Pin#: 4
5	Analog IN - Nr.: 5	Pin#: 5
6	Analog IN - Nr.: 6	Pin#: 6
7	Analog IN - Nr.: 7	Pin#: 7
8	Analog IN - Nr.: 8	Pin#: 8
9	Analog OUT - Nr.: 1	Pin#: 9
10	Analog OUT - Nr.: 2	Pin#: 10
11	Analog OUT - Nr.: 3	Pin#: 11
12	Analog OUT - Nr.: 4	Pin#: 12
13	Analog OUT - Nr.: 5	Pin#: 13
14	Analog OUT - Nr.: 6	Pin#: 14
15	Analog OUT - Nr.: 7	Pin#: 15
16	Analog OUT - Nr.: 8	Pin#: 16
17	GND	
18		
19		
20		
21		
22		
23		
24		
25		
26		
27		
28		
29		
30		
31		
32		

D.2.7 Bus port module II/I

Pin #	Description	DAQ - UNIT II (C: 37)
1	Analog IN 1	Pin#: 3
2	Analog IN 2	Pin#: 22
3	Analog IN 3	Pin#: 4
4	Analog IN 4	Pin#: 23
5	Analog IN 5	Pin#: 5
6	Analog IN 6	Pin#: 24
7	Analog IN 7	Pin#: 6
8	Analog IN 8	Pin#: 25
9	Analog OUT 1	Pin#: 26
10	Analog OUT 2	Pin#: 8
11	Analog OUT 3	Pin#: 27
12	Analog OUT 4	Pin#: 9
13	Analog OUT 5	Pin#: 28
14	Analog OUT 6	Pin#: 10
15	Analog OUT 7	Pin#: 29
16	Analog OUT 8	Pin#: 11
17	GND	Pin#: 21
18	+ 15V	Pin#: 1
19	- 15V	Pin#: 2
20	+ 5V	Pin#: 20
21	External Trigger	Pin#: 7
22		
23		
24		
25		
26		
27		
28		
29		
30		
31		
32		

D.2.8 Bus port module II/II

Pin #	Description	DAQ - UNIT II (C: 37)
32	TTL IN 1	Pin#: 34
31	TTL IN 2	Pin#: 16
30	TTL IN 3	Pin#: 35
29	TTL IN 4	Pin#: 17
28	TTL IN 5	Pin#: 36
27	TTL IN 6	Pin#: 18
26	TTL IN 7	Pin#: 37
25	TTL IN 8	Pin#: 19
24	TTL OUT 1	Pin#: 30
23	TTL OUT 2	Pin#: 12
22	TTL OUT 3	Pin#: 31
21	TTL OUT 4	Pin#: 13
20	TTL OUT 5	Pin#: 32
19	TTL OUT 6	Pin#: 14
18	TTL OUT 7	Pin#: 33
17	TTL OUT 8	Pin#: 15
16	GND	
15		
14		
13		
12		
11		
10		
9		
8		
7		
6		
5		
4		
3		
2		
1		

D.2.9 Bus port module III/I

Pin #	Description	DAQ - UNIT II, No.: II
1	TTL IN - Nr.: 1	Pin#: 32
2	TTL IN - Nr.: 2	Pin#: 31
3	TTL IN - Nr.: 3	Pin#: 30
4	TTL IN - Nr.: 4	Pin#: 29
5	TTL IN - Nr.: 5	Pin#: 28
6	TTL IN - Nr.: 6	Pin#: 27
7	TTL IN - Nr.: 7	Pin#: 26
8	TTL IN - Nr.: 8	Pin#: 25
9	TTL OUT - Nr.: 1	Pin#: 24
10	TTL OUT - Nr.: 2	Pin#: 23
11	TTL OUT - Nr.: 3	Pin#: 22
12	TTL OUT - Nr.: 4	Pin#: 21
13	TTL OUT - Nr.: 5	Pin#: 20
14	TTL OUT - Nr.: 6	Pin#: 19
15	TTL OUT - Nr.: 7	Pin#: 18
16	TTL OUT - Nr.: 8	Pin#: 17
17	GND	
18		
19		
20		
21		
22		
23		
24		
25		
26		
27		
28		
29		
30		
31		
32		

D.2.9 Bus port module III/II

Pin #	Description	Power Supply I and II, No.: I
32	~ 220V	
31		
30		
29	~ 220V	
28		
27		
26	SEC 1 - ~15V	Pin#: 7
25	SEC 1 - ~15V	Pin#: 8
24	SEC 2 - ~15V	Pin#: 9
23	SEC 2 - ~15V	Pin#: 10
22		
21		
20		
19		
18		
17		
16		
15		
14		
13		
12		
11		
10		
9		
8		
7	+ 12V	Pin#: 26
6	- 12V	Pin#: 27
5	+ 5V	
4	+ 15V	Pin#: 29
3	- 15V	Pin#: 30
2	E 240 - X	
1	GND	Pin#: 32

D.2.11 Pin connection of the input terminal

Pin #	Description	Function
1	+ 15V	Supply
2	- 15V	Supply
3	Analog IN 1	Analog
4	Analog IN 3	Analog
5	Analog IN 5	Analog
6	Analog IN 7	Analog
7	External Trigger	Trigger
8	Analog OUT 2	Analog
9	Analog OUT 4	Analog
10	Analog OUT 6	Analog
11	Analog OUT 8	Analog
12	TTL OUT 2	TTL
13	TTL OUT 4	TTL
14	TTL OUT 6	TTL
15	TTL OUT 8	TTL
16	TTL IN 2	TTL
17	TTL IN 4	TTL
18	TTL IN 6	TTL
19	TTL IN 8	TTL
20	+ 5V	Supply
21	GND	Supply
22	Analog IN 2	Analog
23	Analog IN 4	Analog
24	Analog IN 6	Analog
25	Analog IN 8	Analog
26	Analog OUT 1	Analog
27	Analog OUT 3	Analog
28	Analog OUT 5	Analog
29	Analog OUT 7	Analog
30	TTL OUT 1	TTL
31	TTL OUT 3	TTL
32	TTL OUT 5	TTL
33	TTL OUT 7	TTL
34	TTL IN 1	TTL
35	TTL IN 3	TTL
36	TTL IN 5	TTL
37	TTL IN 7	TTL

D.2.12 Table of interconnections

Pin#	Description	Module
24	Analog IN 6 (E 240 - 1)	Photo detector I
6	Analog IN 7 (E 240 - 2)	Photo detector II
25	Analog IN 8 (E 240 - 3)	PSD - Amplifier
29	Analog OUT 7 (E 240 - 4)	Piezo - Driver
11	Analog OUT 8 (E 240 - 5)	DAI - Unit

D.2.13 Photographs of the DAQ Unit

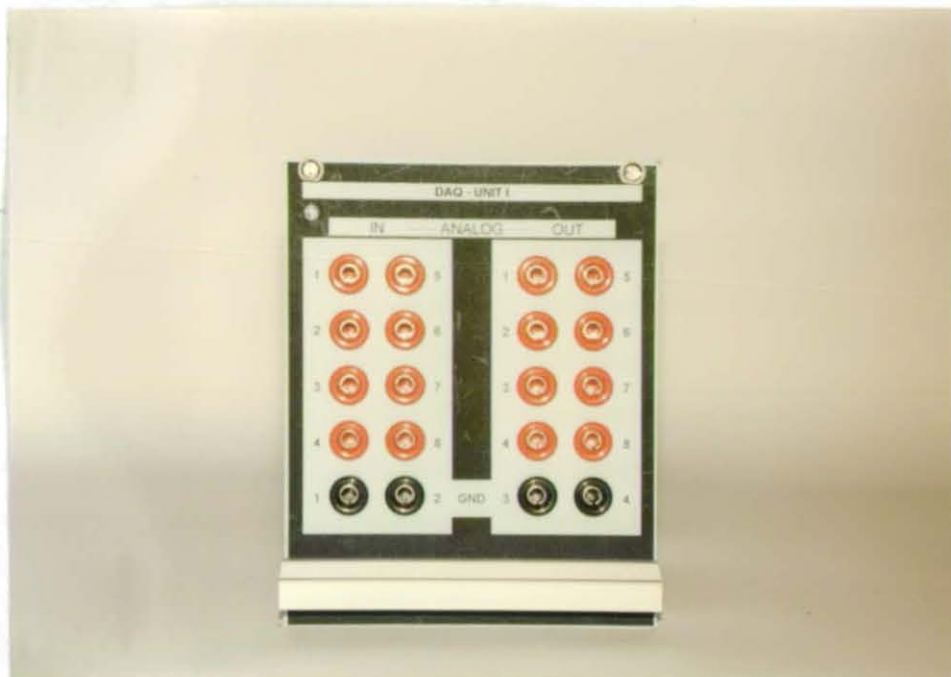


Photo D2: Front view of the DAQ Unit module I

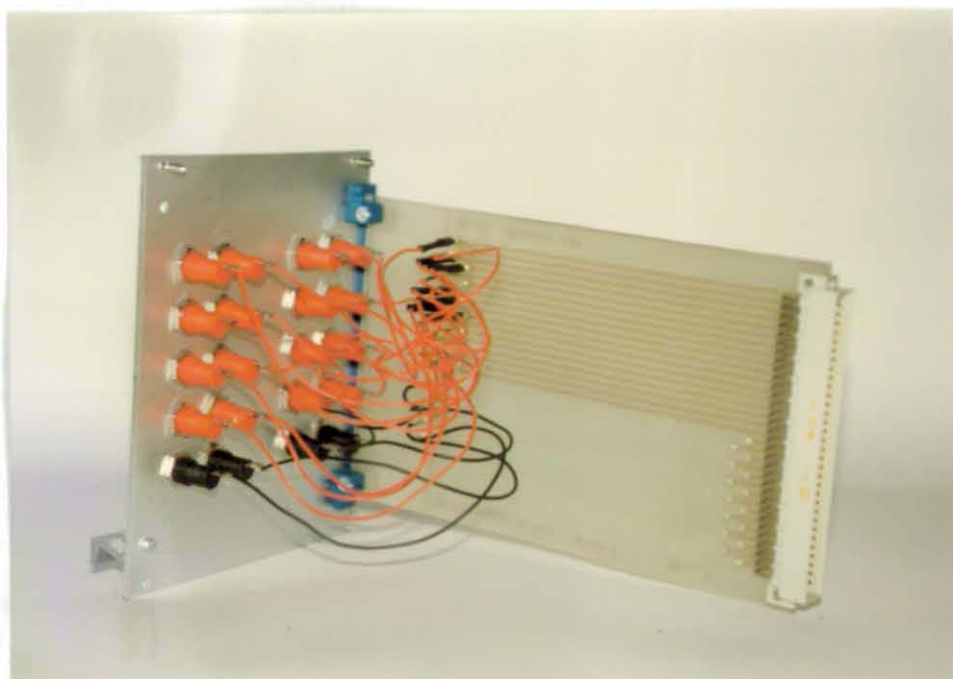


Photo D3: Side view of the DAQ Unit module I



Photo D4: Front view of the DAQ Unit module II

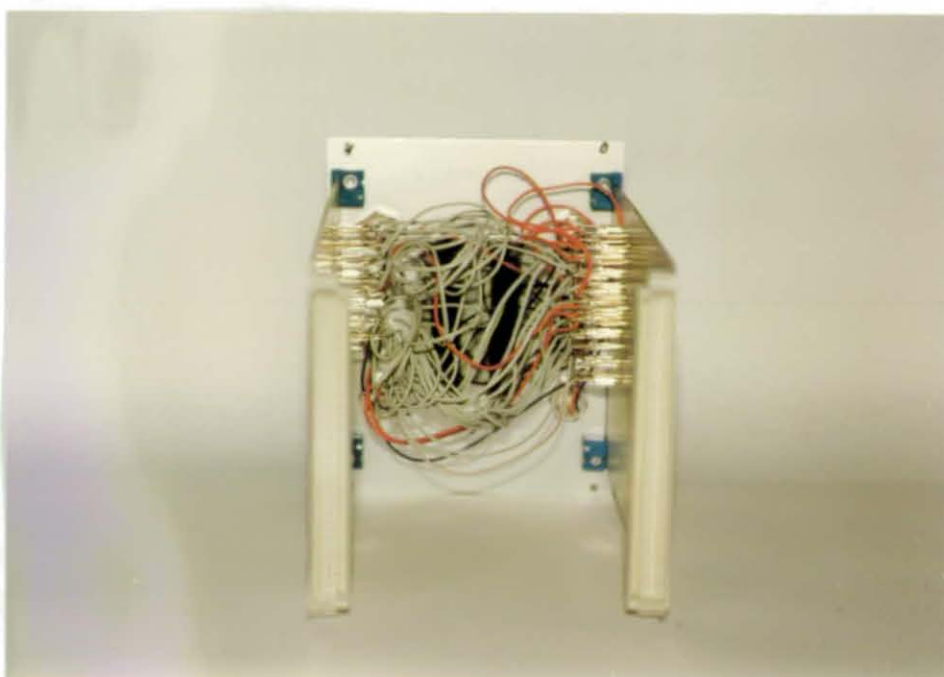


Photo D5: Side view of the DAQ Unit module II

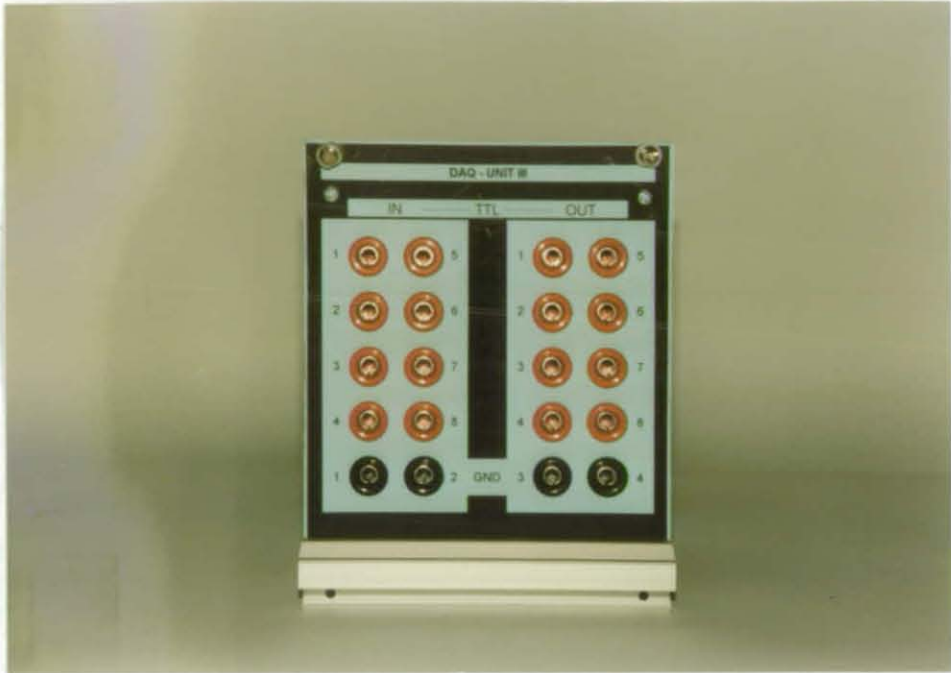


Photo D6: Front view of the DAQ Unit module III

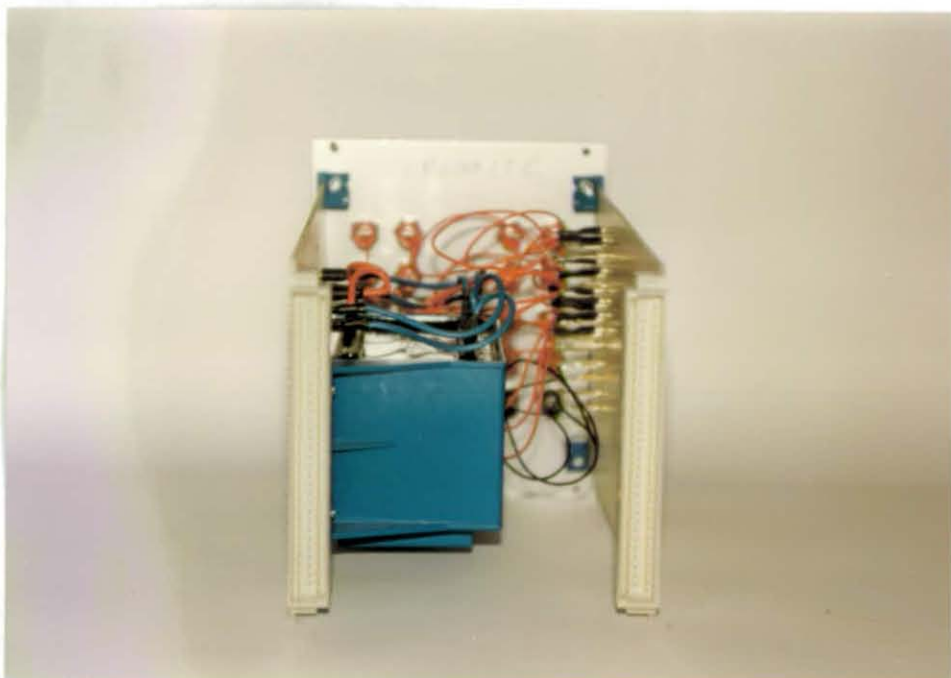
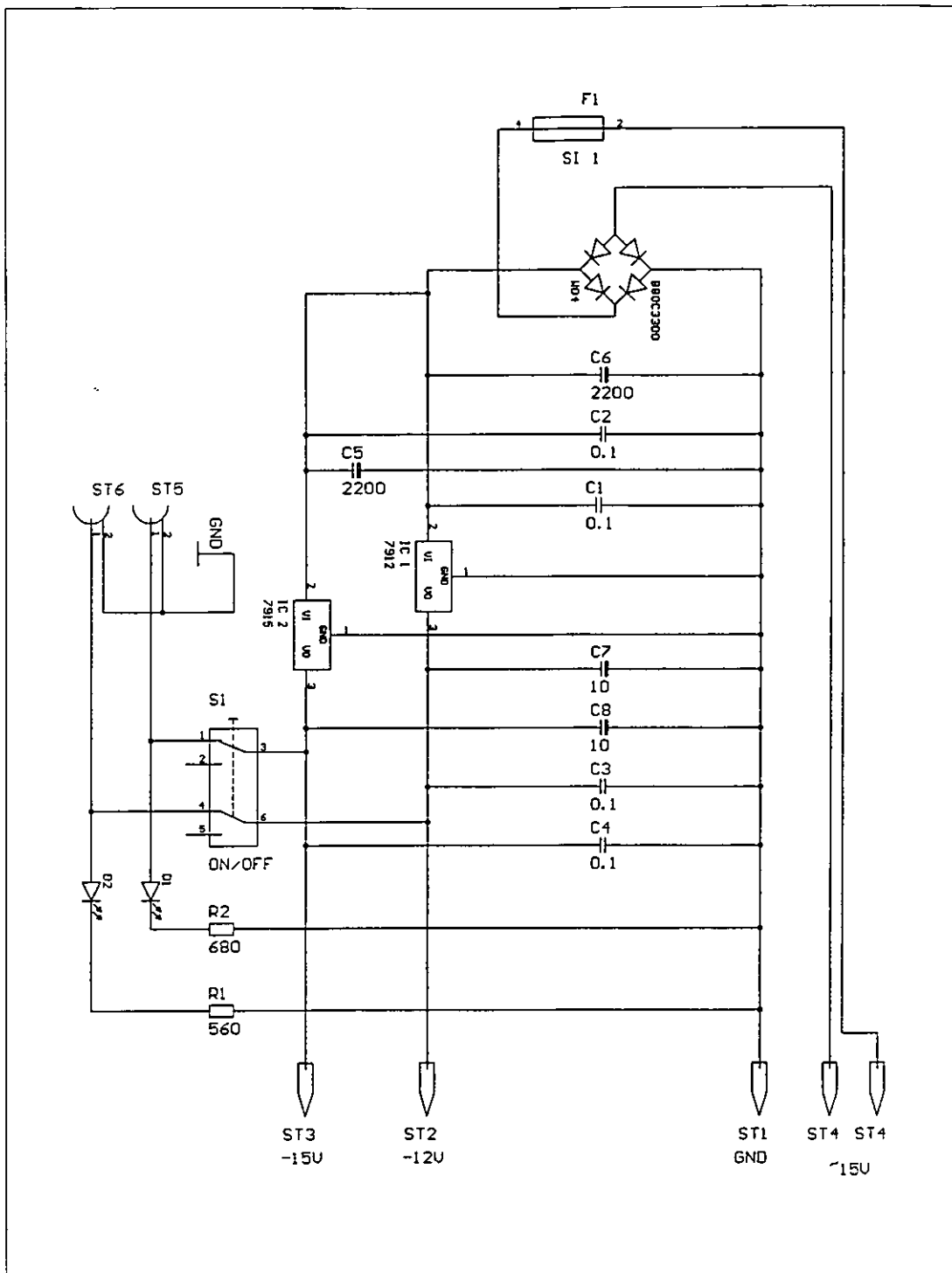


Photo D7: Side view of the DAQ Unit module III

D.3 Power supply I

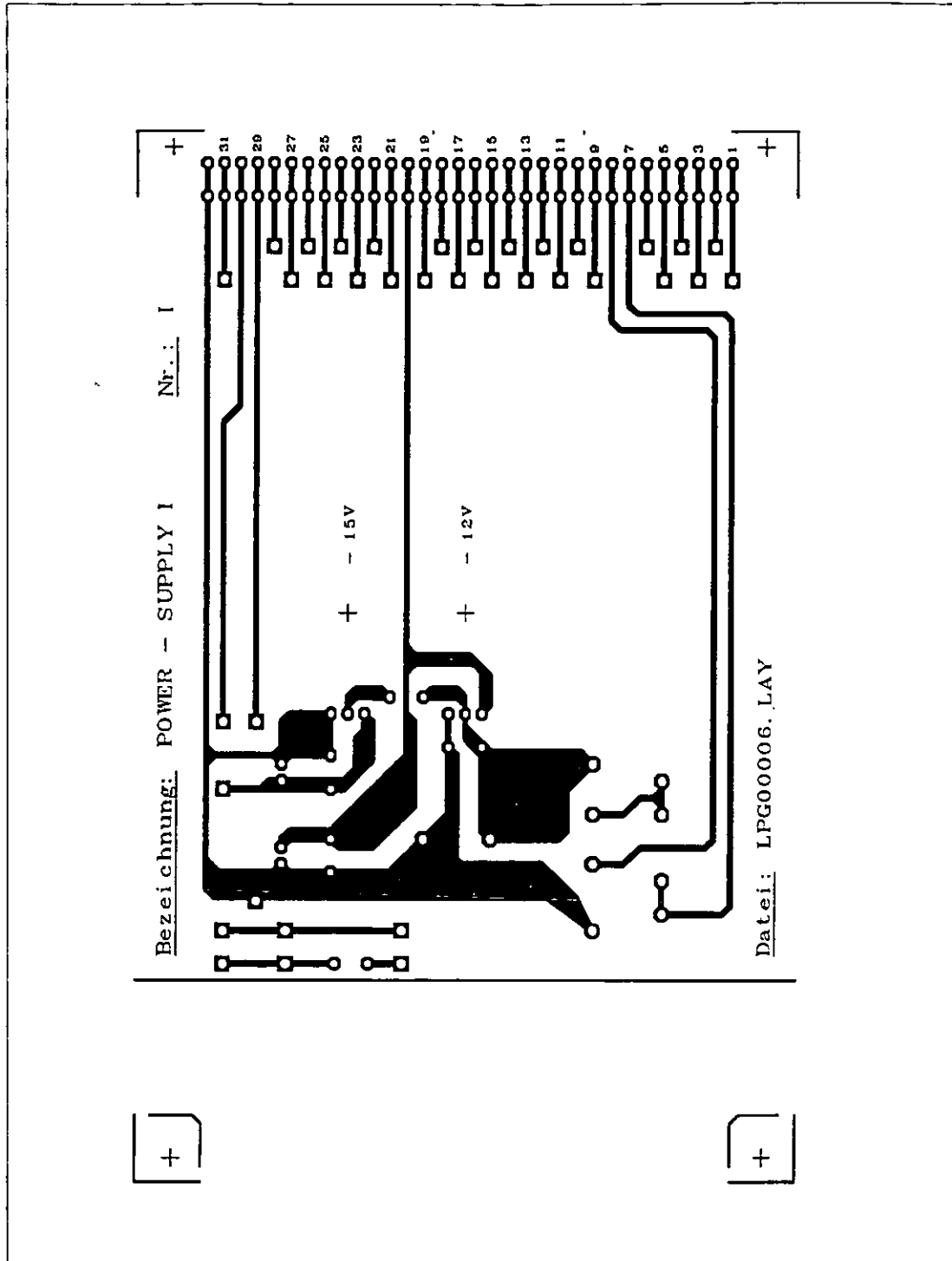
CONTENTS	PAGE #
1. Circuit diagram	D22
2. Parts list	D23
3. PCB layout	D24
4. Bus port	D25
5. Photographs	D26



Part-No.:	Title:
Scale:	Circuit diagram of the power supply I
Material:	
Date: October 1996	FHO-Fachhochschule Ostfriesland -Institut für Lasertechnik Ostfriesland -
ENGR: Dipl.-Ing. U. Samuels	

D.3.2 Parts list

<u>Part No.</u>	<u>Description</u>
R1	Resistor 560 Ω
R2	Resistor 680 Ω
C1	Capacity 0.1 μ F/100V
C2	Capacity 0.1 μ F/100V
C3	Capacity 0.1 μ F/100V
C4	Capacity 0.1 μ F/25V electrolyte
C5	Capacity 2200 μ F/25V electrolyte
C6	Capacity 2200 μ F/25V electrolyte
C7	Capacity 10 μ F / 25V electrolyte
C8	Capacity 10 μ F / 25V electrolyte
D1	LED, 5mm, red
D2	LED, 5mm, red
W04	Bridge rectifier
IC1	7912 (-12V)
IC2	7915 (-15V)
S1	Switch
F1	Fuse 100mA



Part-No.:	Title: PCB of the power supply I
Scale:	
Material:	
Date: October 1996	FHO-Fachhochschule Ostfriesland -Institut für Lasertechnik Ostfriesland -
ENGR: Dipl.-Ing. U. Samuels	

D.3.4 Bus port

Pin #	Description	DAQ - Unit III, Nr.: II
1		
2		
3		
4		
5		
6		
7	SEC 1 - ~15V	Pin#: 26
8	SEC 1 - ~15V	Pin#: 25
9	SEC 2 - ~15V	
10	SEC 2 - ~15V	
11		
12		
13		
14		
15		
16		
17		
18		
19		
20	- 12V	Pin#: 13
21	+ 15V	
22		
23		
24		
25		
26	+ 12V	
27	- 12V	
28	+ 5V	
29	+ 15V	Pin#: 4
30	- 15V	Pin#: 3
31	E 240 - X	
32	GND	Pin#: 1

D.3.5 Photographs

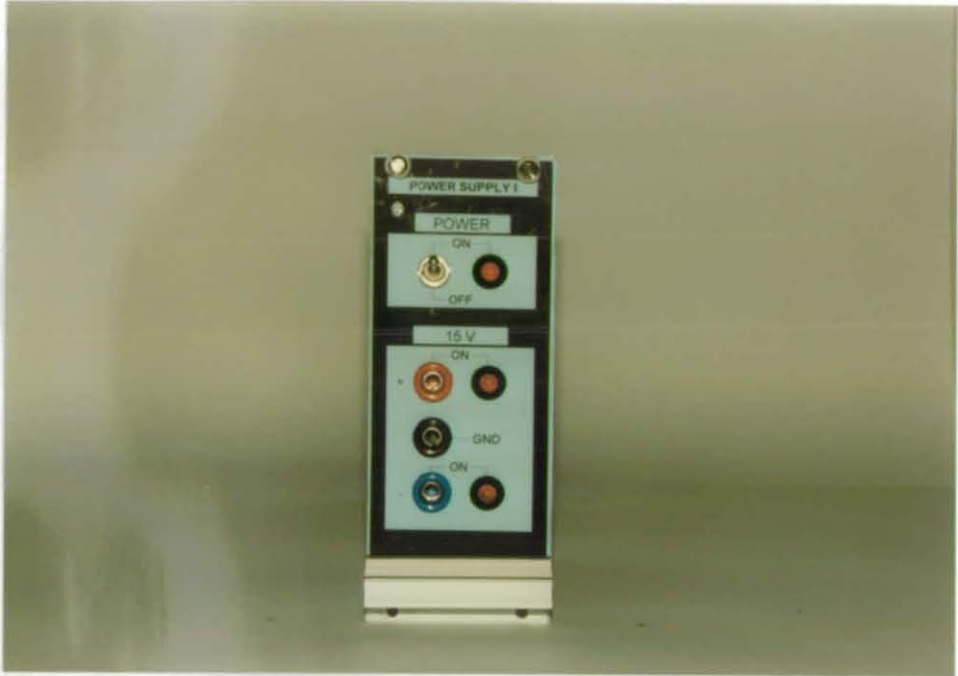


Photo D8: Front view of the power supply I

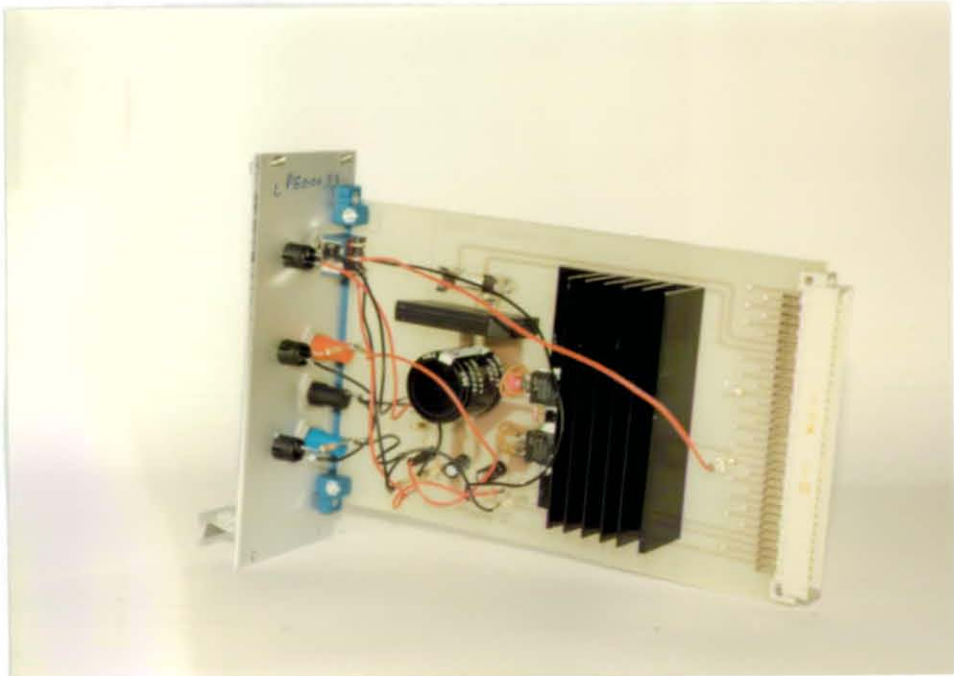
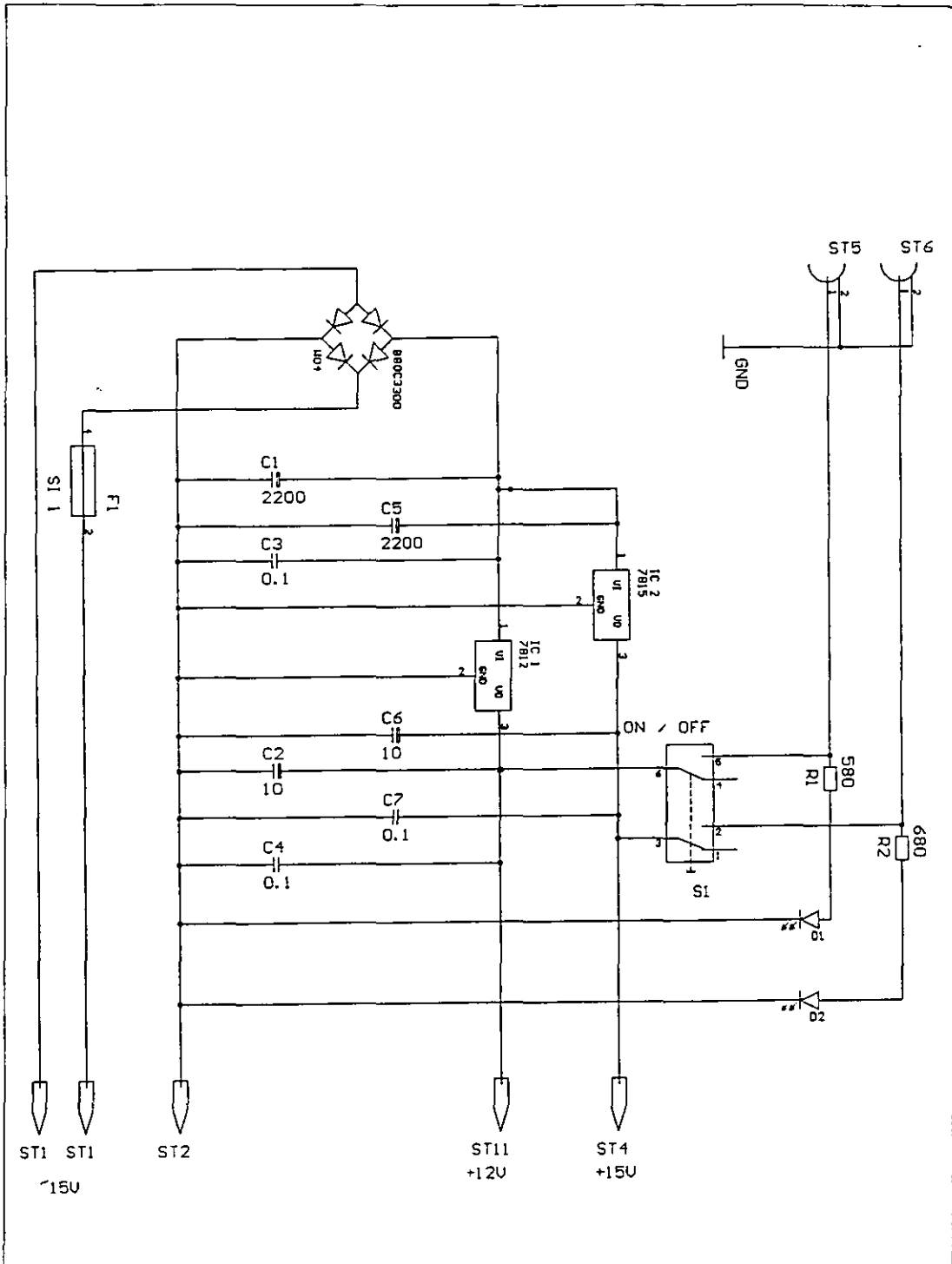


Photo D9: Side view of the power supply I

D.4 Power supply II

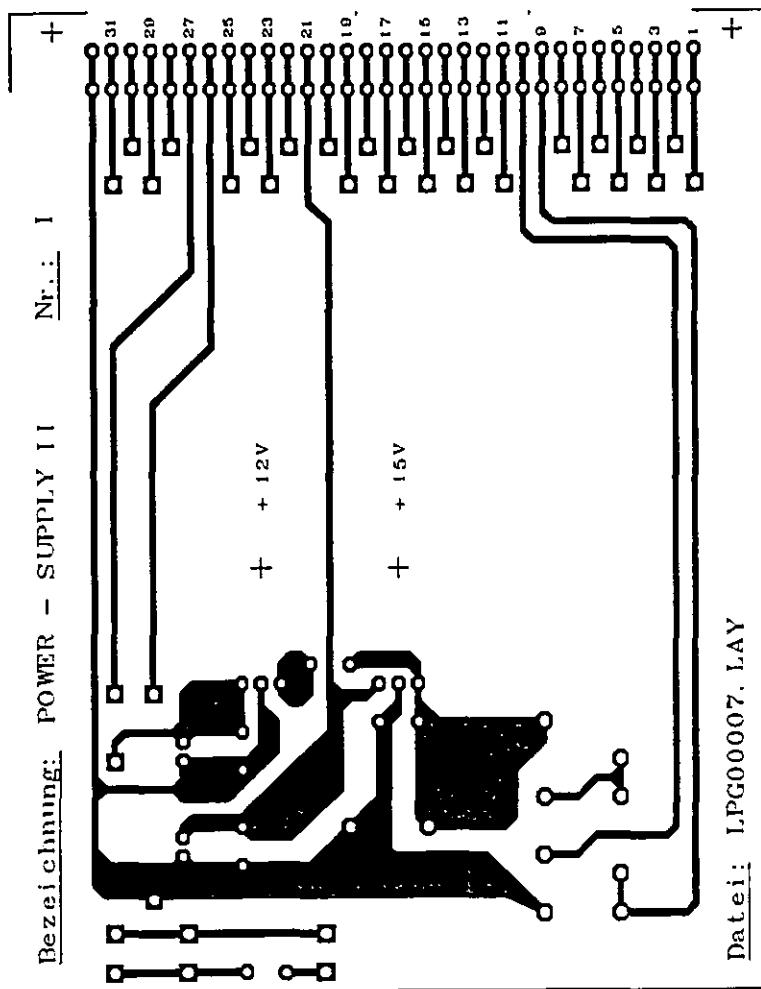
CONTENTS	PAGE #
1. Circuit diagram	D28
2. Parts list	D29
3. PCB layout	D30
4. Bus port	D31
5. Photographs	D32



Part-No.:	Title: Circuit diagram of the power supply II
Scale:	
Material:	
Date: October 1996	FHO-Fachhochschule Ostfriesland -Institut für Lasertechnik Ostfriesland -
ENGR: Dipl.-Ing. U. Samuels	

D.4.2 Parts list

<u>Part No.</u>	<u>Description</u>
R1	Resistor 560 Ω
R2	Resistor 680 Ω
C1	Capacity 2200 μ F/25V electrolyte
C2	Capacity 10 μ F / 25V electrolyte
C3	Capacity 0.1 μ F/100V
C4	Capacity 0.1 μ F/100V
C5	Capacity 2200 μ F/25V electrolyte
C6	Capacity 10 μ F / 25V electrolyte
C7	Capacity 0.1 μ F/25V electrolyte
D1	LED, 5mm, red
D2	LED, 5mm, red
W04	Bridge rectifier
IC1	7812 (+12V)
IC2	7815 (+15V)
S1	Switch
F1	Fuse 100mA



Part-No.:	Title: PCB of the power supply II
Scale:	
Material:	
Date: October 1996	FHO-Fachhochschule Ostfriesland -Institut für Lasertechnik Ostfriesland -
ENGR: Dipl.-Ing. U. Samuels	

D.4.4 Bus port

Pin #	Description	DAQ - Unit III, No.: II
1		
2		
3		
4		
5		
6		
7	SEC 1 - ~15V	
8	SEC 1 - ~15V	
9	SEC 2 - ~15V	Pin#: 24
10	SEC 2 - ~15V	Pin#: 23
11		
12		
13		
14		
15		
16		
17		
18		
19		
20	- 12V	
21	+ 15V	Pin#: 12
22		
23		
24		
25		
26	+ 12V	Pin#: 7
27	- 12V	Pin#: 6
28	+ 5V	
29	+ 15V	
30	- 15V	
31	E 240 - X	
32	GND	Pin#: 1

D.4.5 Photographs

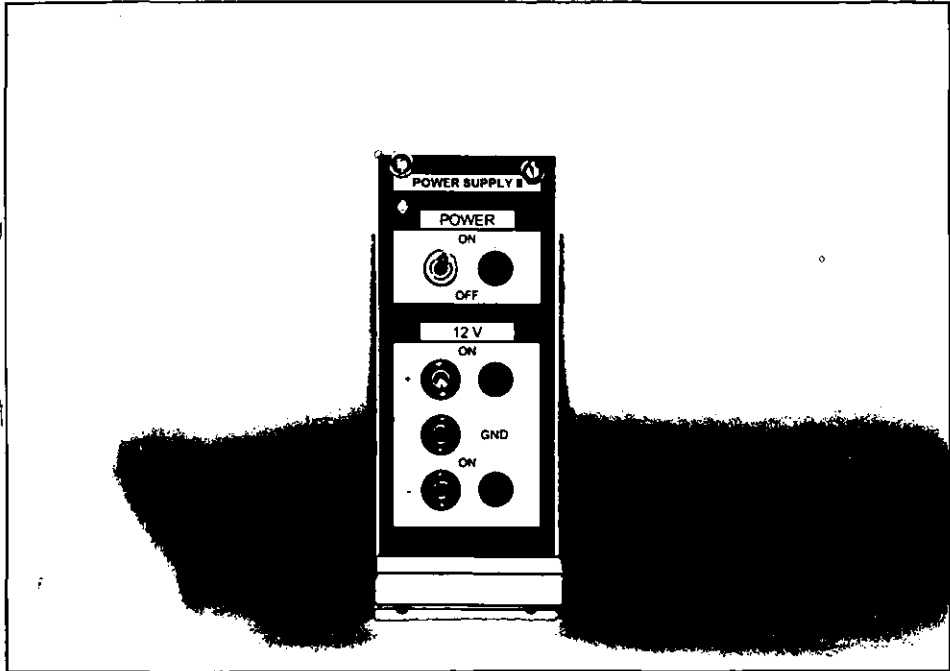


Photo D10: Front view of the power supply II

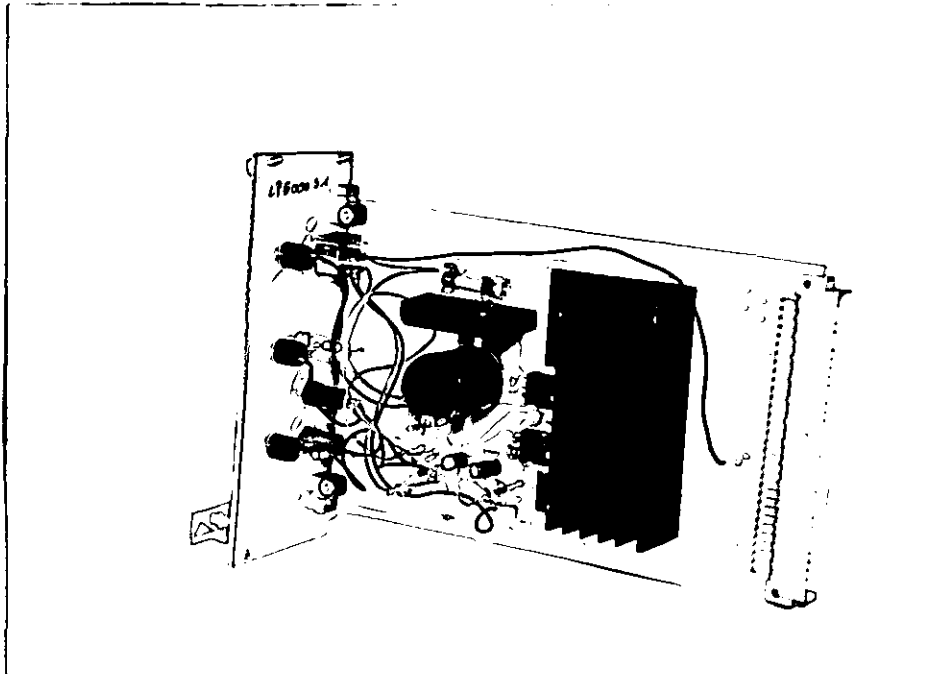


Photo D11: Side view of the power supply II

D.4.5 Photographs



Photo D10: Front view of the power supply II

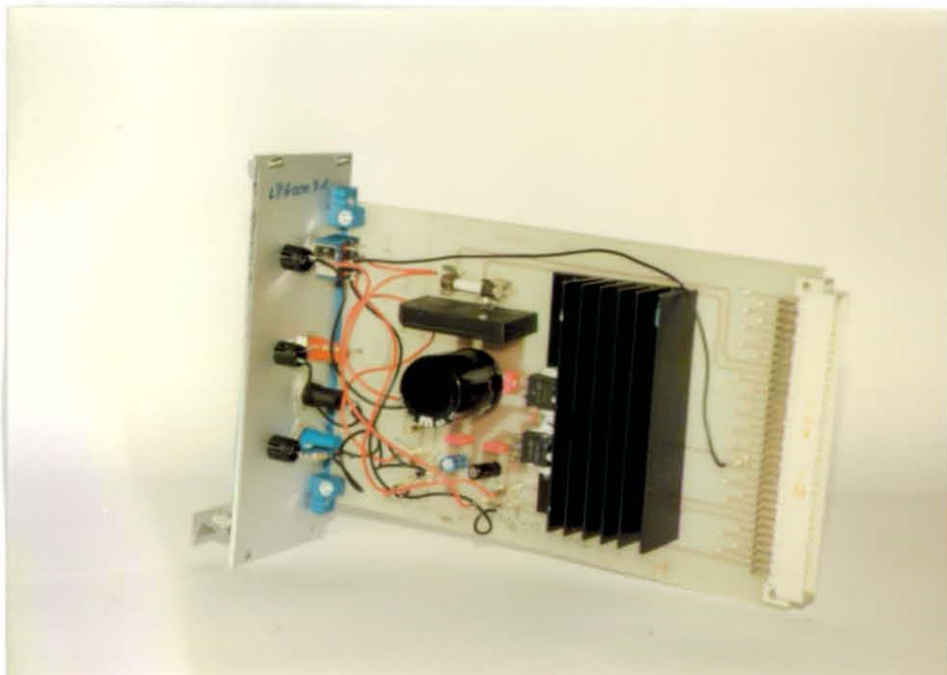
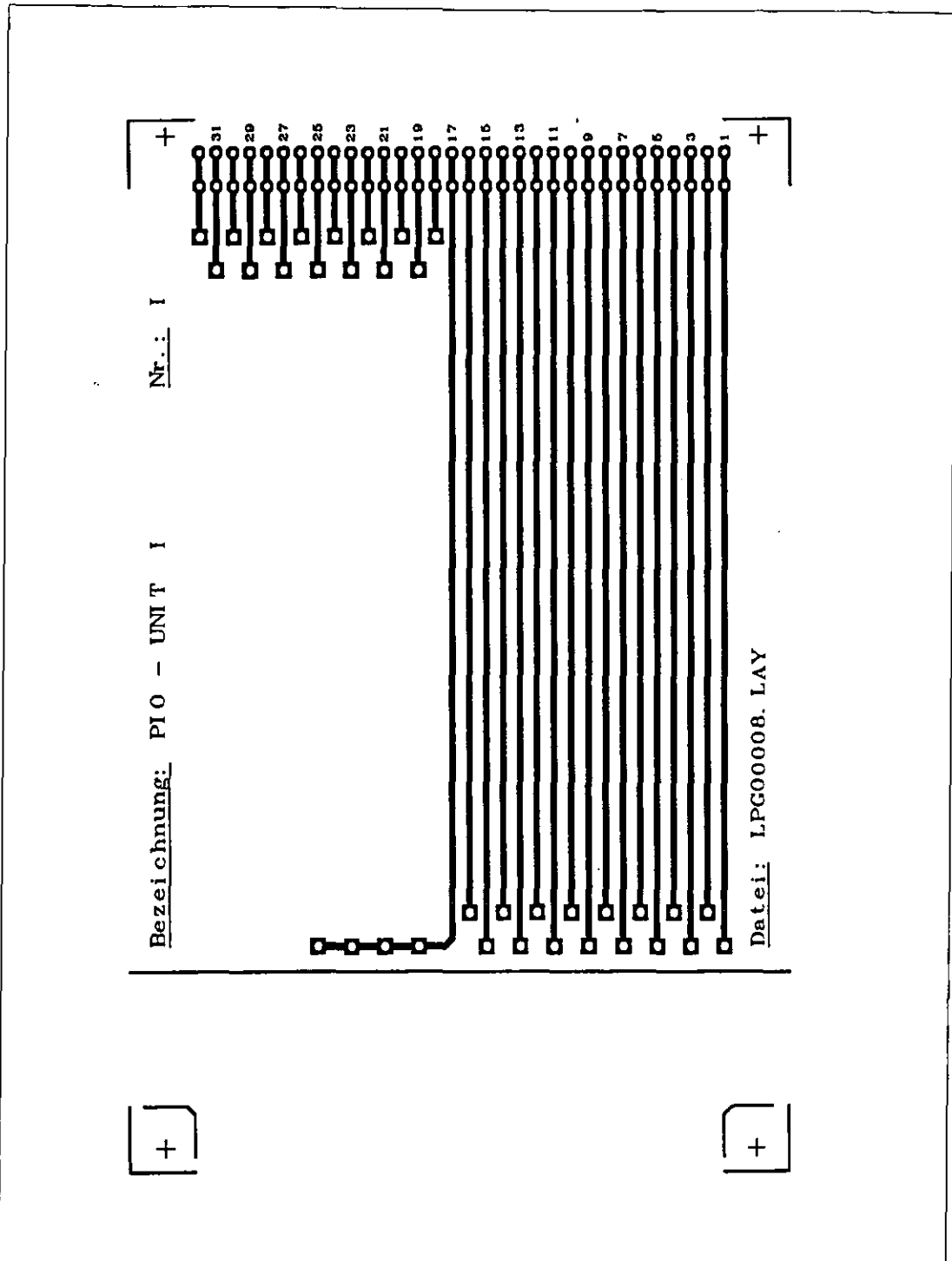


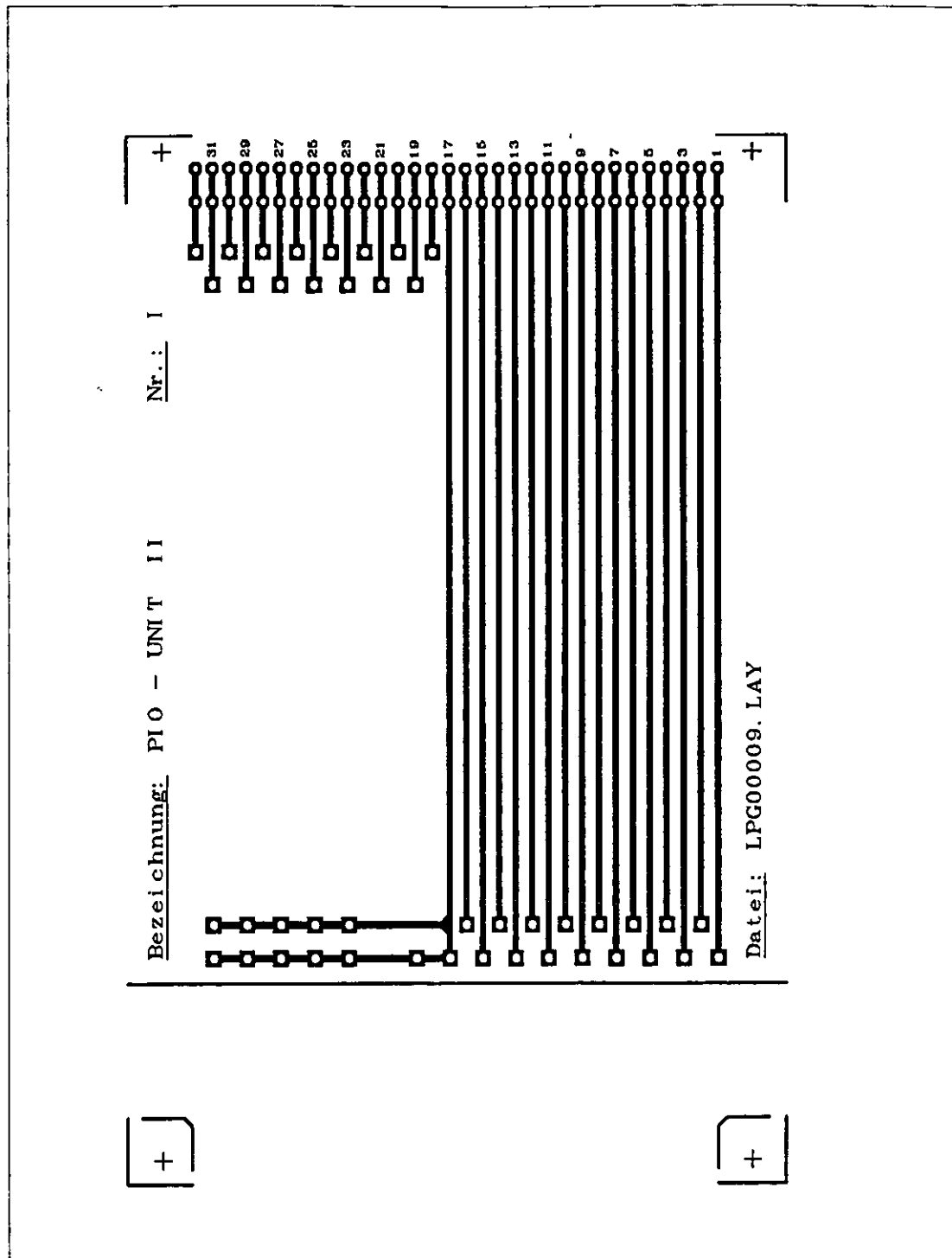
Photo D11: Side view of the power supply II

D.5 PIO Unit

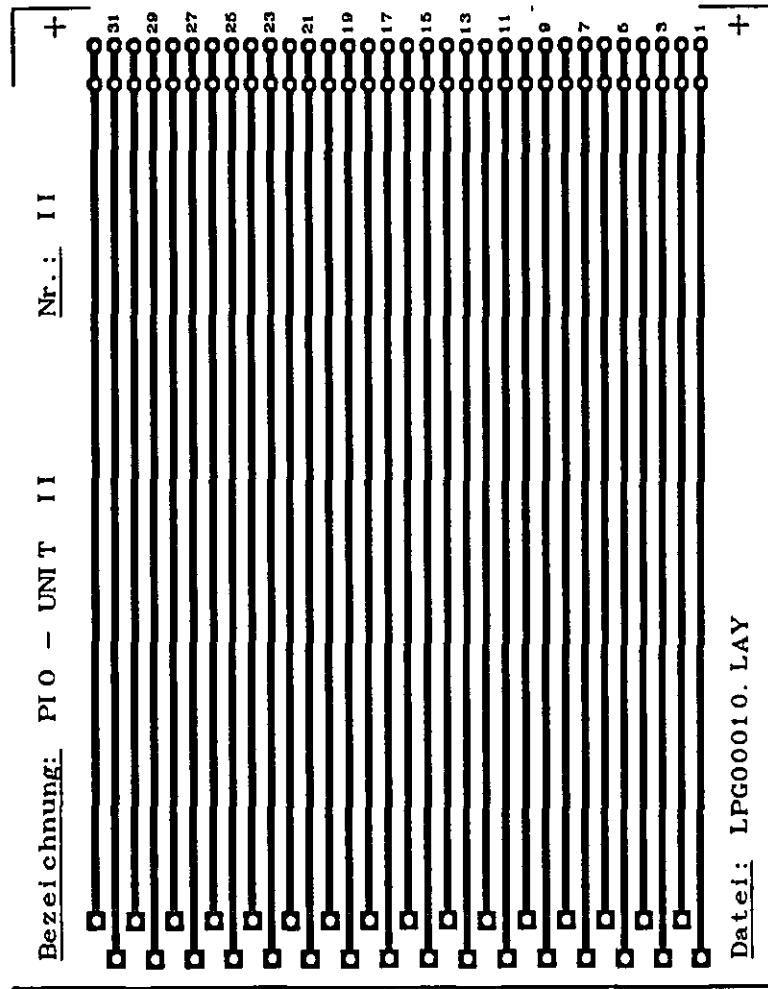
CONTENTS	PAGE #
1. PCB layout module I	D34
2. PCB layout module II/I	D35
3. PCB layout module II/II	D36
4. PCB layout module III	D37
5. PCB layout module IV	D38
6. Bus port module I	D39
7. Bus port module II/I	D40
8. Bus port module II/II	D41
9. Bus port module III	D41
10. Bus port module IV	D43
11. Pin connection of the input terminal	D44
12. Photographs	D45-D48



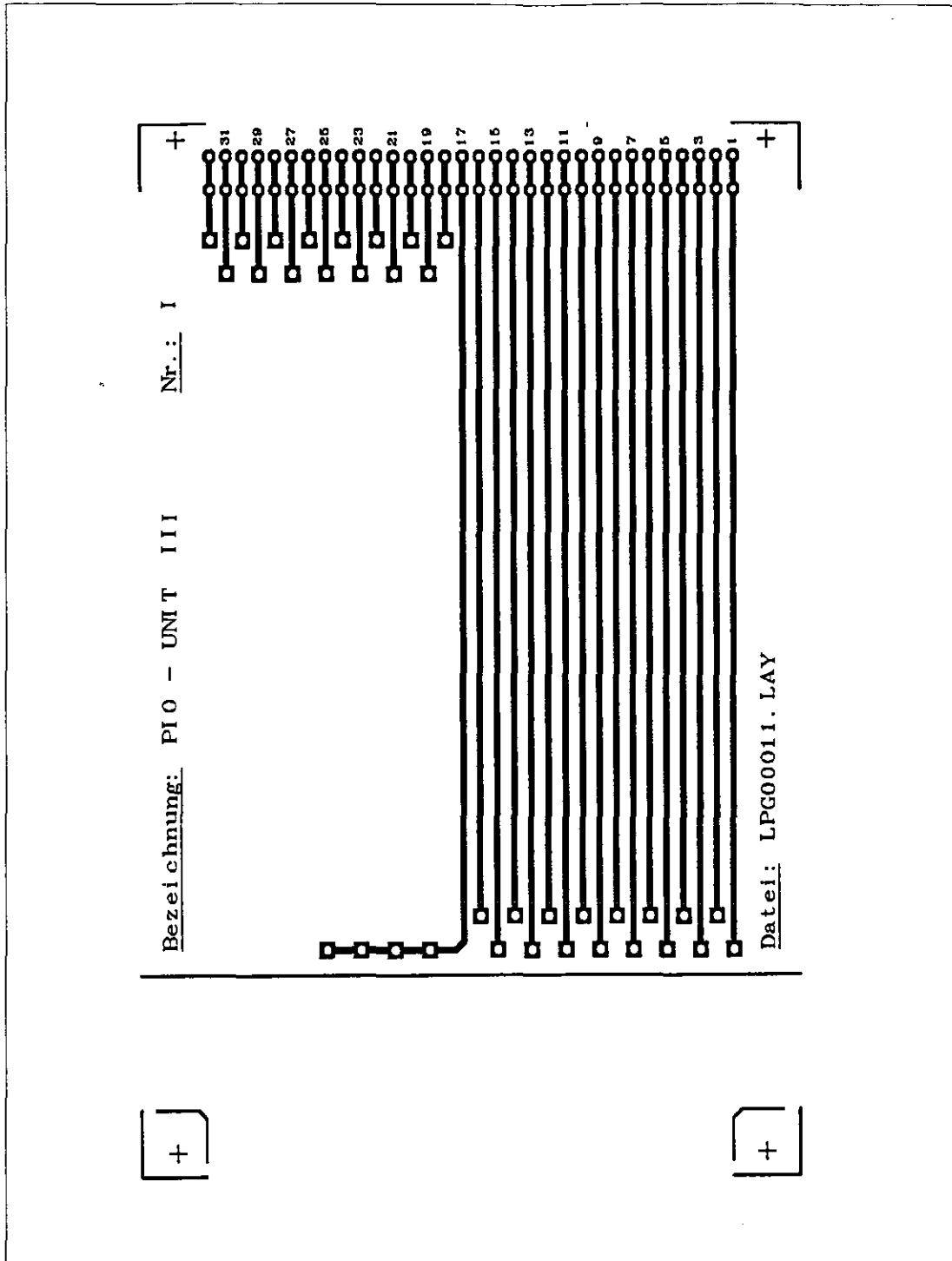
Part-No.:	Title: PCB of the PIO Unit module I
Scale:	
Material:	
Date: October 1996	FHO-Fachhochschule Ostfriesland -Institut für Lasertechnik Ostfriesland -
ENGR: Dipl.-Ing. U. Samuels	



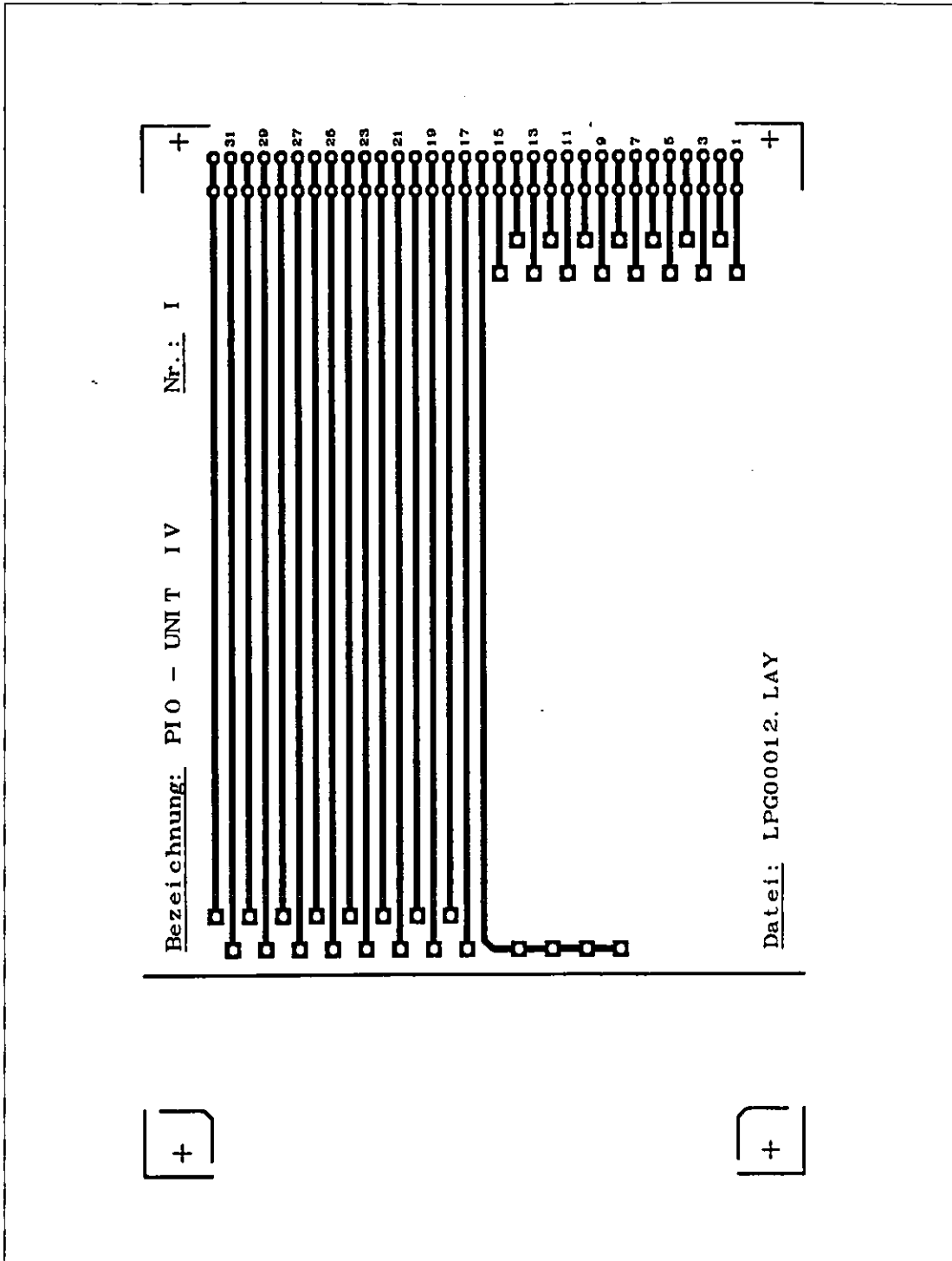
Part-No.:	Title: PCB of the PIO Unit module II/I
Scale:	
Material:	
Date: October 1996	FHO-Fachhochschule Ostfriesland -Institut für Lasertechnik Ostfriesland -
ENGR: Dipl.-Ing. U. Samuels	



Part-No.:	Title: PCB of the PIO Unit module II/II
Scale:	
Material:	
Date: October 1996	FHO-Fachhochschule Ostfriesland -Institut für Lasertechnik Ostfriesland -
ENGR: Dipl.-Ing. U. Samuels	



Part-No.:	Title: PCB of the PIO Unit module III
Scale:	
Material:	
Date: October 1996	FHO-Fachhochschule Ostfriesland -Institut für Lasertechnik Ostfriesland -
ENGR: Dipl.-Ing. U. Samuels	



Part-No.:	Title: PCB of the PIO Unit module IV
Scale:	
Material:	
Date: October 1996	FHO-Fachhochschule Ostfriesland -Institut für Lasertechnik Ostfriesland -
ENGR: Dipl.-Ing. U. Samuels	

D.5.6 Bus port module I

Pin #	Description	PIO - UNIT II, No.: I
1	Port A 1 - Nr.: 1	Pin#: 1
2	Port A 1 - Nr.: 2	Pin#: 2
3	Port A 1 - Nr.: 3	Pin#: 3
4	Port A 1 - Nr.: 4	Pin#: 4
5	Port A 1 - Nr.: 5	Pin#: 5
6	Port A 1 - Nr.: 6	Pin#: 6
7	Port A 1 - Nr.: 7	Pin#: 7
8	Port A 1 - Nr.: 8	Pin#: 8
9	Port A 2 - Nr.: 1	Pin#: 9
10	Port A 2 - Nr.: 2	Pin#: 10
11	Port A 2 - Nr.: 3	Pin#: 11
12	Port A 2 - Nr.: 4	Pin#: 12
13	Port A 2 - Nr.: 5	Pin#: 13
14	Port A 2 - Nr.: 6	Pin#: 14
15	Port A 2 - Nr.: 7	Pin#: 15
16	Port A 2 - Nr.: 8	Pin#: 16
17	GND	
18		
19		
20		
21		
22		
23		
24		
25		
26		
27		
28		
29		
30		
31		
32		

D.5.7 Bus port module II/I

Pin #	Description	PIO - UNIT II (C: 50)
1	PIO 1 Port A Bit 0	Pin#: 1
2	PIO 1 Port A Bit 1	Pin#: 2
3	PIO 1 Port A Bit 2	Pin#: 3
4	PIO 1 Port A Bit 3	Pin#: 4
5	PIO 1 Port A Bit 4	Pin#: 5
6	PIO 1 Port A Bit 5	Pin#: 6
7	PIO 1 Port A Bit 6	Pin#: 7
8	PIO 1 Port A Bit 7	Pin#: 8
9	PIO 2 Port A Bit 0	Pin#: 25
10	PIO 2 Port A Bit 1	Pin#: 26
11	PIO 2 Port A Bit 2	Pin#: 27
12	PIO 2 Port A Bit 3	Pin#: 28
13	PIO 2 Port A Bit 4	Pin#: 29
14	PIO 2 Port A Bit 5	Pin#: 30
15	PIO 2 Port A Bit 6	Pin#: 31
16	PIO 2 Port A Bit 7	Pin#: 32
17	GND	Pin#: 49 and 50
18		
19		
20		
21		
22		
23		
24		
25		
26		
27		
28		
29		
30		
31		
32		

D.5.8 Bus port module II/II

Pin #	Description	PIO - UNIT II (C: 50)
32	PIO 1 Port B Bit 0	Pin#: 17
31	PIO 1 Port B Bit 1	Pin#: 18
30	PIO 1 Port B Bit 2	Pin#: 19
29	PIO 1 Port B Bit 3	Pin#: 20
28	PIO 1 Port B Bit 4	Pin#: 21
27	PIO 1 Port B Bit 5	Pin#: 22
26	PIO 1 Port B Bit 6	Pin#: 23
25	PIO 1 Port B Bit 7	Pin#: 24
24	PIO 2 Port B Bit 0	Pin#: 41
23	PIO 2 Port B Bit 1	Pin#: 42
22	PIO 2 Port B Bit 2	Pin#: 43
21	PIO 2 Port B Bit 3	Pin#: 44
20	PIO 2 Port B Bit 4	Pin#: 45
19	PIO 2 Port B Bit 5	Pin#: 46
18	PIO 2 Port B Bit 6	Pin#: 47
17	PIO 2 Port B Bit 7	Pin#: 48
16	PIO 1 Port C Bit 0	Pin#: 9
15	PIO 1 Port C Bit 1	Pin#: 10
14	PIO 1 Port C Bit 2	Pin#: 11
13	PIO 1 Port C Bit 3	Pin#: 12
12	PIO 1 Port C Bit 4	Pin#: 13
11	PIO 1 Port C Bit 5	Pin#: 14
10	PIO 1 Port C Bit 6	Pin#: 15
9	PIO 1 Port C Bit 7	Pin#: 16
8	PIO 2 Port C Bit 0	Pin#: 33
7	PIO 2 Port C Bit 1	Pin#: 34
6	PIO 2 Port C Bit 2	Pin#: 35
5	PIO 2 Port C Bit 3	Pin#: 36
4	PIO 2 Port C Bit 4	Pin#: 37
3	PIO 2 Port C Bit 5	Pin#: 38
2	PIO 2 Port C Bit 6	Pin#: 39
1	PIO 2 Port C Bit 7	Pin#: 40

D.5.9 Bus port module III

Pin #	Description	PIO - UNIT II, No.: II
1	Port B 1 - Nr.: 1	Pin#: 32
2	Port B 1 - Nr.: 2	Pin#: 31
3	Port B 1 - Nr.: 3	Pin#: 30
4	Port B 1 - Nr.: 4	Pin#: 29
5	Port B 1 - Nr.: 5	Pin#: 28
6	Port B 1 - Nr.: 6	Pin#: 27
7	Port B 1 - Nr.: 7	Pin#: 26
8	Port B 1 - Nr.: 8	Pin#: 25
9	Port B 2 - Nr.: 1	Pin#: 24
10	Port B 2 - Nr.: 2	Pin#: 23
11	Port B 2 - Nr.: 3	Pin#: 22
12	Port B 2 - Nr.: 4	Pin#: 21
13	Port B 2 - Nr.: 5	Pin#: 20
14	Port B 2 - Nr.: 6	Pin#: 19
15	Port B 2 - Nr.: 7	Pin#: 18
16	Port B 2 - Nr.: 8	Pin#: 17
17	GND	
18		
19		
20		
21		
22		
23		
24		
25		
26		
27		
28		
29		
30		
31		
32		

D.5.10 Bus port module IV

Pin #	Description	PIO - UNIT II, No.: II
1		
2		
3		
4		
5		
6		
7		
8		
9		
10		
11		
12		
13		
14		
15		
16	GND	
17	Port C 1 - Nr.: 1	Pin#: 16
18	Port C 1 - Nr.: 2	Pin#: 15
19	Port C 1 - Nr.: 3	Pin#: 14
20	Port C 1 - Nr.: 4	Pin#: 13
21	Port C 1 - Nr.: 5	Pin#: 12
22	Port C 1 - Nr.: 6	Pin#: 11
23	Port C 1 - Nr.: 7	Pin#: 10
24	Port C 1 - Nr.: 8	Pin#: 9
25	Port C 2 - Nr.: 1	Pin#: 8
26	Port C 2 - Nr.: 2	Pin#: 7
27	Port C 2 - Nr.: 3	Pin#: 6
28	Port C 2 - Nr.: 4	Pin#: 5
29	Port C 2 - Nr.: 5	Pin#: 4
30	Port C 2 - Nr.: 6	Pin#: 3
31	Port C 2 - Nr.: 7	Pin#: 2
32	Port C 2 - Nr.: 8	Pin#: 1

D.5.11 Pin connection of the input terminal

Pin #	Description	Function
1	PIO 1 Port A Bit 0	A10
2	PIO 1 Port A Bit 1	A11
3	PIO 1 Port A Bit 2	A12
4	PIO 1 Port A Bit 3	A13
5	PIO 1 Port A Bit 4	A14
6	PIO 1 Port A Bit 5	A15
7	PIO 1 Port A Bit 6	A16
8	PIO 1 Port A Bit 7	A17
9	PIO 1 Port C Bit 0	C10
10	PIO 1 Port C Bit 1	C11
11	PIO 1 Port C Bit 2	C12
12	PIO 1 Port C Bit 3	C13
13	PIO 1 Port C Bit 4	C14
14	PIO 1 Port C Bit 5	C15
15	PIO 1 Port C Bit 6	C16
16	PIO 1 Port C Bit 7	C17
17	PIO 1 Port B Bit 0	B10
18	PIO 1 Port B Bit 1	B11
19	PIO 1 Port B Bit 2	B12
20	PIO 1 Port B Bit 3	B13
21	PIO 1 Port B Bit 4	B14
22	PIO 1 Port B Bit 5	B15
23	PIO 1 Port B Bit 6	B16
24	PIO 1 Port B Bit 7	B17
25	PIO 2 Port A Bit 0	A20
26	PIO 2 Port A Bit 1	A21
27	PIO 2 Port A Bit 2	A22
28	PIO 2 Port A Bit 3	A23
29	PIO 2 Port A Bit 4	A24
30	PIO 2 Port A Bit 5	A25
31	PIO 2 Port A Bit 6	A26
32	PIO 2 Port A Bit 7	A27
33	PIO 2 Port C Bit 0	C20
34	PIO 2 Port C Bit 1	C21
35	PIO 2 Port C Bit 2	C22
36	PIO 2 Port C Bit 3	C23
37	PIO 2 Port C Bit 4	C24
38	PIO 2 Port C Bit 5	C25
39	PIO 2 Port C Bit 6	C26
40	PIO 2 Port C Bit 7	C27
41	PIO 2 Port B Bit 0	B20
42	PIO 2 Port B Bit 1	B21
43	PIO 2 Port B Bit 2	B22
44	PIO 2 Port B Bit 3	B23
45	PIO 2 Port B Bit 4	B24
46	PIO 2 Port B Bit 5	B25
47	PIO 2 Port B Bit 6	B26
48	PIO 2 Port B Bit 7	B27
49	GND	
50	GND	

D.5.12 Photographs

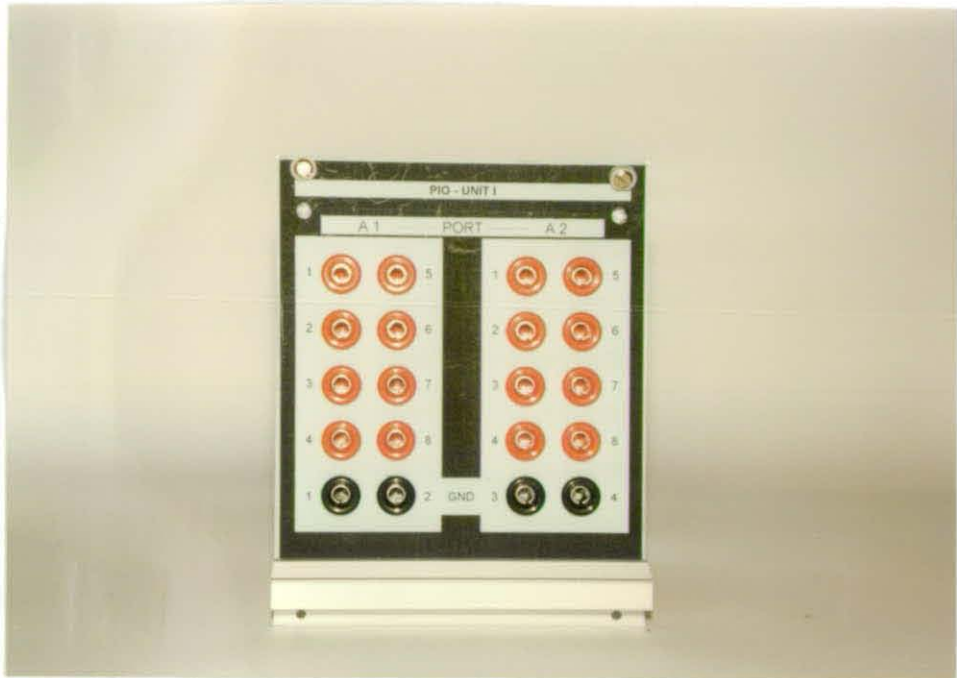


Photo D12: Front view of the PIO Unit module I

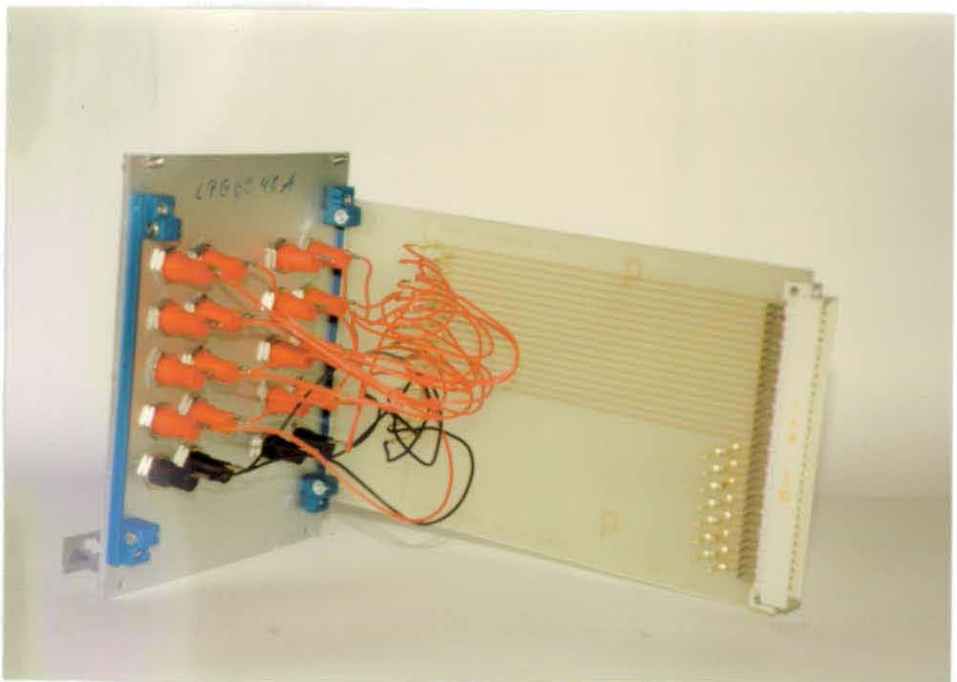


Photo D13: Side view of the PIO Unit module I



Photo D14: Front view of the PIO Unit module II

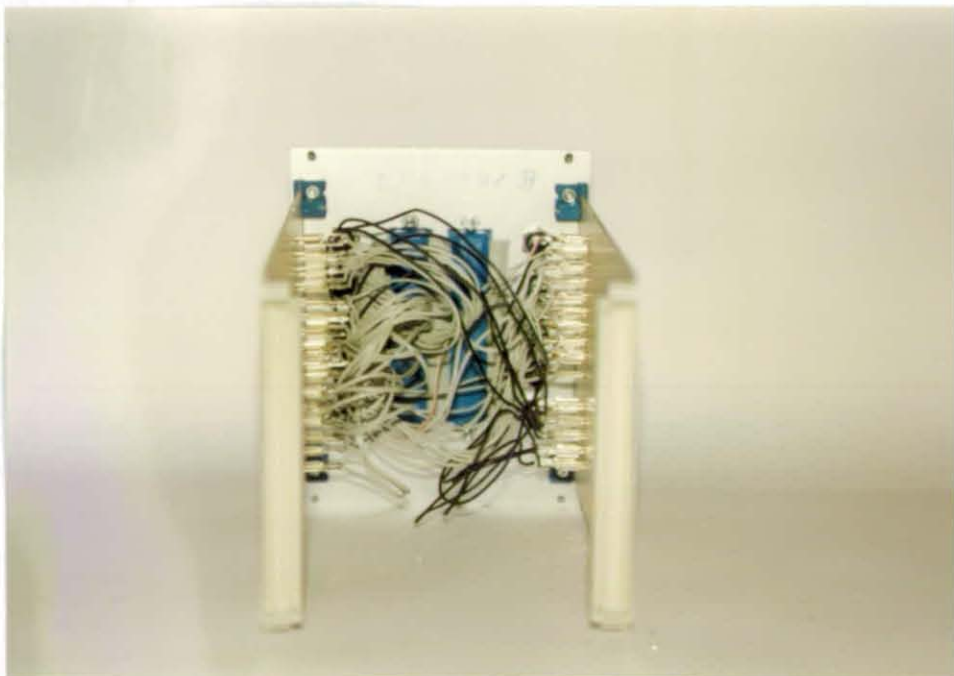


Photo D15: Side view of the PIO Unit module II

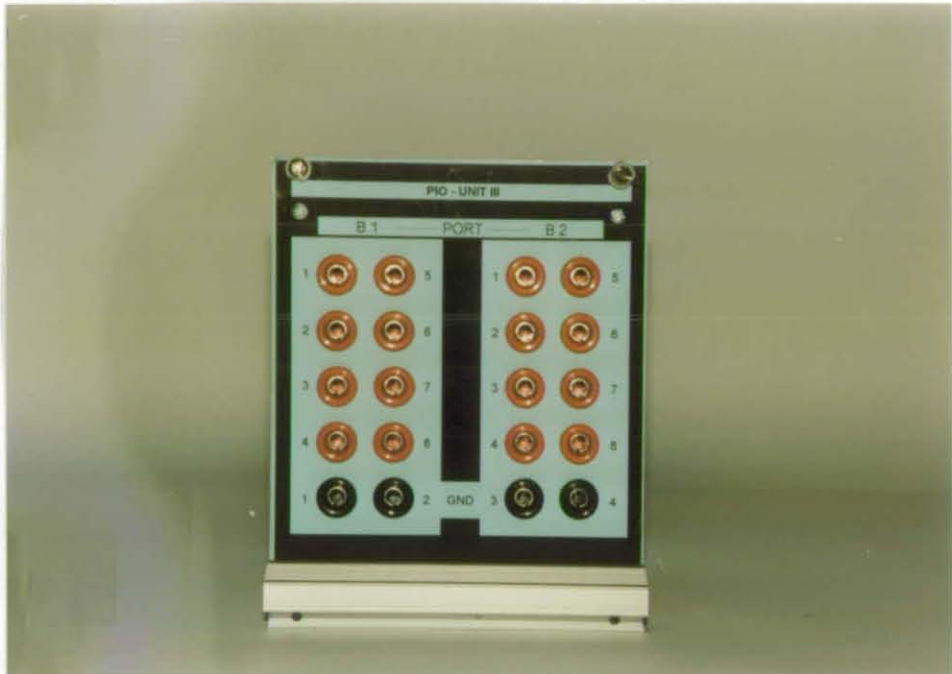


Photo D16: Front view of the PIO Unit module III

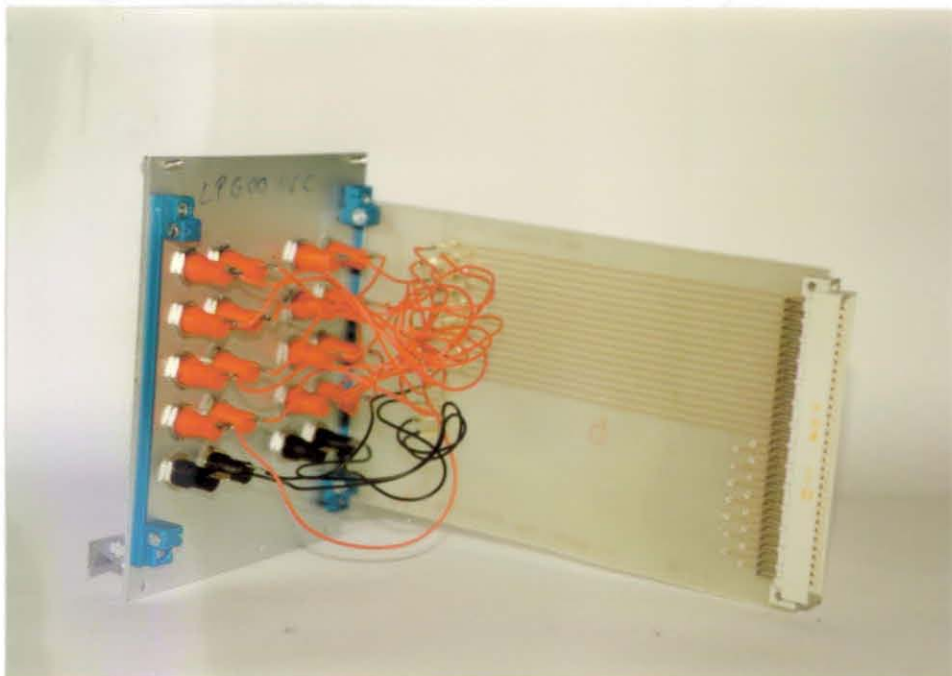


Photo D17: Side view of the PIO Unit module III

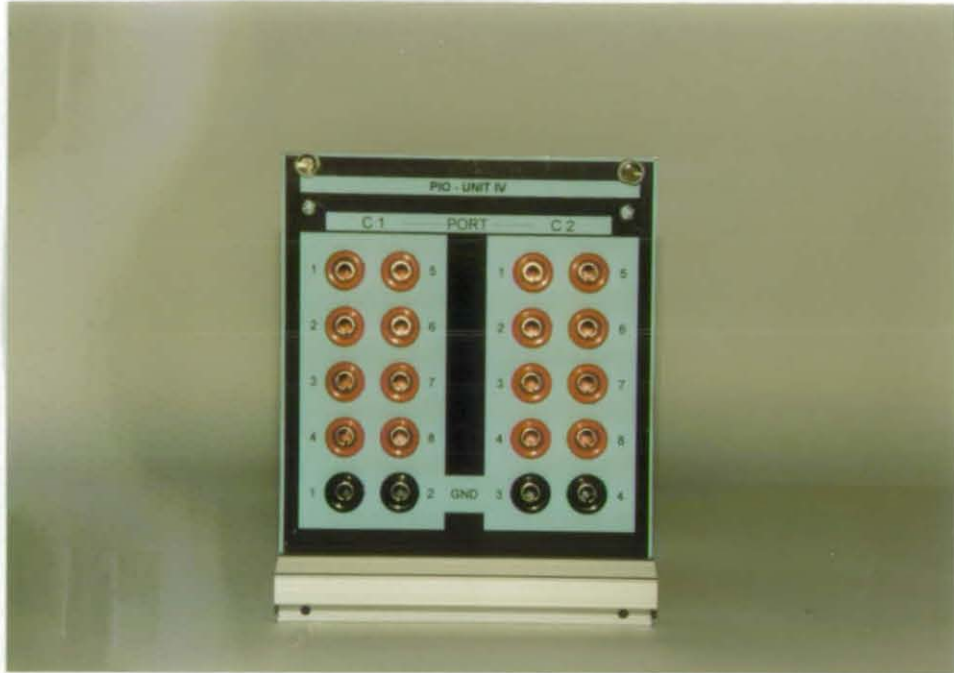


Photo D18: Front view of the PIO Unit module IV

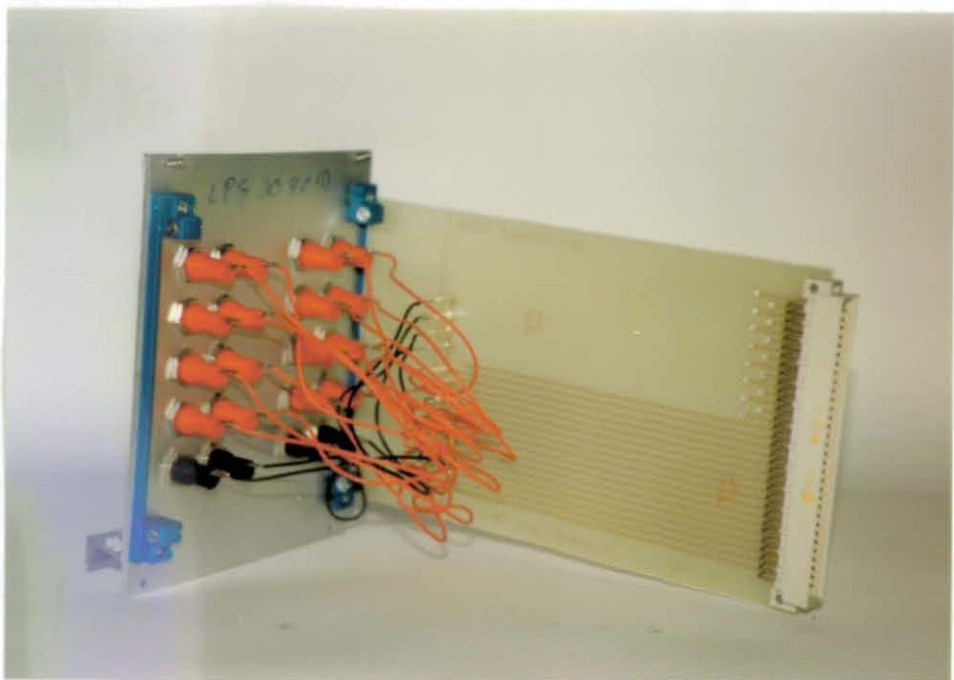


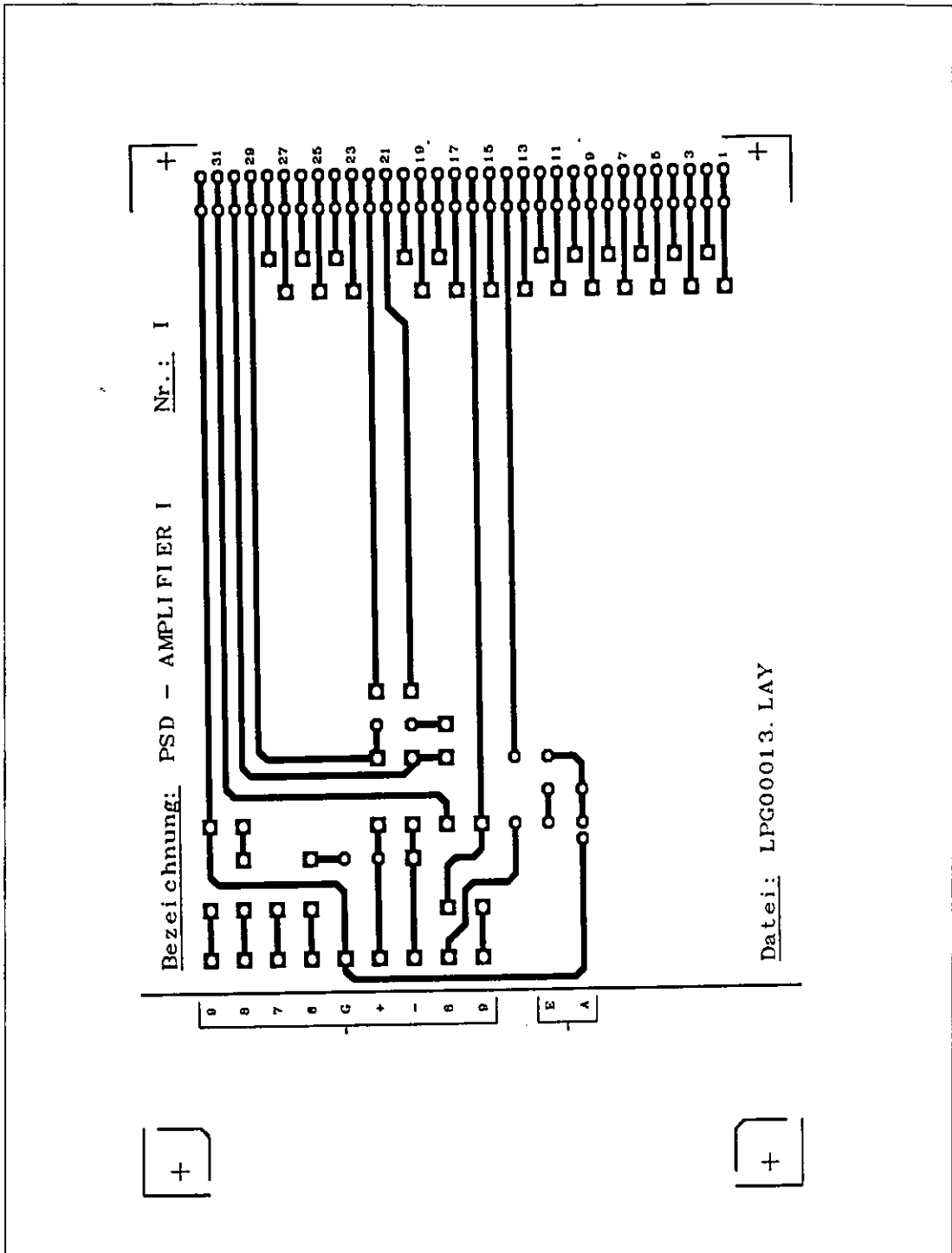
Photo D19: Side view of the PIO Unit module IV

D.6 Signal amplifier

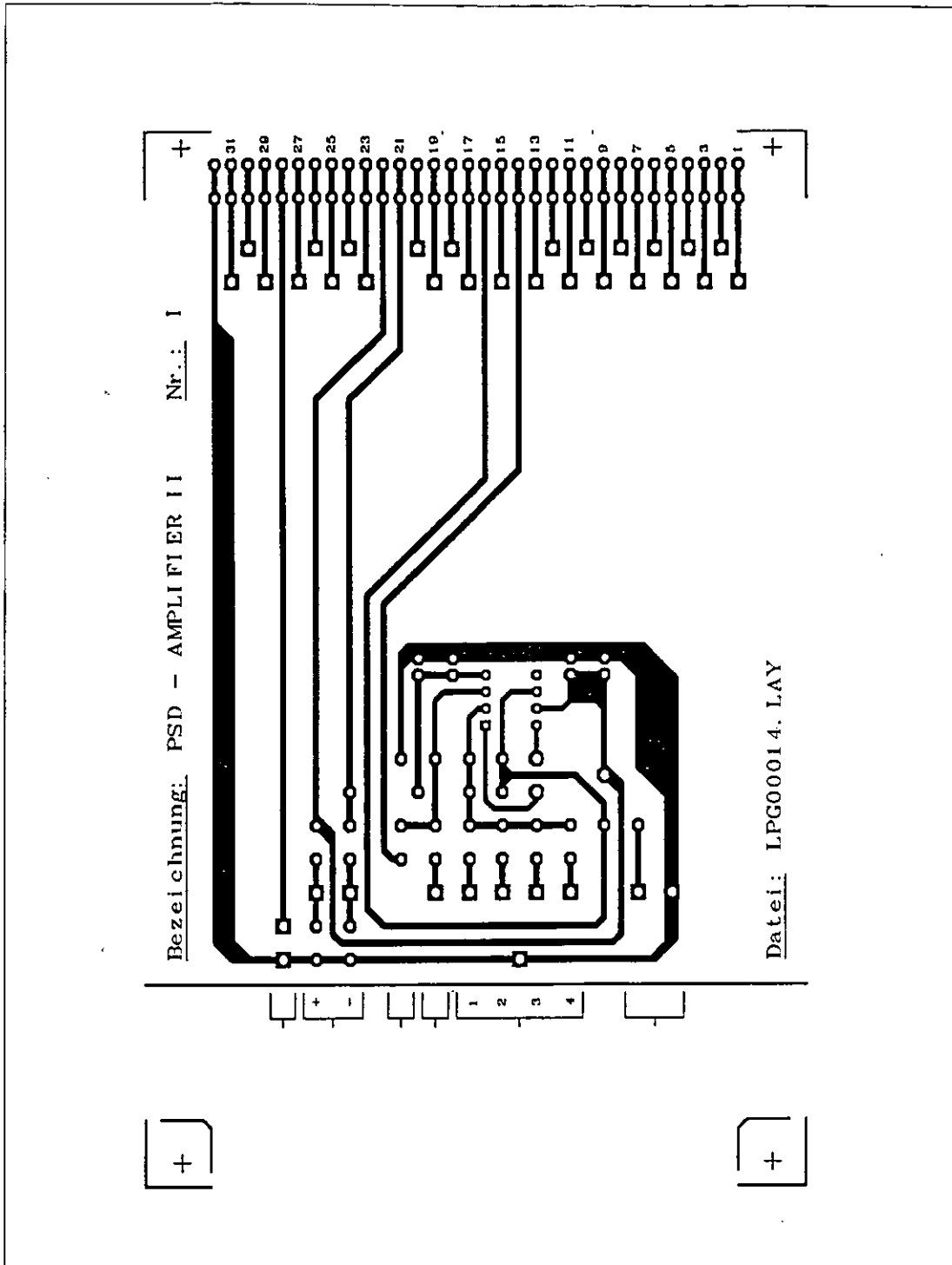
CONTENTS	PAGE #
1. Circuit diagram	D50
2. Parts list	D51
3. PCB layout module I	D52
4. PCB layout module II	D53
5. Bus port module I	D54
6. Bus port module II	D55
7. Terminal connections	D56
8. Photographs	D57-58

D.6.2 Parts list

<u>Part No.</u>	<u>Description</u>
R1	Resistor 1k Ω
R2	Resistor 47K Ω
R3	Resistor 47k Ω
R4	Resistor 10k Ω
R5	Resistor 10k Ω
R6	Resistor 0k Ω
R7	Resistor 10k Ω
R8	Resistor 40k Ω
R9	Resistor 90k Ω
R10	Resistor 10k Ω
R11	Resistor 10k Ω
R12	Resistor 270 Ω
R13	Resistor 47k Ω
R14	Resistor (plugable)
P1	Potentiometer 5k Ω
P2	Potentiometer 10k Ω
C1	Capacity 10pF
C2	Capacity plugable
C3	Capacity 10 μ F
C4	Capacity 100nF
C5	Capacity 100nF
C6	Capacity 10 μ F
D1	LED, 5mm, red
D2	LED, 5mm, red
S1	Six position switch
S2	Snap switch
S3	Four position switch
S4	Snap switch
V1	Rotation coil voltmeter



Part-No.:	Title: PCB of the signal amplifier module I
Scale:	
Material:	
Date: October 1996	FHO-Fachhochschule Ostfriesland -Institut für Lasertechnik Ostfriesland -
ENGR: Dipl.-Ing. U. Samuels	



Part-No.:	Title: PCB of the signal amplifier module II
Scale:	
Material:	
Date: October 1996	FHO-Fachhochschule Ostfriesland -Institut für Lasertechnik Ostfriesland -
ENGR: Dipl.-Ing. U. Samuels	

D.6.5 Bus port module I

Pin #	Description	Signal - Amplier II, No.: I
1		
2		
3		
4		
5		
6		
7		
8		
9		
10		
11		
12		
13		
14	E 240 - 3	Pin#: 14
15		
16	E 240 - 3	Pin#: 16
17		
18		
19		
20		
21	- 15V	Pin#: 21
22	+ 15V	Pin#: 22
23		
24		
25		
26	+ 12V	
27	- 12V	
28	+ 5V	
29	+ 15V	
30	- 15V	

Pin #	Description	DAQ - Unit II, No.: I
31	E 240 - 3	Pin#: 8
32	GND	

D.6.6 Bus port module II

Pin #	Description	Signal - Amplifier I, No.: I
1		
2		
3		
4		
5		
6		
7		
8		
9		
10		
11		
12		
13		
14	E 240 - 3	Pin#: 14
15		
16	E 240 - 3	Pin#: 16
17		
18		
19		
20		
21	- 15V	Pin#: 21
22	+ 15V	Pin#: 22
23		
24		
25		
26	+ 12V	
27	- 12V	
28	+ 5V	
29	+ 15V	
30	- 15V	
31	E 240 - 3	
32	GND	

D.6.7 Terminal connections

Pin #	Description	Function
1	Bias voltage input (V_R)	
2	Analog divider input (V_0)	V_B / V_A (at $V_A > 0$)
3	- V (- 15V)	
4	+ V (+ 15V)	
5	GND	
6	Difference signal input (V_B)	$V_1 - V_2$
7	Head amplifier input (V_1)	
8	Head amplifier input (V_2)	
9	Sum signal input (V_A)	$V_1 + V_2$

D.6.8 Photographs



Photo D20: Front view of the signal amplifier module I

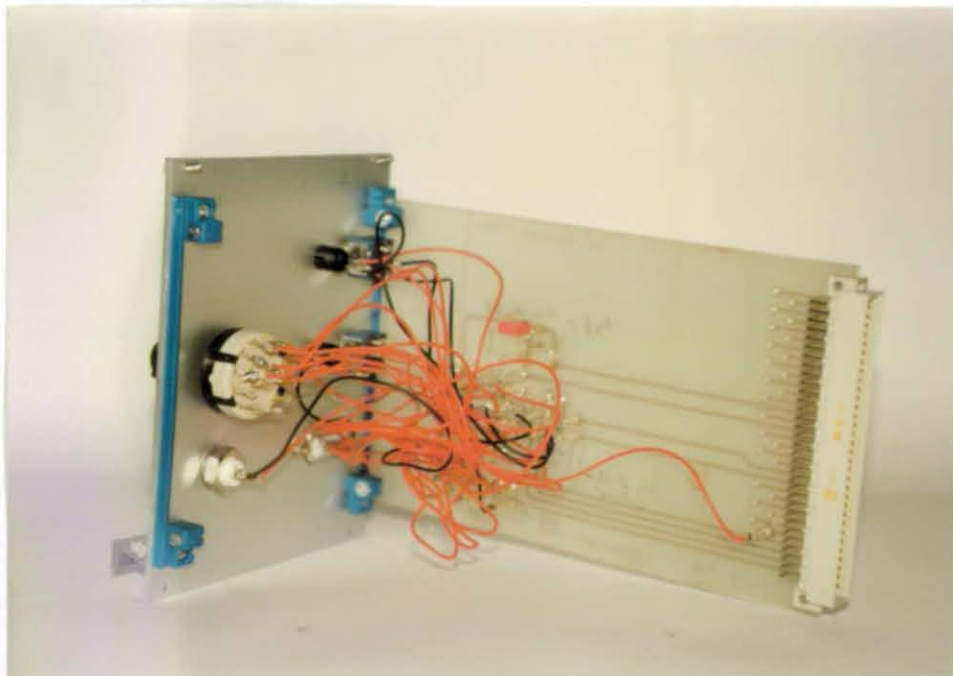


Photo D21: Side view of the signal amplifier module I



Photo D22: Front view of the signal amplifier module II

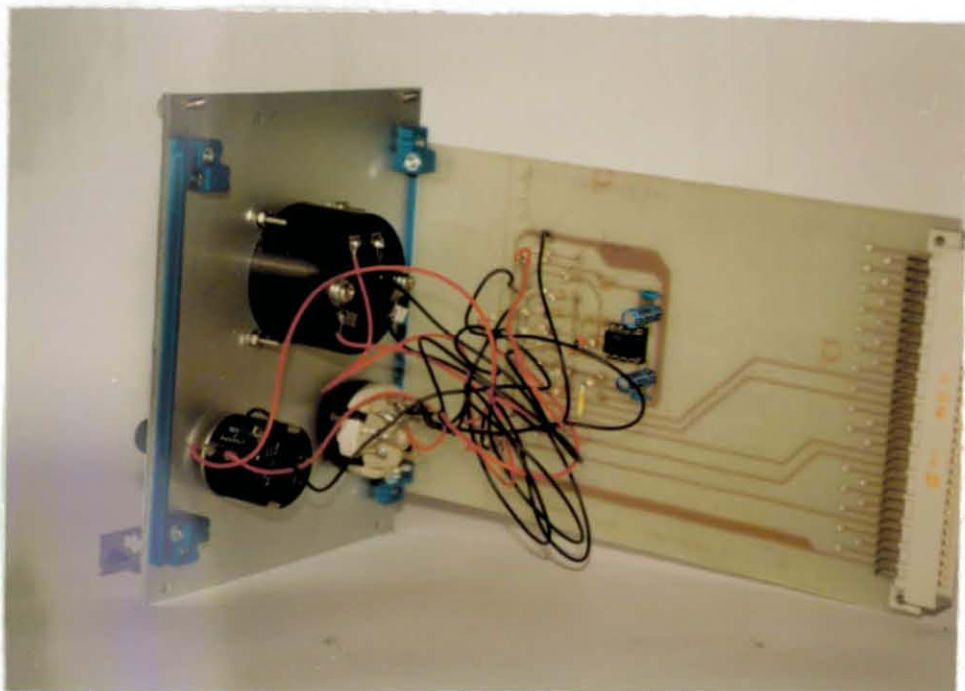
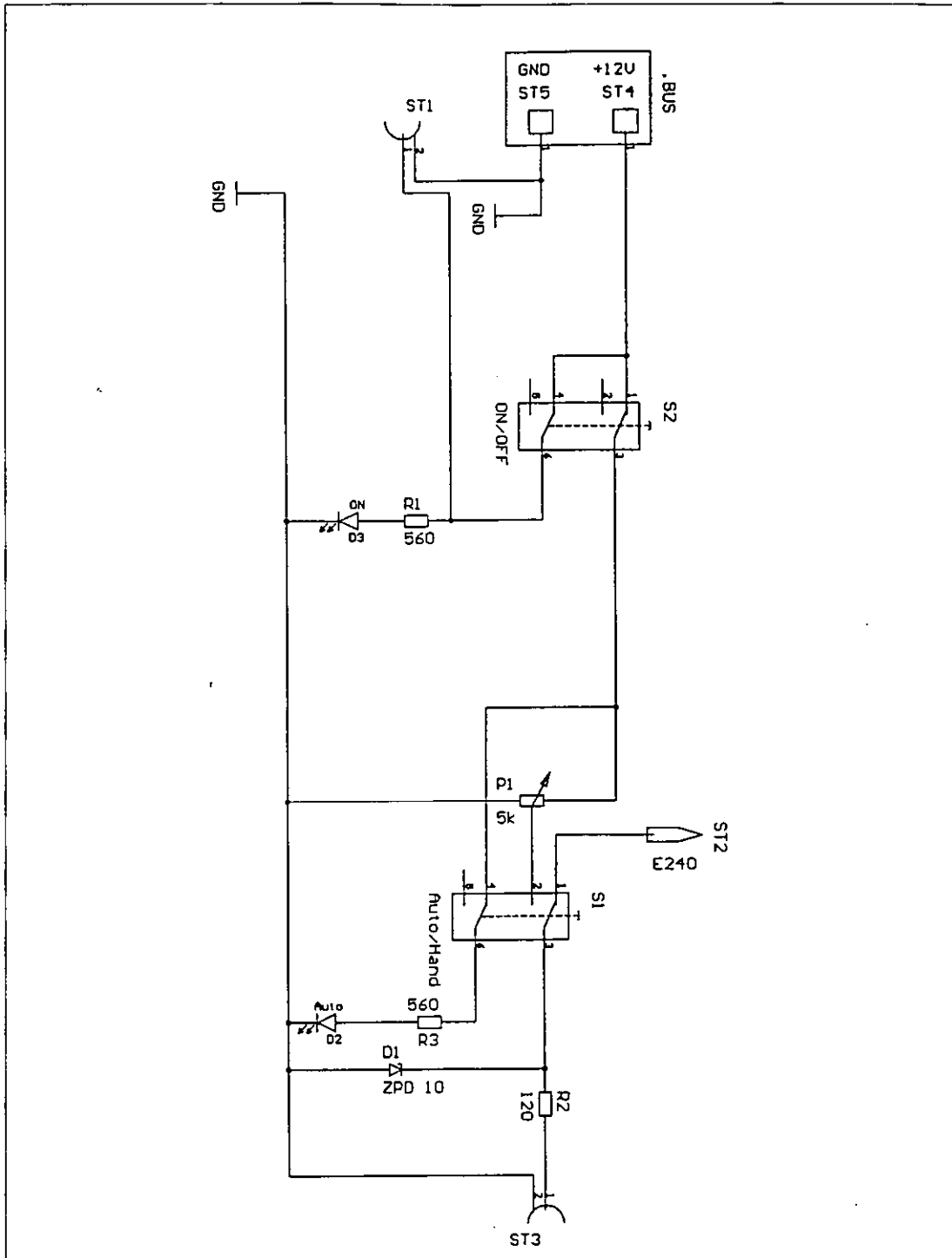


Photo D23: Side view of the signal amplifier module II

D.7 Piezo driver

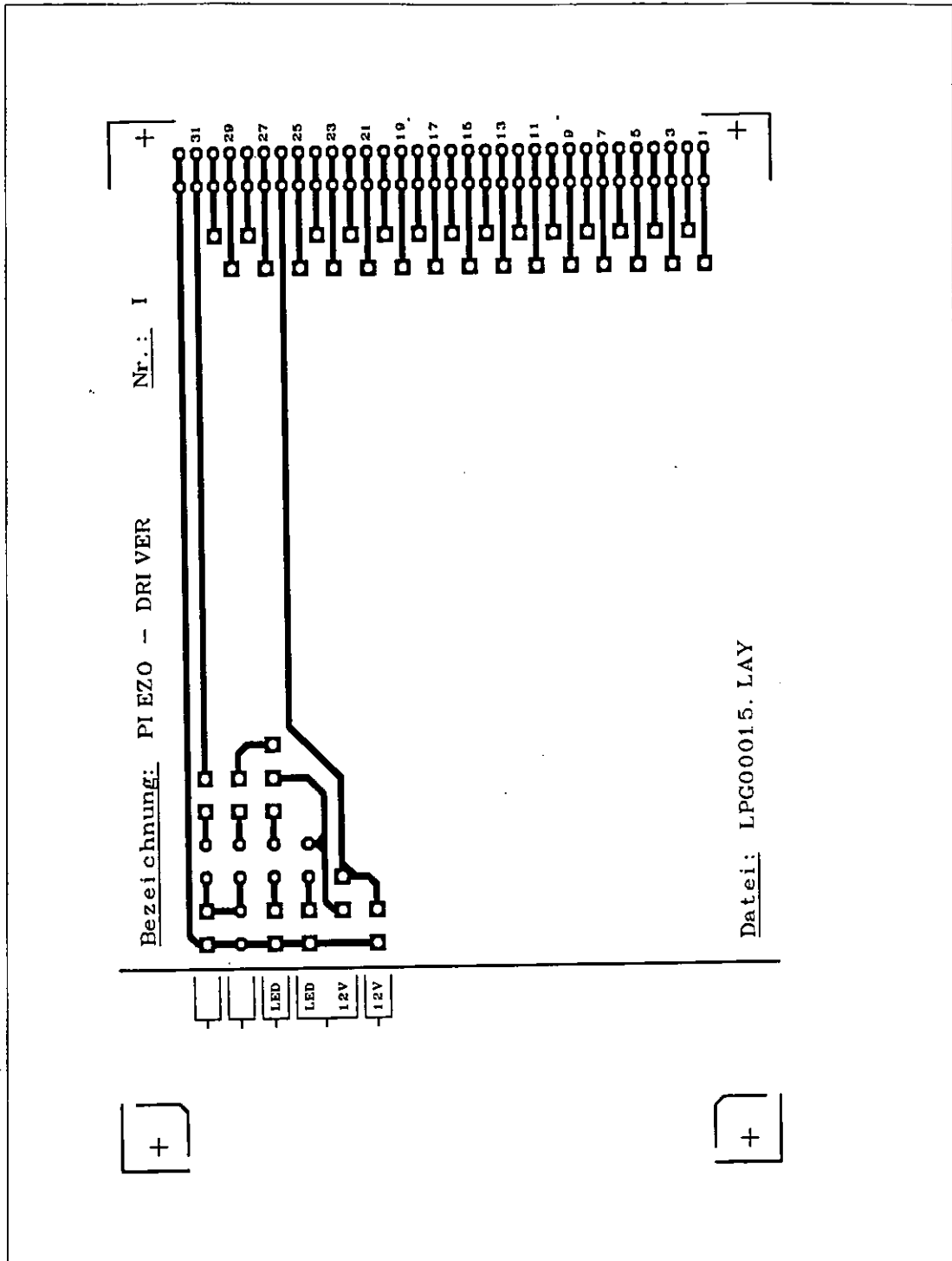
CONTENTS	PAGE #
1. Circuit diagram	D60
2. Parts list	D61
3. PCB layout module I/I	D62
4. PCB layout module I/II	D63
5. Bus port module I/I	D64
6. Bus port module I/II	D65
7. Photographs	D66



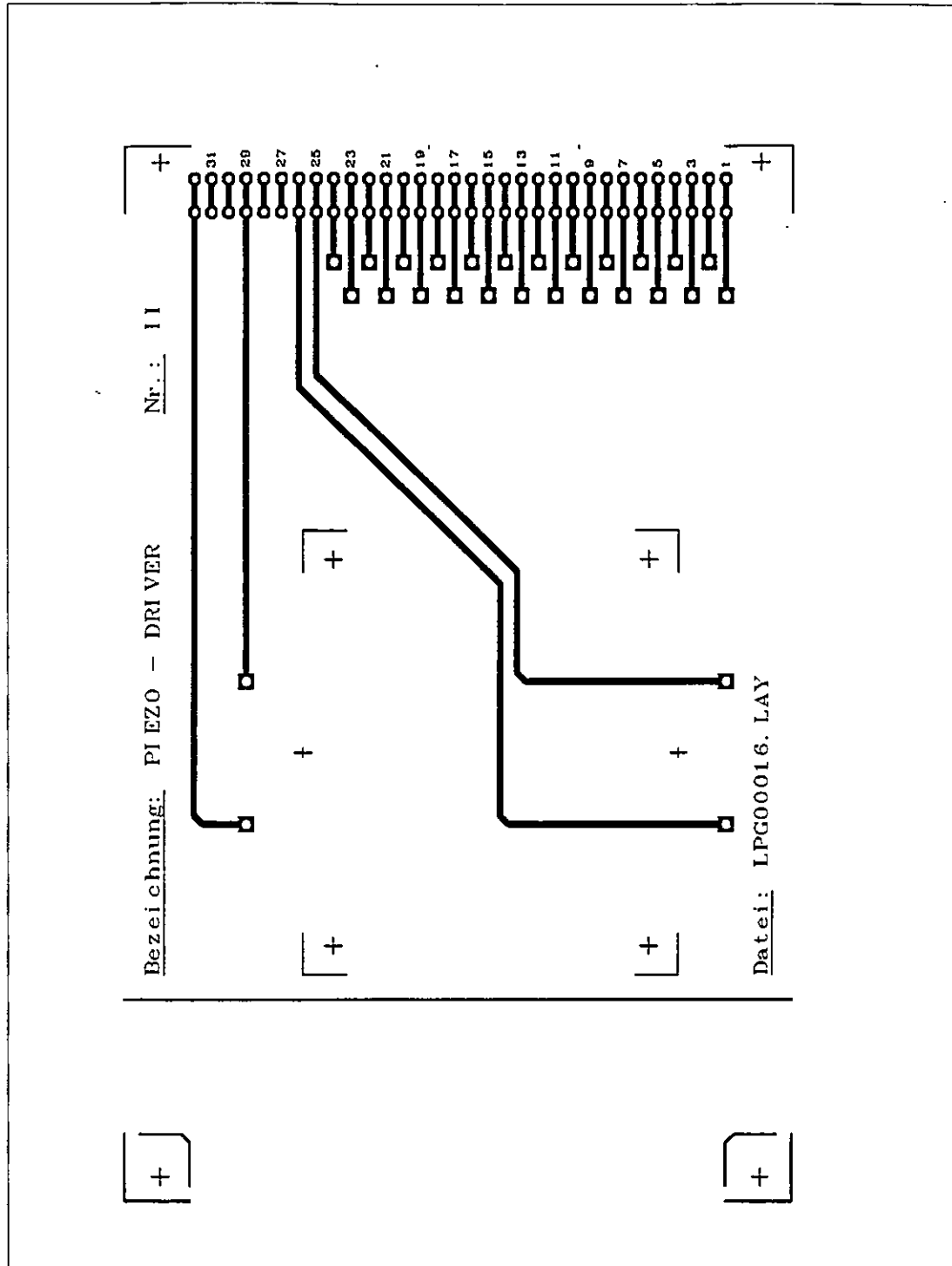
Part-No.:	Title:
Scale:	Circuit diagram of the piezo driver
Material:	
Date: October 1996	FHO-Fachhochschule Ostfriesland -Institut für Lasertechnik Ostfriesland -
ENGR: Dipl.-Ing. U. Samuels	

D.7.2 Parts list

<u>Part No.</u>	<u>Description</u>
R1	Resistor 560 Ω
R2	Resistor 560 Ω
R3	Resistor 120 Ω
P1	Potentiometer 5 k Ω
D1	LED, 5mm, red
D2	LED, 5mm, red
D3	Zener diode 10V
S1	Snap switch
S2	Snap switch



Part-No.:	Title: PCB of the piezo driver module I/I
Scale:	
Material:	
Date: October 1996	FHO-Fachhochschule Ostfriesland -Institut für Lasertechnik Ostfriesland -
ENGR: Dipl.-Ing. U. Samuels	



Part-No.:	Title: PCB of the piezo driver module I/II
Scale:	
Material:	
Date: October	FHO-Fachhochschule Ostfriesland -Institut für Lasertechnik Ostfriesland -
ENGR: Dipl.-Ing. U. Samuels	

D.7.5 Bus port module I/I

Pin #	Description	DAQ - UNIT II, No.: I
1		
2		
3		
4		
5		
6		
7		
8		
9		
10		
11		
12		
13		
14		
15		
16		
17		
18		
19		
20		
21		
22		
23		
24		
25		
26	+ 12V	
27	- 12V	
28	+ 5V	
29	+ 15V	
30	- 15V	
31	E 240 - 4	Pin#: 15
32	GND	

D.7.6 Bus port module I/II

Pin #	Description	Power Supply III, No.: I
32	~ 220V	
31		
30		
29	~ 220V	
28		
27		
26	SEC 1 - ~ 5V	Pin#: 7
25	SEC 1 - ~ 5V	Pin#: 8
24		
23		
22		
21		
20		
19		
18		
17		
16		
15		
14		
13		
12		
11		
10		
9		
8		
7	+ 12V	
6	- 12V	
5	+ 5V	Pin#: 28
4	+ 15V	
3	- 15V	
2	E 240 - X	
1	GND	Pin#: 32

D.7.7 Photographs



Photo D24: Front view of the piezo driver

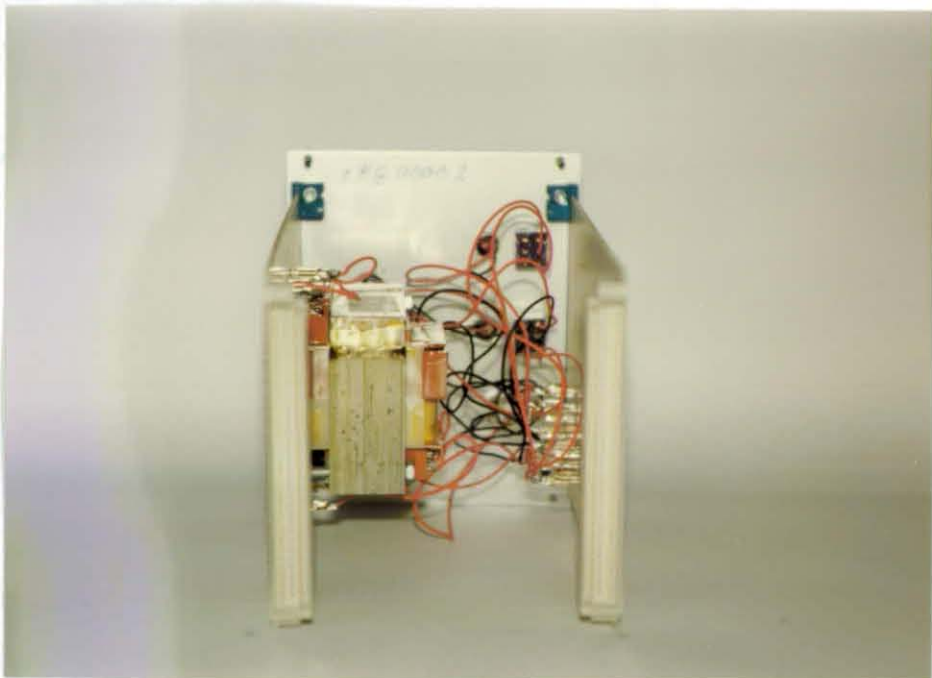
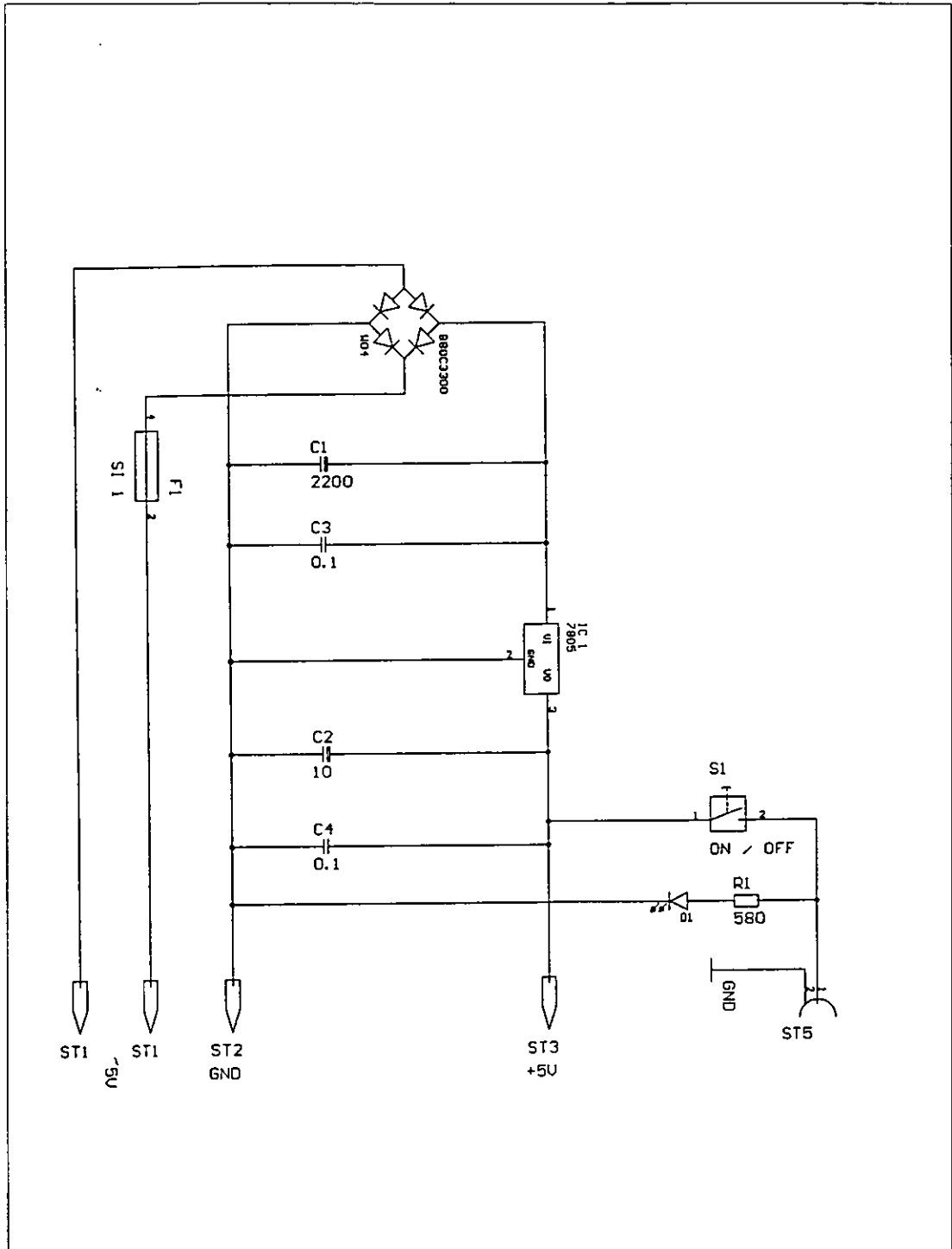


Photo D25: Back view of the piezo driver

D.8 Power supply III

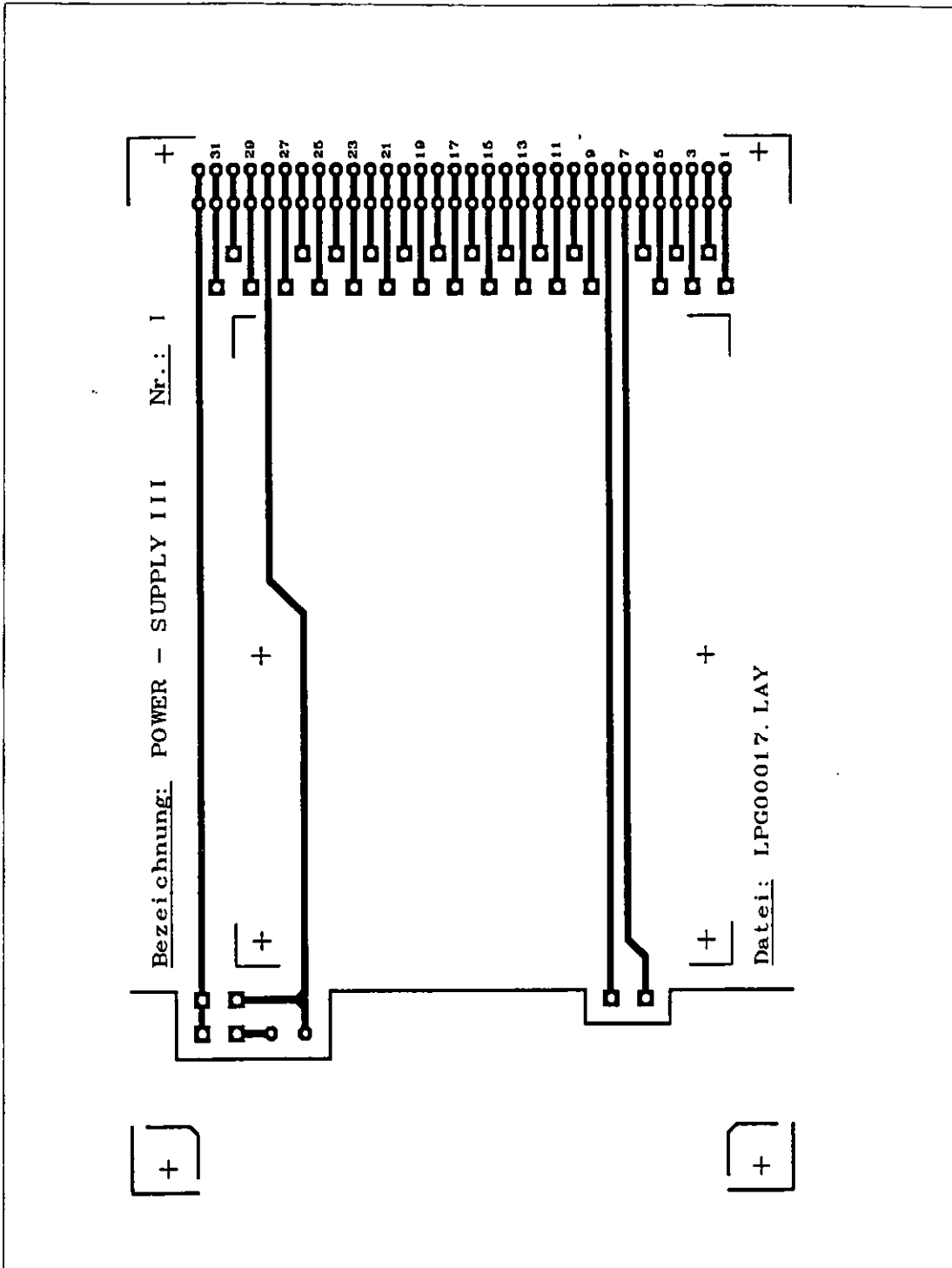
CONTENTS	PAGE #
1. Circuit diagram	D68
2. Parts list	D69
3. PCB layout	D70
4. Bus port	D71
5. Photographs	D72



Part-No.:	Title: Circuit diagram of the power supply III
Scale:	
Material:	
Date: October 1996	FHO-Fachhochschule Ostfriesland -Institut für Lasertechnik Ostfriesland -
ENGR: Dipl.-Ing. U. Samuels	

D.8.2 Parts list

<u>Part No.</u>	<u>Description</u>
R1	Resistor 180Ω
C1	Capacity 2200μF / 25 V (electrolyte)
C2	Capacity 10μF / 25V (electrolyte)
C3	Capacity 0,1μF / 100V
C4	Capacity 0,1μF/100V
D1	LED, 5mm, red
W04	Bridge rectifier
IC1	7805 (+5V)
S1	Snap switch



Part-No.:	Title: PCB of the power supply III
Scale:	
Material:	
Date: October 1996	FHO-Fachhochschule Ostfriesland -Institut für Lasertechnik Ostfriesland -
ENGR: Dipl.-Ing. U. Samuels	

D.8.4 Bus port

Pin #	Description	Piezo Driver, No.: 2
1		
2		
3		
4		
5		
6		
7	SEC 1 - ~5V	Pin#: 26
8	SEC 1 - ~5V	Pin#: 25
9		
10		
11		
12		
13		
14		
15		
16		
17		
18		
19		
20		
21		
22		
23		
24		
25		
26	+ 12V	
27	- 12V	
28	+ 5V	Pin#: 5
29	+ 15V	
30	- 15V	
31	E 240 - X	
32	GND	Pin#: 1

D.8.5 Photographs

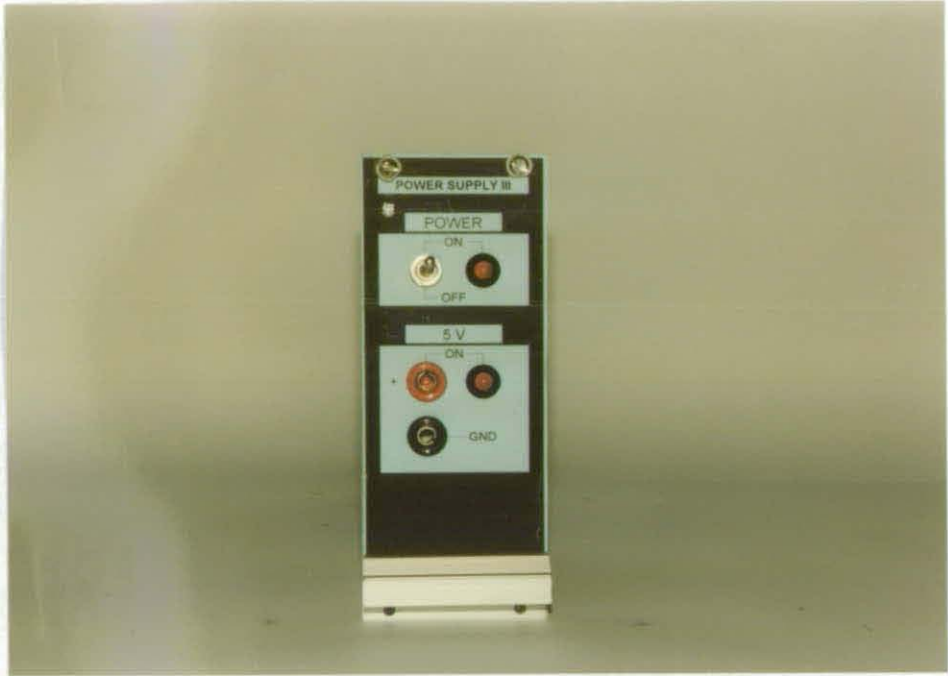


Photo D26: Front view of the power supply III

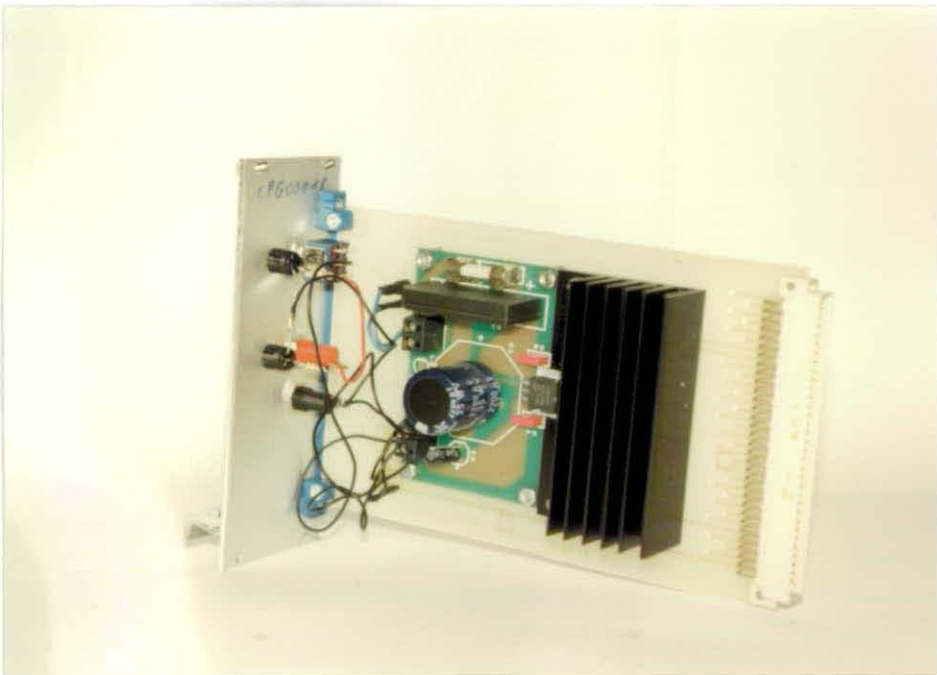
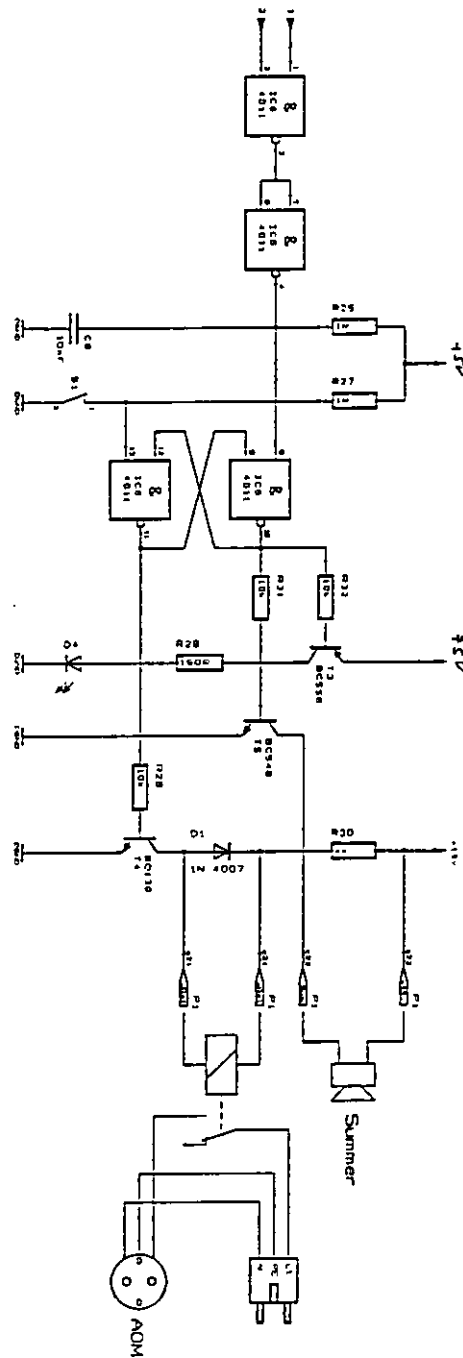


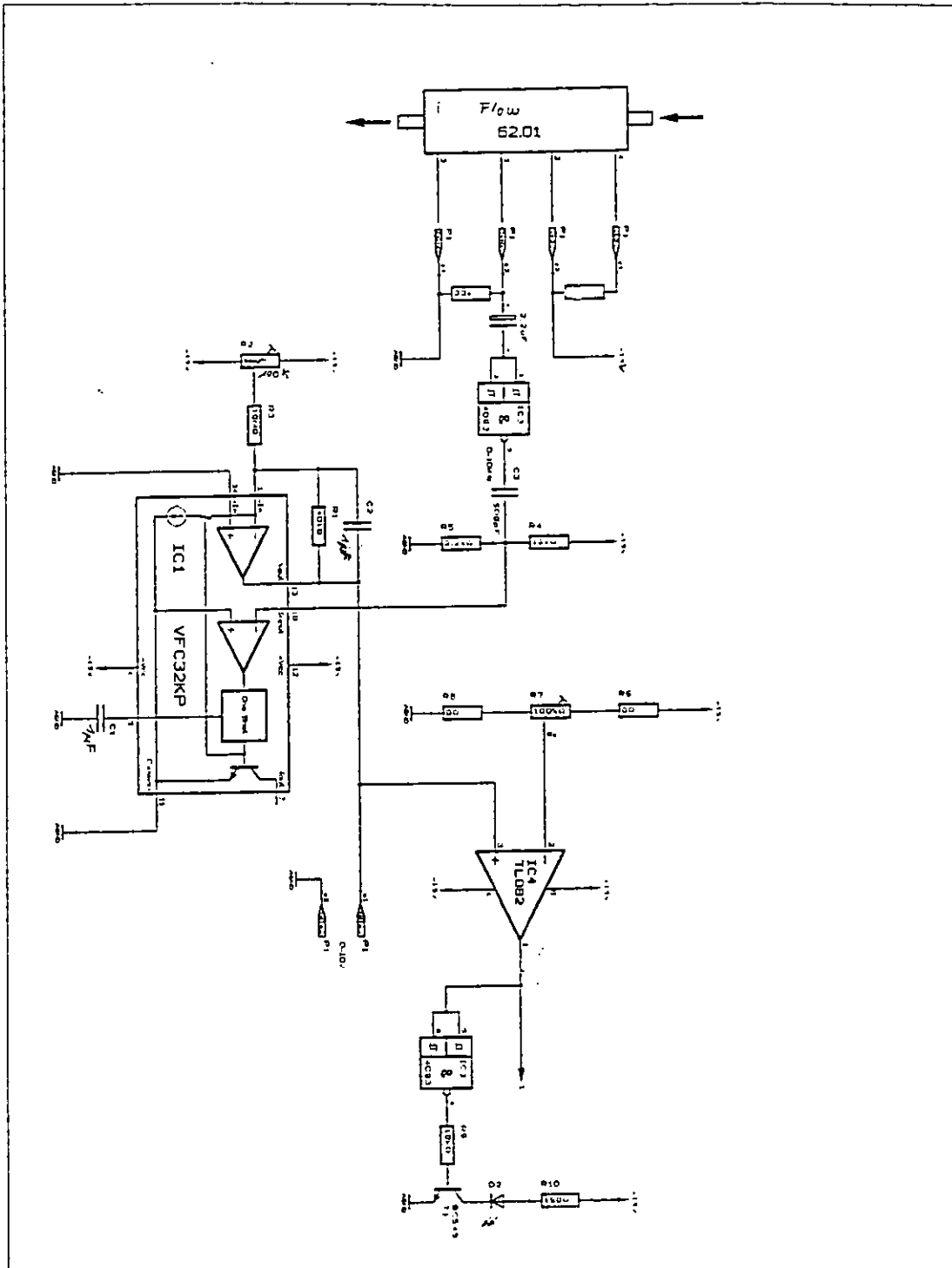
Photo D27: Side view of the power supply III

D.9 AOM protector

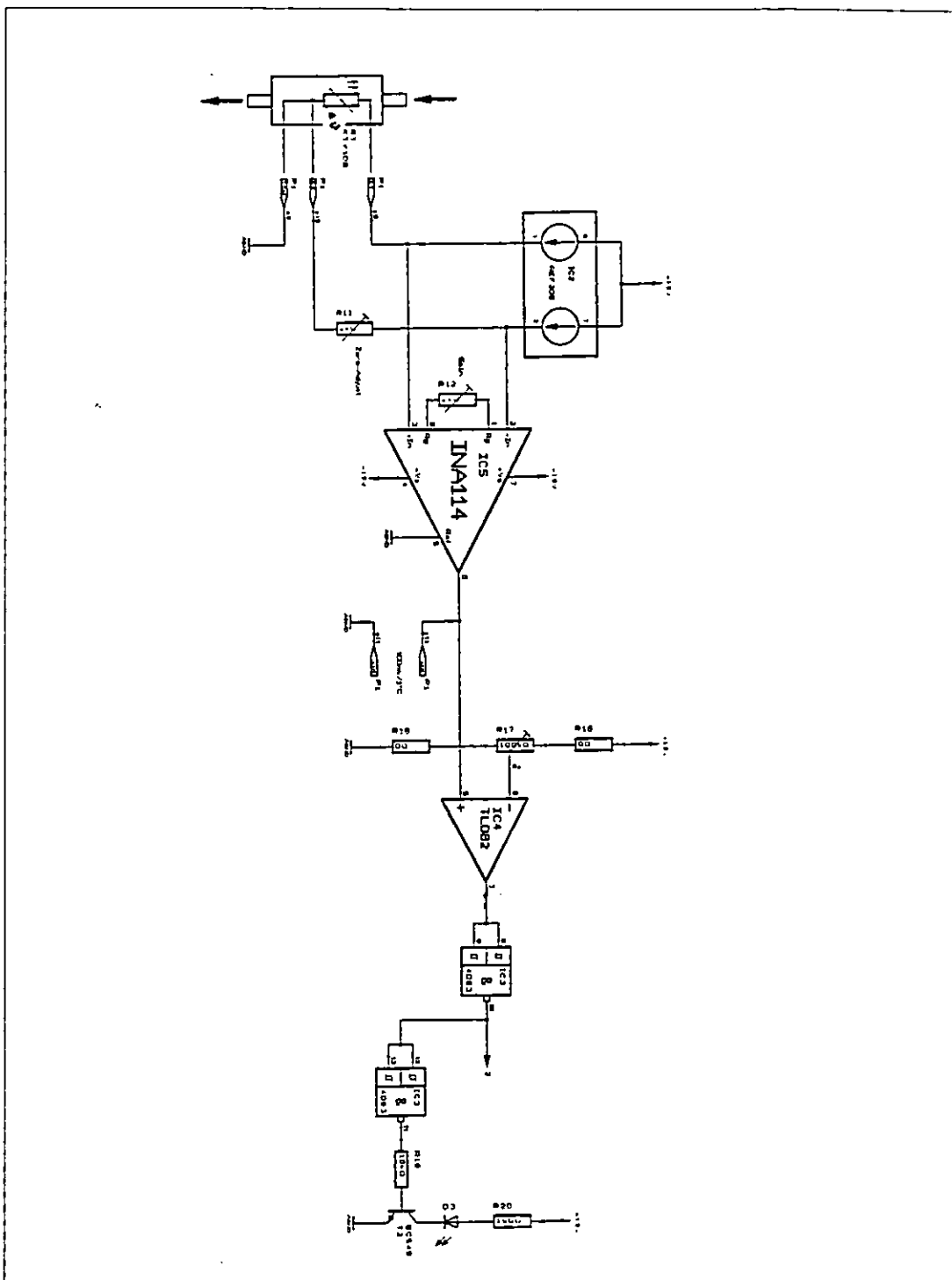
CONTENTS	PAGE #
1. Circuit diagram part I	D74
2. Circuit diagram part II	D75
3. Circuit diagram part III	D76
4. Parts list	D77
5. PCB layout	D78
6. Bus port	D79
7. Photographs	D80



Part-No.:	Title: Circuit diagram of the AOM protector (part I)
Scale:	
Material:	
Date: October 1996	FHO-Fachhochschule Ostfriesland -Institut für Lasertechnik Ostfriesland -
ENGR: Dipl.-Ing. U. Samuels	



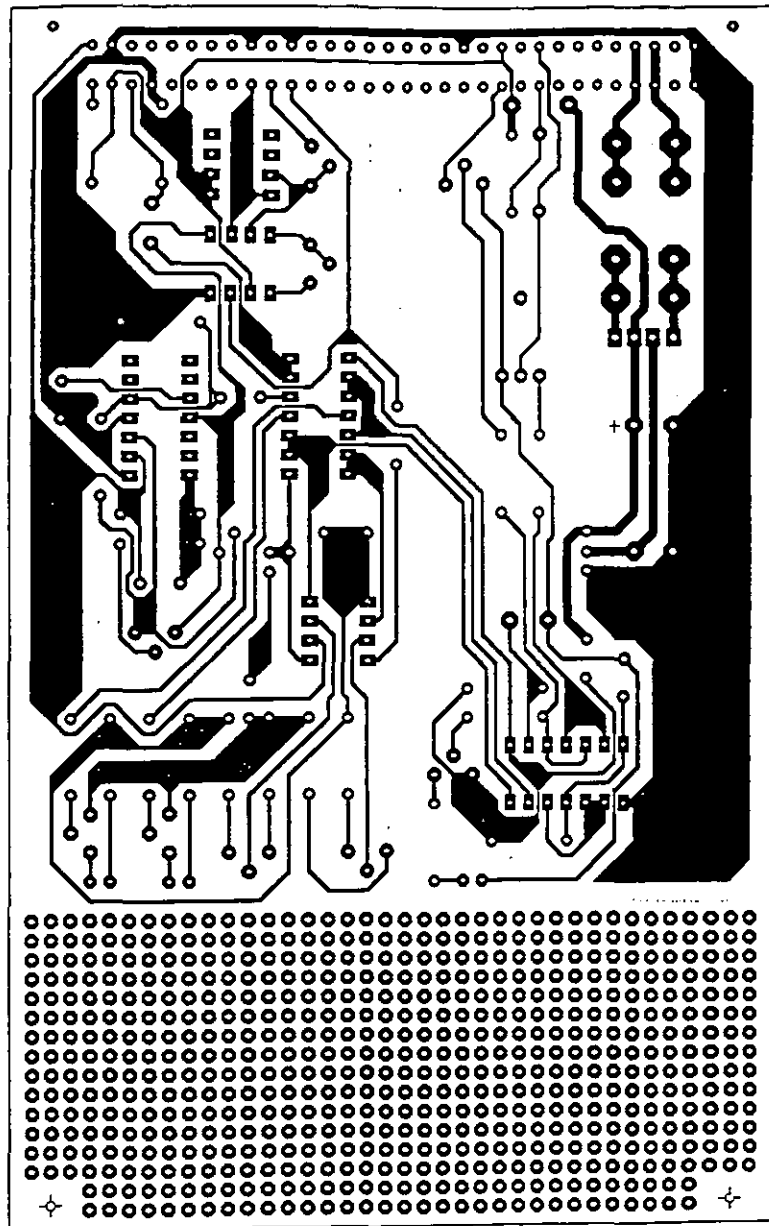
Part-No.:	Title:
Scale:	Circuit diagram of the AOM protector (part II)
Material:	
Date: October 1996	FHO-Fachhochschule Ostfriesland -Institut für Lasertechnik Ostfriesland -
ENGR: Dipl.-Ing. U. Samuels	



Part-No.:	Title:
Scale:	Circuit diagram of the AOM protector (part III)
Material:	
Date: October 1996	FHO-Fachhochschule Ostfriesland -Institut für Lasertechnik Ostfriesland -
ENGR: Dipl.-Ing. U. Samuels	

D.9.5 Parts list

<u>Part No.</u>	<u>Description</u>
R1	Resistor 40k Ω
R2	Resistor 1k Ω
R3	Resistor 10M Ω
R4	Resistor 12k Ω
R5	Resistor 2.2k Ω
R6	-
R7	Resistor 100k Ω
R8	-
R10	Resistor 150 Ω
R11	Resistor 2k Ω
R12	Resistor 2k Ω
R16	-
R17	Resistor 100k Ω
R18	-
R19	Resistor 10k Ω
R20	Resistor 150 Ω
R26	Resistor 1M Ω
R27	Resistor 1M Ω
R28	Resistor 10k Ω
R29	Resistor 150 Ω
R31	Resistor 10k Ω
R32	Resistor 10k Ω
IC1	VFC32KP
IC2	REF200AP
IC3	MOS4093
IC4	TL 082 DIL
IC5	INA114AP
IC6	MOS4011
T1	BC 548B
T2	BC 548B
T3	BC 558B
T4	BD 139
T5	BC 548B
D1	IN4007
D2, D3, D4	LED, 5mm, red
C	Capacity 2.2 μ F
C1	Capacity 3.3nF
C2	Capacity 100nF
C3	Capacity 500pF
C4	Capacity 1000 μ F
C8	Capacity 10nF
C9	Capacity 1000 μ F
S1	Key switch
S2	Snap switch
F1,2	Fuse 50mA



Part-No.:	Title:
Scale:	PCB of the AOM protector
Material:	
Date: October 1996	FHO-Fachhochschule Ostfriesland -Institut für Lasertechnik Ostfriesland -
ENGR: Dipl.-Ing. U. Samuels	

D.9.6 Bus port

Pin #	Description	
1	Flow sensor pin 4	
2	Flow sensor pin 2	
3	Flow sensor pin 1	
4	Flow sensor pin 3	
5		
6		
7		
8	Temperature sensor signal	
9	Temperature sensor GND	
10	Temperature sensor signal	
11		
12		
13		
14		
15		
16		
17		
18		
19		
20		
21		
22	Alarm	
23		
24	Relais +	
25		
26	+ 12V	
27	- 12V	
28	+ 5V	
29	+ 15V	
30	- 15V	
31	E 240 - X	
32	GND	

D.9.7 Photographs

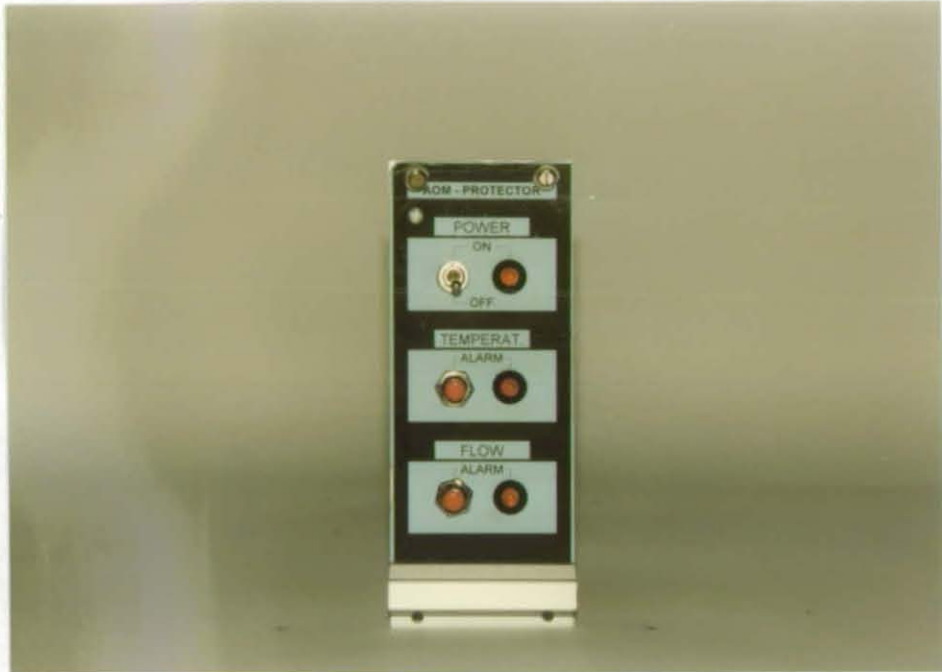


Photo D28: Front view of the AOM protector

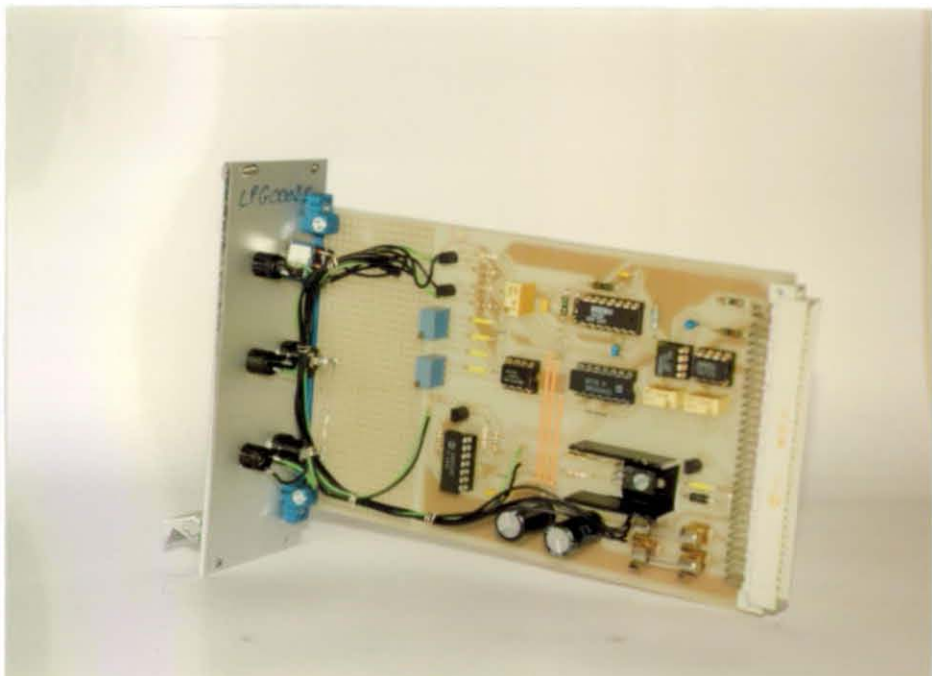
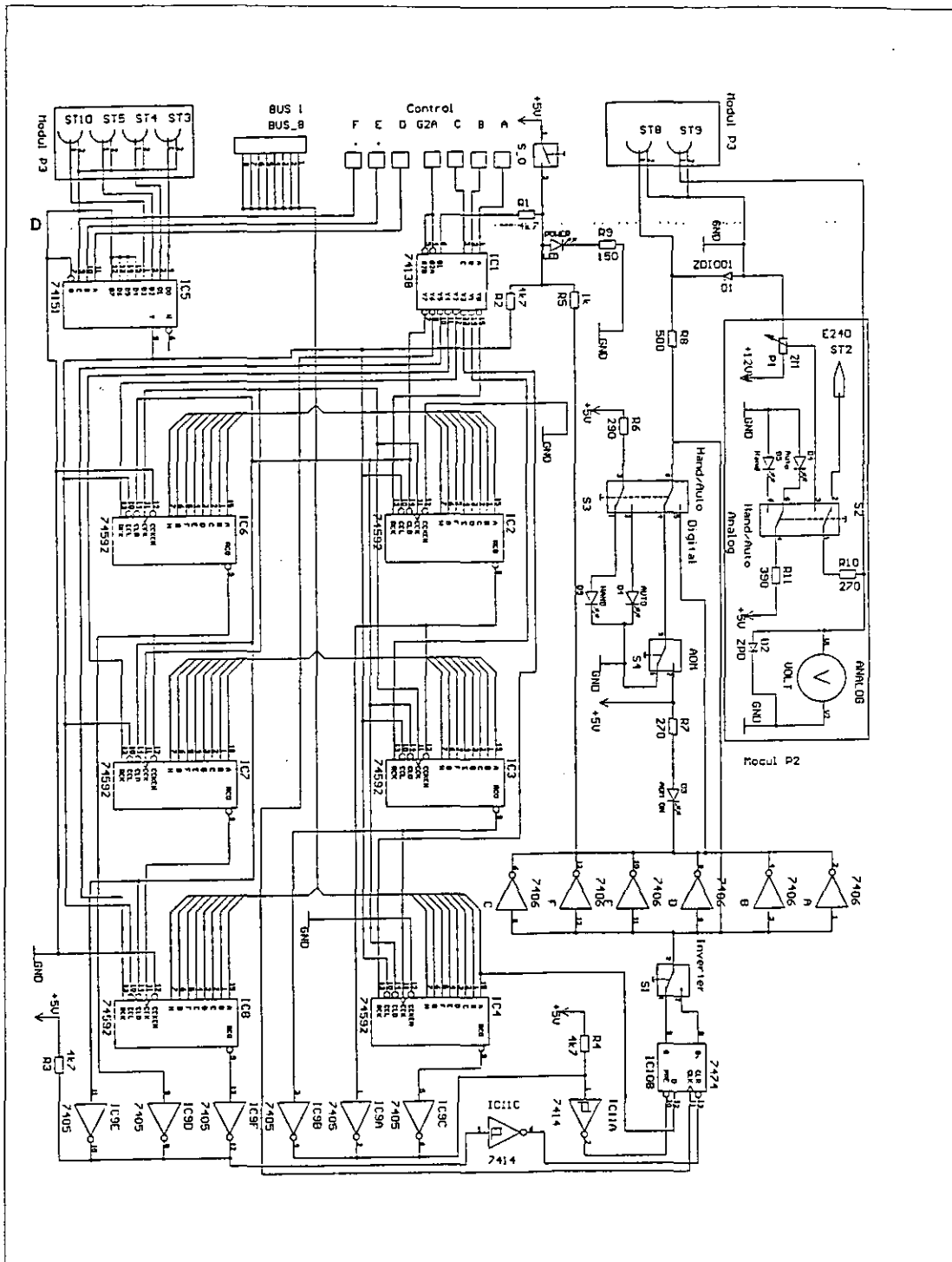


Photo D29: Side view of the AOM protector

D.10 DAI Unit

CONTENTS	PAGE #
1. Circuit diagram	D82
2. Parts list module I	D83
3. Parts list module II	D84
4. Parts list module III	D85
5. PCB layout module I/I	D86
6. PCB layout module I/II	D87
7. PCB layout module II	D88
8. PCB layout module III	D89
9. Bus port module I	D90
10. Bus port module II	D91
11. Bus port module III	D92
12. Table of interconnections	D93
13. Photographs	D94-D96



Part-No.:	Title:
Scale:	Circuit diagram of the DAI Unit
Material:	
Date: October 1996	FHO-Fachhochschule Ostfriesland
ENGR: Dipl.-Ing. U. Samuels	-Institut für Lasertechnik Ostfriesland -

D.10.2 Parts list module I

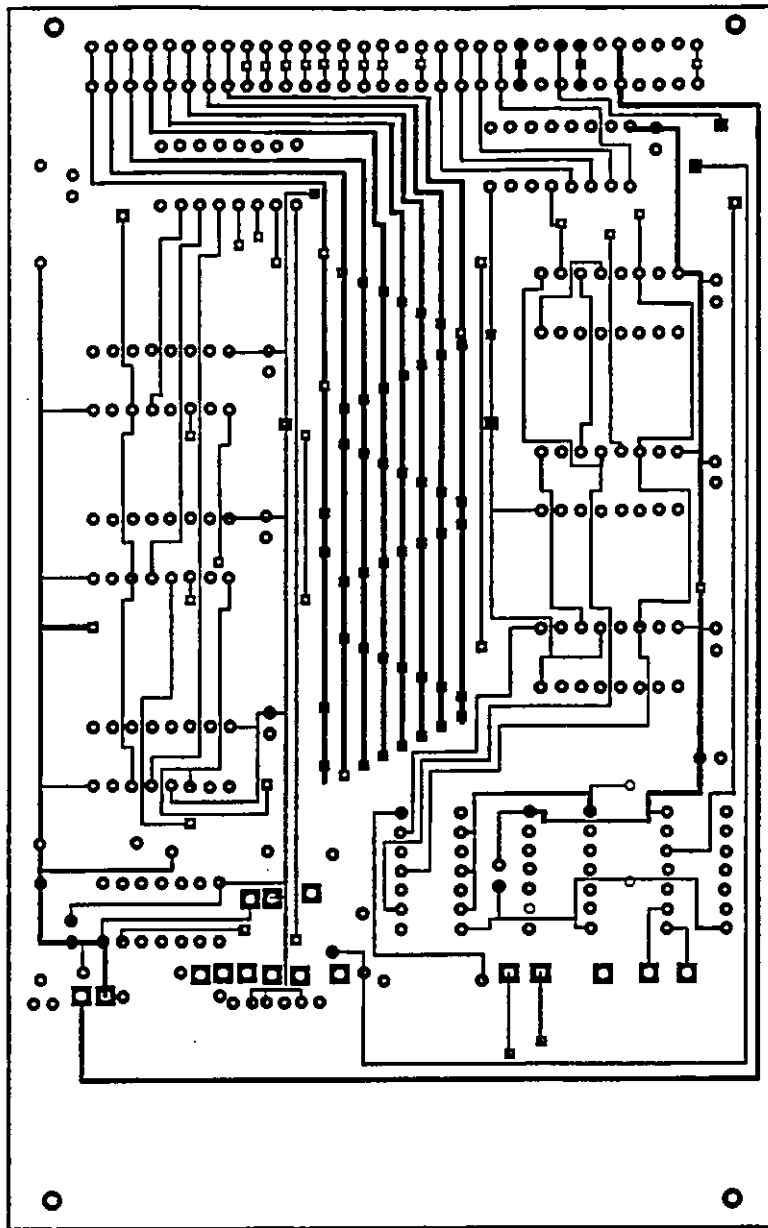
<u>Part No.</u>	<u>Description</u>
R1	Resistor 4.7k Ω
R2	Resistor 4.7k Ω
R3	Resistor 4.7k Ω
R4	Resistor 4.7k Ω
R5	Resistor 1k Ω
R6	Resistor 290 Ω
R7	Resistor 270 Ω
R8	Resistor 500 Ω
R9	Resistor 150 Ω
D1	Zener diode 5V
D2	LED, 5mm, red
IC1	SN74LS138
IC2	SN74LS592
IC3	SN74LS592
IC4	SN74LS592
IC5	SN74LS151
IC6	SN74LS592
IC7	SN74LS592
IC8	SN74LS592
IC9a	SN74LS05
IC9b	SN74LS05
IC9c	SN74LS05
IC9d	SN74LS05
IC9e	SN74LS05
IC9f	SN74LS05
IC10a	SN74LS74
IC11a	SN74LS14
IC11b	SN74LS14
IC11d	SN74LS06
IC12a	SN74LS06
IC12c	SN74LS06
So	Snap switch

D.10.3 Parts list module II

<u>Part No.</u>	<u>Description</u>
R10	Resistor 270 Ω
R11	Resistor 390 Ω
P1	Potentiometer 2M Ω
D3	LED
D4	LED
D5	LED
D6	Zener diode 10V
S1	Snap switch
S2	Snap switch
S3	Snap switch
V1	Rotating coil voltmeter

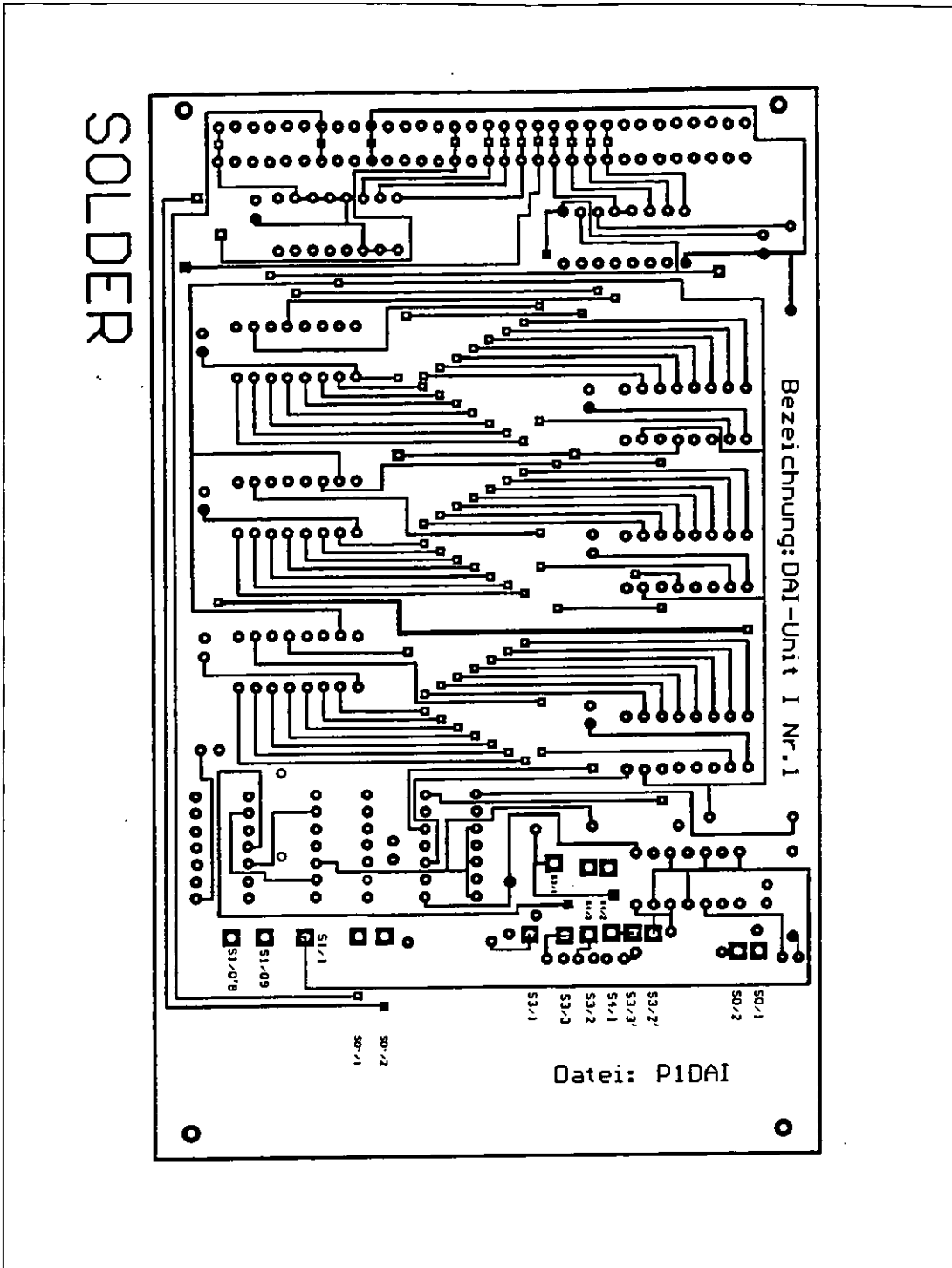
D.10.4 Parts list module III

<u>Part No.</u>	<u>Description</u>
St3	BNC connector
St4	BNC connector
St5	BNC connector
St8	BNC connector
St9	BNC connector
St10	BNC connector

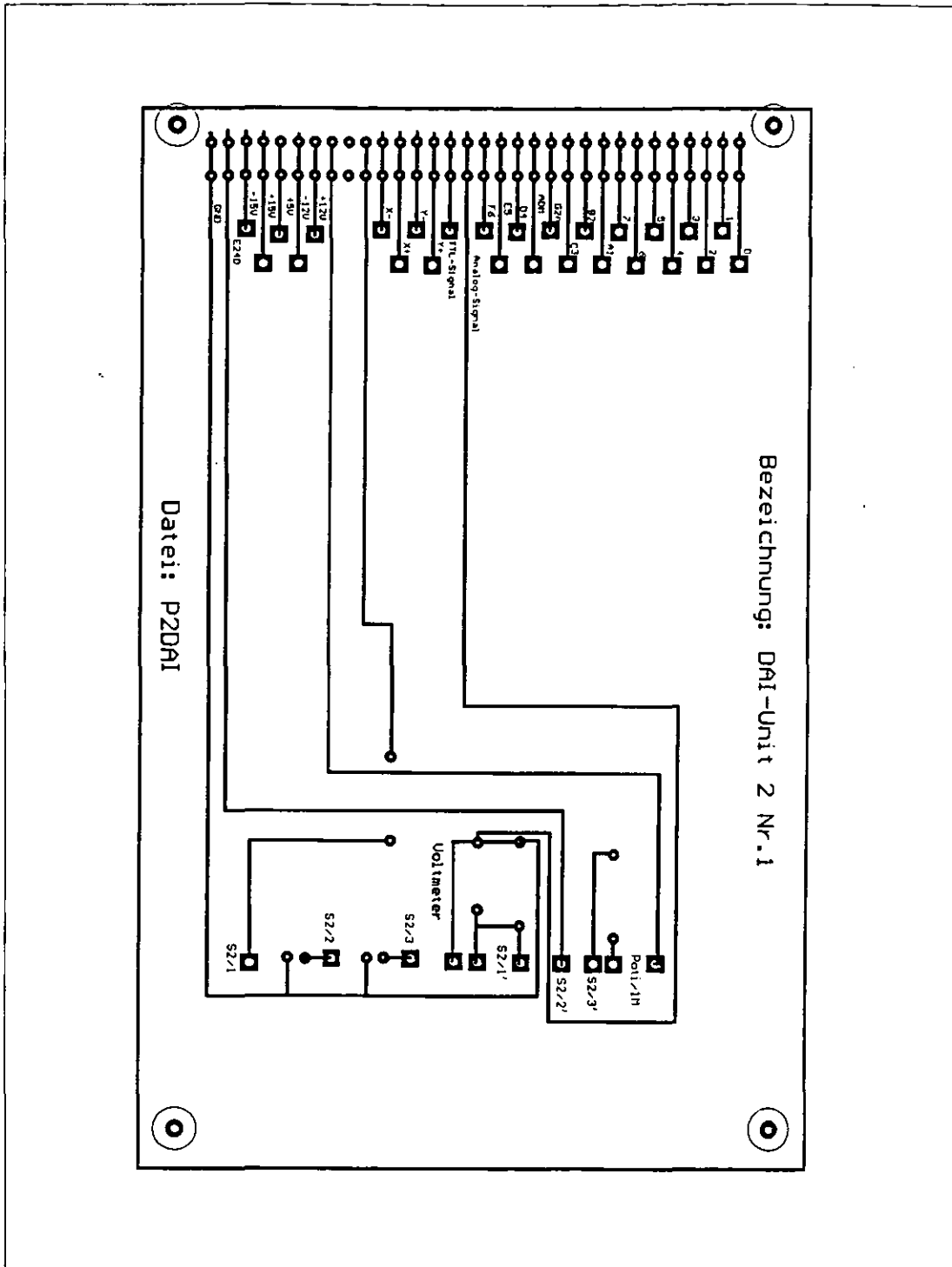


COMPONENTS

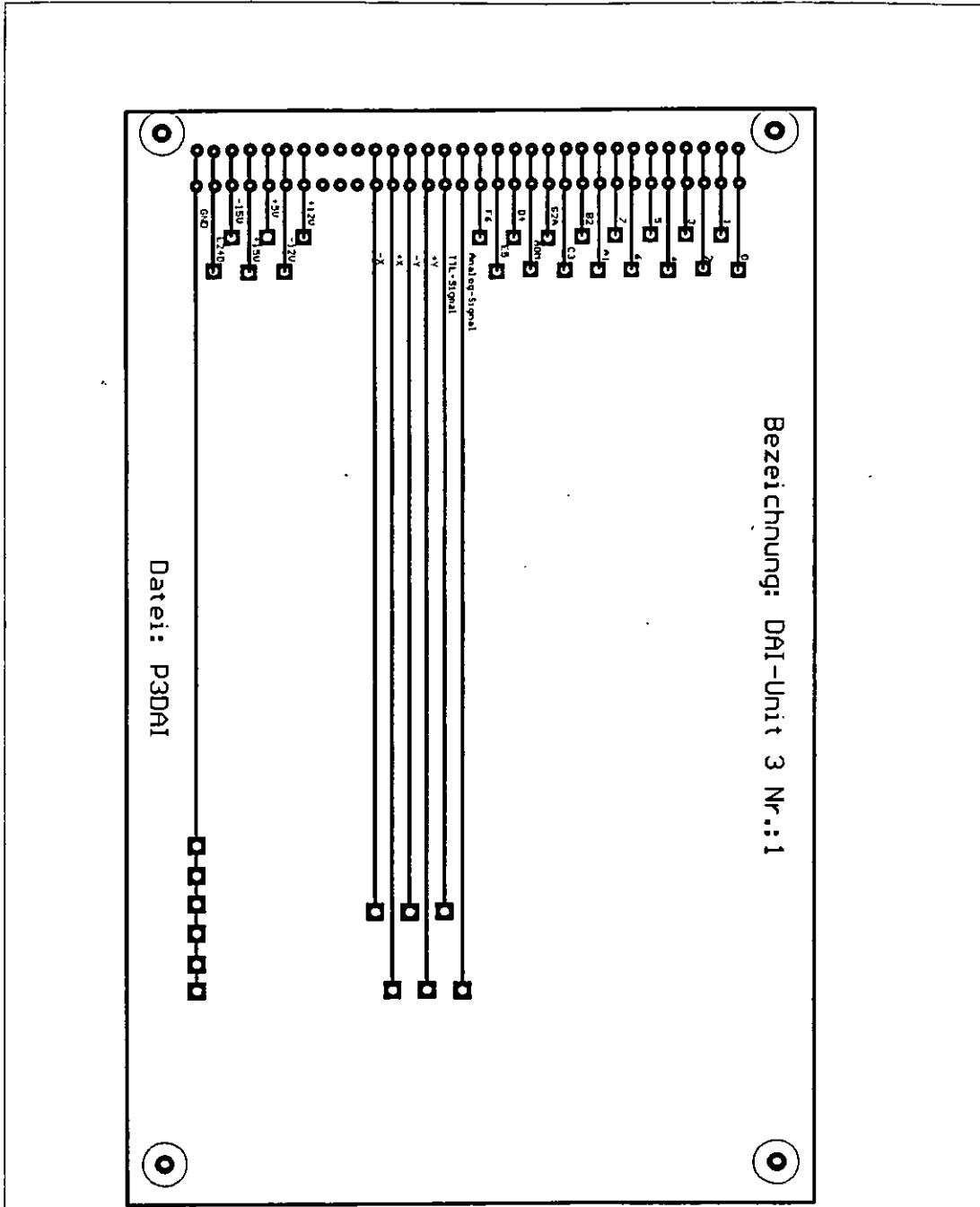
Part-No.:	Title: PCB of the DAI Unit module I (component side)
Scale:	
Material:	
Date: October 1996	FHO-Fachhochschule Ostfriesland -Institut für Lasertechnik Ostfriesland -
ENGR: Dipl.-Ing. U. Samuels	



Part-No.:	Title: PCB of the DAI Unit module I (solder side)
Scale:	
Material:	FHO-Fachhochschule Ostfriesland -Institut für Lasertechnik Ostfriesland -
Date: October 1996	
ENGR: Dipl.-Ing. U. Samuels	



Part-No.:	Title:
Scale:	PCB of the DAI Unit module II
Material:	
Date: October 1996	FHO-Fachhochschule Ostfriesland
ENGR: Dipl.-Ing. U. Samuels	-Institut für Lasertechnik Ostfriesland -



Bezeichnung: DAI-Unit 3 Nr.: 1

Datei: P3DAI

Part-No.:	Title: PCB of the DAI Unit module III
Scale:	
Material:	
Date: October 1996	FHO-Fachhochschule Ostfriesland -Institut für Lasertechnik Ostfriesland -
ENGR: Dipl.-Ing. U. Samuels	

D.10.9 Bus port module I

Pin #	Description	PIO Unit
1	PIO 1 Port A Bit 0	No.II/I Pin#: 1
2	PIO 1 Port A Bit 1	No.II/I Pin#:2
3	PIO 1 Port A Bit 2	No.II/I Pin#:3
4	PIO 1 Port A Bit 3	No.II/I Pin#:4
5	PIO 1 Port A Bit 4	No.II/I Pin#:5
6	PIO 1 Port A Bit 5	No.II/I Pin#:6
7	PIO 1 Port A Bit 6	No.II/I Pin#:7
8	PIO 1 Port A Bit 7	No.II/I Pin#:8
9	PIO 1 Port B Bit 0	No.II/II Pin#:32
10	PIO 1 Port B Bit 1	No.II/II Pin#:31
11	PIO 1 Port B Bit 2	No.II/II Pin#:30
12	PIO 1 Port B Bit 3	No.II/II Pin#:29
13	PIO 1 Port B Bit 4	No.II/II Pin#:28
14	PIO 1 Port B Bit 5	No.II/II Pin#:27
15	PIO 1 Port B Bit 6	No.II/II Pin#:26
16	PIO 1 Port B Bit 7	No.II/II Pin#:25
17	Analog Signal	No. II/I and III/I Pin#:17
18	TTL Signal	No. II/I and III/I Pin#:18
19	+ Y	No. II/I and III/I Pin#:19
20	- Y	No. II/I and III/I Pin#:20
21	+ X	No. II/I and III/I Pin#:21
22	- X	No. II/I and III/I Pin#:22
23		
24		
25		
26	+ 12V	
27	- 12V	
28	+ 5V	
29	+ 15V	
30	- 15V	
31	E 240 - 5	DAQ II/I Pin #: 16
32	GND	

D.10.10 Bus port module II

Pin #	Description	DAI - UNIT I and III, No.: I
1	PIO 1 Port A Bit 0	
2	PIO 1 Port A Bit 1	
3	PIO 1 Port A Bit 2	
4	PIO 1 Port A Bit 3	
5	PIO 1 Port A Bit 4	
6	PIO 1 Port A Bit 5	
7	PIO 1 Port A Bit 6	
8	PIO 1 Port A Bit 7	
9	PIO 1 Port B Bit 0	
10	PIO 1 Port B Bit 1	
11	PIO 1 Port B Bit 2	
12	PIO 1 Port B Bit 3	
13	PIO 1 Port B Bit 4	
14	PIO 1 Port B Bit 5	
15	PIO 1 Port B Bit 6	
16	PIO 1 Port B Bit 7	
17	Analog Signal	Pin#: 17
18	TTL Signal	Pin#: 18
19	+ Y	Pin#: 19
20	- Y	Pin#: 20
21	+ X	Pin#: 21
22	- X	Pin#: 22
23		
24		
25		
26	+ 12V	
27	- 12V	
28	+ 5V	
29	+ 15V	
30	- 15V	
31	E 240 - 5	Pin#: 31
32	GND	

D.10.11 Bus port module III

Pin #	Description	DAI - UNIT I and II, No.: I
1	PIO 1 Port A Bit 0	
2	PIO 1 Port A Bit 1	
3	PIO 1 Port A Bit 2	
4	PIO 1 Port A Bit 3	
5	PIO 1 Port A Bit 4	
6	PIO 1 Port A Bit 5	
7	PIO 1 Port A Bit 6	
8	PIO 1 Port A Bit 7	
9	PIO 1 Port B Bit 0	
10	PIO 1 Port B Bit 1	
11	PIO 1 Port B Bit 2	
12	PIO 1 Port B Bit 3	
13	PIO 1 Port B Bit 4	
14	PIO 1 Port B Bit 5	
15	PIO 1 Port B Bit 6	
16	PIO 1 Port B Bit 7	
17	Analog Signal	Pin#: 17
18	TTL Signal	Pin#: 18
19	+ Y	Pin#: 19
20	- Y	Pin#: 20
21	+ X	Pin#: 21
22	- X	Pin#: 22
23		
24		
25		
26	+ 12V	
27	- 12V	
28	+ 5V	
29	+ 15V	
30	- 15V	
31	E 240 - 5	Pin#: 31
32	GND	

D.10.12 Table of interconnections

Pin #	Description	PIO - UNIT II, No.: I
1	PIO 1 Port A Bit 0	Pin#: 1
2	PIO 1 Port A Bit 1	Pin#: 2
3	PIO 1 Port A Bit 2	Pin#: 3
4	PIO 1 Port A Bit 3	Pin#: 4
5	PIO 1 Port A Bit 4	Pin#: 5
6	PIO 1 Port A Bit 5	Pin#: 6
7	PIO 1 Port A Bit 6	Pin#: 7
8	PIO 1 Port A Bit 7	Pin#: 8

Pin #	Description	PIO - UNIT II, No.: II
9	PIO 1 Port B Bit 0	Pin#: 32
10	PIO 1 Port B Bit 1	Pin#: 31
11	PIO 1 Port B Bit 2	Pin#: 30
12	PIO 1 Port B Bit 3	Pin#: 29
13	PIO 1 Port B Bit 4	Pin#: 28
14	PIO 1 Port B Bit 5	Pin#: 27
15	PIO 1 Port B Bit 6	Pin#: 26
16	PIO 1 Port B Bit 7	Pin#: 25

Pin #	Description	DAI - Unit II and III, No.: I
17	Analog Signal	Pin#: 17
18	TTL Signal	Pin#: 18
19	+ Y	Pin#: 19
20	- Y	Pin#: 20
21	+ X	Pin#: 21
22	- X	Pin#: 22

Pin #	Description	DAI - Unit II and III, No.: I
31	E 240 - 5	Pin#: 16
32	GND	

D.10.13 Photographs



Photo D30: Front view of the DAI Unit module I

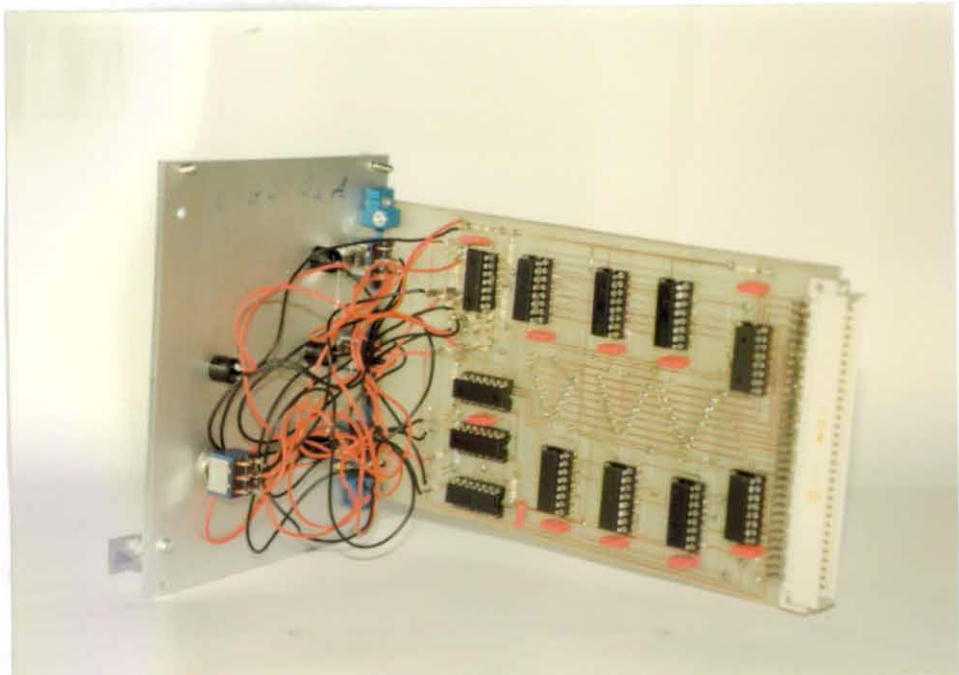


Photo D31: Side view of the DAI Unit module I



Photo D32: Front view of the DAI Unit module II

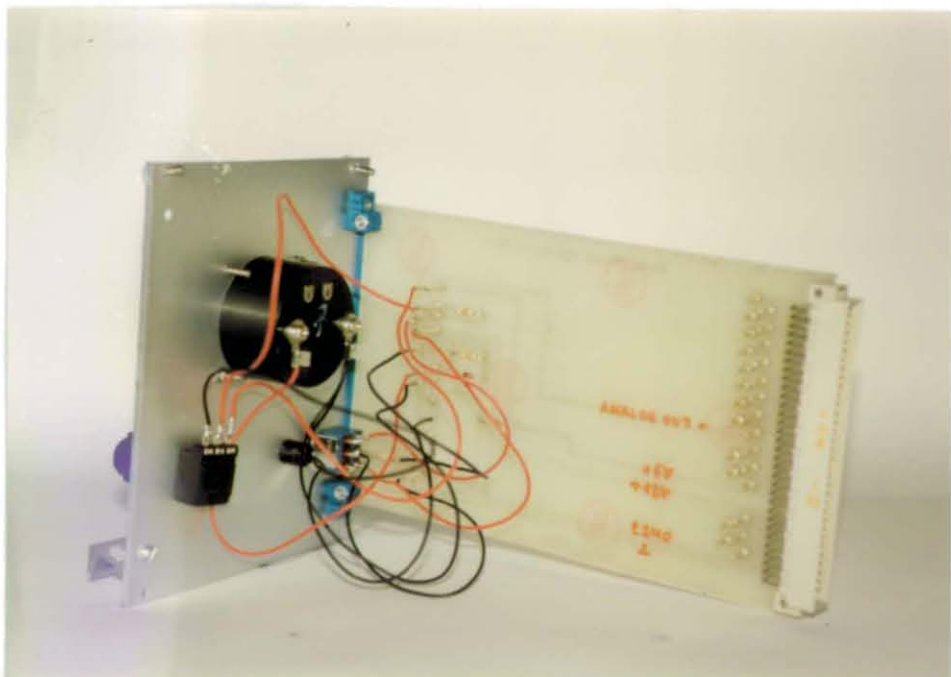


Photo D33: Side view of the DAI Unit module II



Photo D34: Front view of the DAI Unit module III

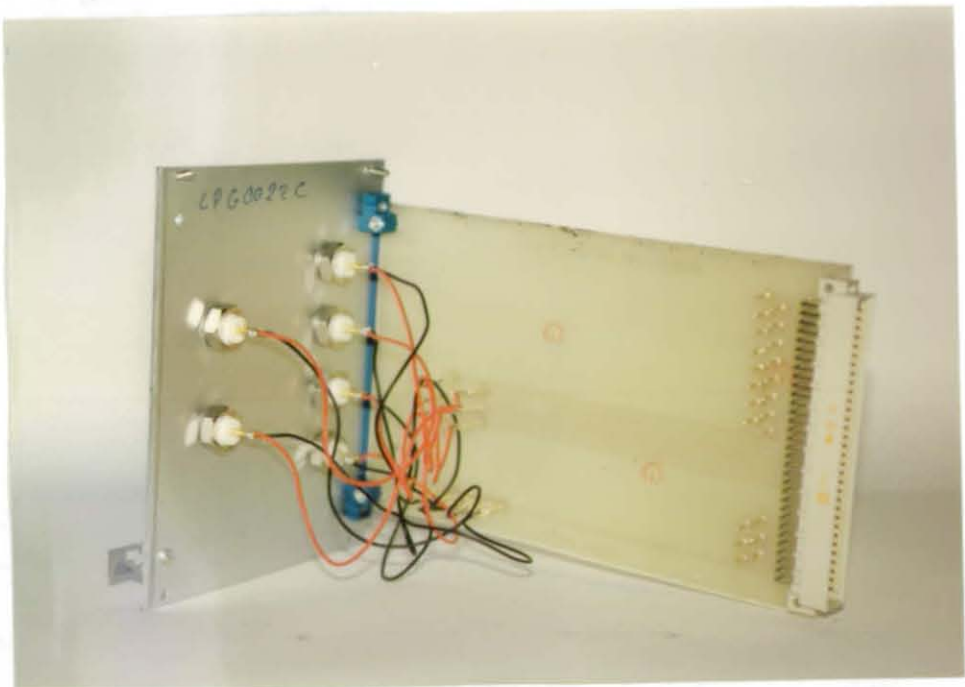
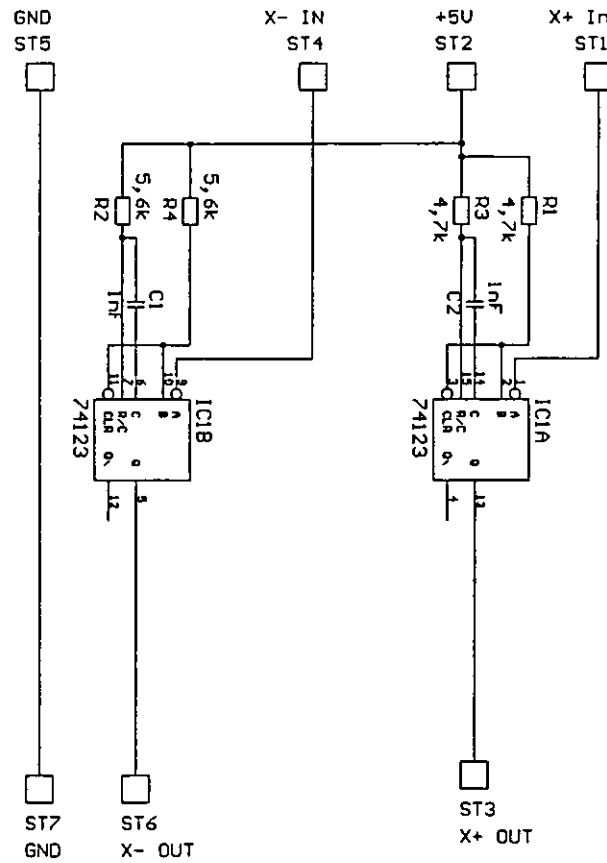


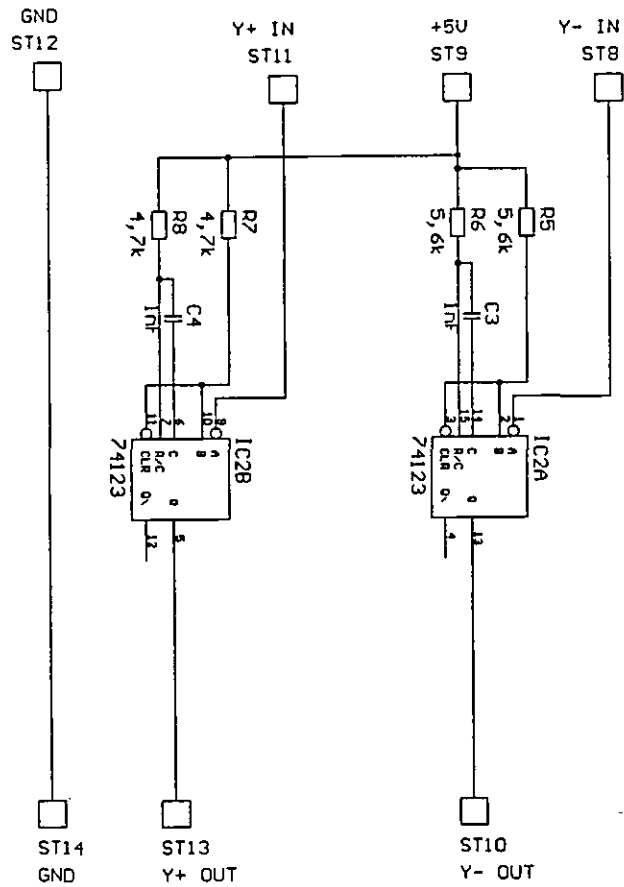
Photo D35: Side view of the DAI Unit module III

D.11 Pulse stretcher

CONTENTS	PAGE #
1. Circuit diagram (x-axis)	D98
2. Circuit diagram (y-axis)	D99
3. Parts list (x-axis)	D100
4. Parts list (y-axis)	D101
5. PCB layout	D102
6. Interfacing diagram	D103
7. Photograph	D104



Part-No.:	Title: Circuit diagram of the pulse stretcher (x-axis)
Scale:	
Material:	
Date: October 1996	FHO-Fachhochschule Ostfriesland -Institut für Lasertechnik Ostfriesland -
ENGR: Dipl.-Ing. U. Samuels	



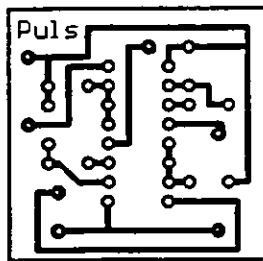
Part-No.:	Title:
Scale:	Circuit diagram of the pulse strecher (y-axis)
Material:	
Date: October 1996	FHO-Fachhochschule Ostfriesland -Institut für Lasertechnik Ostfriesland -
ENGR: Dipl.-Ing. U. Samuels	

D.11.3 Parts list (x-axis)

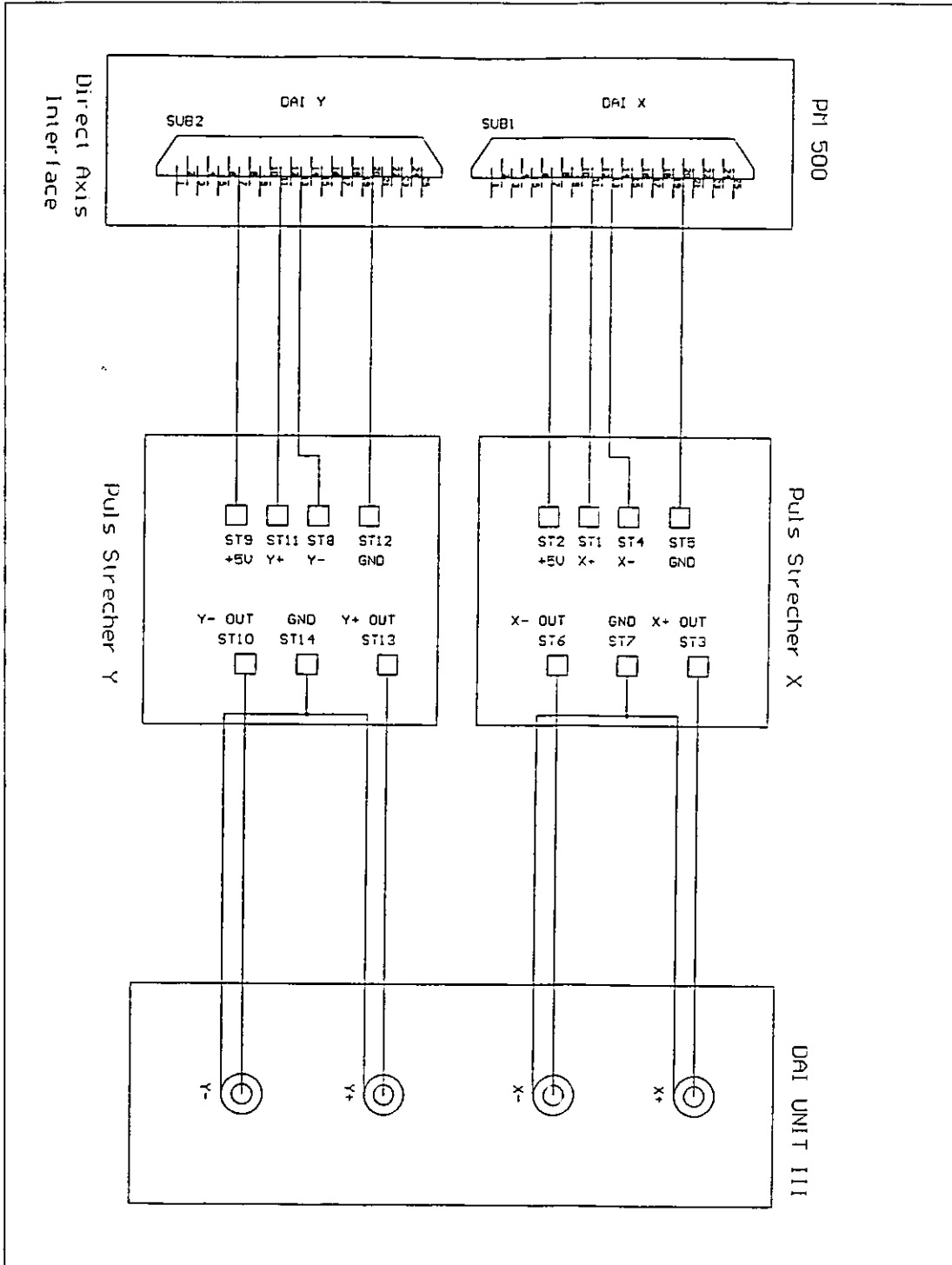
<u>Part No.</u>	<u>Description</u>
R1	Resistor 4.7k Ω
R2	Resistor 5.6k Ω
R3	Resistor 4.7k Ω
R4	Resistor 5.6k Ω
C1	Capacity 1nF (ceramic)
C2	Capacity 1nF (ceramic)
IC1	SN74LS123

D.11.4 Parts list (y-axis)

<u>Part No.</u>	<u>Description</u>
R1	Resistor 4.7k Ω
R2	Resistor 5.6k Ω
R3	Resistor 4.7k Ω
R4	Resistor 5.6k Ω
C1	Capacity 1nF (ceramic)
C2	Capacity 1nF (ceramic)
IC1	SN74LS123



Part-No.:	Title: PCB of the pulse strecher
Scale:	
Material:	
Date: October 1996	FHO-Fachhochschule Ostfriesland -Institut für Lasertechnik Ostfriesland -
ENGR: Dipl.-Ing. U. Samuels	



Part-No.:	Title:
Scale:	Interfacing of the pulse stretcher
Material:	
Date: October 1996	FHO-Fachhochschule Ostfriesland -Institut für Lasertechnik Ostfriesland -
ENGR: Dipl.-Ing. U. Samuels	

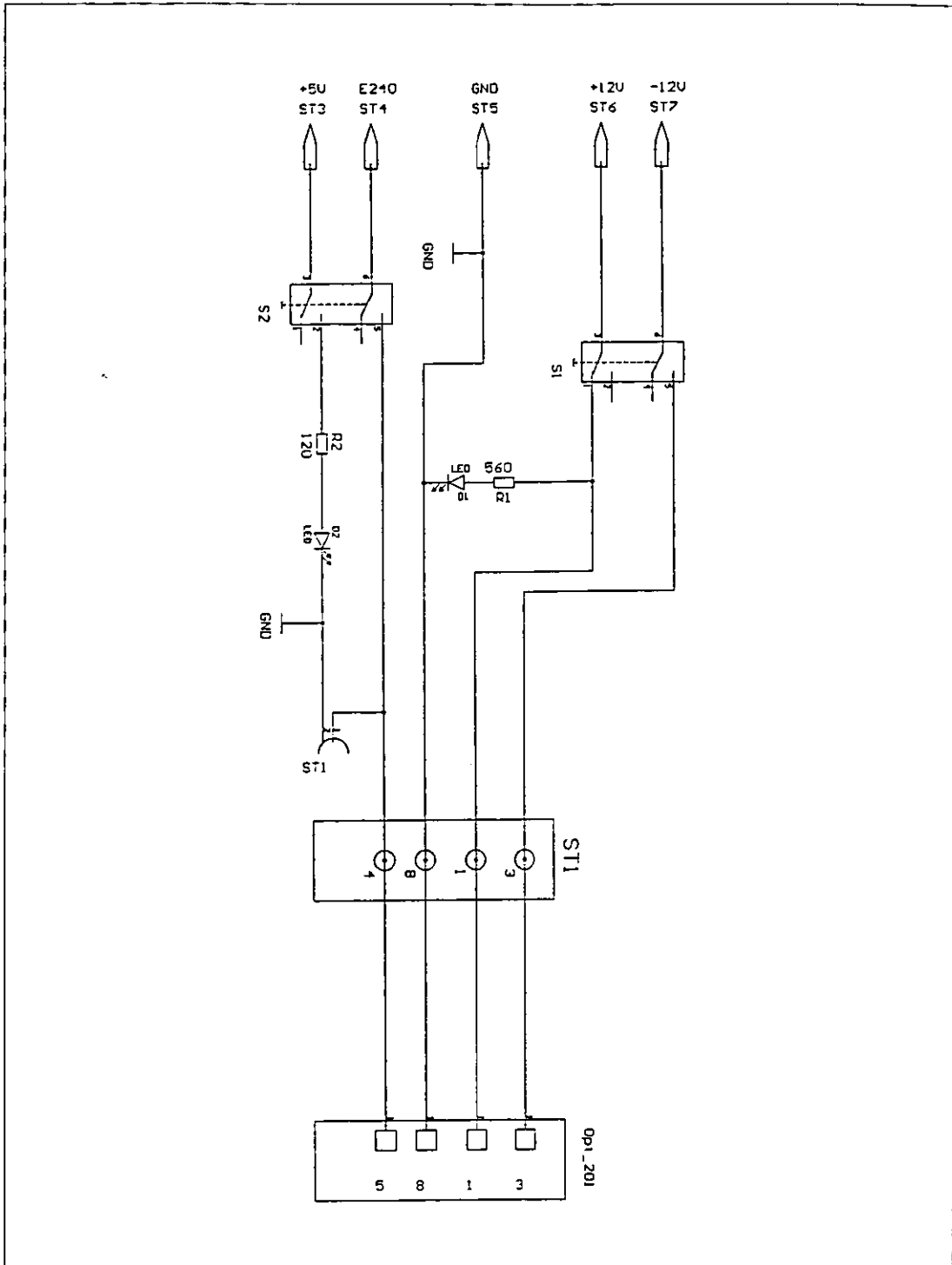
D.11.7 Photograph



Photo D36: Pulse strecher

D.12 Photo detector I

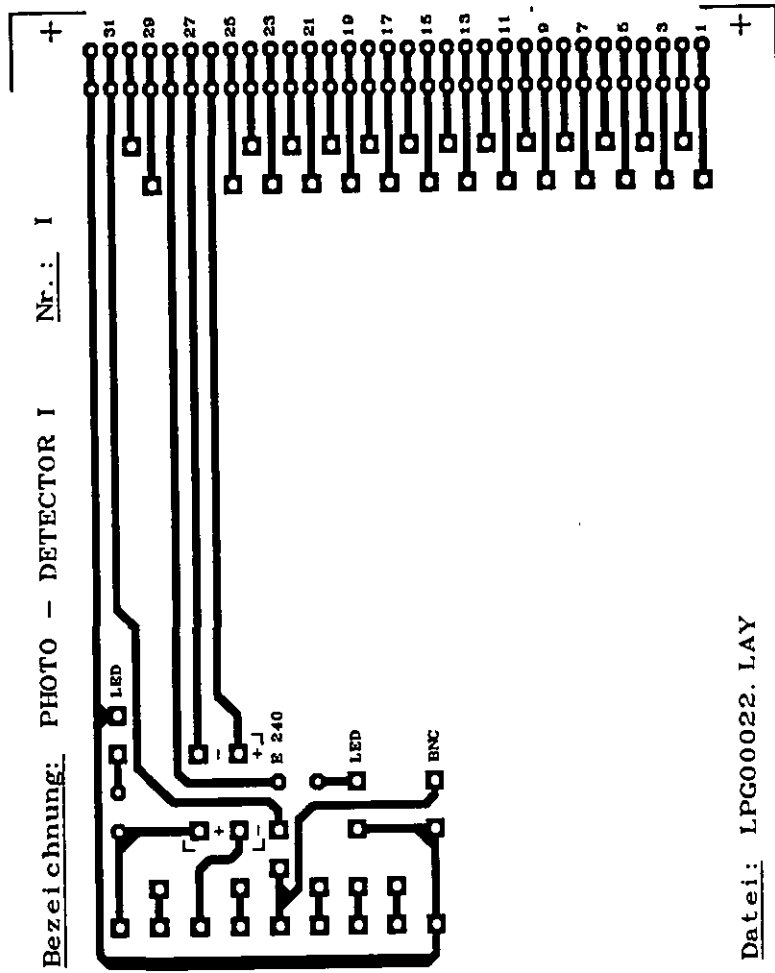
CONTENTS	PAGE #
1. Circuit diagram	D106
2. Parts list	D107
3. PCB layout	D108
4. Bus port	D109
5. Pin connections of the terminal	D110
6. Detector connections	D110
7. Photographs	D111



Part-No.:	Title:
Scale:	Circuit diagram of the photo detector I
Material:	
Date: October 1996	FHO-Fachhochschule Ostfriesland
ENGR: Dipl.-Ing. U. Samuels	-Institut für Lasertechnik Ostfriesland -

D.12.2 Parts list

<u>Part No.</u>	<u>Description</u>
R1	Resistor 560 Ω
R2	Resistor 120 Ω
D1	LED, 5mm, red
D2	LED, 5mm, red
S1	Snap switch
S2	Snap switch



Part-No.:	Title: PCB of the photo detector I
Scale:	
Material:	
Date: October 1996	FHO-Fachhochschule Ostfriesland -Institut für Lasertechnik Ostfriesland -
ENGR: Dipl.-Ing. U. Samuels	

D.12.4 Bus port

Pin #	Description	DAQ - UNIT II, No.: I
1		
2		
3		
4		
5		
6		
7		
8		
9		
10		
11		
12		
13		
14		
15		
16		
17		
18		
19		
20		
21		
22		
23		
24		
25		
26	+ 12V	
27	- 12V	
28	+ 5V	
29	+ 15V	
30	- 15V	
31	E 240 - 1	Pin#: 6
32	GND	

D.12.5 Pin connections of the terminal

Pin #	Description	Connection
1	+ V (+ 12V) (yellow)	
2		
3	- V (- 12V) (white)	
4		
5	V ₀ (0 ... 10V) (brown)	E 240 - 1
6		
7		
8		
9	GND (green)	

D.12.6 Detector connections

Pin #	Description	Colour
1	+ V (+ 12V)	yellow
2		
3	- V (- 12V)	white
4		
5	Out: V ₀ (0 ... 10V) E 240	brown
6		
7		
8	GND	green

D.12.7 Photographs

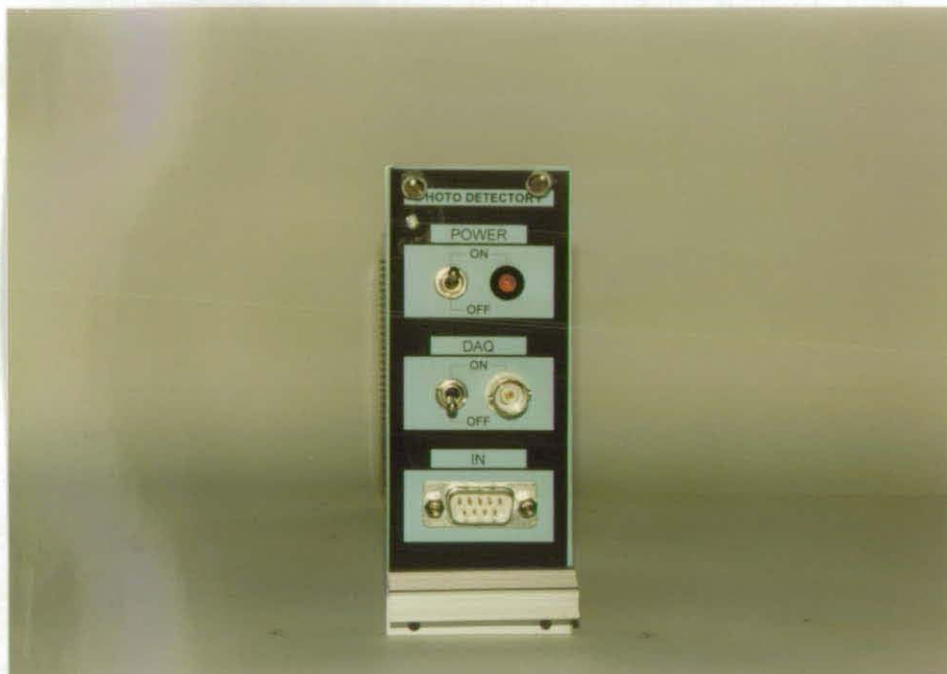


Photo D37: Front view of the photo detector I

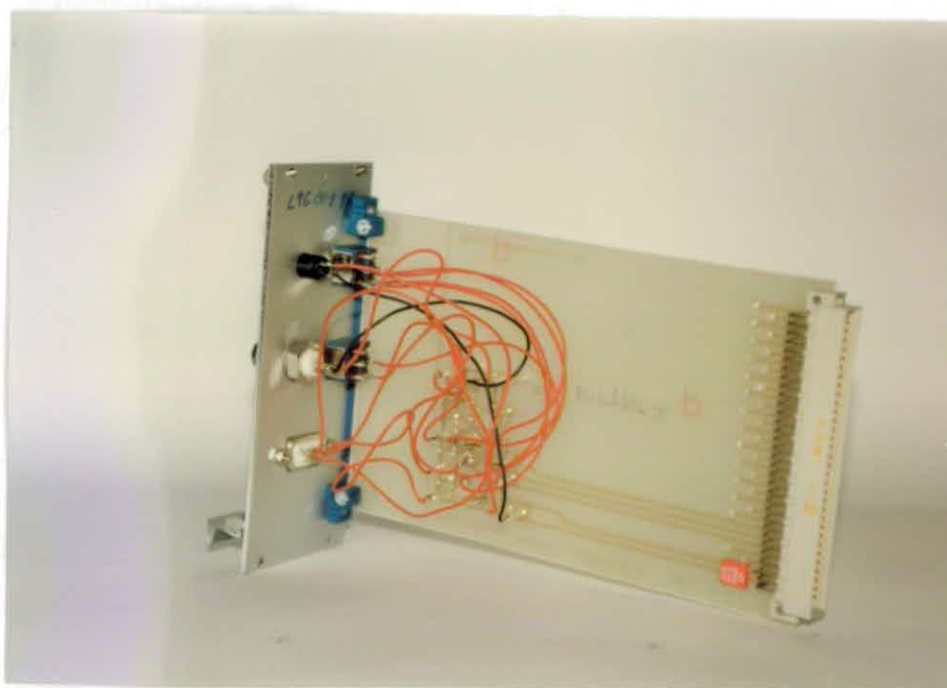
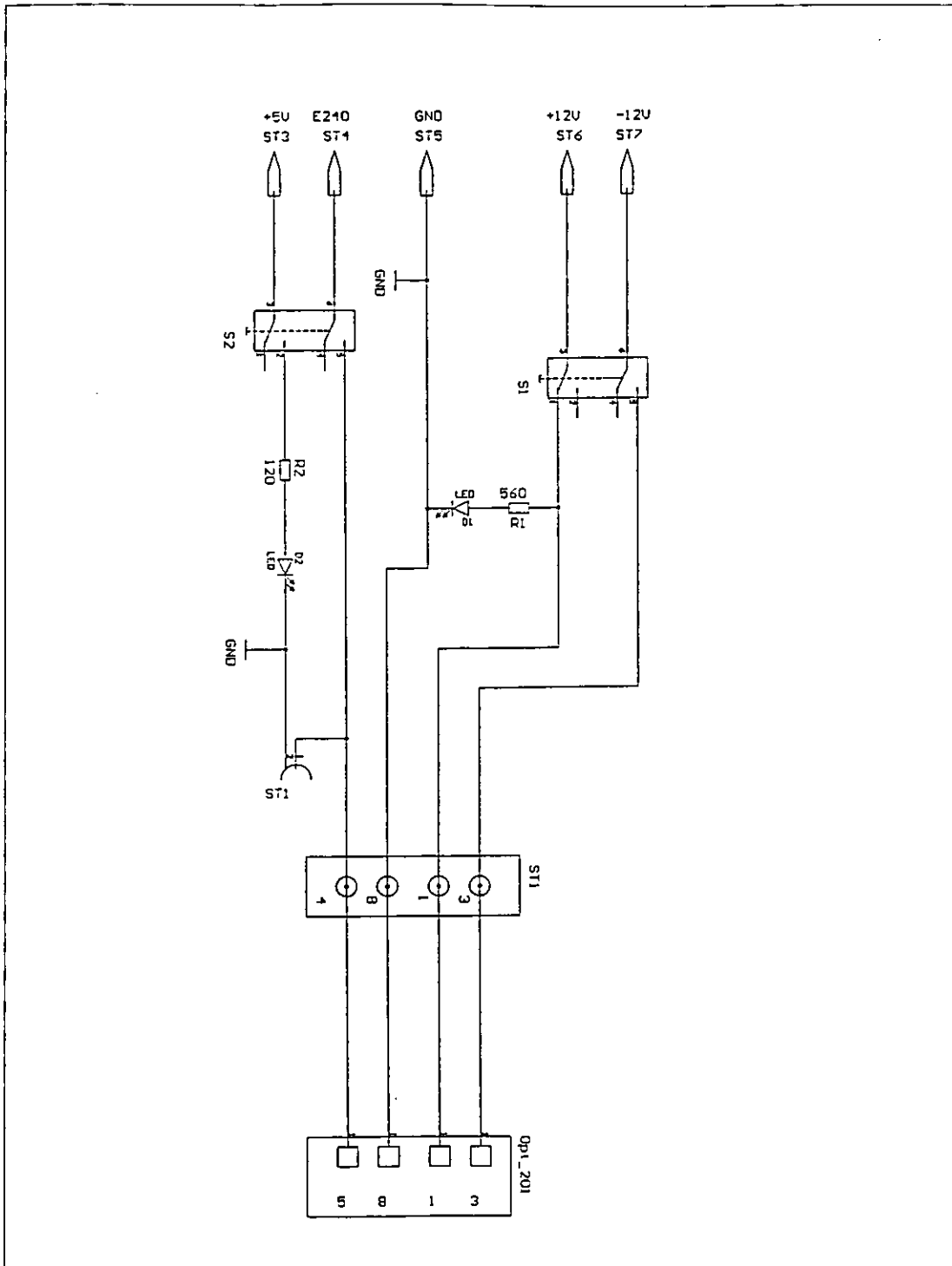


Photo D38: Side view of the photo detector I

D.12 Photo detector II

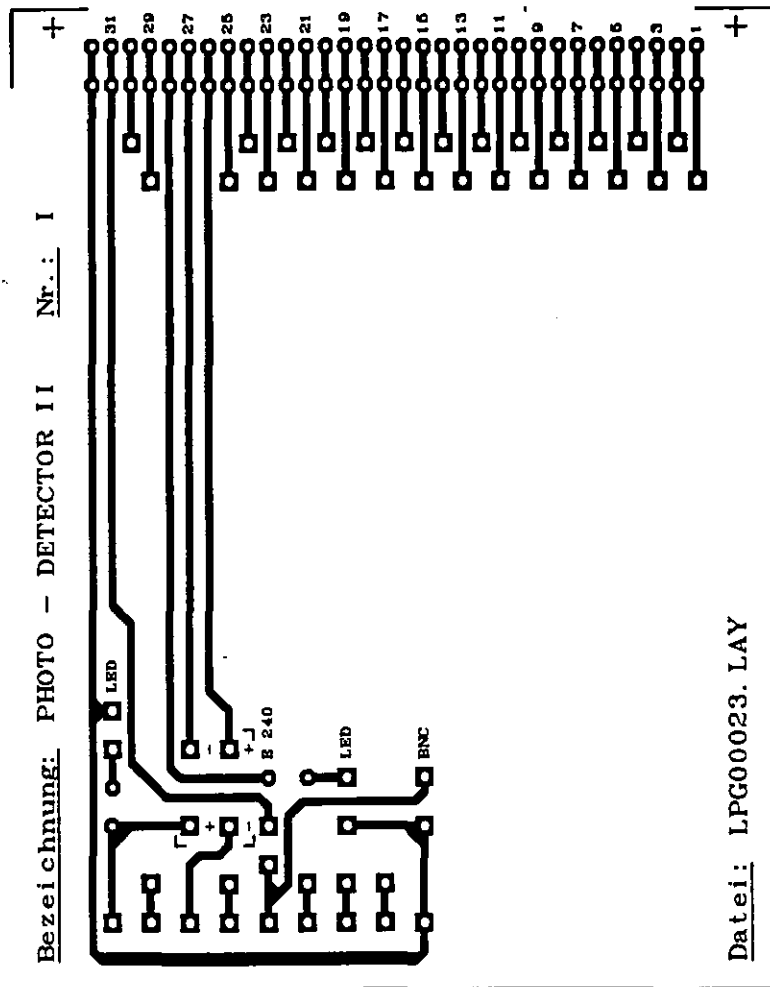
CONTENTS	PAGE #
1. Circuit diagram	D113
2. Parts list	D114
3. PCB layout	D115
4. Bus port	D116
5. Pin connections of the terminal	D117
6. Detector connections	D117
7. Photographs	D118



Part-No.:	Title:
Scale:	Circuit diagram of the photo detector II
Material:	
Date: October 1996	FHO-Fachhochschule Ostfriesland -Institut für Lasertechnik Ostfriesland -
ENGR: Dipl.-Ing. U. Samuels	

D.13.2 Parts list

<u>Part No.</u>	<u>Description</u>
R1	Resistor 560 Ω
R2	Resistor 120 Ω
D1	LED, 5mm, red
D2	LED, 5mm, red
S1	Snap switch
S2	Snap switch



Part-No.:	Title: PCB of the photo detector II
Scale:	
Material:	
Date: October 1996	FHO-Fachhochschule Ostfriesland -Institut für Lasertechnik Ostfriesland -
ENGR: Dipl.-Ing. U. Samuels	

D.13.4 Bus port

Pin #	Description	DAQ - UNIT II, No.: I
1		
2		
3		
4		
5		
6		
7		
8		
9		
10		
11		
12		
13		
14		
15		
16		
17		
18		
19		
20		
21		
22		
23		
24		
25		
26	+ 12V	
27	- 12V	
28	+ 5V	
29	+ 15V	
30	- 15V	
31	E 240 - 2	Pin#: 7
32	GND	

D.13.5 Pin connections of the terminal

Pin #	Description	Connection
1	+ V (+ 12V) (yellow)	
2		
3	- V (- 12V) (white)	
4		
5	V ₀ (0 ... 10V) (brown)	E 240 - 2
6		
7		
8		
9	GND (green)	

D.13.6 Detector connections

Pin #	Description	Colour
1	+ V (+ 12V)	yellow
2		
3	- V (- 12V)	white
4		
5	Out: V ₀ (0 ... 10V) E 240	brown
6		
7		
8	GND	green

D.13.7 Photographs

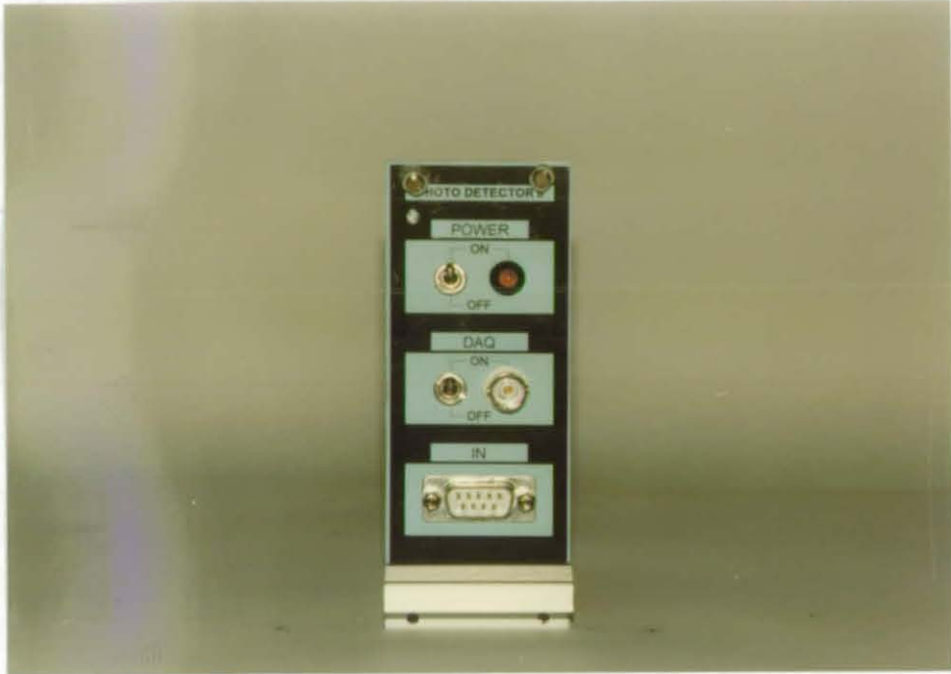


Photo D39: Front view of the photo detector II

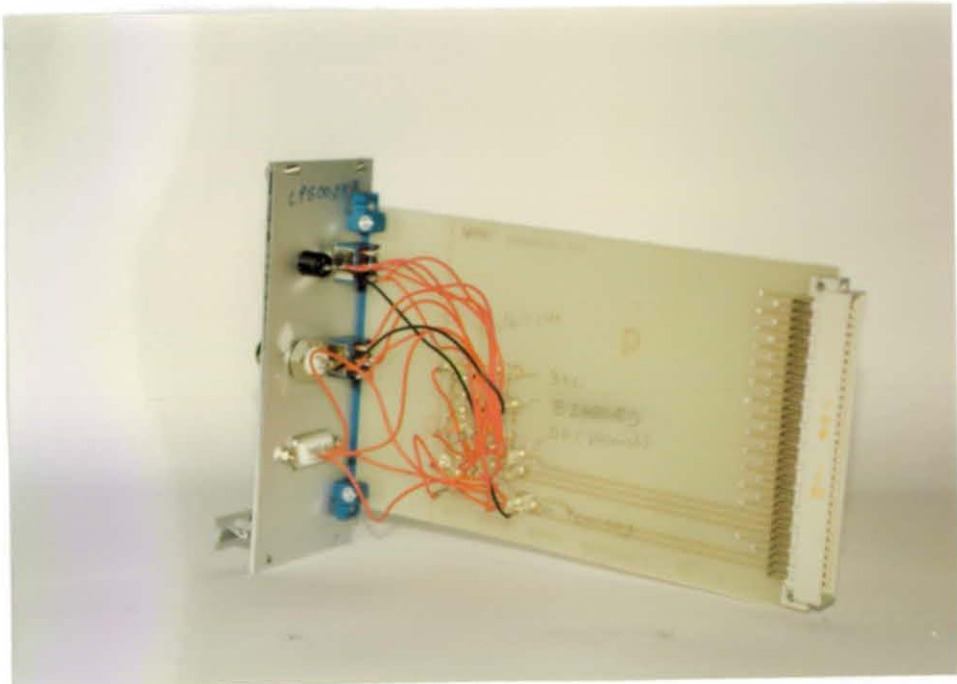


Photo 40: Side view of the photo detector II

E. LPG Software

CONTENTS	PAGE #
1. System requirements	E1
2. Axis control	E2
3. Evaluation of the interferometer signal	E7
4. DAI programming	E11
5. Intensity control	E16
6. Focal position control	E22
7. Module test system	E28
8. Laser stability	E29
9. Positioning tracing	E33
10. Positioning accuracy	E36
11. Error compensation	E41
12. Exposure program	E47
13. Floppy disk	E51

E.1 System requirements

Computer: Personal computer with Intel 80386 processor and VGA screen

Interfaces:

- A 12 bit A/D and D/A converter DAQ-1212A from Physik Instrumente (PI)
- A 48 channel PIO card from Conrad Electronics
- A 3 channel 24 bit counter card from Kolter Electronics
(All cards are described in chapter 3.1.3.1)

Compiler: Turbo Pascal 6.0 from Borland

Tools: Real-Time graphics and measurement/control tools for Turbo Pascal 6.x Version 2.0 from Quinn Curtis

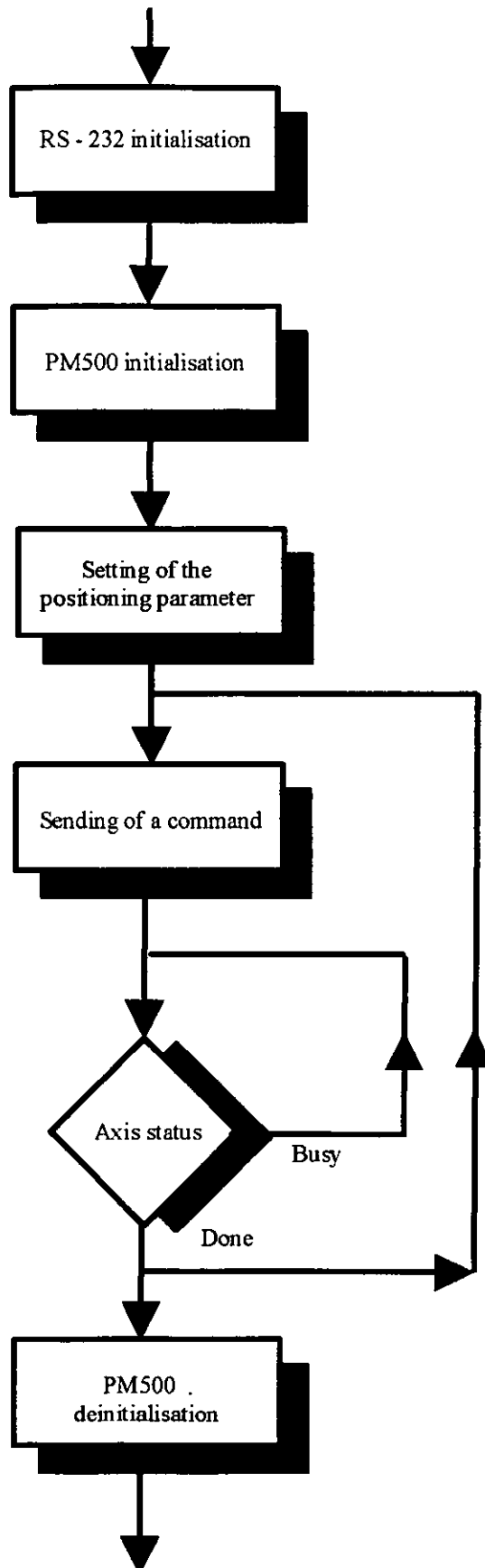
Hardware:

- The complete optical system described in chapter 3.1.1
- The complete positioning system described in chapter 3.1.2
- The complete control system described in chapter 3.1.3

E.2 Axis control

CONTENTS	PAGE #
1. Flow chart	E3
2. Description of the procedures and functions	E4
3. Procedures and functions	E5

E.2.1 Flow chart



E.2.2 Description of the procedures and functions

FUNCTION PM500Command(Befehl: PChar):INTEGER;
Sending a command string to the PM500 and controlling the status signal of the PM500 (L=Limit and D=Done) of the selected axis

FUNCTION PM500Init:INTEGER;
Initialisation of the serial RS-232 interface with the same parameter as the interface of the PM500

PROCEDURE PM500Close;
Closing of the RS-232 interface

The procedures can be found in Appendix E13 : \Modules\PM500

E.2.3 Procedures and functions

```

{*****}
FUNCTION PM500Command(Befehl: PChar):INTEGER;
VAR
  Ch  : Char;
  Strg : STRING;
  Erg,i : INTEGER;
BEGIN
  i := 0;
  REPEAT
    Ch := Befehl[i];
    IF Ch=#0 THEN Ch:=#13;
    SendCom(1,Ch,Erg);
    INC(i);
  UNTIL(Erg<>0) OR (Ch=#13);
  IF Erg=0 THEN BEGIN
    Strg := "";
    REPEAT
      CheckCom(1,Ch,Erg);
      IF Erg=0 THEN Strg := Strg+Ch;
    UNTIL Erg<>0;
    IF Erg=6 THEN Erg := 0;
  END;
  IF Erg=0 THEN
    BEGIN
      IF (Pos('XD',Strg)<>0) OR
        (Pos('XL',Strg)<>0) THEN Erg:=Erg OR PM500DoneX;
      IF (Pos('YD',Strg)<>0) OR
        (Pos('YL',Strg)<>0) THEN Erg:=Erg OR PM500DoneY;
      IF (Pos('AD',Strg)<>0) OR
        (Pos('AL',Strg)<>0) THEN Erg:=Erg OR PM500DoneA;
    END
  ELSE
    Erg := PM500Err;
  PM500Befehl := Erg;
END;

{*****}

```

```
{*****}
FUNCTION PM500Init:INTEGER;
VAR
  Err :INTEGER;
BEGIN
  { Com port 2, 9600 baud, no parity, 2 stop bit, 8 data bits }
  OpenCom(1,9600,'N',2,8,Err);
  SetHandshakeMode(1,1);
  SetHardHandshake(1,$10);
  IF (Err=0) THEN PM500Init:=0 ELSE PM500Init:=PM500Err;
END;

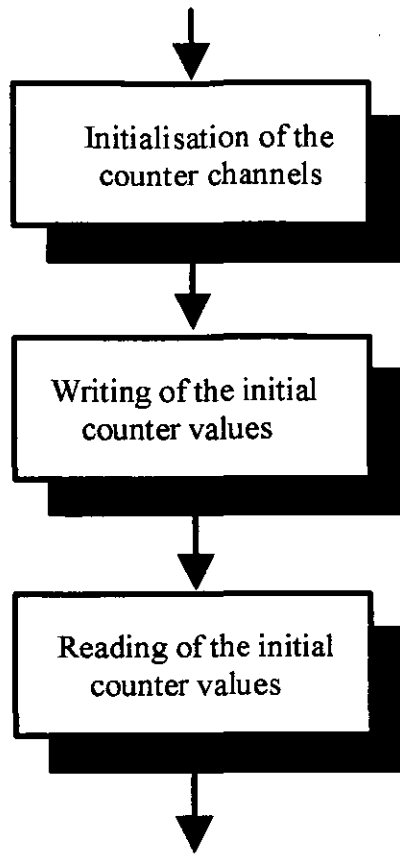
{*****}
PROCEDURE PM500Close;
BEGIN
  CloseCom(1);
END;

{*****}
```

E.3 Evaluation of the interferometer signal

CONTENTS	PAGE #
1. Flow chart	E8
2. Description of the procedures and functions	E9
3. Procedures and functions	E10

E.3.1 Flow chart



E.3.2 Description of the procedures and functions

PROCEDURE KolterInit; {Kolterkarte Initialisieren}

 Initialisation of the input channels of the counter card

PROCEDURE KolterSet(Achsenkennung:WORD;Weg:REAL);

 Setting of the initial counter value in μm of the selected axis

FUNCTION KolterRead(Achsenkennung:WORD):REAL;

 Reading of the actual counter value in μm

The procedures can be found in Appendix E13:\Modules\Kolter

E.3.3 Procedures and functions

```
{*****}
PROCEDURE KolterInit;
BEGIN
  Port[SteuerPort] := 128;
  Port[PortC]      := 255;
  Port[PortA]      := ModusX + 8 * ModusY;
  Port[PortB]      := ModusZ;
END;
```

```
{*****}
PROCEDURE KolterSet(Achsenkennung:WORD;Weg:REAL);
VAR
  Soll : TDreiViertelLong;
BEGIN
  Soll.Long := ROUND(Weg/MueProImp) shl 8;
  Port[Achsenkennung+0] := Soll.Hi;
  Port[Achsenkennung+1] := Soll.Mi;
  Port[Achsenkennung+2] := Soll.Lo;
END;
```

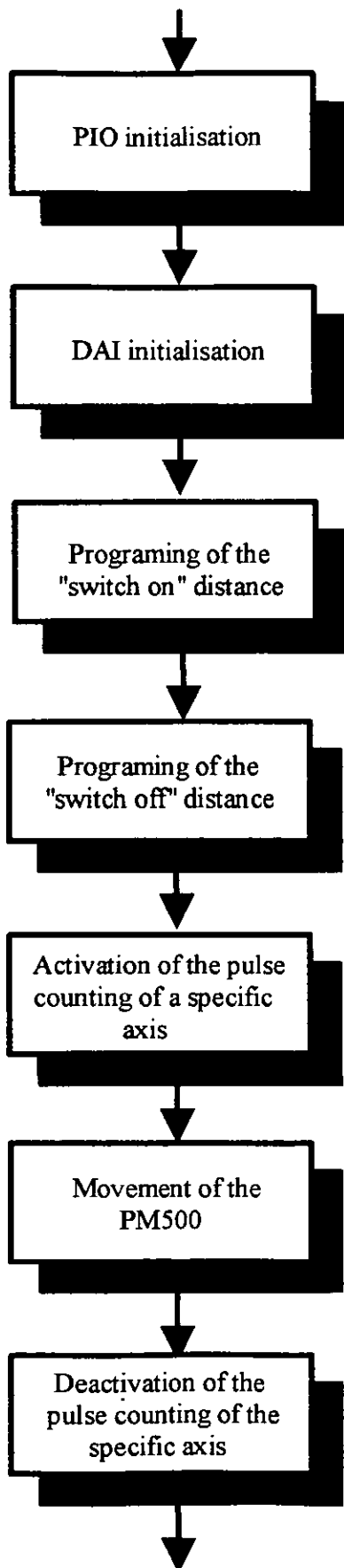
```
{*****}
FUNCTION KolterRead(Achsenkennung:WORD):REAL;
VAR
  Erg : TDreiViertelLong;
BEGIN
  Erg.Hi := Port[Achsenkennung+0];
  Erg.Mi := Port[Achsenkennung+1];
  Erg.Lo := Port[Achsenkennung+2];
  KolterLies := (Erg.Long DIV $100)*MueProImp;
END;
```

```
{*****}
```

E.4 DAI programming

CONTENTS	PAGE #
1. Flow chart	E12
2. Description of the procedures and functions	E13
3. Procedures and functions	E14

E.4.1 Flow chart



E.4.2 Description of the procedures and functions

PROCEDURE Set8Bit(ChipNr,Wert:BYTE);

Setting of one byte to the input lines of a selected IC

PROCEDURE Set24Bit(ChipNr:BYTE;Wert:LONGINT);

Setting of three bytes to the input lines of the selected ICs

PROCEDURE DaiInit;

Initialisation of the DAI unit, so that no DAI signal is counted and the laser is switched off

PROCEDURE DaiOff;

Switches laser off

PROCEDURE DaiOn;

Switches laser on

PROCEDURE DaiWayOn(s:REAL);

Programming of the DAI pulses after that the laser has to be switched on

PROCEDURE DaiWayOff(s:REAL);

Programming of the DAI pulses after that the laser has to be switched off

PROCEDURE DaiAxis(AchsenKennung:BYTE);

Selection of the axis that has to be counted

The procedures can be found in Appendix E13:\Modules\DAI

E.4.3 Procedures and Functions

```

{*****}
PROCEDURE Set8Bit(ChipNr,Wert:BYTE);
BEGIN
  Port[PortA] := Wert;
  Port[PortB] := (Port[PortB] AND $f0) OR ChipNr;
  Port[PortB] := Port[PortB] OR 8;
  Port[PortB] := (Port[PortB] AND $f0) OR 7;
  Port[PortB] := Port[PortB] OR 8;
END;

{*****}
PROCEDURE Set24Bit(ChipNr:BYTE;Wert:LONGINT);
VAR
  i : INTEGER;
BEGIN
  FOR i := ChipNr TO ChipNr+2 DO BEGIN
    Port[PortA] := Wert AND $ff;
    Port[PortB] := (Port[PortB] AND $f0) OR i;
    Port[PortB] := Port[PortB] OR 8;
    Wert := Wert shr 8;
  END;
  Port[PortB] := (Port[PortB] AND $f0) OR 7;
  Port[PortB] := Port[PortB] OR 8;
END;

{*****}
PROCEDURE DaiInit;
BEGIN
  Port[SteuerPort] := $80;
  Port[PortB] := $0f;
  DaiAxis(DAI_nul);
  DaiOff;
END;

{*****}
PROCEDURE DaiOff;
BEGIN
  Set8Bit(6,1);
END;
{*****}

```

```
{*****}
PROCEDURE DaiOn;
BEGIN
  Set8Bit(6,0);
END;
```

```
{*****}
PROCEDURE DaiWayOn(s:REAL);
BEGIN
  Set24Bit(0,-ROUND(s/MueProImp));
END;
```

```
{*****}
PROCEDURE DaiWayOff(s:REAL);
BEGIN
  Set24Bit(3,-ROUND(s/MueProImp));
END;
```

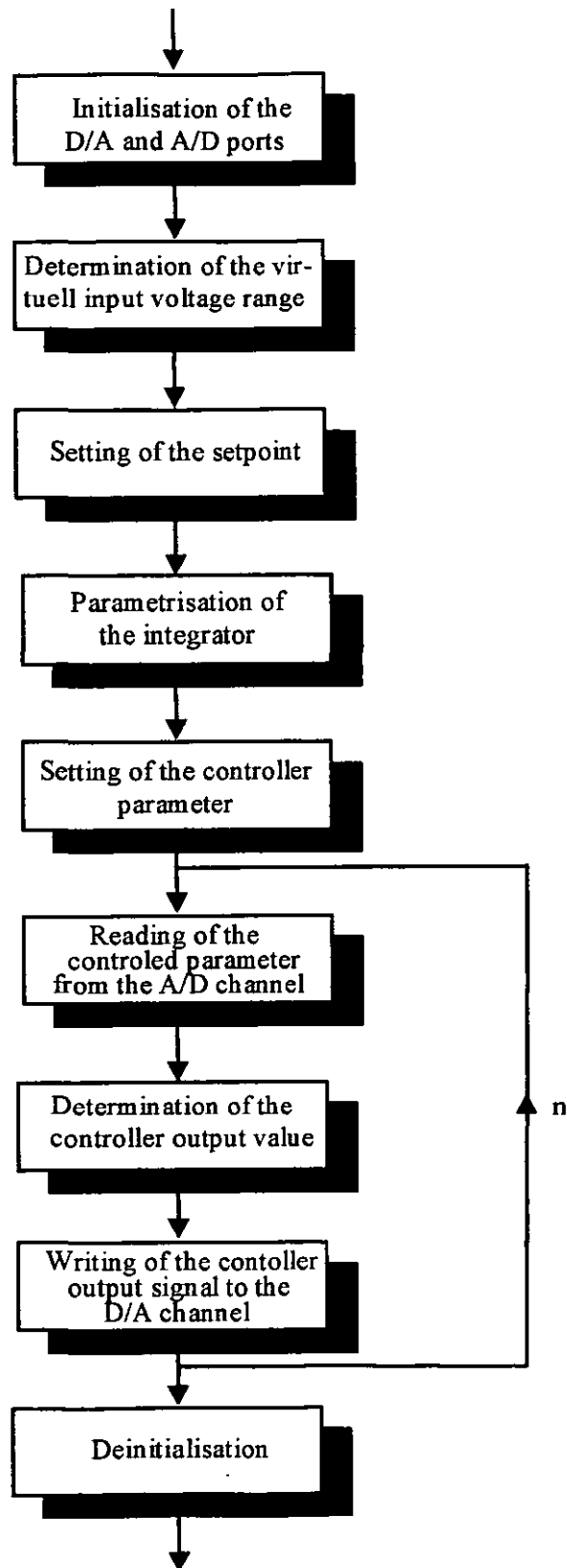
```
{*****}
PROCEDURE DaiAxis(AchsenKennung:BYTE);
BEGIN
  Port[PortB] := (Port[PortB] AND $1f) OR AchsenKennung*$20;
END;
```

```
{*****}
```

E.5 Intensity control

CONTENTS	PAGE #
1. Flow chart	E17
2. Description of the procedures and functions	E18
3. Procedures and functions	E19

E.5.1 Flow chart



E.5.2 Description of the procedures and functions

FUNCTION ReadValue:REAL;

Reads the actual control parameter value from the A/D channel

PROCEDURE Output(StellWert:REAL);

Output of the controller output signal to the D/A converter

FUNCTION IntenSetpoint(x:REAL):BOOLEAN;

Setting of the setpoint

FUNCTION IntenSetParam(kp,yi,yd:REAL):BOOLEAN;

Setting of the controller parameter

FUNCTION IntenUmr(Umin,Umax:REAL;Tiefp:BOOLEAN):BOOLEAN;

Internal signal conversion

FUNCTION IntenControl:BOOLEAN;

Call of the software controller

The procedures can be found in Appendix E13:\Modules\Inti

E.5.3 Procedures and functions

```

{*****}
FUNCTION ReadValue:REAL;
VAR
  Dummy      : WORD;
  Digits     : WORD;
  TempTimer  : TTimer;
BEGIN
  Port[DAC+ 1] := Param.AdCCR+6;
  Port[DAC+ 2] := Param.AdGCR;      {GainControlRegister}
  Port[DAC+10] := $0000;           {clear conversion bit}
  Dummy := Port[DAC+12];          {start conversion}
  TimerInit(TempTimer,1000);      {max. 1ms ConversionTime}
  REPEAT
  UNTIL ((PortW[DAC+15] AND $8000)<>0) OR
  TimerInterrupt(TempTimer);
  Digits := (PortW[DAC+ 0] AND $fff);
  Port[DAC+10] := $0000;          {clear conversion bit}
  Info.IstAD := Param.a*Digits+Param.b;
  Info.Ist := Param.c*Info.IstAD+Param.d;
  IF Info.Ist<-5 THEN Info.Ist:=-5;
  IF Info.Ist>+5 THEN Info.Ist:=+5;
  LiesIstWert := Info.Ist;
END;

{*****}
PROCEDURE Output(StellWert:REAL);
VAR
  Digits: INTEGER;
BEGIN
  Param.StellDA := Param.StellDA + Param.StellKi*Stellwert/TakteProSek;
  IF Param.StellDA< 1 THEN Param.StellDA:= 1;
  IF Param.StellDA> 3 THEN Param.StellDA:= 3;

  Info.Stell := Stellwert;
  Info.StellDA := Param.StellDA;

  Digits := TRUNC(Param.StellDA*($7ff/10)) + $800;
  Port[DAC+ 3] := $0007;  {Channel7}
  Port[DAC+ 4] := Digits AND $ff;
  Port[DAC+ 5] := Digits SHR 8;
  Port[DAC+ 6] := $0001;  {change output with new data values}
END;

{*****}

```

```

{*****}
FUNCTION IntenSetpoint(x:REAL):BOOLEAN;
BEGIN
  Param.Soll := x;
END;

```

```

{*****}
FUNCTION IntenSetParam(kp,yi,yd:REAL):BOOLEAN;
BEGIN
  RtResetErrorTerms(1);           {information software controller}
  RTSetPIDParameters(1,          {LoopNum }
    0,                            {Position Algorithmen}
    Param.Soll,                   {Setpoint[V]}
    0.0,                          {SteadyState [V] }
    kp,                           {Proportional parameter [1] }
    yi,                            {Integral parameter(1/Tn) [1/s] }
    yd,                           {Derivative parameter (Tv) [s] }
    -5,                            {Low Clamp [V] }
    5,                             {HighClamp [V] }
    1000,                         {RateClamp [1/s] }
    1/TakteProSek,               {Seconds Per Sample [s] }
    0.1);                         {FilterConst [1] }

END;

```

```

{*****}
FUNCTION IntenControl:BOOLEAN;
BEGIN
  IF TimerInterrupt(TimerParam) THEN
    SetzStellWert(RTCalcPID(1,    {LoopNum}
      ReadValue,                 {Actual value [V] }
      Param.Soll));              {Set point [V] }
  END;

```

```

{*****}

```

```

{*****}
FUNCTION IntenUmr(Umin,Umax:REAL;Tiefp:BOOLEAN):BOOLEAN;
VAR
  kb,kr,k2,k5,kg : INTEGER; {AD-converter Bits}
  Ux,k25g:REAL;
  dUad : REAL;
  UADmin : REAL;
  UADmax : REAL;
BEGIN
  IF (Umin<-20) OR (Umin>+20) OR
     (Umax<-20) OR (Umax>+20) OR
     (ABS(Umax-Umin)<0.0001) THEN BEGIN
    Umin := -5;
    Umax := +5;
  END;

  IF (Umin<0) OR (Umax<0) THEN kb:=0 ELSE kb:=1;           {kb}
  IF ABS(Umin)>ABS(Umax) THEN Ux:=ABS(Umin) ELSE
  Ux:=ABS(Umax);
  IF Ux*(2-kb)>10 THEN kr:=0 ELSE kr:=1;                     {kr}
  k25g := Ux*(2-kb)/10.001/(2-kr);
  kg := 123-Trunc(ln(k25g*2)/ln(10)+123);
  IF kg<0 THEN kg:=0;
  IF kg>4 THEN kg:=4;                                       {kg}
  k25g := k25g*exp(kg*ln(10));
  IF k25g>2 THEN k5:=0 ELSE k5:=1;                           {k5}
  IF k25g/(5-4*k5)>1 THEN k2:=0 ELSE k2:=1;                  {k2}
  Param.AdCCR := kb*$80+kr*$40;
  Param.AdGCR := k5*$40+k2*$20+$10+kg;
  IF k5*k2=1 THEN Param.AdGCR:=kg;
  IF Tiefp THEN Param.AdGCR:=Param.AdGCR+$80;

  dUad := 10*(2-kr)*(2-k2)*(5-4*k5)/exp(kg*ln(10));
  UADmax := dUad/(2-kb);
  UADmin := UADmax-dUad;

  Param.a := (UADmax-UADmin)/4096;
  Param.b := UADmin;
  Param.c := 10/(Umax-Umin);
  Param.d := 5-Param.c*Umax;

END;

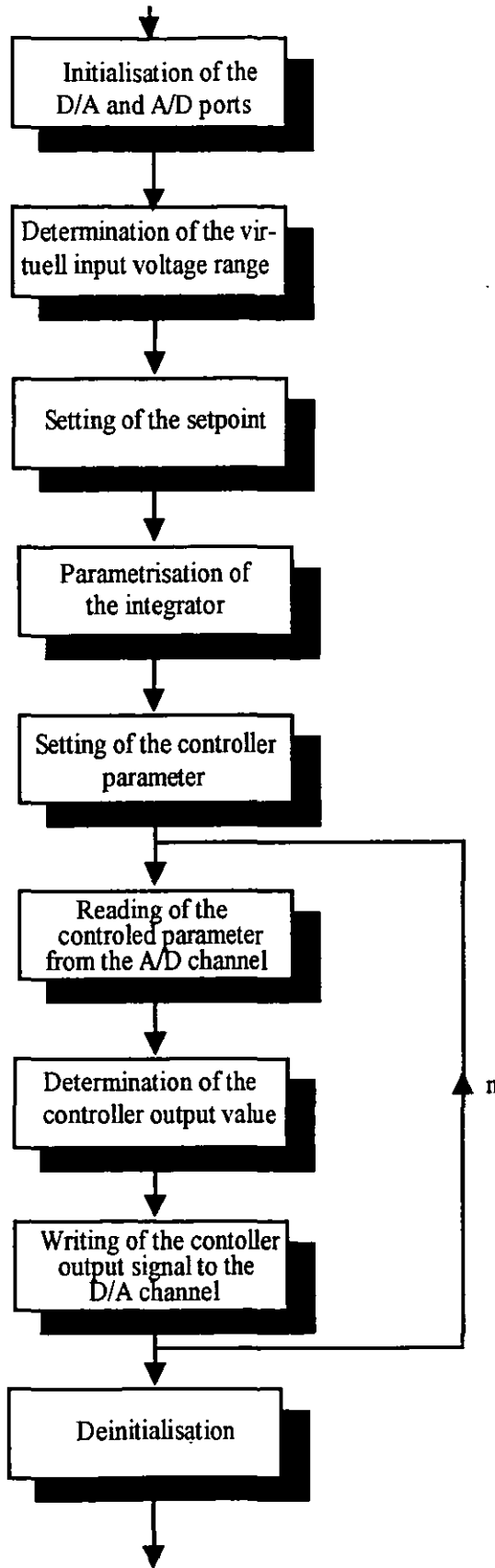
{*****}

```

E.6 Focal position control

CONTENTS	PAGE #
1. Flow chart	E23
2. Description of the procedures and functions	E24
3. Procedures and functions	E25

E.6.1 Flow chart



E.6.2 Description of the procedures and functions

FUNCTION ReadValue:REAL;

 Reads the actual control parameter value from the A/D channel

PROCEDURE Output(StellWert:REAL);

 Output of the controller output signal to the D/A converter

FUNCTION FocalSetpoint(x:REAL):BOOLEAN;

 Setting of the setpoint

FUNCTION FocalSetParam(kp,yi,yd:REAL):BOOLEAN;

 Setting of the controller parameter

FUNCTION FocalUmr(Umin,Umax:REAL;Tiefp:BOOLEAN):BOOLEAN;

 Internal signal conversion

FUNCTION FocalControl:BOOLEAN;

 Call of the software controller

The procedures can be found in Appendix E13:\Modules\Foki

E.6.3 Procedures and functions

```

{*****}
FUNCTION ReadValue:REAL;
VAR
  Dummy   : WORD;
  Digits  : WORD;
  TempTimer : TTimer;
BEGIN
  Port[DAC+ 1] := Param.AdCCR+7;
  Port[DAC+ 2] := Param.AdGCR;           {GainControlRegister}
  Port[DAC+10] := $0000;                 {clear conversion bit }
  Dummy := Port[DAC+12];                 {start conversion}
  TimerInit(TempTimer,1000);             {max. 1ms ConversionTime}
  REPEAT
  UNTIL ((PortW[DAC+15] AND $8000) <> 0) OR
  TimerInterrupt(TempTimer);
  Digits := (PortW[DAC+ 0] AND $ff);
  Port[DAC+10] := $0000;                 {clear conversion bit }
  Info.IstAD := Param.a*Digits+Param.b;
  Info.Ist := Param.c*Info.IstAD+Param.d;
  IF Info.Ist<-5 THEN Info.Ist:=-5;
  IF Info.Ist>+5 THEN Info.Ist:=+5;
  LiesIstWert := Info.Ist;
END;

{*****}
PROCEDURE Output(StellWert:REAL);
VAR
  Digits: INTEGER;
BEGIN
  Param.StellDA := Param.StellDA + Param.StellKi*Stellwert/TakteProSek;
  IF Param.StellDA< 0 THEN Param.StellDA:= 0;
  IF Param.StellDA>10 THEN Param.StellDA:=10;

  Info.Stell := Stellwert;
  Info.StellDA := Param.StellDA;

  Digits := TRUNC(Param.StellDA*($7ff/10)) + $800;
  Port[DAC+ 3] := $0006;                 {Channel6}
  Port[DAC+ 4] := Digits AND $ff;
  Port[DAC+ 5] := Digits SHR 8;
  Port[DAC+ 6] := $0001;                 {new output value}
END;

{*****}

```

```

{*****}
FUNCTION FocalSetpoint(x:REAL):BOOLEAN;
BEGIN
  Param.Soll := x;
END;

```

```

{*****}
FUNCTION FocalSetParam(kp,yi,yd:REAL):BOOLEAN;
BEGIN
  RtResetErrorTerms(0);           {information software controller}
  RTSetPIDParameters(0,          {LoopNum}
    0,                            {PositionAlgorithmus}
    Param.Soll,                   {Sollwert [V]}
    0.0,                          {SteadyState [V]}
    kp,                            {Proportional parameter [1]}
    yi,                            {Integral parameter (1/Tn) [1/s]}
    yd,                            {Derivative parameter (Tv) [s]}
    -5,                            {Low Clamp [V] }
    5,                             {HighClamp [V]}
    1000,                          {RateClamp [1/s]}
    1/TakteProSek,                 {Seconds per Sample [s]}
    0.1);                          {FilterConst [1]}

END;

```

```

{*****}
FUNCTION FocalControl:BOOLEAN;
BEGIN
  IF TimerInterrupt(TimerParam) THEN
    SetzStellWert(RTCalcPID(0,      {LoopNum}
      Read Value,                   {Actual value [V] }
      Param.Soll));                 {Setpoint[V] }
  END;

```

```

{*****}

```

```

{*****}
FUNCTION FocalUmr(Umin,Umax:REAL;Tiefp:BOOLEAN):BOOLEAN;
VAR
  kb,kr,k2,k5,kg : INTEGER; {AD-Wandler Bits}
  Ux,k25g:REAL;
  dUad : REAL;
  UADmin : REAL;
  UADmax : REAL;
BEGIN
  IF (Umin<-20) OR (Umin>+20) OR
    (Umax<-20) OR (Umax>+20) OR
    (ABS(Umax-Umin)<0.0001) THEN BEGIN
    Umin := -5;
    Umax := +5;
  END;

  IF (Umin<0) OR (Umax<0) THEN kb:=0 ELSE kb:=1;           {kb}
  IF ABS(Umin)>ABS(Umax) THEN Ux:=ABS(Umin) ELSE
  Ux:=ABS(Umax);
  IF Ux*(2-kb)>10 THEN kr:=0 ELSE kr:=1;                     {kr}
  k25g := Ux*(2-kb)/10.001/(2-kr);
  kg := 123-Trunc(ln(k25g*2)/ln(10)+123);
  IF kg<0 THEN kg:=0;
  IF kg>4 THEN kg:=4;                                       {kg}
  k25g := k25g*exp(kg*ln(10));
  IF k25g>2 THEN k5:=0 ELSE k5:=1;                           {k5}
  IF k25g/(5-4*k5)>1 THEN k2:=0 ELSE k2:=1;                 {k2}
  Param.AdCCR := kb*$80+kr*$40;
  Param.AdGCR := k5*$40+k2*$20+$10+kg;
  IF k5*k2=1 THEN Param.AdGCR:=kg;
  IF Tiefp THEN Param.AdGCR:=Param.AdGCR+$80;

  dUad := 10*(2-kr)*(2-k2)*(5-4*k5)/exp(kg*ln(10));
  UADmax := dUad/(2-kb);
  UADmin := UADmax-dUad;

  Param.a := (UADmax-UADmin)/4096;
  Param.b := UADmin;
  Param.c := 10/(Umax-Umin);
  Param.d := 5-Param.c*Umax;
END;

{*****}

```

E.7 Module test system

E.7.1 Program description

The modules described in the Appendices E2 to E6 are combined to a program that meets the windows SAA standard.

The program can be found in Appendix E13 :\\Help\\LTest

E.8 Laser stability

CONTENTS

PAGE #

1. Program description
2. Selected procedures

E30

E31

E.8.1. Program description

Using the procedure **AnalogueValue** a constant voltage is subsequently applied to the control input channel of the AOM, so that the photodetector measures the intensity of the first diffraction order of the laser beam. The procedure **Read_A2D** reads the voltage to the detector into the program.

The procedures **Save** and **SaveTime** permit storage of the measured intensity values and system time in a file which can be visualised in using a spreadsheet program (e.g. Excel).

The program can be found in Appendix E13:\Help\Stable

E. 8.2 Selected procedures

```

{*****}
FUNCTION Read_A2D : word;
var index, a : integer;
BEGIN
  index := 0;
  PortW[$32a] := 1;           {15 bit Status register}
  a := PortW[$32c];          {start}
  REPEAT
    delay(10);
  UNTIL (portw[$32f] and ($8000) <> 0); {statusregister 15. bit = 1}
  read_A2D := Portw[$320] and $0fff;
  Portw[$32a] := 0;          {15. bit status register null}
  END;

```

```

{*****}
PROCEDURE Analoguevalue (value : integer);
BEGIN
  PORT[DAQ_Command] := $0;
  PORT[DAQ_LSB] := value AND $07FF;
  PORT[DAQ_MSB] := value SHR 8;
  PORT[DAQ_LOAD] := 1;
END;

```

```

{*****}
PROCEDURE save;
var
  pfad : string;
  f : text;
begin
  clrscr;
  pfad:='b:\daten.txt';
  writeln('Filne name (including Path) :',pfad);
  assign(f,pfad);
  Writeln('Saven');
  rewrite(f);
  for n :=1 to 3600 do
  begin
    writeln(f,VA[n]);
  end;
  close(f);
end;

```

```

{*****}

```

```
{*****}
PROCEDURE savetime;
var
  pfad    : string;
  f       : text;
begin
  pfad:='b:\Zeiten.txt';
  writeln ('File name (including path) :',pfad);
  assign(f,pfad);
  Writeln('Saven');
  rewrite(f);
  writeln(f,'Anfangszeit: ',houreaanfang,' ',minuteanfang,' ',secanfang);
  writeln(f,'Ende      : ',hourende,' ',minuteende,' ',secende);
  writeln(f,'Zeitformat : Stunde, Minute, Sekunde');
  close(f);
end;

{*****}
```

E.9 Positioning tracing

CONTENTS	PAGE #
1. Program description	E34
2. Selected procedures	E35

E.9.1 Program description

After initialisation of the interface and adjustment of the parameters of the PM500, the selected axis (x-axis in this case) is moved by a defined linear path. While movement takes place the procedure **Save_Repro** calls the procedure **ReadCounter-Xaxis**, that determines the actual x-position and stores this position as well as the related system time into a file. These steps will be repeated until the final position of the axis has been reached. The stored data of this file will be displayed on a monitor as the st-diagram of the movements.

The program can be found in Appendix E13:\Help\Position

E.9.2 Selected procedures

```

{*****}
PROCEDURE ReadCounter-Xaxis;
  var LowerByteX,MediumByteX,HigherByteX : longint;
      GesamtByteX                          : longInt;
begin
  LowerByteX :=port[LowerByteC1];
  MediumByteX :=port[MediumByteC1];
  HigherByteX :=port[HigherByteC1];
  GesamtByteX := HigherByteX * 256*256 +
                MediumByteX * 256+LowerByteX;
  if HigherByteX > 127 then {Minus}
    dec(GesamtByteX,16777215);
  if ZwischenSpeicherX <> GesamtByteX then
    begin
      ZwischenSpeicherX := GesamtByteX;
      Anzeige_X(GesamtByteX,LowerByteX,MediumBYteX,
                HigherByteX);
    end;
end;

```

```

{*****}
PROCEDURE Save_Repro(Zahl      : integer;
                    CSignal    : char;
                    Achse,Position : string);
begin
  { if upcase(Achse)='X' then ReadCounter1;
    If upcase(Achse)='Y' then ReadCounter2;
    If upcase(Achse)='Z' then ReadCounter3;}

  if (achse ='X')or (achse='x') then ReadCounter1;
  begin
    { ReadingCounter1; }
    writeln(ProtokollDatei,Zahl,',',clock,',',
            ZwischenSpeicherX * Aufloesung,',',
            ZwischenSpeicherY * Aufloesung,',',
            ZwischenSpeicherZ * Aufloesung,',',
            Position,',N;N;',
            'N;N;N;',
            'N;N;N;',
            'N;N;N;',
            'X;',CSignal,',R;');
  end;
end;
end;

```

```

{*****}

```

E.10 Positioning accuracy

CONTENTS	PAGE #
1. Program description	E37
2. Selected procedures	E38

E.10.1 Program description

Beginning at the starting position, the axis alternately will be displaced to the left and to the right by equally sized linear paths after which the axis is moved back to the starting position. After being placed back to the starting position, the actual position is determined by means of an interferometer. Normally one will find deviations between original and finally reached starting positions which are statistically distributed around an average value. The procedure **Average** calculates the average of the deviations between the values of controller and interferometer while the procedure **StuVa** calculates the associated standard deviation and variance. The function **Gauss** determines the actual gaussian value at the examined position. All calculated values will be displayed on the monitor afterwards.

The program can be found in Appendix E13:\Help\Gauss

E.10.2 Selected procedures and functions

```
{*****}
FUNCTION Gauss(X,S,M : Extended) : Extended;

    {X : X-Value}
    {S : standard deviation}
    {M : arithmetic average value}

begin

    Gauss := ( 1/( (Sqrt(2*Pi))*S ) ) * exp( (-1/2)*Sqr( (X-M)/S ) );

end;

{*****}
```

```

{*****}
PROCEDURE Average (Achse: Char;
                  var MittelC,MaxAbwC,MittelI,MaxAbwI : Extended);

var N    : LongInt;           {number of the read dervations}
    WertC : Extended;        {read deviation - Controller}
    WertI : Extended;        {read deviation - Interferometer}

    {Achse : X- and Y-Axis }
    {MittelC : Average value of the deviation - Controller}
    {MittelI : Average value of the deviation - Interferometer}

begin
  D_Anzahl := 0;
  N := 0;
  MittelC := 0;
  MittelI := 0;
  MaxAbwC := 0;
  MaxAbwI := 0;
  WertC := 0;
  WertI := 0;
  Reset(MessDaten);           {Resetting of the file pointer}
  while not EoF(MessDaten) do
  begin
    ReadLn(MessDaten,Zeile);
    if Gauss_Check then      {Line for Gaussian}
    begin
      Inc(N);
      Abweichungsweg(Achse,WertC,WertI);
      MittelC := MittelC + WertC;
      MittelI := MittelI + WertI;
      if Abs(WertC) > Abs(MaxAbwC) then MaxAbwC := WertC;
      if Abs(WertI) > Abs(MaxAbwI) then MaxAbwI := WertI;
    end;
  end;
  MittelC := (MittelC / N);   {Average value - Controller}
  MittelI := (MittelI / N);   {Average value- Interferometer}
end;

{*****}

```

```

{*****}
PROCEDURE StuVa(Achse : Char; MittelC,MittelI : Extended;
                var StC,VaC,StI,VaI : Extended);

var N    : LongInt;           {number of the read derivation}
    WertC : Extended;        {read deviation - Controller}
    WertI : Extended;        {read deviation - Interferometer}

    {Axis      : X- or Y-Axis}
    {MittelC   : Average value - Controller}
    {MittelI   : Average value - Interferometer}
    {StC       : Standard deviation - Controller}
    {VaC       : Varianz - Controller}
    {StI       : Standard deviation - Interferometer}
    {VaI       : Varianz - Interferometer}

begin
  D_Anzahl := 0;
  N := 0;
  WertC := 0;
  WertI := 0;
  StC := 0;
  StI := 0;
  Reset(MessDaten);           {Resetting of the file pointer}
  while not EoF(MessDaten) do
  begin
    ReadLn(MessDaten,Zeile);
    if Gauss_Check then       {Line for Gaussian }
    begin
      Inc(N);
      Abweichungsweg(Achse,WertC,WertI);
      StC := StC + Sqr(WertC-MittelC);
      StI := StI + Sqr(WertI-MittelI);
    end;
  end;
  VaC := (StC/(N-1));         {Varianz - Controller }
  StC := (Sqr(StC/(N-1)));    {Standard deviation - Controller }
  VaI := (StI/(N-1));         {Varianz - Interferometer }
  StI := (Sqr(StI/(N-1)));    {Standard deviation-Interferometer}
end;

{*****}

```

E.11 Compensation program

CONTENTS	PAGE #
1. Program description	E42
2. Selected procedures	E43
3. Mathcad simulation	E44

E.11.1 Program description

First of all, the axis under consideration will be surveyed using the program **PM500f**. For that purpose the axis will be displaced and the desired (nominal) value and the measured (actual) value, measured by means of an interferometer, will be compared. The positioning error (nominal - actual value), being a function of the nominal value, will be stored in a file. The function indicates a periodical error of the axis movement. The file is examined using the software application Mathcad (see appendix E.11.3) which determines Fourier terms of the Fourier approximation of the error function. The program **PM500U** uses this Fourier table. The function **ErrorCorrection** establishes a control optimisation by replacing the original command value of the PM500 with a value optimised by the functions calculation.

The program can be found in Appendix E13:\Help\Error

E.11.2 Selected procedures

```

{*****}
FUNCTION ErrorCorrection(Var Achse:Char;Var KVal:String):Integer;

Var    Soll_Str,g_Command_str,
        Send_str      : String;
        sz,erg        : Integer;
        RVal          : Real;

Begin
  g_Command_str:="";
  Send_str:="";
  If Achse = 'x' then
    Begin
      erg:=KorrekturX(RVal);
      If (erg=0) then
        Begin
          PM500KorrX:=Round((PM500SollX-RVal)/XAchse_dx)*XAchse_dx;
          Str(PM500KorrX:10:3,Soll_str);
          g_Command_str:='xg'+Soll_str;      { absolute position }
          For sz:= 1 to length(g_Command_str) do if g_Command_str[sz]<>' ' then
            Send_str:=Send_str+g_Command_str[sz]; { delete blanks }
          KVal:=Send_str;
          End
        Else erg:=1
        End
      Else
        Begin
          erg:=KorrekturY(RVal);
          If (erg=0) then
            Begin
              PM500KorrY:=Round((PM500SollY-RVal)/YAchse_dx)*YAchse_dx;
              Str(PM500KorrY:10:3,Soll_str);
              g_Command_str:='yg'+Soll_str;
              For sz:= 1 to length(g_Command_str) do if g_Command_str[sz]<>' ' then
                Send_str:=Send_str+g_Command_str[sz]; { delete blanks }
              KVal:=Send_str;
              End
            Else erg:=1
            End;
          FehlerKorrektur:=erg;
        End;
    End;
  End;

```

E.11.3 Mathcad simulation

Sample points of the measured positioning characteristics

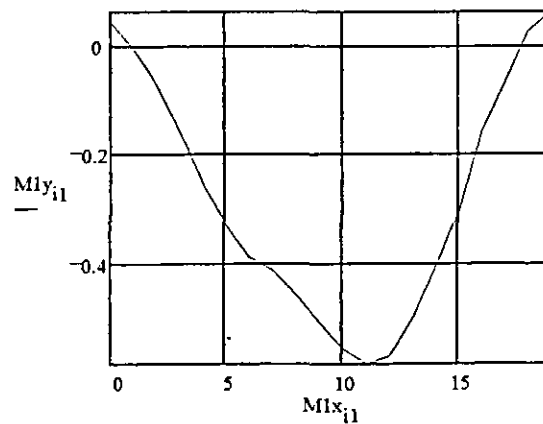
$M1x :=$	0	$M1y :=$	0.042748
	1		-0.008306
	2		-0.072364
	3		-0.159176
	4		-0.255732
	5		-0.329536
	6		-0.39034
	7		-0.415402
	8		-0.459968
	9		-0.511024
	10		-0.558828
	11		-0.587136
	12		-0.573208
	13		-0.50402
	14		-0.412086
	15		-0.307158
	16		-0.159972
	17		-0.06805
	18		0.023892
	19		0.060576

$\text{länge}(M1y) = 20$

$k1 := \text{länge}(M1x) - 1$ $k1 = 19$

$i1 := 0..k1$

Visualisation of the measured curve



Cubic Spline Interpolation

$$v1x := \frac{M1x \cdot 2 \cdot \pi}{M1x_{k1}}$$

$$v1y := 2 \cdot \left(\frac{M1y - \min(M1y)}{\max(M1y - \min(M1y))} \right) - 1$$

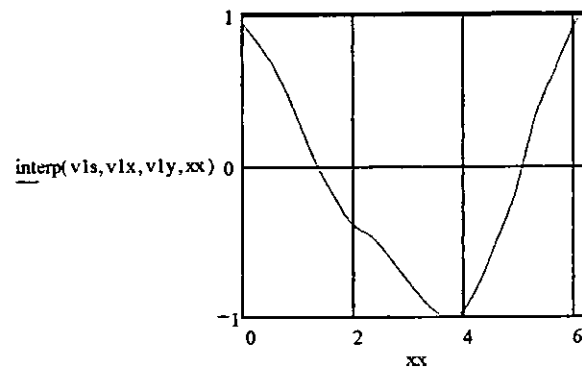
$$v1s := \text{kspline}(v1x, v1y)$$

$$N := 512 \quad n := 0..2 \cdot N - 1$$

$$dx := \frac{\pi}{N} \quad xx := 0, dx..2 \cdot \pi$$

$$x_n := \frac{\pi \cdot n}{N}$$

Visualisation of the spline interpolation curve



Determination of the Fourier parameter

$$Y1 := \overrightarrow{\text{interp}(v1s, v1x, v1y, x)} \quad k := 0..N$$

$$A1_k := \frac{1}{N} \cdot \left(\sum_n Y1_n \cdot \cos(x_n \cdot k) \right) \quad B1_k := \frac{1}{N} \cdot \left(\sum_n Y1_n \cdot \sin(x_n \cdot k) \right)$$

$$\text{AufPM500} := 25$$

$$\text{Periode1} := (\max(M1x) - \min(M1x)) + M1x_1 - M1x_0 \quad \text{Periode1} = 20$$

$$\text{AnzahlWerte1} := \frac{\text{Periode1} \cdot 1000}{\text{AufPM500}} \quad \text{AnzahlWerte1} = 800$$

$$dx1 := \frac{2 \cdot \pi}{\text{AnzahlWerte1}} \quad dx1 = 0.008$$

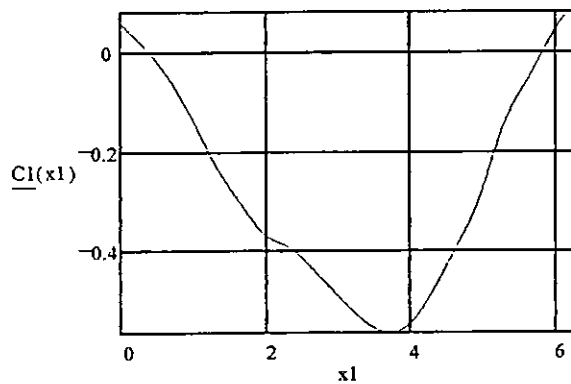
$$x1 := 0, dx1.. 2 \cdot \pi$$

$$h1 := \frac{\max(M1y) - \min(M1y)}{2}$$

$$b1 := \max(M1y) - \left[\left(\sum_k A1_k \right) \cdot h1 \right] \quad b1 = -0.209$$

$$C1(x1) := \left[\left(\sum_k B1_k \cdot \sin(k \cdot x1) \right) \cdot h1 + \left(\sum_k A1_k \cdot \cos(k \cdot x1) \right) \cdot h1 + b1 \right]$$

Visualisation of the result



Export of the result

$$\text{PRNSCHREIBEN}(x1_pi) := x1$$

$$dx1 := \frac{\text{AufPM500}}{1000} \quad dx1 = 0.025$$

$$x1 := 0, dx1.. \text{Periode1}$$

$$\text{PRNSCHREIBEN}(x1) := x1$$

E.12 Exposure program

CONTENTS	PAGE #
1. Program description	E48
2. Selected procedures	E49

E.12.1 Program description

Calling the procedure **Data** will read following exposure data from a file:

- focal position
- intensity
- exposure duration
- radius

This file can be generated using a standard text editor.

Calling the function **Plott_Circle** will establish the exposure of a circle by using these parameters. The positioning movement is exclusively performed through linear axes.

The program can be found in Appendix E13:\Exposure

E.12.2 Selected procedures

```

{*****}
PROCEDURE Data (j:Integer);
Const  datname='B:\code1.txt';
VAR    zeile :Array[1..4000] of real;
        o :Integer;
        datei :Text;

Begin
  Assign(datei,datname);
  Reset(datei);
  For o:=2 to i*4 Do readln(Datei);
  Readln(datei,zeile[j]);
  Radius:=zeile[j];           {Radius}
  Readln(datei,zeile[j+1]);
  Focal:=zeile[j+1];         {Focal position}
  Readln(datei,zeile[j+2]);
  Intensity:=zeile[j+2];     {Intensity}
  Readln(datei,zeile[j+3]);
  Duration:=zeile[j+3];      {Exposure duration}
  If Eof(datei) Then Dateiende:=1 Else Dateiende:=0;
  Close(Datei);
End;

{*****}

```

```
{*****}
{Main}
Begin
  put_ttl($44);
  Clrscr;
  PM500ini;
  Mitte;
Repeat
  Writeln('Press any key');
Until Keypressed;

  Radius_alt:=0;
  Delay(500);
  i:=0;
  Repeat
    clrscr;
    Inc(i);
    Data(i);
    writeln('Number',i);
    mitte;
    plot_circle(radius, Focal, Intensity, Duration);
  Until Dateiende=1;
  PM500Close;
End.

{*****}
```

E.13 Floppy disk

The floppy disk contains the following directories:

```
: \    MODULES  \PM500
          \Kolter
          \DAI
          \Inti
          \Foki
      HELP  \Ltest
          \Stable
          \Position
          \Gauss
          \Error
      EXPOSURE
      LASSI
```

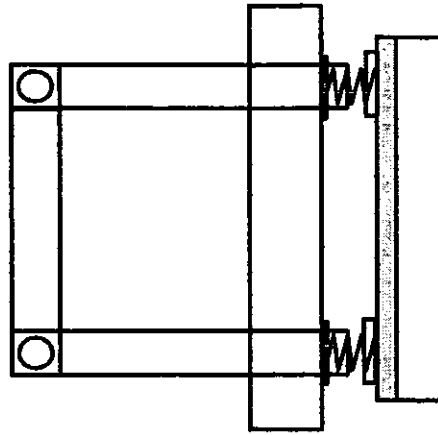
F.MECHANICAL SYSTEM OF THE LPG

CONTENTS	PAGE #
1. LPG construction	F1-F6
2. Positioning units	F7-F14
3. Optical planes	F15-F21

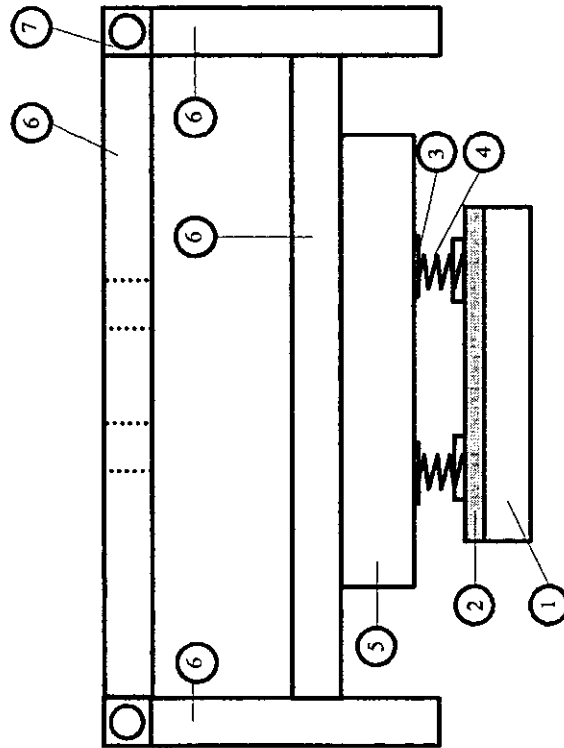
F.1 LPG construction

CONTENTS	PAGE #
1. Rack	F1
2. Parts list of rack	F3
3. Optical table	F4
4. Parts list of the optical table	F5
5. Photographs	F6

Side view



Front view



Part-No.:

Scale: Arbitrary

Material:

Date: October 1996

ENGR: Dipl.-Ing. U. Samuels

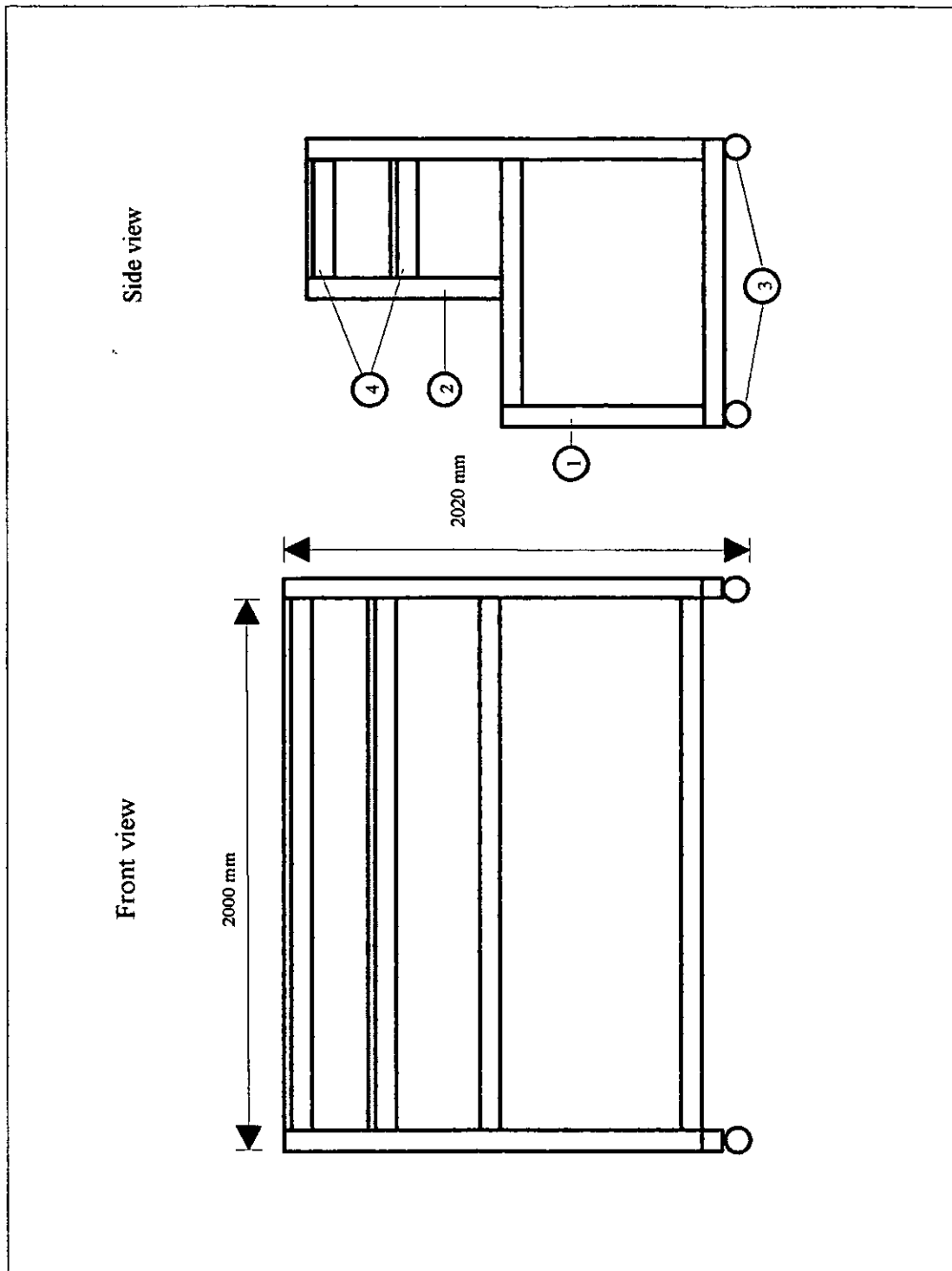
Title:

Optical table of the LPG

FHO-Fachhochschule Ostfriesland
-Institut für Lasertechnik Ostfriesland -

F.1.2 Parts list of the rack

<u>Part No.</u>	<u>Description</u>
1	Button module of the rack
2	Top module of the rack
3	Reel
4	Board



Part-No.:	Title: Rack of the LPG
Scale: Arbitrary	
Material:	
Date: October 1996	FHO-Fachhochschule Ostfriesland -Institut für Lasertechnik Ostfriesland -
ENGR.: Dipl.-Ing. U. Samuels	

F.1.4 Parts list of the optical table

<u>Part No.</u>	<u>Description</u>
1	Styropore plate
2	Wodden plate
3	Holder
4	Spring
5	Marmor plate
6	X95-profile
7	Combiner cube

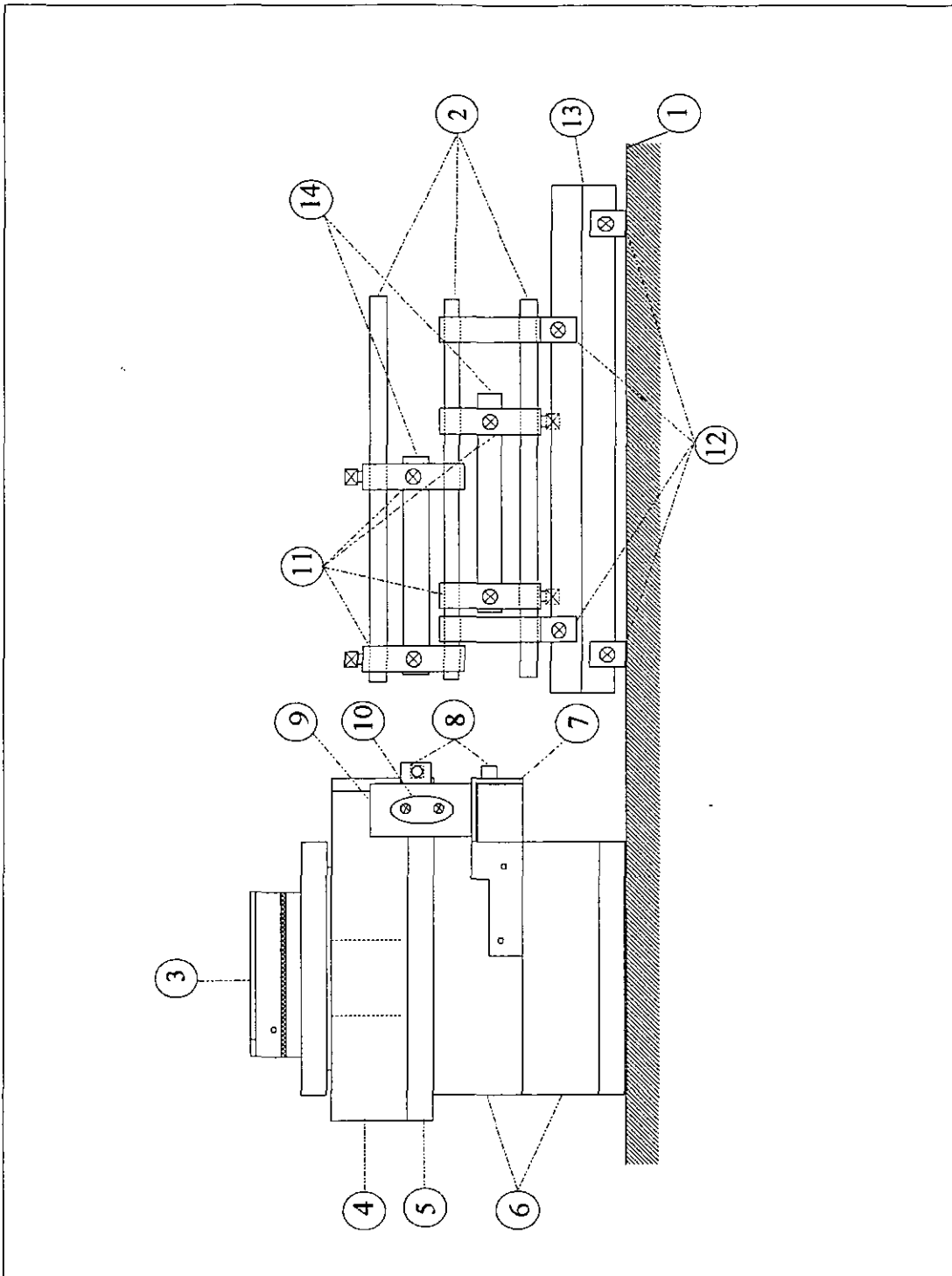
F.1.5 Photographs



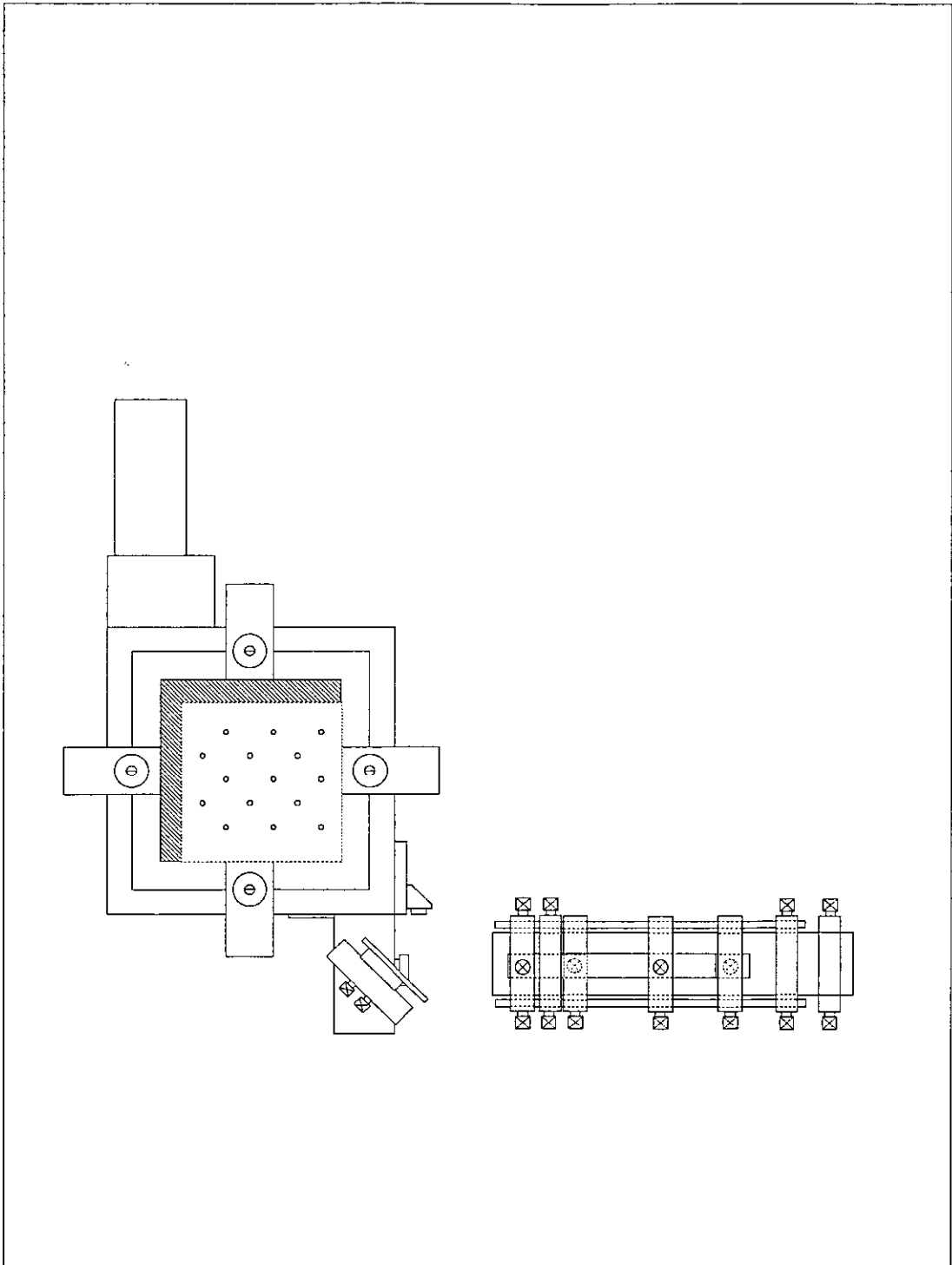
Photo F1: LPG system

F.2 Positioning units

CONTENTS	PAGE #
1. Side view of the positioning system	F8
2. Top view of the positioning system	F9
3. Parts list of the positioning system	F10
4. Photographs of the positioning system	F11
5. Construction of the processing head	F12
6. Parts list of the processing head	F13
7. Photographs of the processing head	F14



Part-No.:	Title:
Scale: Arbitrary	Side view of the positioning system
Material:	
Date: October 1996	FHO-Fachhochschule Ostfriesland -Institut für Lasertechnik Ostfriesland -
ENGR.: Dipl.-Ing. U. Samuels	



Part-No.:	Title: Top view of the positioning system
Scale: Arbitrary	
Material:	
Date: October 1996	FHO-Fachhochschule Ostfriesland -Institut für Lasertechnik Ostfriesland -
ENGR.: Dipl.-Ing. U. Samuels	

F.2.3 Parts list of the positioning system

<u>Part No.</u>	<u>Description</u>
1	Bread board
2	Precision rods
3	Substrate holder
4	Rotary stage
5	Adapter
6	Linear axis
7	Mounting board
8	Retro reflector
9	Mount
10	Tilt mirror
11	x,y mini stages
12	X25 carriger
13	X25 profile
14	Interferometer head

F.2.4 Photographs of the positioning system

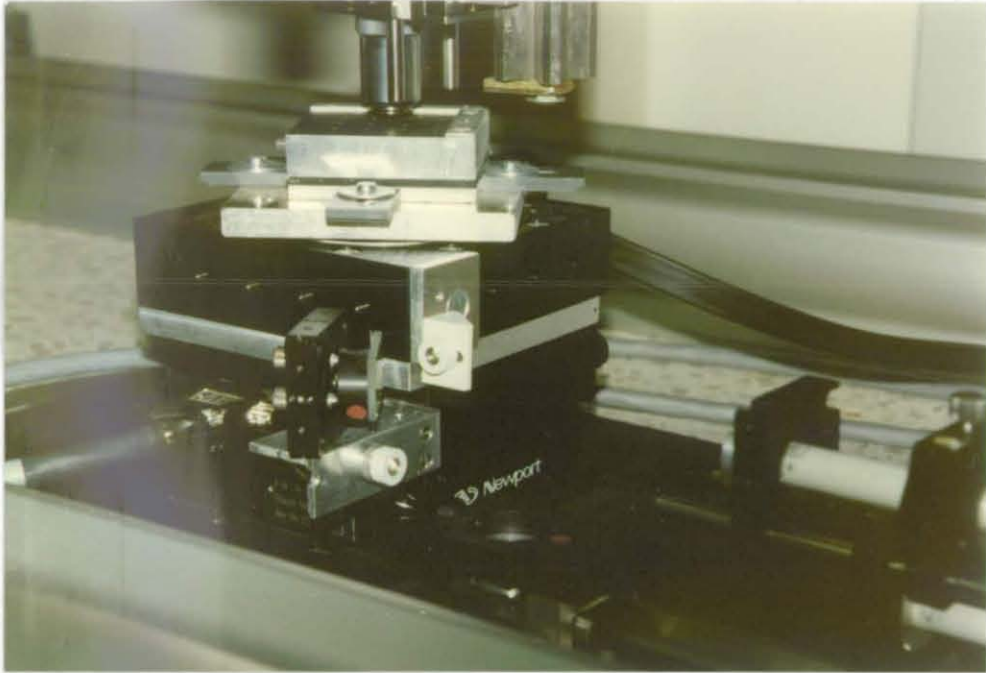


Photo F2: Positioning system

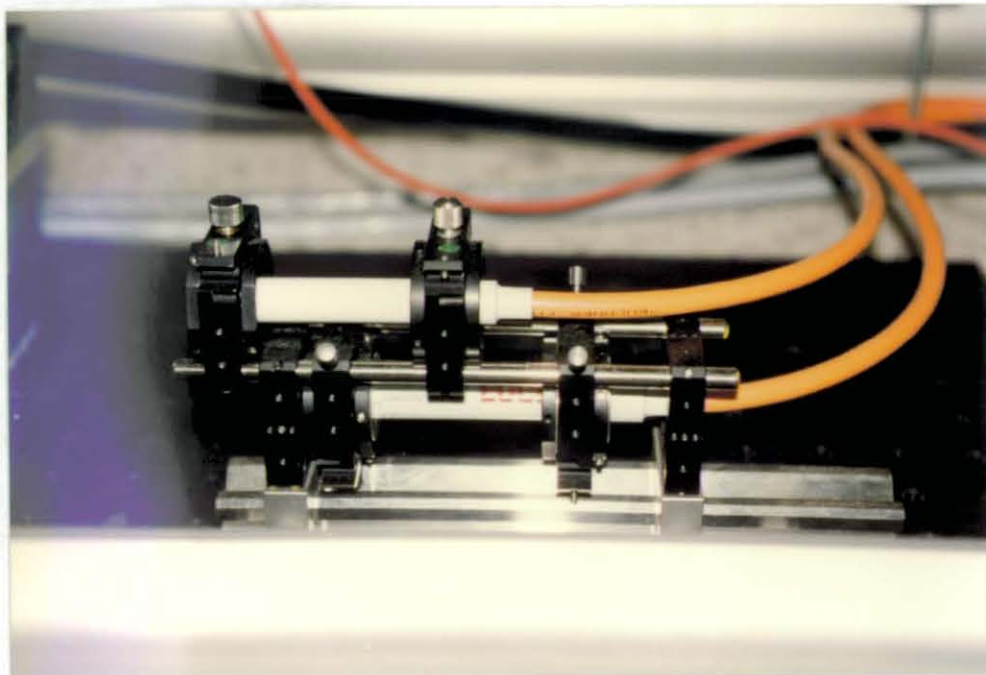
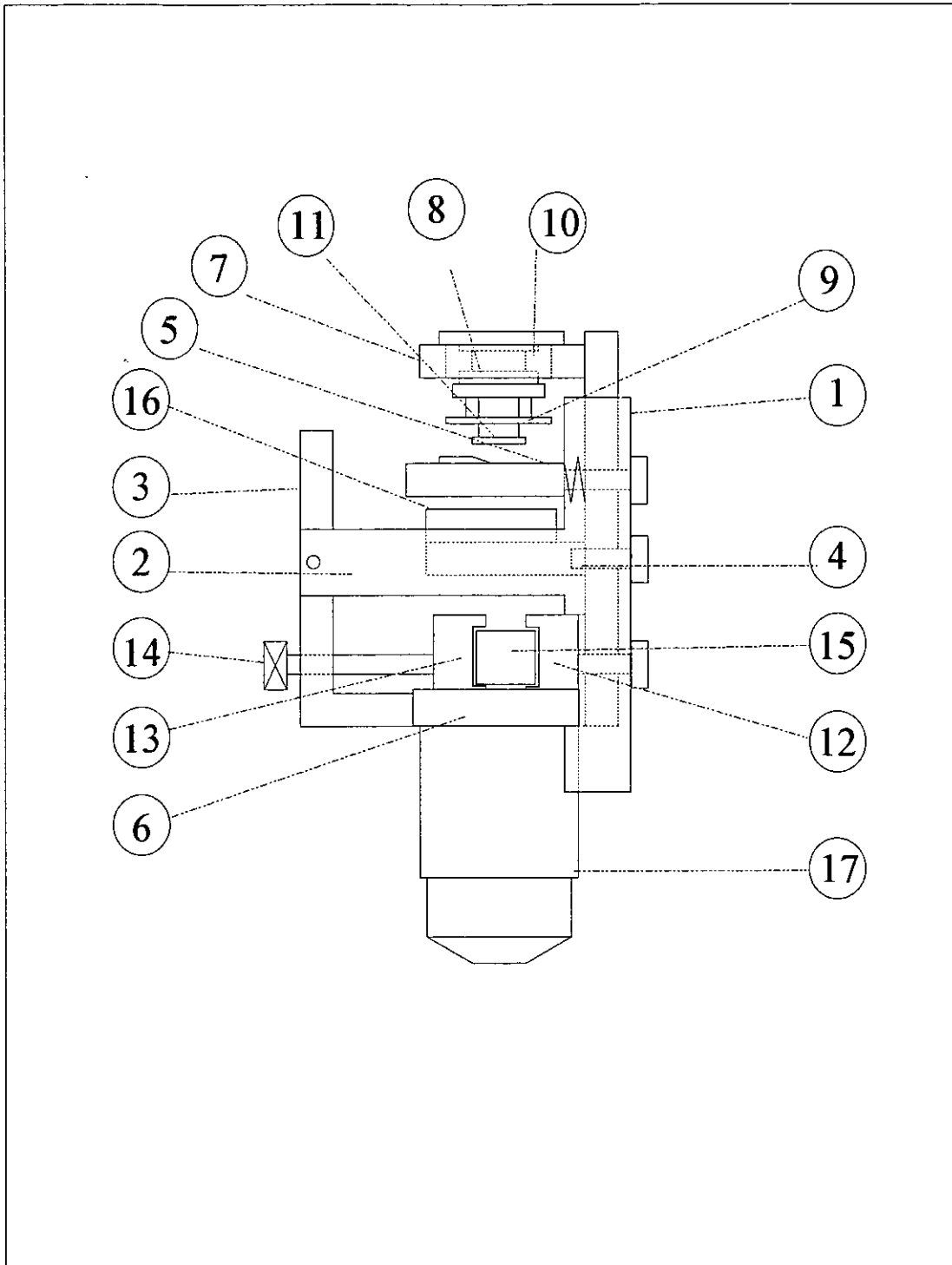


Photo F3: Laser interferometer head



Part-No.:	Title:
Scale: Arbitrary	Assembly schematic of the optimised processing head
Material:	
Date: October 1996	FHO-Fachhochschule Ostfriesland -Institut für Lasertechnik Ostfriesland -
ENGR.: Dipl.-Ing. U. Samuels	

F.2.6 Parts list of the processing head

<u>Part No.</u>	<u>Description</u>
1	Base plate
2	Connector plate
3	Adapter for the piezo translator
4	Lens mount with lens $f=20\text{mm}$
5	Beam stop mount with beam stop
6	Microscope objective mount
7	PSD adjustment unit
8	PSD mount
9	PCB for the PSD
10	Leaf spring
11	PSD
12	Beam splitter holder a
13	Beam splitter holder b
14	Threaded rod
15	Beam splitter
16	Interference filter
17	Microscope objective

F.2.7 Photographs of the processing head

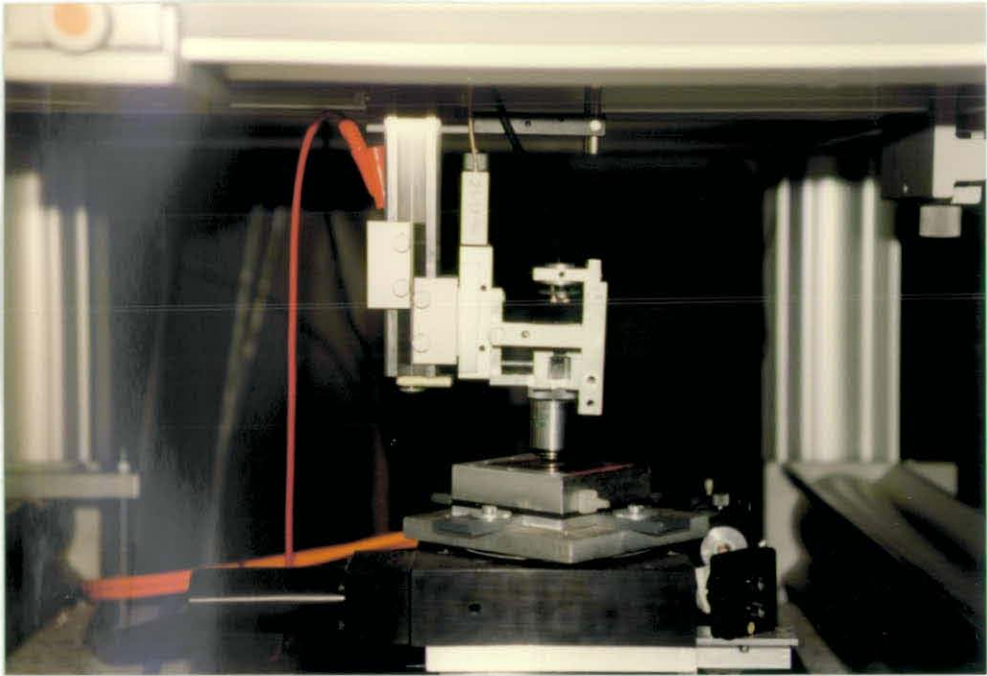
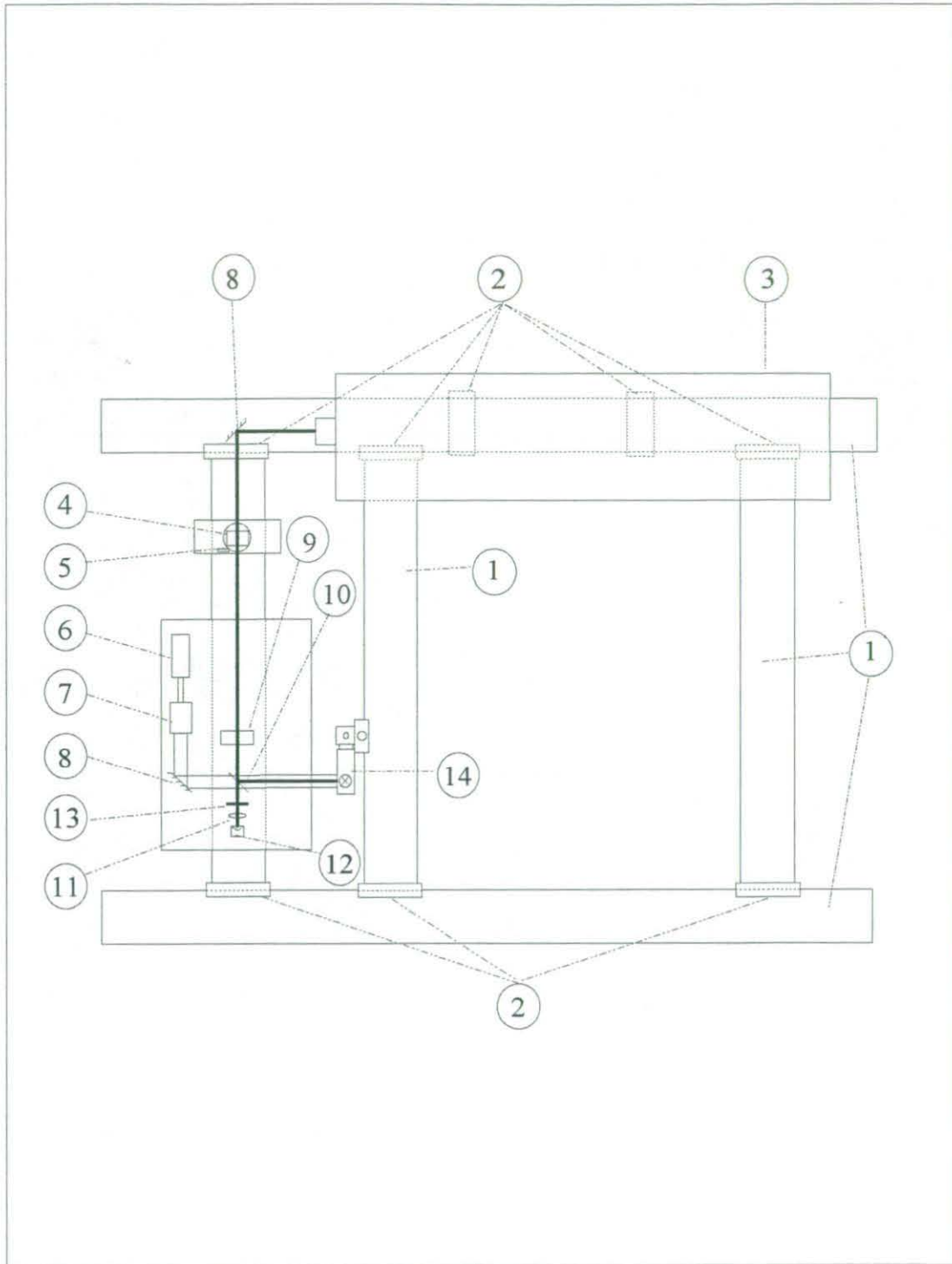


Photo F4: Processing head

F.3 Optical planes

CONTENTS	PAGE #
1. Construction of the x,y plane	F16
2. Parts list of the x,y plane	F17
3. Photographs of the x,y plane	F18
4. Construction of the z plane	F19
5. Parts list of the z plane	F20
6. Photographs of the z plane	F21



Part-No.:	Title: X,Y plane of the LPG
Scale: Arbitrary	
Material:	
Date: October 1996	FHO-Fachhochschule Ostfriesland -Institut für Lasertechnik Ostfriesland -
ENGR.: Dipl.-Ing. U. Samuels	

F.3.2 Parts list of the x,y plane

<u>Part No.</u>	<u>Description</u>
1	X95 profile
2	X95 carriger
3	He-Cd laser
4	Micro rotary stage
5	AOM
6	Semiconductor laser
7	Telescope
8	Mirror
9	ND filter
10	Beam splitter
11	Mount with lens $f=20\text{mm}$
12	Photo detector
13	Beam stop
14	z axis

F.3.3 Photographs of the x,y plane

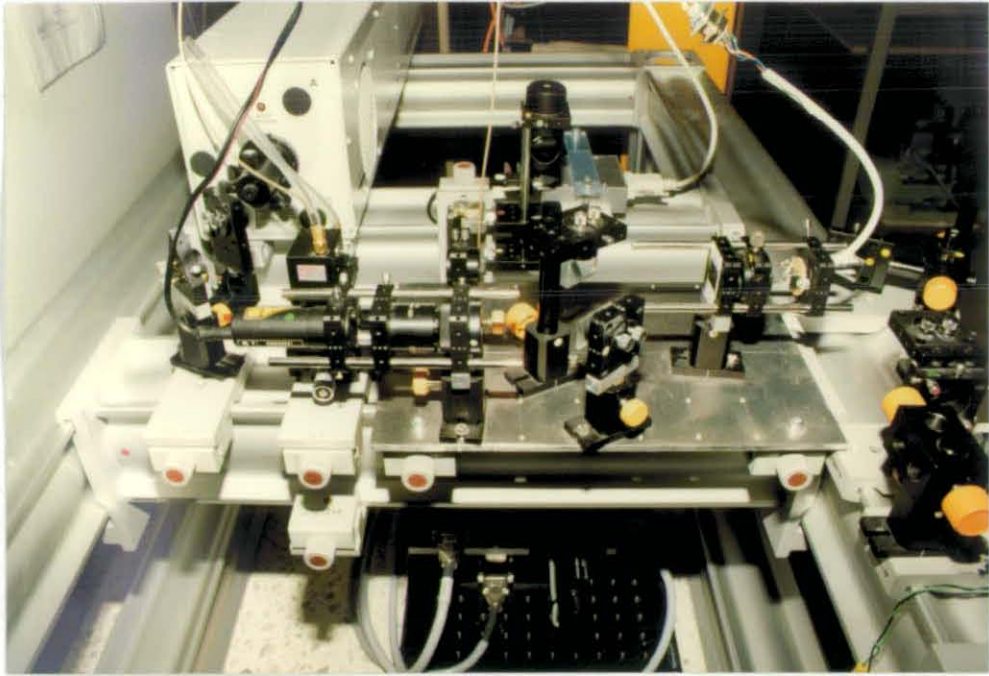


Photo F5: x,y plane of the optical system

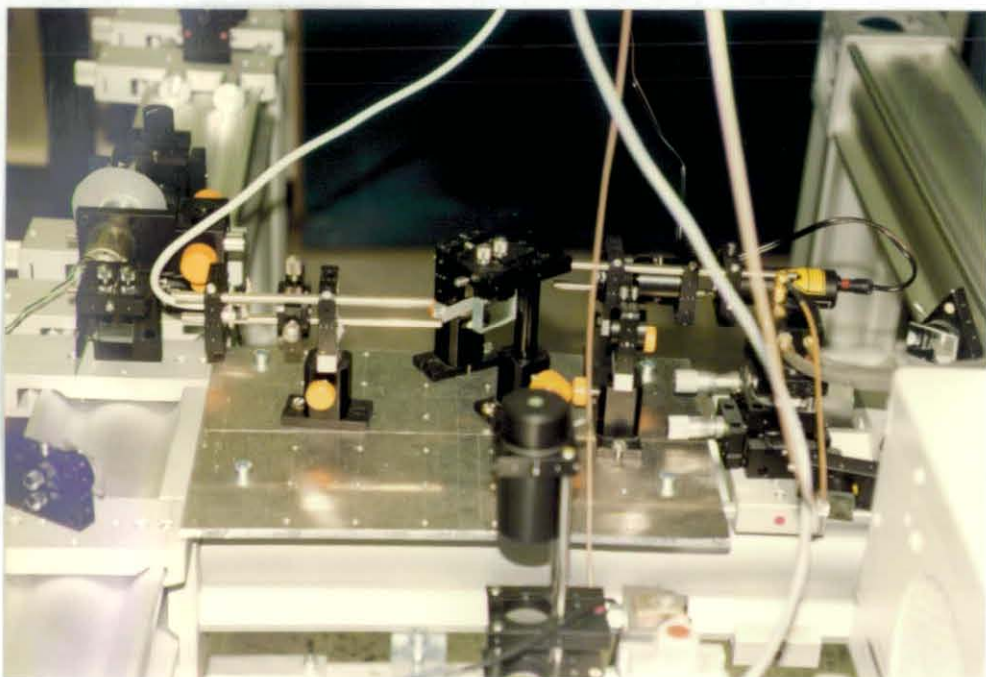
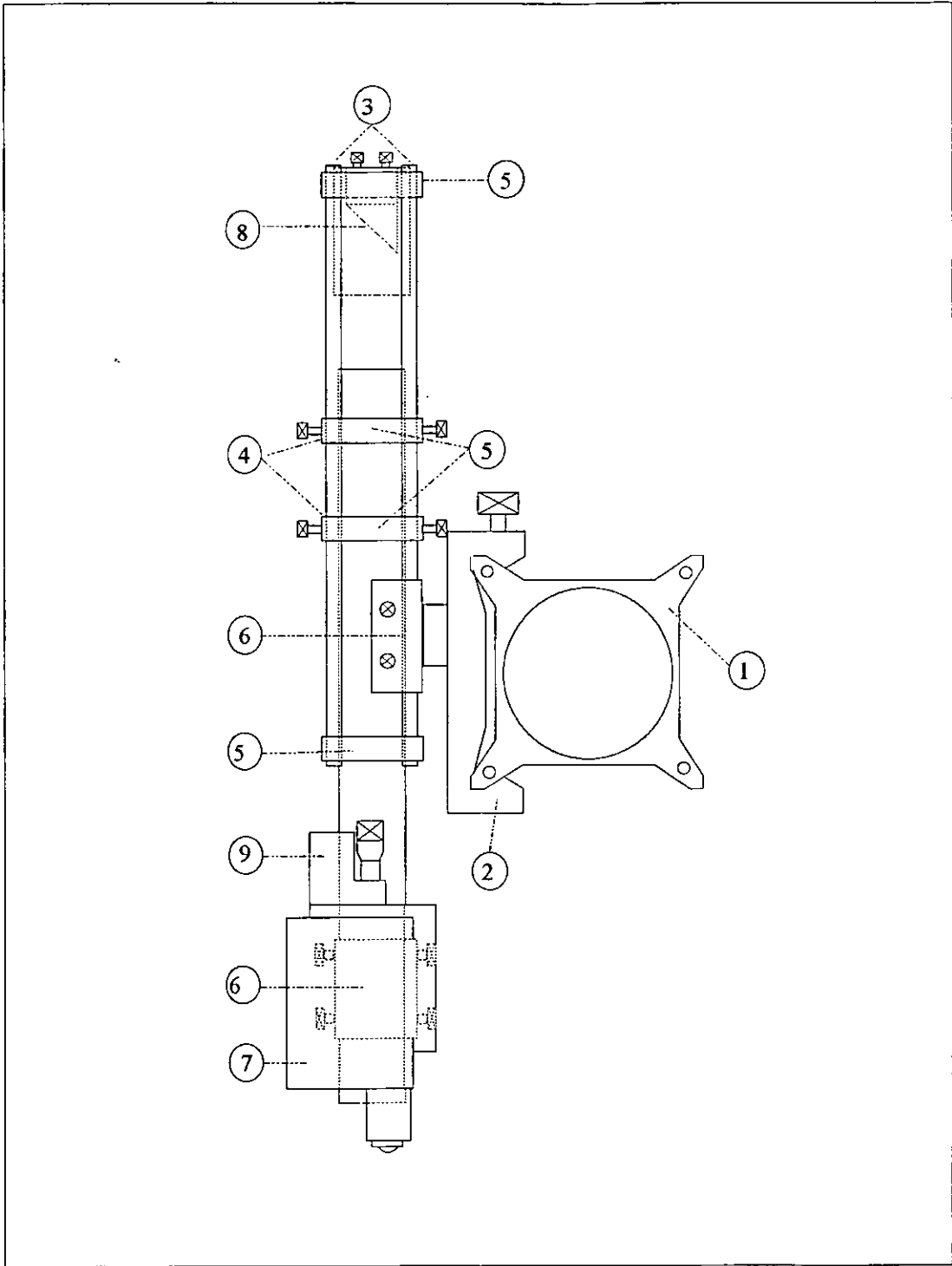


Photo F6: Details of the x,y plane of the optical system



Part-No.:	Title:
Scale: Arbitrary	Z-axis of the LPG
Material: Aluminium	
Date: October 1996	
ENGR.: Dipl.-Ing. U. Samuels	FHO-Fachhochschule Ostfriesland -Institut für Lasertechnik Ostfriesland -

F.3.5 Parts list of the z plane

<u>Part No.</u>	<u>Description</u>
1	X95 profile
2	X95 carriger
3	Precision rods
4	X25 carriger (small)
5	Mount
6	X25 carriger (large)
7	Autofocus sensor
8	Tilt mirror
9	Piezo translator

F.3.6 Photographs of the z plane

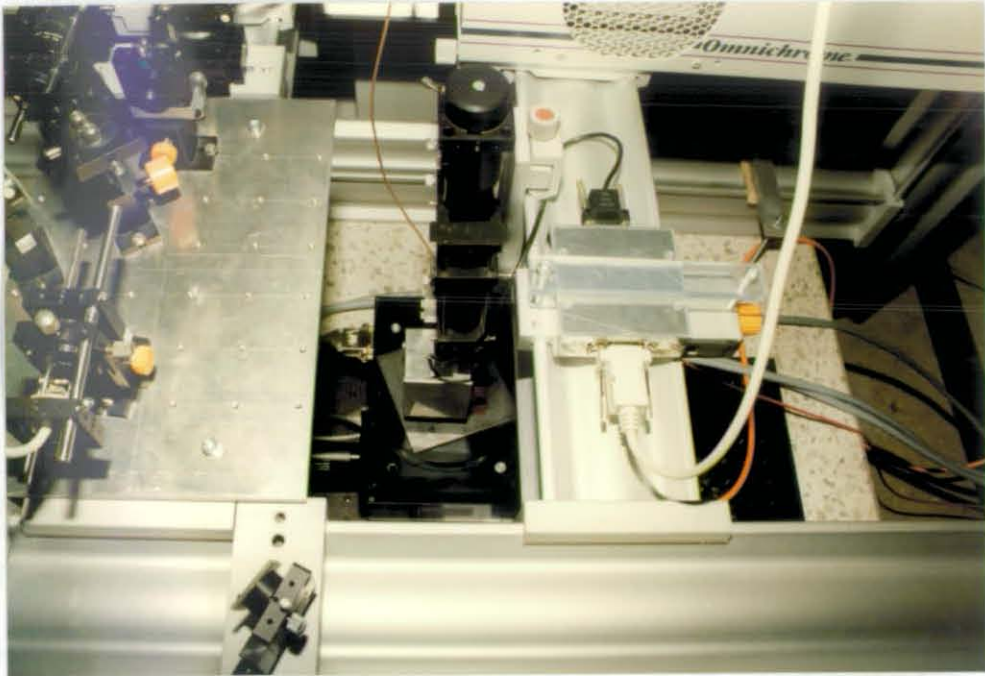


Photo F7: z plane of the LPG

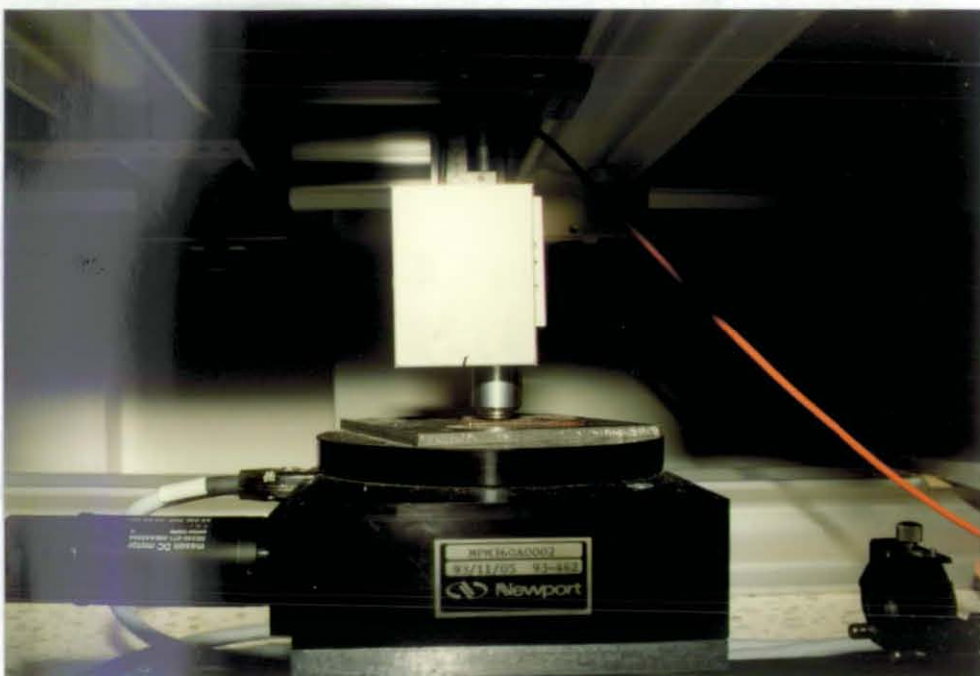


Photo F8: z plane of the LPG

G. SIMULATION PROGRAM *LASSI*

CONTENTS	PAGE #
1. Program description	G1
2. System requirements	G1
3. Flow chart „Lassi.pas“	G2
4. Flow chart „Menue.pas“	G3
5. Flow chart „Laser.pas“	G4
6. Flow chart „Etchtime.pas“	G5
7. Flow chart „Remove.pas“	G6

G.1 Program description

Program **LASSI** permits simulation of a resist exposure using a serial laser beam and followed by a resist etching. Following sub program parts can be called through the main menu:

- Input of all exposure parameters
- Input of all resist parameters
- Output of the exposure results
- Output of the development results

With a key stroke, all exposure and development results will be stored into a PCX-file which permits examination of the output results after being printed on a printer or the monitor.

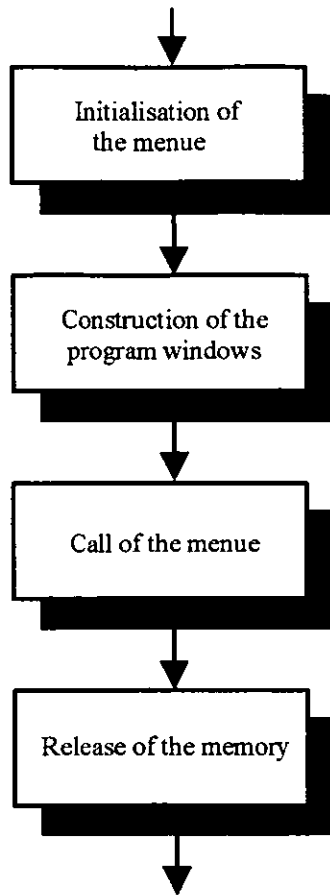
The program is in appendix E13:\Lassi

G.2 System requirements

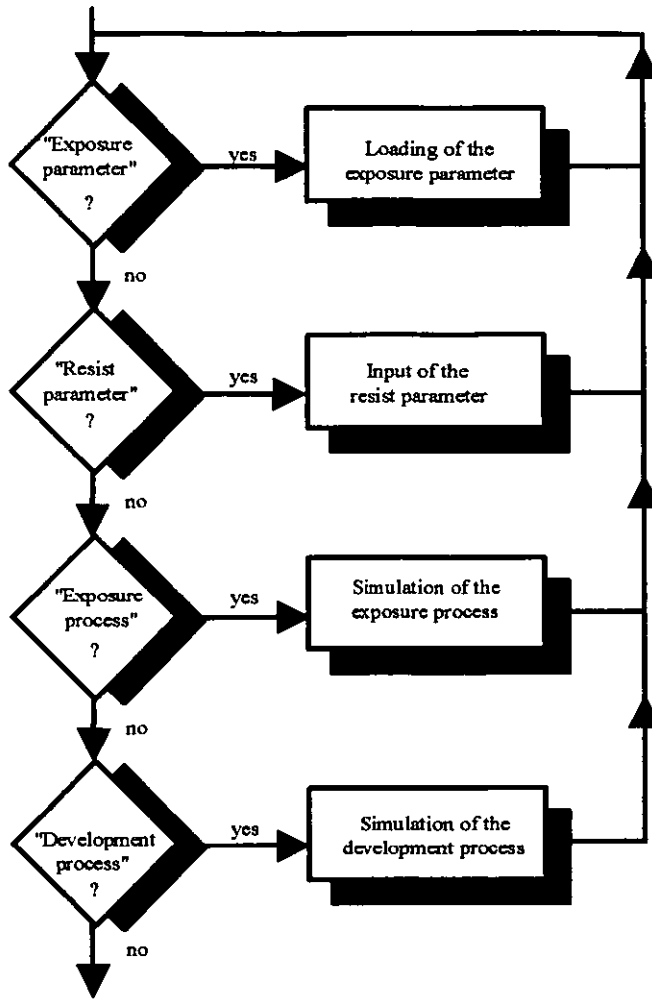
Computer: Personal computer with Intel 80386 processor and VGA monitor

Compiler: Turbo Pascal 6.0 from Borland

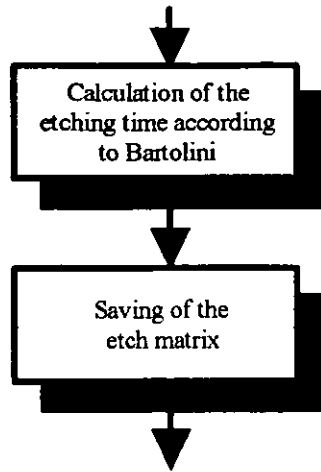
G.3 Flow chart „LASSI.pas“



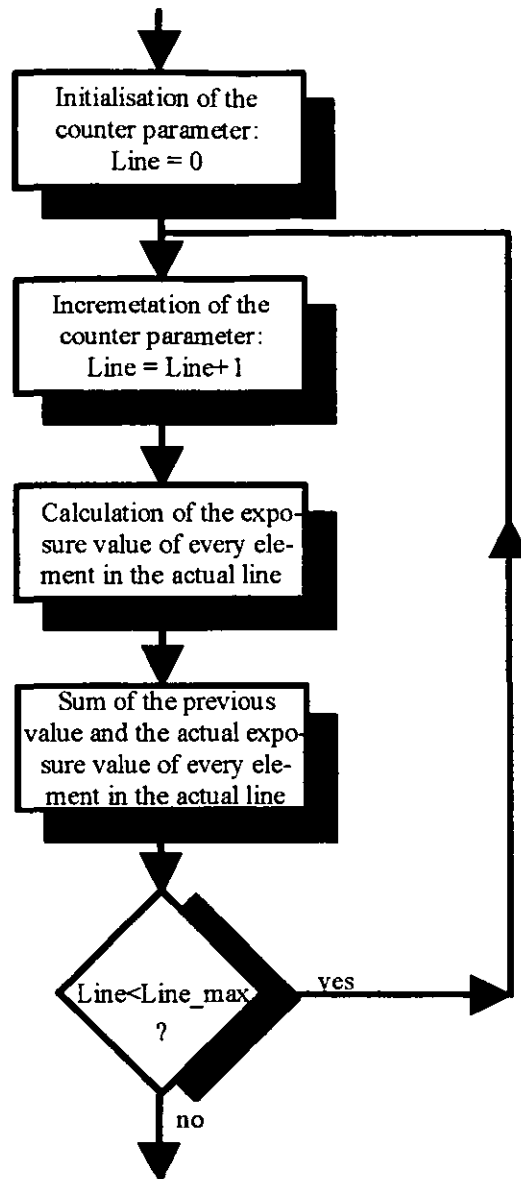
G.4 Flow chart „Menue.pas“



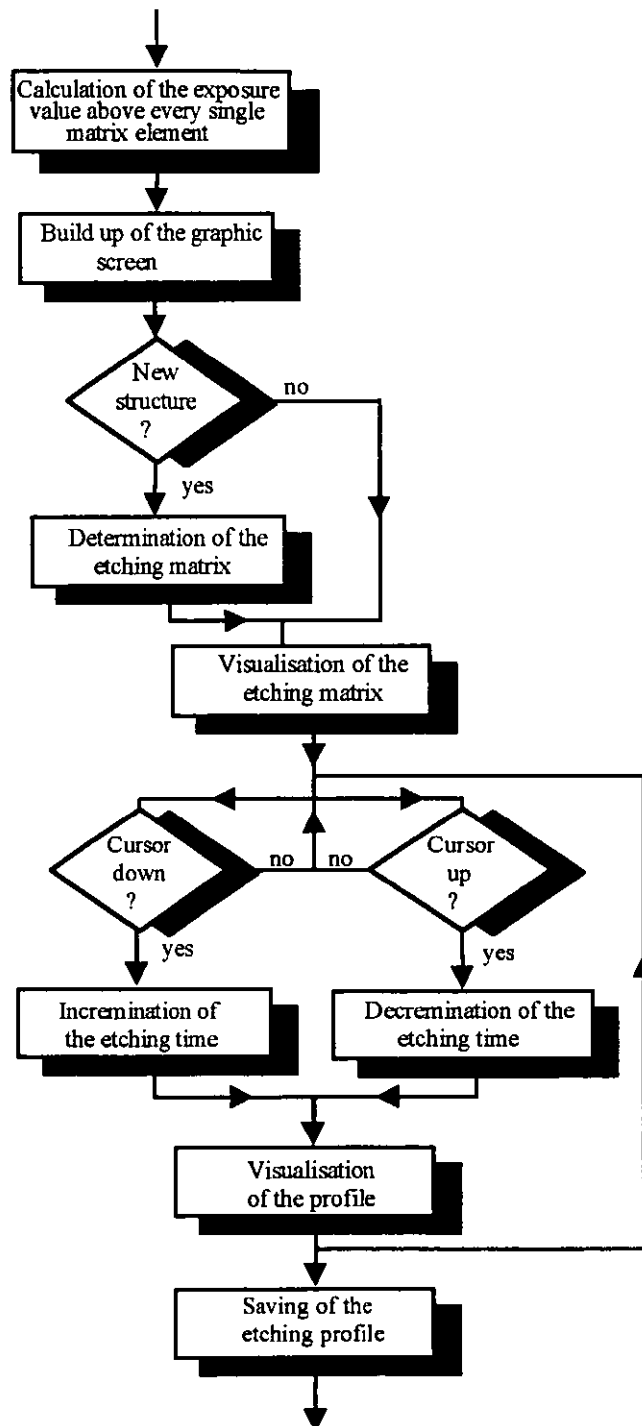
G.5 Flow chart „Laser.pas“



G.6 Flow chart „Etchtime.pas“



G.7 Flow chart „Remove.pas“



H. PUBLICATIONS

CONTENTS	PAGE #
1. List of publications	H1-H2
2. Fiber optical sensor for absolute measurement of rotation angles	H3-H13
3. Measurement of absolute rotation angles by combining fiber-optics distance sensors with gravity deformed cantilevers	H14-H17
3. Automated Surface Measurement by Laser Tomography	H18-H19
4. Automated Surface Measurement Via Laser Profiling	H20-H32
5. Precise Wavelength Tuning of a Dye Laser Using an Active Diffractive Optical Element	H33-H39
6. Automated plant propagation by use of image processing and laser beam cutting	H40-H43
7. Combined Communication and Navigation System for Automated Guided Vehicles (AGV)	H44-H47
8. Optimised autofocus sensor for flexible distance and profile measurement without moving sensor parts	H48-H53
9. Laser Pattern Generator (LPG) for flexible microstructuring	H54-H59

H.1 List of publications

1. H. Kreitlow, U. Samuels
Fiber optical sensor for absolute measurement of rotation angles
Proc. SPIE Vol. 2341, pp.260-270, Interferometry '94, Interferometric Fiber Sensing, Eric Udd, Ralph P. Tatam, Eds, Warsaw, Poland, May 16.-20.,1994
2. H. Kreitlow, U. Samuels, D. Wöbber, L. Tiase
Measurement of absolute rotation angle by combining fiber-optics distances sensors with gravity deformed cantilevers
Proceedings of the Laser '95, ISBN 3-540-61316-1, Springer Verlag Berlin, pp. 547-550, München, June 19. - 23., 1995
3. U. Samuels, R. M. Parkin, H. Kreitlow
Automated surface measurement by laser tomography
IEE, Innovations in Manufacturing control through mechatronics, ISSN 0963-3308, pp. P6.1-P6.2, Digest 95/214, Newport (GB), Gwent, November 22., 1995,
4. U. Samuels, H. Kreitlow, R.M. Parkin
Automated plant propagation by use of image processing and laser beam cutting
Proceedings of „Vision and control aspects of mechatronic“ , ISBN 972-8063-07-5 pp. 163-166, Ed. R.M. Parkin, M. Lima, T.G. King, Guimaraes, Portugal, September 16.-21., 1996
5. R.M. Parkin, J. Miesner, U. Samuels
Combined communication and navigation system for automated guided vehicles (AGV)
Proceedings of „Vision and control aspects of mechatronic“ , ISBN 972-8063-07-5 pp. 171-174, Ed. R.M. Parkin, M. Lima, T.G. King, Guimaraes, Portugal, September 16.-21., 1996
6. U. Samuels, R.M. Parkin, H. Kreitlow
Laser Pattern Generator (LPG) for flexible microstructuring
Proceedings of „Vision and control aspects of mechatronic“ , ISBN 972-8063-07-5 pp. 181-186, Ed. R.M. Parkin, M. Lima, T.G. King, Guimaraes, Portugal, September 16.-21., 1996
7. U. Samuels, R.M. Parkin, H. Kreitlow
Optimised autofocus sensor for flexible distance and profile measurement without moving sensor parts
Proceedings of „Vision and control aspects of mechatronic“ , ISBN 972-8063-07-5 pp. 211-216, Ed. R.M. Parkin, M. Lima, T.G. King, Guimaraes, Portugal, September 16.-21., 1996

8. U. Samuels, H. Kreitlow, S.C. Wright, CH. Budzinski, H.J. Tiziani
**Precise Wavelength Tuning of a Dye Laser
Using an Active Diffractive Optical Element**
Optics & Laser Technology, Vol. 28, No.6, pp. 423-429, 1996 ✓

9. U. Samuels, R.M. Parkin, H. Kreitlow
Automated surface measurement via laser profiling
Submitted for publication in Control Theory and Applications ✕

Fiber optical sensor for
absolute measurement of rotation angles

H. Kreitlow and U. Samuels

Fachhochschule Ostfriesland
Fachbereich Naturwissenschaftliche Technik
Constantiaplatz 4, 26723 Emden, Germany

ABSTRACT

A fiber optical sensor (FOS) for sensitive measurements of absolute angles has been developed. The sensor principle is based on the well defined angular dependence of the bending of a cantilever under the influence of its own weight. The cantilever bending is measured via a non-contact and high resolution method using two fiber optical sensors. These sensors are oriented perpendicular to each other and fixed opposite to the cantilever so that they are rotated synchronously during every angular movement. The current values of the rotation angle, the angular velocity, and the angular acceleration are determined in an analysing and data processing unit and visualised on the computer monitor.

This high precision absolute rotation-angle sensor has the advantages of being compact, insensitive to external influences such as electromagnetic fields, humidity, atmospheric density fluctuations, and nuclear radiation and is therefore applicable in nearly every kind of angular measurement problem and in unfavorable environmental conditions.

1. CANTILEVER THEORY

The cantilever with length l , width b , and height h is clamped at one end for bending under its own weight. Figure 1 describes the geometry and the coordinate system used, where q is the load per unit length caused by the density of the cantilever material.

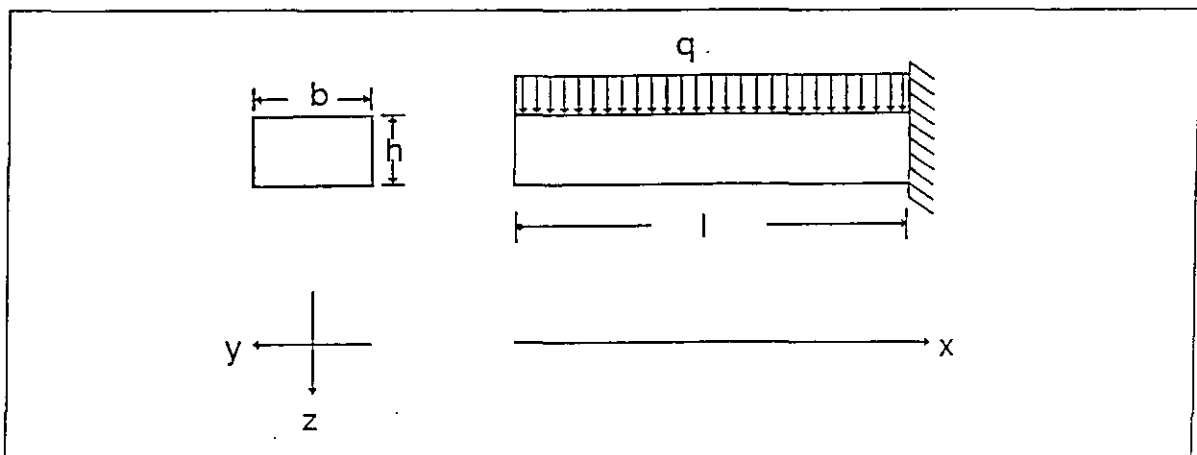


Figure 1: Cantilever model

The displacement $W(x)$ of the free end depends on the shear force and is defined by equation (1) where I is the moment of inertia and E is the module of elasticity. The product of E and I is called the rigidity.

$$W(x) = \frac{q \cdot l^4}{8 \cdot E \cdot I} * \left[1 - \frac{4}{3} * \frac{x}{l} + \frac{1}{3} * \frac{x^4}{l^4} \right] \quad (1)$$

The derivative $dW(x)/dx$ of equation (1) is necessary for the calculation of the slope (surface tangent) of the cantilever at point x which affects the angle between the incident and reflected light beams and has, therefore, to be taken into account for further considerations concerning the FOS-bending sensor described in chapter 2.

$$\frac{dW(x)}{dx} = \frac{q \cdot l^4}{8 \cdot E \cdot I} * \left[-\frac{4}{3} * \frac{1}{l} + \frac{4}{3} * \frac{x^3}{l^4} \right] = \tan(\beta) \quad (2)$$

Figure 2 illustrates the characteristic bending curve of the cantilever as well as the surface tangent at the point of maximum deflection f .

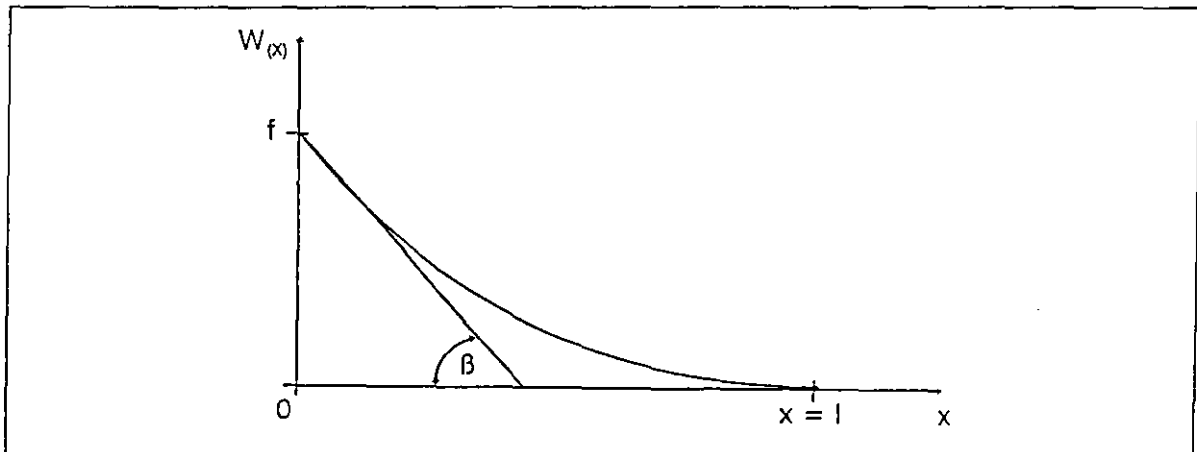


Figure 2: Cantilever deflection W as a function of x

The maximum deflection $f(y)$ and $f(z)$ at point $x=0$ in the two directions of the principle axes of the cantilever y and z , (see figure 1) depending on its angular orientation α with respect to the vertical can be obtained by rotation of the employed coordinate system by α .

$$f(y) = W(0) * \sin(\alpha) \quad (3)$$

$$f(z) = W(0) * \cos(\alpha) \quad (4)$$

Using cantilevers with square cross section ($b=h$) and isotropic material the moment of inertia I is equal in both directions y and z .

$$I(y) = I(z) = \frac{h^4}{12} \quad (5)$$

The load per unit length (q) is given by

$$q = \frac{F}{l} = \delta * b * h * g = \delta * h^2 * g \quad (6)$$

and, therefore, the deflection along the two principle axes at the point $x=0$ of maximum deflection is given by equations (7) and (8) where δ is the density of the cantilever material and g is the acceleration due to gravity at the Earth's surface.

$$f(y) = \frac{3 * \delta * g * l^4}{2 * E * h^2} * \sin(\alpha) \quad (7)$$

$$f(z) = \frac{3 * \delta * g * l^4}{2 * E * h^2} * \cos(\alpha) \quad (8)$$

Using this result, the cantilever as one part of the whole sensor can be optimized with respect to the FOS as the second important part of the rotation angle sensor.

2. FIBER OPTICAL SENSOR (FOS)

A wide variety of physical quantities can be measured using fiber optical sensors.² By means of a FOS, the mechanical bending of a cantilever as depends on its orientation compared to the vertical can be measured. to give the absolute rotation angle.

For measuring the cantilever deflection with highest possible sensitivity, a fiber optical sensor based on the principle of external light intensity modulation was employed as described in earlier work: the light from a light source (guided to the cantilever surface by the sending fiber) is reflected and scattered back from the cantilever surface into the coaxial receiving fibers for opto-electronic conversion by a photodiode.²

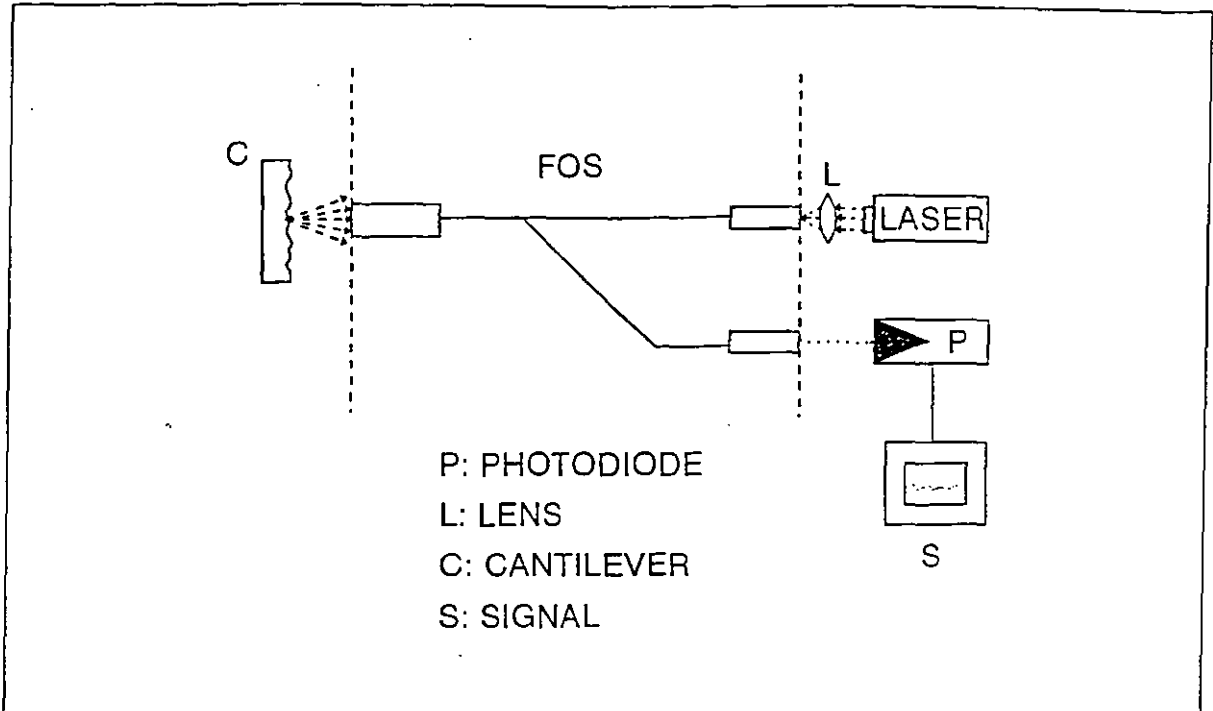


Figure 3: Principle of the fiber optical sensor (FOS)

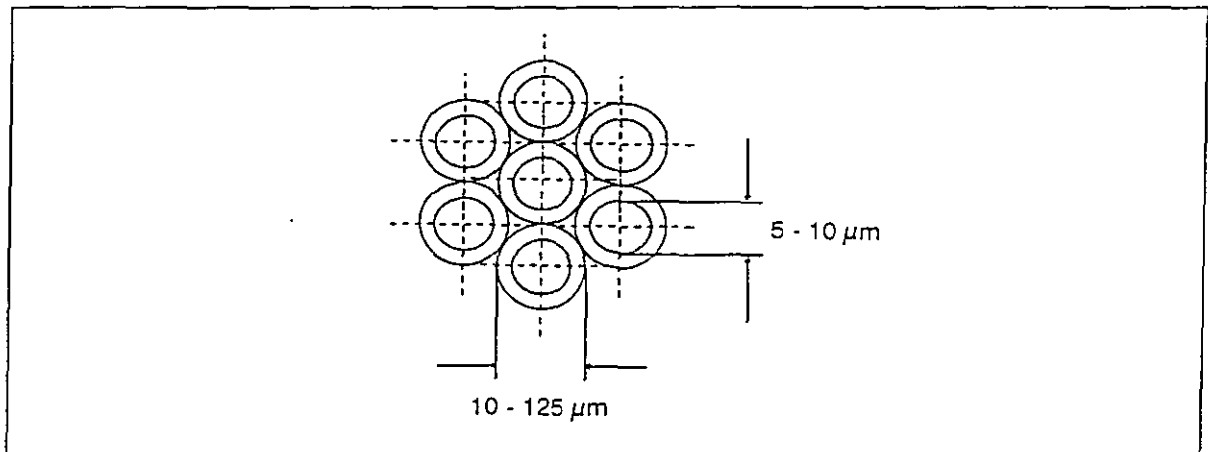


Figure 4: Cross-section of the FOS measuring head with the central (sending) fiber and the coaxial receiving fibers

The voltage output signal of the FOS is a function of the distance from and orientation of a reflecting and scattering surface at the points of light contact as shown in figure 5.

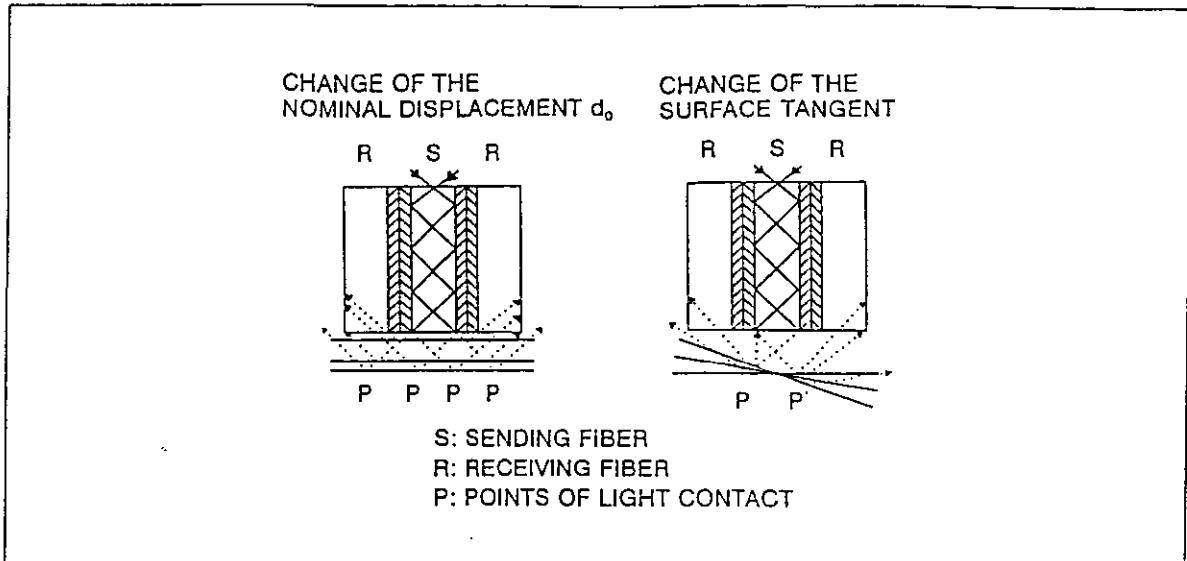


Figure 5: Input of the reflected light in the fiber optical sensor depending on the distance and the orientation of the reflecting and scattering surface

3. MEASUREMENT PRINCIPLE

With regards to sensor construction, the smallest measurable parameter changes and the measurement range are the major demands. In this development the rotation angle sensor has to work over the full-angle (360 degrees) with a resolution as high as possible. For this reason, the cantilever has to have a maximum angular-dependent bending amplitude. According to equations (7) and (8), the deflection of the cantilever is nearly linear at some ranges of both deflection curves with the additional advantage that these are also the high slope parts required for sensitive measurements (see figure 6).

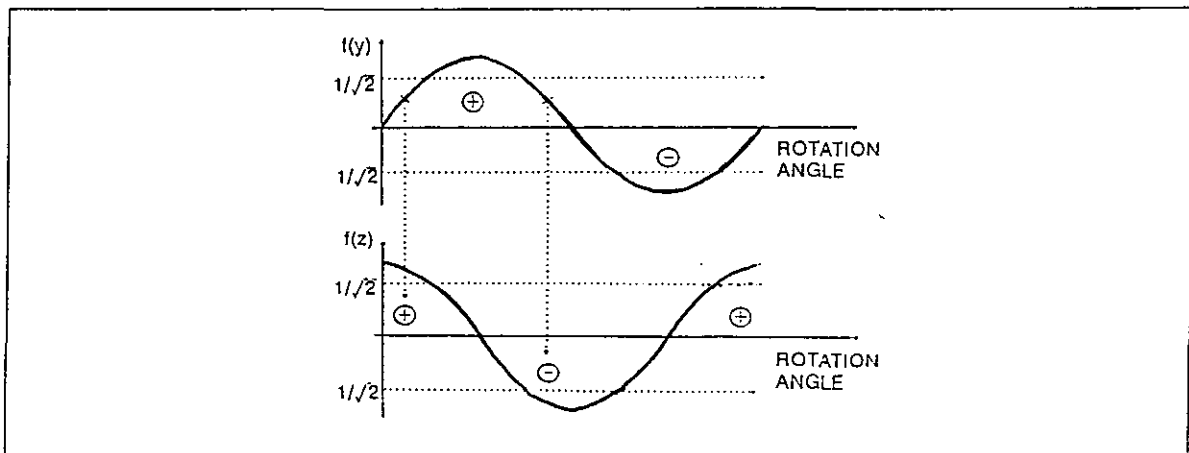


Figure 6: Bending of the cantilever as a function of the rotation angle

Using a cantilever with square cross section, the deflection curves $f(y)$ and $f(z)$ have equal amplitudes. Since the sine function bending characteristic is nearly linear in a range from 0 degree up to 45 degrees while the cosine function showing the bending of the orthogonal component delivers a nearly linear bending in the range from 45 degrees up to 90 degrees, these two curves should be used alternatively for linear rotation angle determination. Following from the behaviour of the sine- and cosine function, this method of angle determination is also applicable for angles between 90 and 360 degrees. Since the above mentioned ranges have also the characteristic of the highest slope, that is, within the deflection range between 0 and $1/\sqrt{2}$ of the maximum signal value, the angle measurement is also performed with highest sensitivity. In order to eliminate the ambiguity in the angle determination (each amplitude of both signals can be obtained by two different angles) an additional piece of information is required. Figure 6 shows the principle of angle determination where, at a given time, the bold lines in one of the curves can be used for angle determination and the other curve for elimination of the ambiguity by examining the sign which indicates the quadrant of the analysed signal. Usable maximum deflection amplitudes are limited by the linear output signal of the FOS in combination with the cantilever bending. The range of the linear portion of the characteristic curve of the FOS depends on the diameter of the receiving fibers and their distance from the sending fiber, as shown in figure 5.

4. ANALYSING AND DATA PROCESSING UNIT

For the determination of the rotation-angle value, a special system for analysing and evaluating the two FOS signals is required. To this end, a computer in combination with an interface to the sensor can be used. The analogue output signals of the sensor have to be transformed for the computer using an A/D converter with an appropriate number of characteristic bits for the signal representation influencing the obtainable quantisation accuracy. As described in chapter 3, only signals up to $1/\sqrt{2}$ of the maximum amplitude in the linear regions have to be analysed. The maximum quantisation error is caused at the point of $1/\sqrt{2}$ of the maximum amplitude and can be calculated depending on the number of A/D converter bits and can be compared with the value at the point of maximum amplitude.

MAXIMUM QUANTISATION ERROR/DEGREES		
BITS	$A=A_{(max)}$	$A=1/\sqrt{2} \cdot A_{(max)}$
8	7.16	0.629
10	3.58	0.158
12	2.53	0.04
14	1.79	$9.89 \cdot 10^{-3}$
16	1.27	$2.47 \cdot 10^{-3}$
18	0.90	$6.18 \cdot 10^{-4}$
20	0.63	$1.55 \cdot 10^{-4}$
22	0.45	$3.86 \cdot 10^{-5}$
24	0.32	$9.66 \cdot 10^{-6}$

Table 1: Maximum quantisation error as a function of A/D converter bits

The A/D converted signal value can be used in an algorithm for comparison of the signal values with:

- those in a look-up table or
- computer calculated sine and cosine functions incrementing the argument or
- a numerical approximation of the linear signal portions

to determine the current rotation angle. The computer program can be used to visualize the current angular value or the value over a longer period. Furthermore, the angular velocity and angular acceleration can be calculated and also presented on the computer monitor. By means of the D/A converter, all angular and angular dependent values can be used as control data for further applications.

5. EXPERIMENTAL OPTIMIZATION OF THE SENSOR

Optimization of the sensor was performed in two stages: optimization of the FOS and the resulting adaptation of the cantilever. The FOS was comprised of the following components:

- a semi-conductor laser as the light source
- a sending-fiber
- six receiving-fibers
- an opto-electronic signal converter (photodiode)
- a DC power supply (12V)

The sending and receiving fibers were of polymethylmethacrylate (PMMA) with a diameter of $50\mu\text{m}$. The output signal of the FOS for a given geometry (fiber diameter and separation between the fibers), is dependent upon the distance between the FOS and the surface of the cantilever (which is the sum of the nominal distance d_0 and the rotation-dependent deflection $W(\alpha)$) as well as the inclination of the surface tangent of the cantilever as a result of the bending at the position of measurement with respect to the FOS axis (see figures 5 and 7). Analysis of the characteristics of the output signal in relation to the above geometrical parameters allows one to choose the most linear operating region, thus optimizing the sensor for high precision rotation angle measurements. For this reason, two experiments were performed, in which a systematic study of the effect of the two parameters d_0 and W on the output signal were recorded. In order to ensure the reproducibility of the measurements, cantilevers with similar surface microstructures were used in all of the experiments.

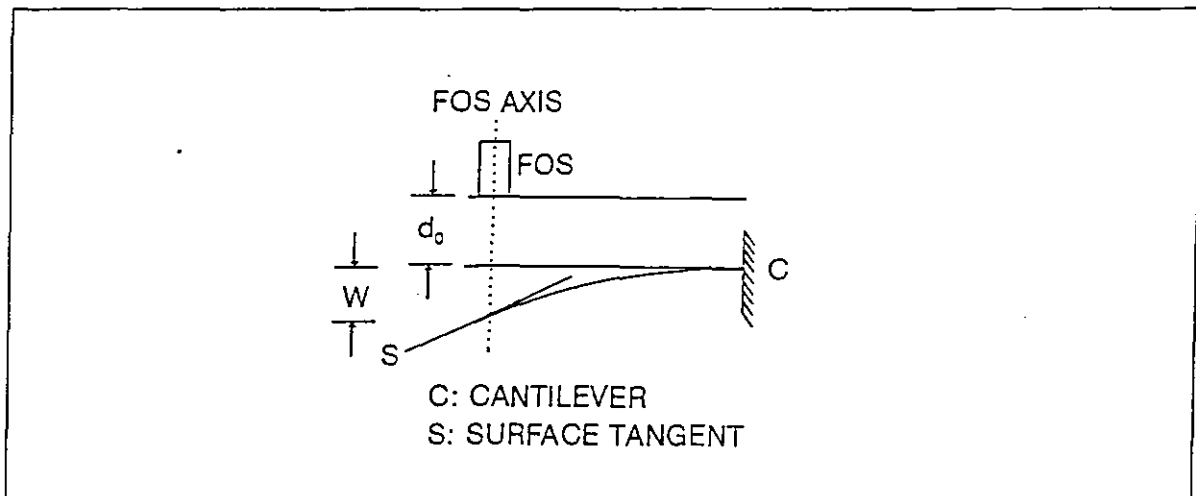


Figure 7: Geometrical parameters affecting the amplitude of the measured signal

In the first experiment, the dependence of the output of the FOS on the nominal displacement, d_0 , was determined by displacing the FOS in a well defined manner with a micrometer screw relative to the cantilever surface, which was oriented perpendicular to the FOS, and measuring the resulting reflected and scattered laser light collected by the receiving fibers.

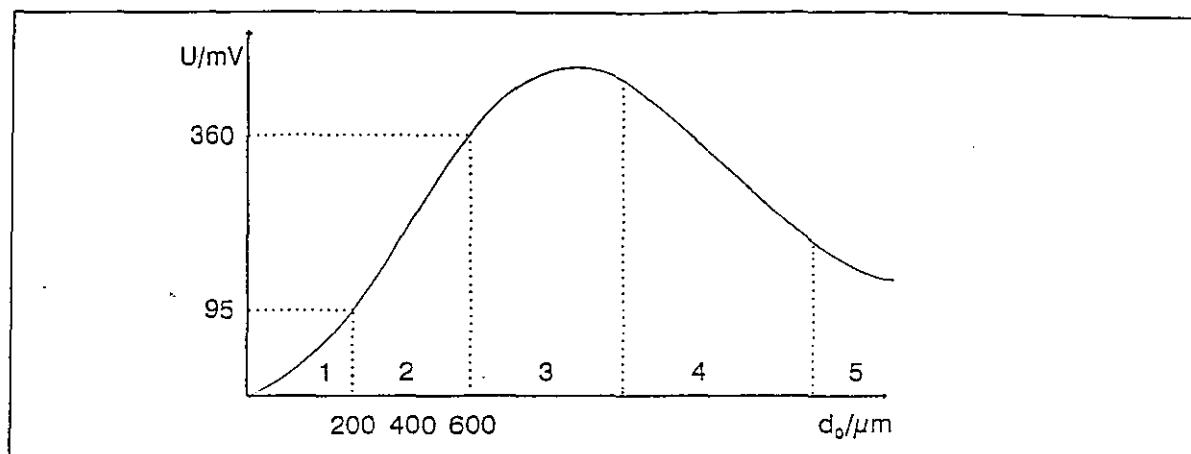


Figure 8: Output, S , of the FOS versus nominal displacement, d_0 , from the reflecting and scattering cantilever surface

d_0 : nominal displacement between cantilever surface and FOS

U : output signal from the FOS

1,3 and 5: non-linear signal regions

2 and 4: linear signal regions

Regions 2 and 4 are both characterized by a linear dependence of the signal on displacement, with the difference that region 2 ($200\mu\text{m} < d_0 < 600\mu\text{m}$) is more suitable for high-precision measurements of the deflection of the cantilever owing to its greater slope ($0.66\text{ mV}/\mu\text{m}$), resulting in a sensitivity of 10nm .

A second experiment was necessary to determine the influence of the cantilever deflection, W , on the output signal. For various values of d_0 within the linear region 2 (as determined above), the cantilever was deformed via a second micrometer screw and the output signal as a function of this well defined deflection recorded. The linear working range of the system was then defined as the smaller of the two ranges of linearity about the nominal displacement of the cantilever (that is, displacements due to deflection towards or away from the FOS). From Figure 9, one sees that the largest linear working range for deflections is $70\mu\text{m}$ when d_0 is set to $400\mu\text{m}$, that is, with d_0 set to the middle of the linear range from the first experiment (see figure 8).

Figure 10 shows that for a cantilever deflection of $70\mu\text{m}$ in both directions, a linear signal is obtained with a total signal variation of $\Delta U=400\text{mV}$. In comparison to figure 8, the reduction of the linear working range and the increase in sensitivity to $2.82\text{ mV}/\mu\text{m}$ are a result of the inclination of the surface tangent of the cantilever with respect to the FOS during deflection. This results in an increased sensitivity of the measurement system.

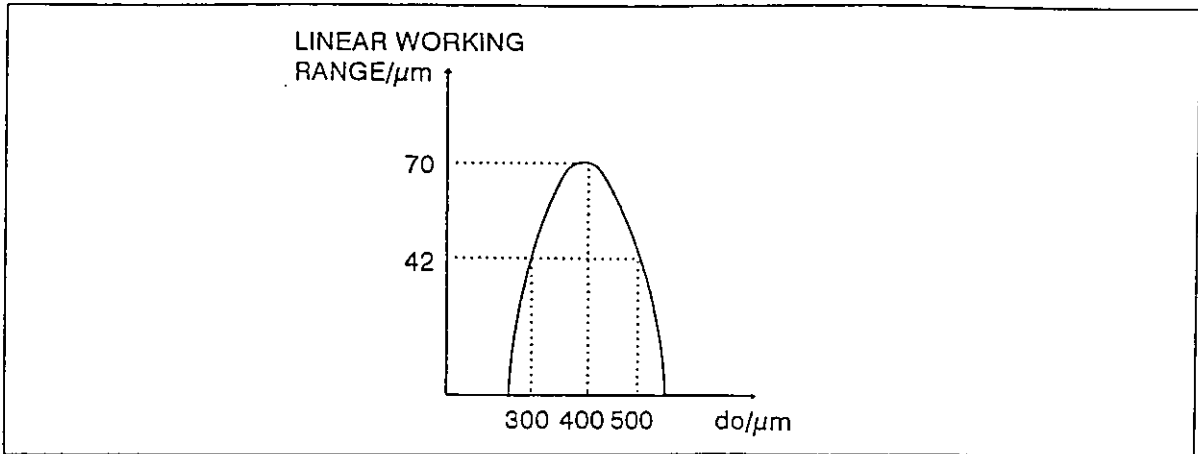


Figure 9: Linear working range of the FOS as a function of the nominal displacement, d_0 , between the FOS and the cantilever surface

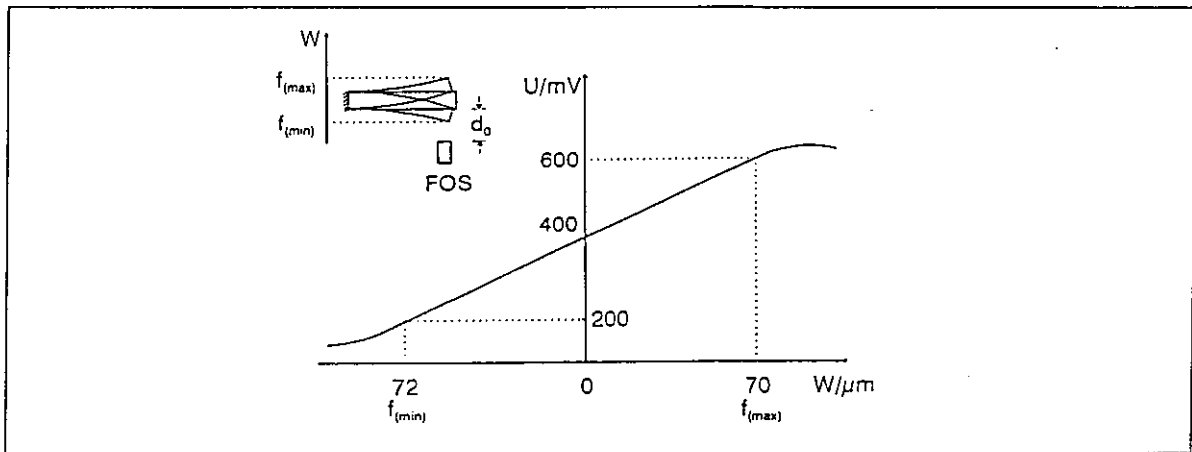


Figure 10: Dependence of the output signal from the FOS on the cantilever deflection, W , for a nominal displacement, d_0 , of $400\mu\text{m}$

Through use of equations (7) and (8), various combinations of parameters may be found, allowing optimal design of the cantilever using the full linear working range determined above. The following parameters were chosen:

MATERIAL:	BRASS (RED)
E:	98GPa
δ :	8.8Kg/dm
l:	0.15m
h=b:	3.1mm

Table 2: Cantilever parameters

6. MEASUREMENT CHARACTERISTICS OF THE ROTATION ANGLE SENSOR

To determine the measurement characteristics of the rotation angle sensor described in chapter 5 (see figure 11), a computer controlled apparatus was developed employing a high-precision rotation stage with a resolution of 1/1000 degree to rotate the cantilever about the horizontal axis.

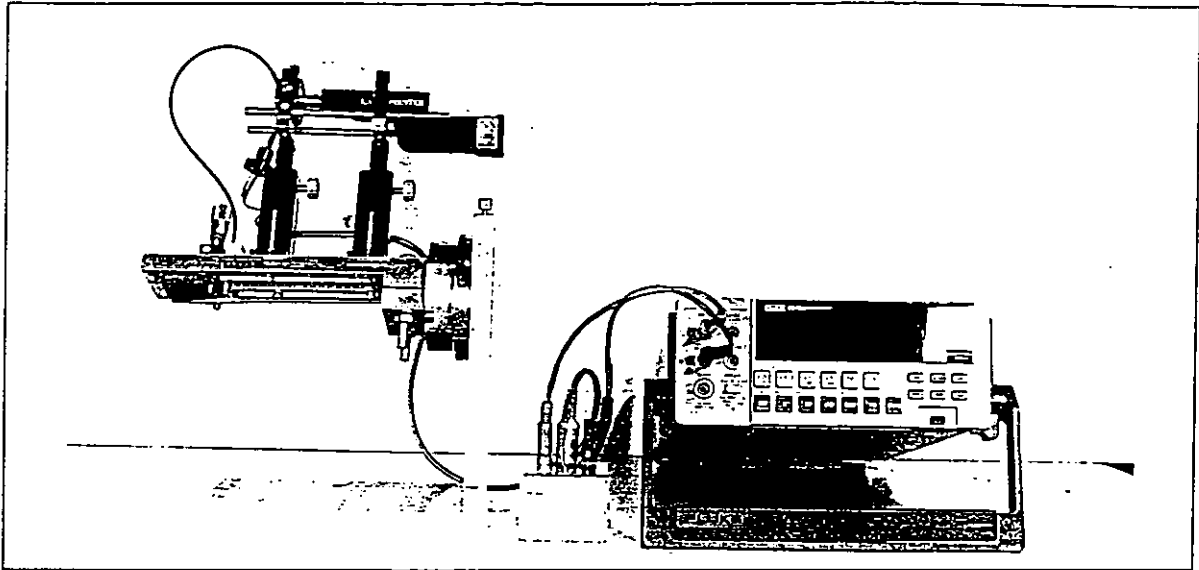


Figure 11: Rotation angle sensor construction

The dependence of the measured FOS-signal on the rotation angle, α , is confirming the theoretical description given by equations (7) and (8). The experiments result a signal of more than $7\mu\text{V}$ per rotary motion step of 1/1000 degree. In order to unambiguously determine the true rotation angle from these FOS-signals, a data processing unit was developed based on a PC with an integrated A/D and D/A converter, as described in chapter 4.

The current value of the rotation angle (which was updated every $10\mu\text{s}$ by polling the interface), the angular velocity, the angular acceleration as well as their development in time are displayed on the computer monitor with a measurement period of 30s (see figure 12).

These values are also made available at the output port of the D/A converter for systems control applications. The data processing algorithm developed, uses only the nearly-linear regions of the FOS-signals (sine and cosine functions) for the determination of the rotation angle, as described in chapter 3. In this manner, the sensitivity was increased and a minimal digitization error could be obtained, since only the signal values up to $1/\sqrt{2}$ of the maximum signal amplitude were used for the computation. The current value of the rotation angle is determined by the software by comparing the signals of the FOS with computer-generated sine and cosine functions, whose arguments could be incremented in steps of 1/1000 degrees. Due to the high resolution of the FOS developed, the optimization of the cantilever and the intelligent data processing algorithm using only signal regions of highest sensitivity which results in minimal digitization error during the A/D conversion, this rotation angle sensor delivers high-precision signals, whose precision is limited only by the characteristics of the digital conversion. For this reason, the A/D conversion card should be chosen to have the highest possible digital resolution. In order to isolate the system against undesirable external influences, the whole sensor was integrated into an enclosure.

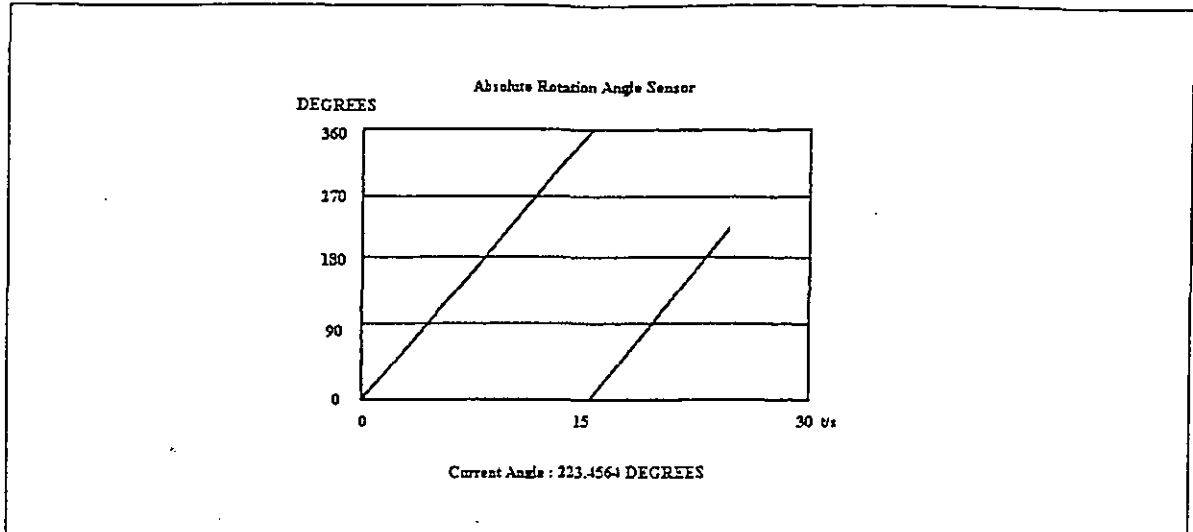


Figure 12: Monitor display of the rotation angle sensor signal

7. AREAS OF APPLICATION

The rotation-angle sensor can be used in a wide range of applications where highly precise information on angular orientation is required. Compared to other rotation-angle sensors such as code-discs and incremental counters, this sensor has the advantage of measuring absolute angles. Furthermore, the use of light as the information carrier as well as fiber optics ensures that this sensor is insensitive to environmental influences such as electromagnetic fields, humidity, and atmospheric density fluctuations. Using fiber optical links, long distances between the rotation-angle sensor and the analysing and data processing unit do not restrict the application of the sensor because of the small attenuation of the light in the fiber. The choice of a cantilever material with a small temperature expansion coefficient makes this sensor suitable for high temperature applications, since quartz or sapphire based fiber optics can be used up to 1000°C without influencing the measurements. Furthermore, this sensor is also useful in regions with up to 100 Krad nuclear radiation where electronic signals cannot be used.

8. REFERENCES

1. Szabó, I., "Einführung in die Technische Mechanik", Berlin, Springer-Verlag, 1966
2. Kreitlow, H., "Faseroptische Sensoren" in Pfeifer, T., et. al., "Optoelektronische Verfahren zur Messung geometrischer Größen in der Fertigungstechnik", Ehningen, expert-verlag, 1993

Measurement of absolute rotation angle by combining fiber-optics distance sensors with gravity-deformed cantilevers

H. Kreitlow, U. Samuels, L. Tiase, K. Boer, M. Schlaf
 Fachhochschule Ostfriesland
 Fachbereich Naturwissenschaftliche Technik
 Institut für Lasertechnik
 Constantiaplatz 4, D-26723 Emden

ABSTRACT

The principle of a fiber optical sensor (FOS) for sensitive measurements of absolute angles has been investigated. The sensor principle is based on the well defined angular dependence of the bending of a cantilever under the influence of its own weight. The cantilever bending is measured via a non-contact and high resolution method using two fiber optical sensors. These sensors are oriented perpendicular to each other and fixed opposite to the cantilever so that they are rotated synchronously during every angular movement. The current values of the rotation angle are determined in an analysing and data processing unit and visualised on the computer monitor.

This high precision absolute rotation angle sensor has the advantages of being compact, insensitive to external influences such as humidity, atmospheric density fluctuations, electromagnetic fields, and nuclear radiation and is therefore applicable in nearly every kind of angular measurement problem and in unfavorable environmental conditions.

1. CANTILEVER

The cantilever with length l , width b , and height h is clamped at one end for bending under its own weight (see figure 1).

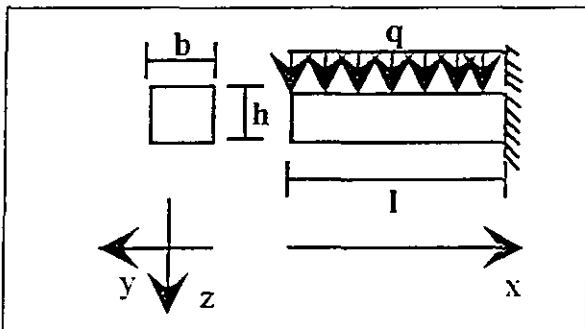


Figure 1: Cantilever model

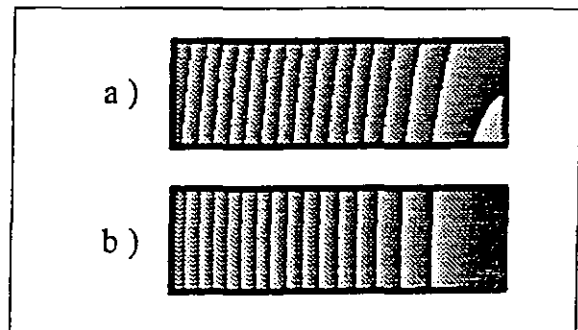


Figure 2: Fringe pattern simulation for cantilever optimization by holographic interferometry: a.) torsion; b.) ideal adjustment

The angular dependent deflection of a cantilever with square cross section ($b=h$) and isotropic material along the two principle axes at the point of maximum deflection is given by equations (1) and (2) where ρ is the density of the cantilever material, g is the acceleration due to gravity at the Earth's surface, and E is the module of elasticity.

$$f_y(\alpha) = \frac{3\rho g l^4}{2Eh^2} \sin(\alpha) \quad (1)$$

$$f_z(\alpha) = \frac{3\rho g l^4}{2Eh^2} \cos(\alpha) \quad (2)$$

Using this result, the cantilever as one part of the whole sensor can be optimized theoretically with respect to the FOS as the second important part of the rotation angle sensor. Experimental optimization of the cantilever was performed by holographic interferometry supported by a computer programme for holographic fringe pattern simulation (see figure 2).

2. FIBER OPTICAL SENSOR (FOS)

By means of a FOS, the mechanical bending of a cantilever as depends on its orientation compared to the vertical can be measured, to give the absolute rotation angle. For measuring the cantilever deflection with highest possible sensitivity, fiber optical sensors based on the principle of external light intensity modulation is employed as described: the light from a light source (guided to the cantilever surface by the sending fiber) is reflected and scattered back from the cantilever surface into the coaxial receiving fibers for opto-electronic conversion by a photodiode [1,2], see figures 3, 4, 5.

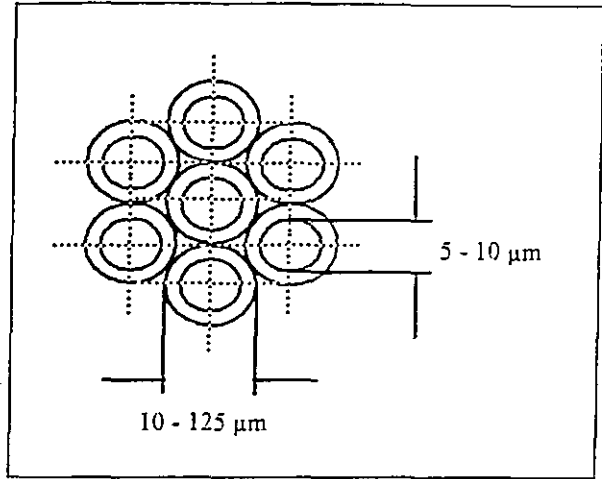
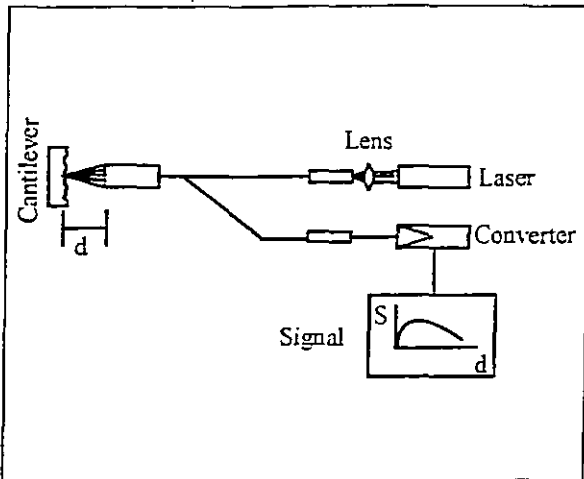


Figure 3: Principle of the fiber optical sensor (FOS) Figure 4: Cross-section of the FOS measuring head with the central (sending) fiber and the coaxial (receiving) fibers

The voltage output signal of the FOS is a function of the distance from and orientation of a reflecting and scattering surface at the points of light contact as shown in figure 5 and 6.

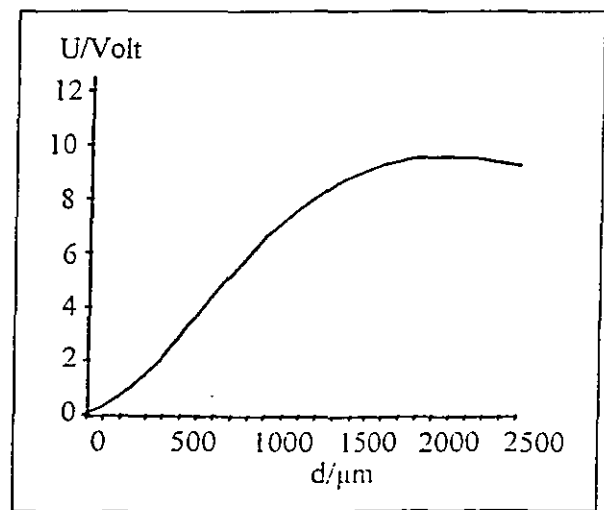
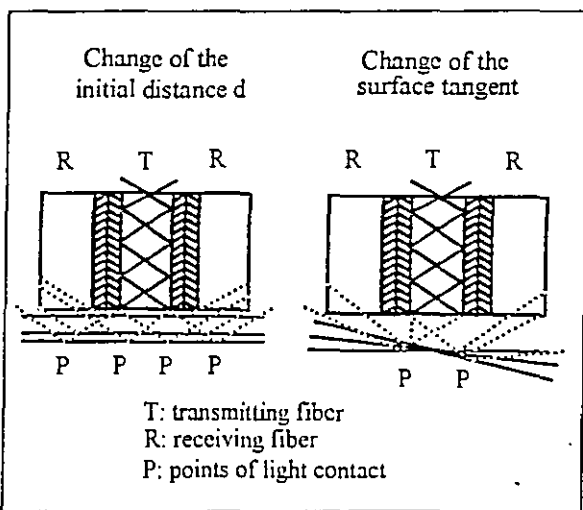


Figure 5: Input of the reflected light in the fiber optical sensor depending on the distance and the orientation of the reflecting and scattering surface

Figure 6: Output U of the FOS as a function of the nominal displacement d

3. COMBINATION OF FOS AND CANTILEVER

With regards to sensor construction, the smallest measurable parameter changes and the measurement range are the major demands. In this development the rotation angle sensor has to work over the full-angle (360 degrees) with a resolution as high as possible. For this reason, the cantilever has to have a maximum angular-dependent bending amplitude. According to equations (1) and (2), the deflection of the cantilever is nearly linear at some ranges of both deflection curves with the additional advantage that these are also the high slope parts required for sensitive measurements. Using a cantilever with square cross section, the deflection curves $f_y(\alpha)$ and $f_z(\alpha)$ have equal amplitudes. Since the sine function bending characteristic is nearly linear in a range from 0 degree up to 45 degrees while the cosine function showing the bending of the orthogonal component delivers a nearly linear bending in the range from 45 degrees up to 90 degrees, these two curves should be used alternatively for linear rotation angle determination. Following from the behaviour of the sine and cosine function, this method of angle determination is also applicable for angles between 90 and 360 degrees. Since the above mentioned ranges have also the characteristic of the highest slope, that is, within the deflection range between 0 and $1/\sqrt{2}$ of the maximum signal value, the angle measurement is also performed with highest sensitivity. In order to eliminate the ambiguity in the angle determination (each amplitude of both signals can be obtained by two different angles) an additional piece of information is required.

Through use of equations (1) and (2), various combinations of parameters may be found, allowing optimal design of the cantilever using the full linear working range determined above. The following parameters were chosen:

material:	Ceramtec [®]
E:	360kN/mm ²
ρ :	3.8Kg/dm ³
l:	50mm
h:	0.1mm
b:	5mm

Table 1: Cantilever parameters

4. SENSOR DESIGN

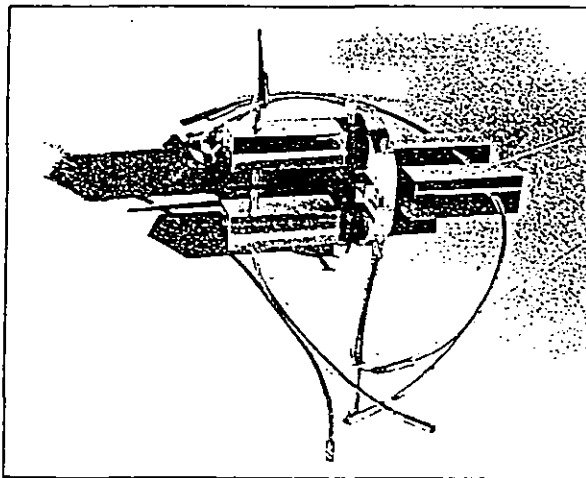


Figure 7: Design of the full angle sensor

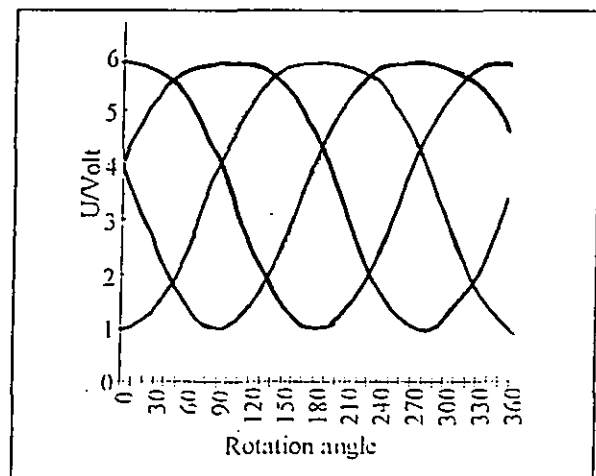


Figure 8: Output signal of the full angle sensor

For the measurement of absolute rotation angles with a measurement range of 360 degrees, a sensor was developed which is based on two cantilevers which are fixed perpendicular to each other in

combination with four FOS which are rotated synchronously with the cantilever. Figure 7 shows a picture of the full-angle sensor. The output signal of the four FOS as a function of the rotation angle is sketched in figure 8.

For special applications a miniaturized sensor for a measurement range of 180 degrees based on one FOS has been developed (see figure 9). The output signal of this sensor is shown in figure 10.

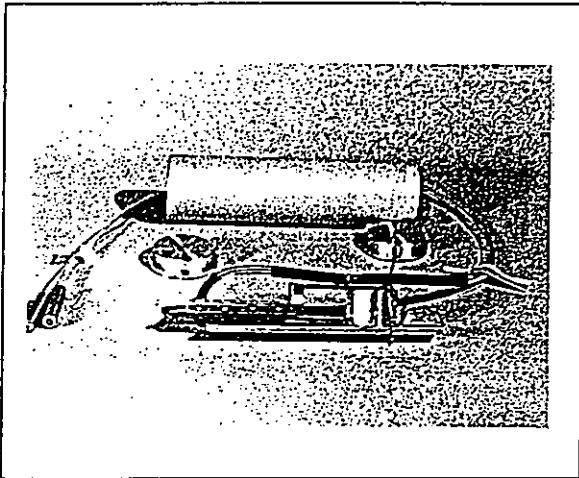


Figure 9: Miniaturized sensor design

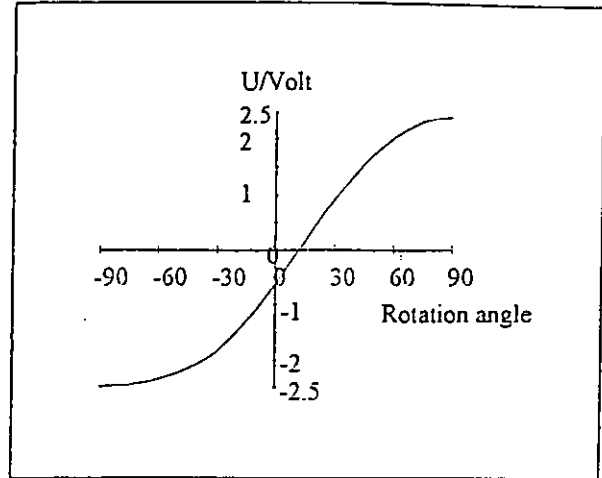


Figure 10: Output signal of the miniaturized sensor

5. RESULTS

The characteristics of the sensor developments are summarized in the following table

- measurement range: 360 degrees
- resolution :1/1000 degree
- no measurement influence due to:
 - humidity
 - high temperature
 - electromagnetic fields
 - nuclear radiation < 100krad
- flexible signal guiding by modular fiber system
- noise minimized electronics for signal conversion and analysing
- measurement of angular acceleration and angular velocity by computer signal evaluation
- miniaturized sensor for measurement range: 180 degrees

REFERENCES

1. Kreitlow, H., "Faseroptische Sensoren" in Pfeifer, T., et. al., "Optoelektronische Verfahren zur Messung geometrischer Größen in der Fertigungstechnik", Ehningen, expert-verlag, 1993
2. Kreitlow, H., Samuels, U., "Fiber optical sensor for absolute measurement of rotation angles", presented on the SPIE Conference "Interferometry '94", Warsaw, 1994

AUTOMATED SURFACE MEASUREMENT VIA LASER TOMOGRAPHY

U.Samuels, R. Parkin, H. Kreitlow*

Loughborough University of Technology, Mechanical Engineering Department,
Ashby Road, Loughborough, LE 11 3 TU, England

* Fachhochschule Ostfriesland, Forschungsschwerpunkt Lasertechnik
Constantiaplatz 4, 26723 Emden, Germany

1. Introduction

Increasingly high demands in quality assurance during the manufacture of high precision components e.g. in the automotive, aerospace, optical and bearing industries, require continuous improvements in measurement techniques. The measurement of roundness as well as shape measurement of technical components, for example turbine blades, are typical examples of demanding measurements. The measurement of complete three-dimensional object shapes can be performed by the determination and combination of the shapes of several single cross-sectional planes, which can be advantageously described in cylindrical coordinates. All of the roundness measurement systems presented can be classified by use of table 1.

Principle	Movement		Sensor		
	Sensor	Object	Contact	Signal	Dimension
1	Stationary	Rotating	Yes	Incremental	One
2	Rotating	Stationary	No	Absolute	Multi

Table 1: Classification of measurement principles for roundness measurement

2. Construction of the laser tomographical system

The here presented measurement principle is based on a high precision positioning system for object rotation, in conjunction with an optical distance sensor based on an autofocus principle. A personal computer equipped with special interfaces delivers the motor voltage (pulse width signal) for the desired object rotation speed and reads the signal from the high resolution incremental angular encoder in order to control the object rotation speed. Furthermore, the

computer also performs the reading of the sensor distance signal as well as the subsequent storage and visualisation of the evaluated measurement data.

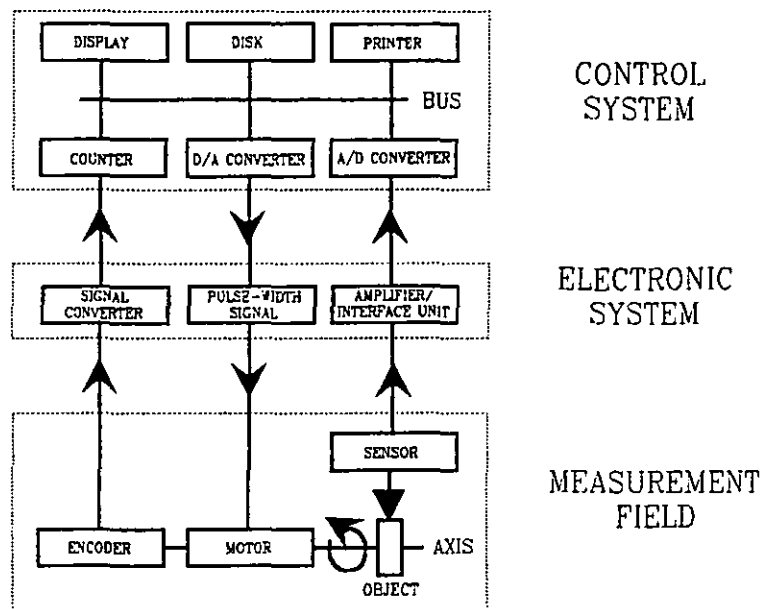


Figure 1: Principle construction of the automated system for roundness measurement

In order to optimise the sensor for different applications, the measurement range as well as the resolution of the autofocus sensor can be tuned by system adjustment. Experimental investigations have shown largest measurement ranges of $100\mu\text{m}$ and highest resolution of 200nm . The numerous surface classes which can be inspected in a non-contact and feed-back free manner is an advantage of this procedure.

3. Application

The use of this non-contact measurement procedure enables especially the investigation of ultra soft and ultra hard materials which are difficult to investigate with contact measuring systems. The large dynamic range of the sensor because of the elimination of all moving parts can be used for the investigation of periodic and transient dynamic behaviours of technical components required for example for the investigation of the oscillation characteristics of turbine blades. The application of the surface measurement system is demonstrated on selected objects.

AUTOMATED SURFACE MEASUREMENT VIA LASER PROFILING

U.Samuels, R. Parkin, H. Kreitlow*

Loughborough University of Technology, Mechanical Engineering Department,
Ashby Road, Loughborough, LE 11 3 TU, England

* Fachhochschule Ostfriesland, Institut für Lasertechnik Ostfriesland
Constantiaplatz 4, 26723 Emden, Germany

1. Introduction

Increasingly high demands in quality assurance during the manufacture of high precision components e.g. in the automotive, aerospace and optical industries, require continuous improvement in measurement techniques. The measurement of the shape of technical components is a typical example in quality assurance, where for the investigation of roundness of axially symmetrical objects special measurement systems are designed. In these systems either the sensor rotates around the object or the object rotates in front of a stationary sensor. All the sensors used in these roundness measurement systems presented can be classified by any combination of the categories presented in Table 1.

Principle

- Contact
- Non contact

Signal type

- Incremental
- Absolute

Dimension

- One dimension
- Multi dimension

Table 1: Classification of measurement techniques for roundness measurement

Most systems are designed for the static roundness investigation and they use tactile distance sensors with sub micron resolution [1-4]. For the investigation of the dynamic behaviour and/or on sensitive materials they have disadvantages due to their contact with the test object. Other non-contact measurement principles like autofocus sensors or triangulation sensors have either the disadvantage of low bandwidth or too small resolution so that they are not applicable to dynamic investigations or exact profile determination [5-6].

For these reasons a new automatic laser profile measurement system has been developed. According to Table 1 the principle of the optimised autofocus sensor delivers absolute distance signals in a non-contact manner on one axis. Due to its high resolution and its large bandwidth it is suitable for various applications. For the roundness measurement the sensor is fixed while the object is rotated.

After the description of the autofocus sensor and the automated measurement system the measurement task for roundness determination will be investigated in detail. Then typical applications of the system will be presented followed by suggestions of further improvements of the measurement setup.

2. Description of the autofocus principle

Optical distance sensors have captured new application fields in modern engineering, particularly because of its non-contact measuring principle applicable to very sensitive and/or on fast moving components. The measurement technique of the autofocus sensor is based on the principle used within CD players. It is one of the well known representatives of this class of sensors having a sub micron resolution. The typical setup of an autofocus sensor operates on the principle of dynamic focussing, where the whole sensor or the laser beam focussing lens of the sensor is moved, such that the focal position is kept on the surface to be profiled. The required movement is measured by an additional measurement system whose signal represents the profile. As a result of the moving sensor parts this principle requires relatively large equipment effort and the measurement characteristic has a limited dynamic range [5-8]. For this reasons a more advantageous sensor principle, shown in Fig. 1, has been realised, which is based on a modified setup of a previously described principle [9].

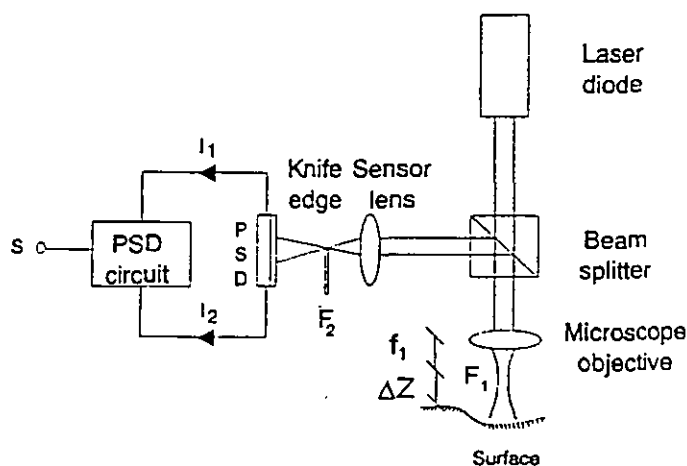


Figure 1: Principle of the autofocus sensor [9]

In front to the surface the beam of a laser diode is strongly focussed by a microscope objective to a focal spot diameter of $2\mu\text{m}$. Part of the reflected beam from the surface is separated from the incoming beam line using a beam splitter cube and is then manipulated by a sensor lens and a knife edge. As a result of this setup a light spot can be detected in the detector (PSD: position sensitive detector) plane. The light spot diameter between the focal plane F_1 and the test surface D is a function of the measured distance ΔZ and can be described by the following equation

$$D = D_0 + K\Delta Z \quad (1)$$

with the initial diameter D_0

$$D_0 = 2w \frac{(l_2 - f_2)}{f_2} \quad (3)$$

and the sensitivity constant K

$$K = 4w \frac{(f_1 l_2 - f_1 f_2 - l_1 l_2 + l_1 f_2 - l_2 f_2)}{f_1^2 f_2} \quad (4)$$

Where l_1 means the distance between the microscope objective and the sensor lens, l_2 the distance between the sensor lens and the light detector, f_1 the focal length of the microscope objective, f_2 the focal length of the sensor lens and w the beam waist radius of the measurement laser (for derivation see Appendix). Following the detection of the laser light spot in the detector plane by means of the PSD, a signal conditioning circuit combines the two characteristic PSD currents I_1 and I_2 to the signal S according to:

$$S = \frac{I_1 - I_2}{I_1 + I_2} \quad (5)$$

I_1 and I_2 are functions of the PSD illumination. If the PSD, the sensor lens, and the knife edge are properly aligned then the output signal S of the sensor can be described by [10]:

$$S \approx S_0 + K\Delta Z \quad (6)$$

Where S_0 means the initial signal and $K\Delta Z$ the change of the signal as a function of the measured distance (compare equation (1)). Equation (6) shows that a nearly linear relationship between the measurement value and the sensor signal is achieved. Varying the sensitivity constant K according to equation (4), the measurement sensitivity and the measurement range of the sensor can be tuned in relatively large ranges, where largest measurement ranges of up to $100\mu\text{m}$ and highest resolutions of up to 200nm were achieved. In contrast to other autofocus sensors this sensor has no moving parts so that the dynamic range is only restricted by the electronic characteristic and is therefore comparably large.

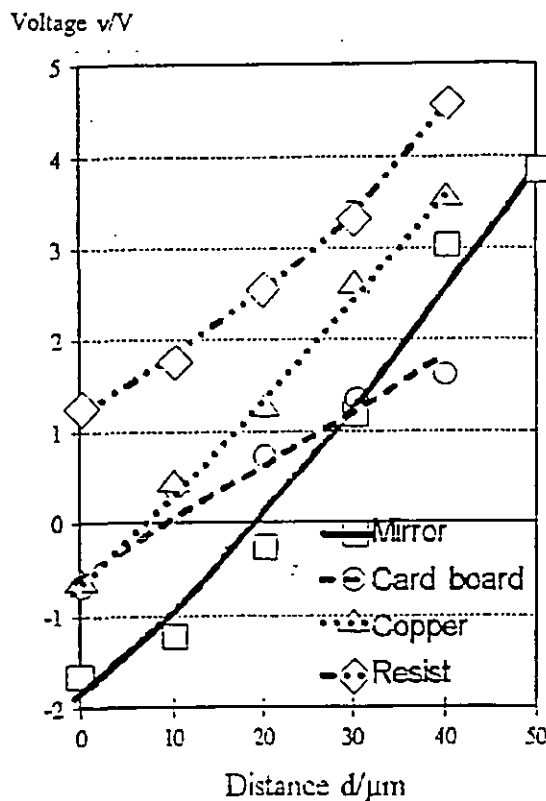


Figure 2: Measurement characteristics of the distance sensor

Figure 2 shows four typical measurement curves which were determined for the different surface materials mirror, copper, resist, and cardboard using the same sensor with equal alignment. It is apparent that different surfaces deliver measurement curves slightly varying in slope and offset but all having a linear characteristic in a large working range. For this reason the sensor has to be calibrated to any new surface, whereby the measurement on a known surface can be performed using calibration parameters from a look-up table. Furthermore, these surfaces have to be homogenous and free of contamination (by e.g. oxidation or oil).

3. Automated measurement system

For automated measuring the following system has been designed (see Figure 3). It consists of a control system, an electronic system, and the measurement field: This system is used for the synchronisation of the rotational speed of the test object and the sensor signal sampling rate.

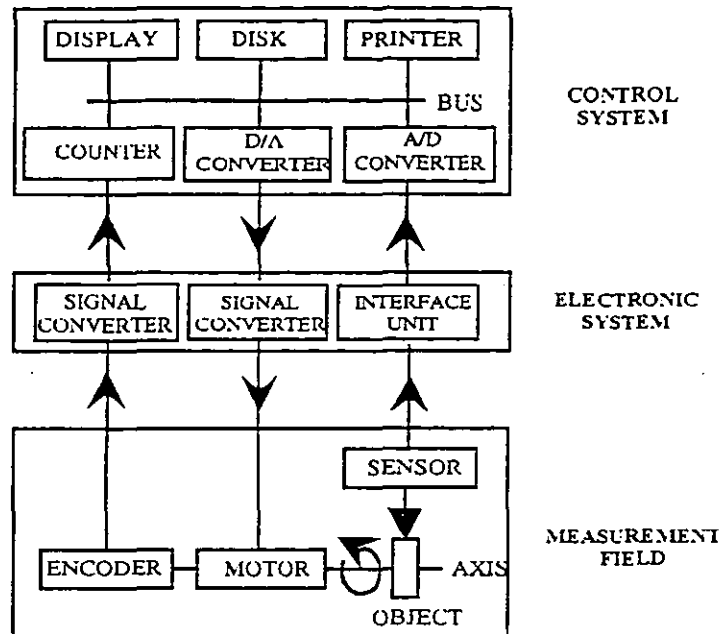


Figure 3: Block diagram of the automated roundness measurement system

The control system is a computer with a display for signal presentation, a floppy disk and a hard disk for signal storage, a printer for documentation, and interfaces for data exchange with the environment. In order to control the rotational speed of the rotation axis the D/A converter delivers a signal to the motor which is converted in a pulse-width-signal by means of the electronic system. The actual axis rotation speed is detected by an incremental encoder and transferred to the computer via a signal converter. In order to determine the new output signal of the D/A converter for the motor, the computer compares the actual rotation speed with the setpoint. This system affects as a closed loop control system for the rotation speed of the axis. During the rotation of the axis the autofocus sensor signal is sampled, amplified, and transferred to the A/D converter in the control system for the subsequent data storage, analysis, and visualisation. For the setup shown, the object to be measured is fixed on the rotation axis or can be the axis shaft itself.

4. Description of the measurement task

The automated system enables the measurement of the distance between the surface of objects with round cross sections and the sensor while the object is rotated in front of the sensor. Due to the fixed position of the sensor and for homogeneous surface characteristics of the object the measurement signal is a function of the object shape and the accuracy of the object rotation.

For an ideal rotation axis, that means an axis without a radial runout, the measurement signal describes the eccentricity of the object so that its cross section of the object is obtained. A real axially symmetrical object has in general a deviation from absolute roundness. If its cross section can be classified as round it has still a surface characteristic affected by waviness and roughness. These parameters can be distinguished by the frequency of the profile. In comparison to waviness the roughness has a much higher frequency and is superpositioned to the waviness[3]. For this reason the output signal of the sensor for an object with a round cross section rotated with an ideal rotation axis having a constant rotation speed can be separated by the frequency in the two parts describing the eccentricity of the object. The first part with the lower frequency describes the waviness and the second part with the higher frequency describes the roughness.

For a non-ideal rotation axis, that means an axis with radial runout, the signal to be measured describes the overall system consisting of the object and the rotation axis. Therefore, the signal is more difficult to interpret. If the radial runout movement influences the signal in the frequency range of the waviness and in the frequency range of the roughness the sensor signal is equivocal. This is due the fact that the signal parts which stem from the radial runout movements of the axis or by the object surface cannot be distinguished by their frequencies.

For the high precision axis used in the measurement setup the radial runout movements are in the same frequency range as the axis rotation frequency and, for this reason, also in the range of the waviness. Therefore, when a correct frequency filtering is performed, the roughness describing signal with a much higher frequency can be separated from radial runout signal and the waviness signal. But due to the same fact the signal obtained by the radial runout movements can not be separated correctly from the waviness by simple frequency filtering. Therefore, different measurement curves will be determined for different rotation speeds because the radial runout is in general dependent on the rotation speed.

5. Measurement examples

The measurement of the surface roughness of the shaft of the precise rotating axis is the first application. The sensor was tuned according to equation (4) so that a measurement resolution of 200nm in a linear measurement range of nearly 50 μm was achieved. A high pass filtering of the sensor signal, adjusted in accordance with the very slow rotation speed (quasi static investigation) ensures that the waviness and the radial runout are not influence the signal so that only the roughness of the axis surface is detected. Figure 4 shows in polar coordinates the measured roundness deviation curve of the axis. The maximum eccentricity value is 12.00 μm and the minimum eccentricity value is 7.27 μm , so that the R_t (Roughness Total) value of 4.73 μm is determined.

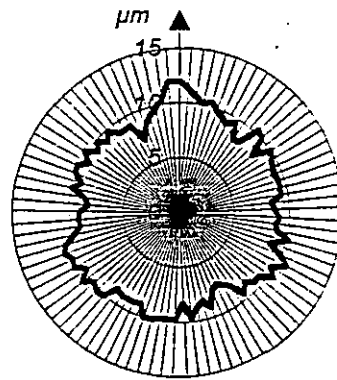
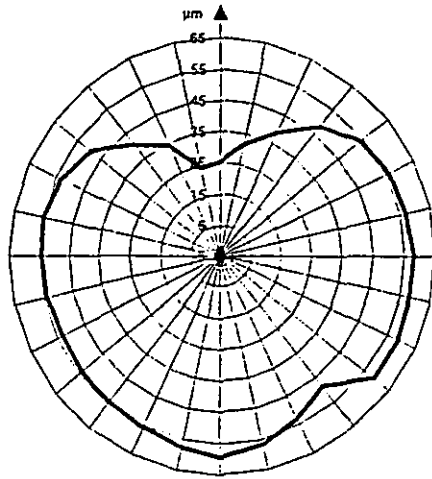


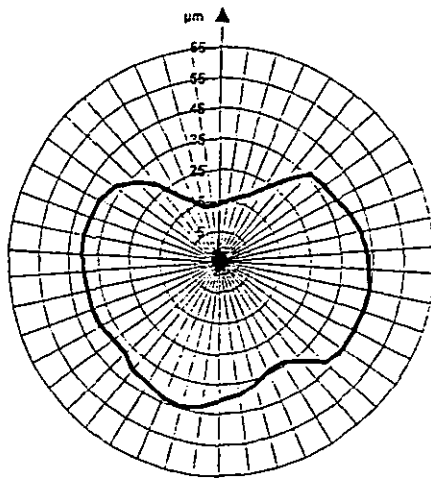
Figure 4: Example of static investigation using the laser profiling system

In a second example the application of the laser profiling system for the investigation of fast rotating objects (dynamic investigation) has to be demonstrated. With the above mentioned sensitivity of the sensor the shaft of the same axis was investigated. A low pass filtering of the sensor signal, tuned to the rotation speed, ensures the reverse clipping of the influence on the sensor signal, so that the signal is only a function of the waviness of the axis surface and the radial runout of the axis and not influenced by the surface roughness.

The minimum value of the signal shown in Figure 5a is 23.82 μm and the maximum value is 59.52 μm , so that a peak to peak value of 35.7 μm is determined for a rotation speed of 240rpm. Figure 5b) shows a minimum value of 13.53 μm and a maximum value of 44.83 μm , so that a peak to peak value of 31.3 μm is determined at a rotation speed of 2400rpm. It can be seen that different values of rotation speed result in curves with the same characteristic but with different amplitudes of the measured value.



a) 240rpm



b) 2400rpm

Figure 5: Examples of dynamic investigation using the laser profiling system

6. Optimised measurement system

Every measurement requires the presence of a reference. For the special case of the determination of roundness deviation compared to a circle, the reference is in general a high precision bearing that allows the precise rotation of the measurement object [3,4]. Every rotational deviation of the bearing influences the measurement result so that this procedure can only be used for the determination of roundness deviations that are large compared to the radial runout of the spindle in use. Further problems are observed concerning large objects that are difficult to handle. In these cases the use of the 3 point method is preferred [1,2]. By combination of two three point measurement systems to a four point system [11] and a suitable angle adjustment between supporting points and the sensor [12] the measurement accuracy can

be further improved. To preserve the advantages of the non-contact measurement technique for dynamic investigations and/or the measurement of sensitive objects in a 3 or 4 point method the reference determination has to be performed in a non-contact manner as well. The tunability of the autofocus sensor makes this sensor also applicable for this task. For the investigation at a high rotation speed also a fast signal analysis and evaluation is required. For most accurate and flexible signal evaluation the Fourier transform can be applied. Based on geometrical relations of the mechanical measurement system, consisting of the sensor and the supporting points, the transfer function of the spectrum of the measured signal to the desired roundness deviation can be determined.

7. Conclusion

An automated laser profiling system based on an autofocus sensor in combination with a rotational axis has been presented, which allows the roundness deviation measurement of axially symmetrical objects. By use of the non-contact autofocus sensor working without any moving part the measurement of ultra hard and ultra soft objects in static and dynamic applications can be performed. The system can be used e.g. in quality assurance of precisely manufactured objects and roll bearings as well as in rapid prototyping.

References

- [1] Westkämper, E., Michel, S., Gente, A., Lange, D.: Prozeßnahe Rundheitsmeßtechnik mit 3-Punkte Meßsystem, Research description on the Interkama exhibition, Düsseldorf, 1995
- [2] Mitsui, K.: Development of a new measurement method for spindle rotation accuracy by three points method, Proceedings of the 23rd conference on machine tool design and research MTDR, 1982
- [3] Stevens, D.M.: An investigation into the use of a wide range interferometric transducer for roundness measurement, MPhil Thesis, CNAAL, Leicester Polytechnic, August 1989
- [4] Moore, D.: Design consideration in multiprobe roundness measurement, J.Phys.E:Sci. Instr., 1989, Vol.22
- [5] Breitmeyer, U., Lasermeßtechnik zur Oberflächen-Qualitätskontrolle, Laser und Optoelektronik, 24(2), 1992
- [6] Overmeyer, L., Dickmann, K., Dynamischer Autofokussensor zur dreidimensionalen Mikrostrukturerfassung, tm, Technisches Messen, 59/1992

- [7] Tönshoff, H.K., Heekenjann, P.B., Overmeyer, L., Autofocus sensor for micromachining, *Laser und Optoelektronik*, 25(6), 1993
- [8] Brodmann, R., Messen in CD-Qualität, *Laser* 3/1989
- [9] Dupuy, M.O., High precision optical profilometer for the study of micro-geometrical surface defects, *Proc. Instn. Engrs.* 1967-68, Vol. 182 Pt 3K
- [10] Samuels, U.: Focal position controlled processing head for a laser pattern generator (LPG) for flexible microstructuring, MPhil Thesis, Loughborough University of Technology, November 1995
- [11] Zhang, G.X., Wang, R.K.: Four point of roundness and spindle error measurements, *Annals of the CIRP*, Vol. 42/1, 1993
- [12] Steger, A.: Über die Möglichkeiten und Grenzen der Dreipunktmessung zur Bestimmung der Formabweichung vom Kreis. PhD Thesis TH Karl-Marx-Stadt, 1976

Appendix

Derivation of the sensor equation

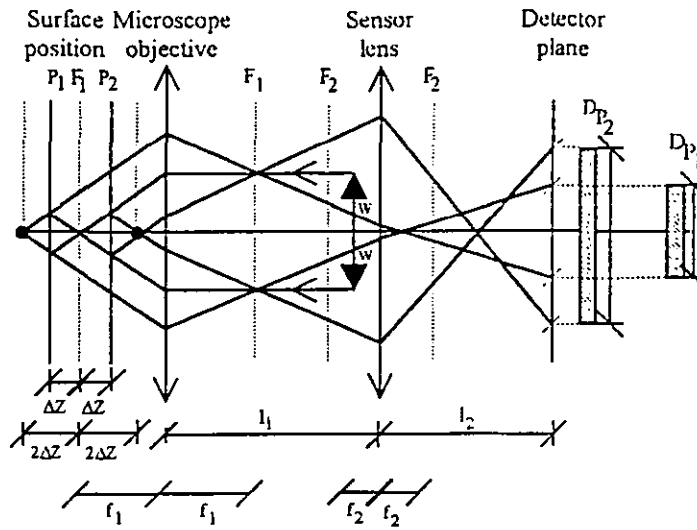


Figure A1: Principle of the beam guiding system of the sensor

The input beam of the measuring laser with the radius w and parallel boundary rays is focussed by the lens of the microscope into the focal plane F_1 . Depending on the distance ΔZ of the measured surface to the focal plane f_1 of the microscope objective, the reflected boundary rays take different paths through the system which consists of microscope objective, sensor lens separated by the distance l_1 , and the detector plane displaced with respect to the sensor lens by a distance l_2 . In the detector plane a spot is obtained whose diameter D is a result of the distance ΔZ of the measuring surface. This spot is reduced to a semi-circle by the knife edge (not sketched in Figure A1) and detected by the PSD. The mathematical description of the sensor will be investigated in three principal steps:

I) In following the influence of the focal length f_1 and the distance l_1 will be investigated. The microscope objective images a point whose apparent location is at the position

$$a_1 = f_1 + 2\Delta Z \quad (\text{A1})$$

The image location a_1' can be found using the well known lens equation

$$a_1' = \frac{f_1(f_1 + 2\Delta Z)}{f_1 + 2\Delta Z - f_1} = f_1 \frac{(f_1 + 2\Delta Z)}{2\Delta Z} \quad (\text{A2})$$

Because of the location of image at a_1' and the fact that every beam has a diameter w of the input beam at the back focal plane of the microscope objective, the principle beam propagation between the lenses can be drawn as seen in Figure A2.

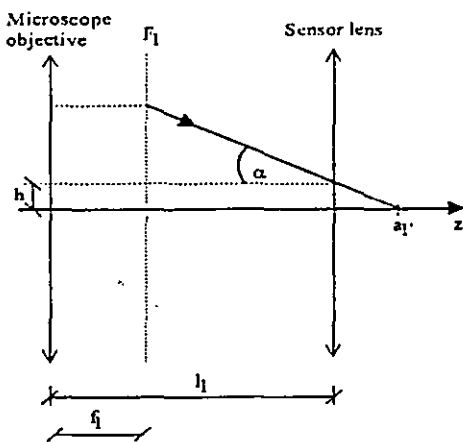


Figure A2: Geometry of the beam propagation between the lenses

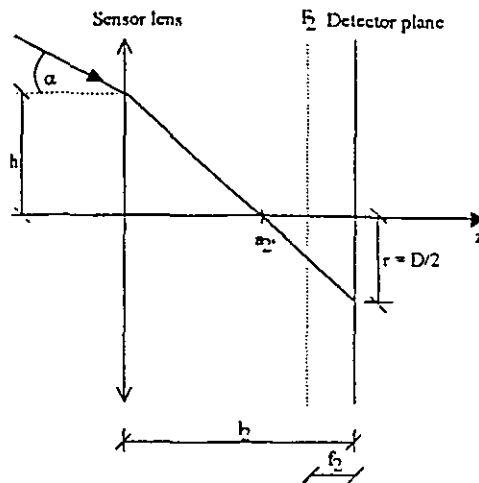


Figure A3: Geometry of the beam propagation between the sensor lens and the detector plane

Using the information in Figure A2 and basic geometry, and equation (A2) the following expression can be found for the angle between the incident beam and the principle plane of the sensor lens

$$\alpha = \arctan\left(\frac{w}{f_1 \frac{(f_1 + 2\Delta Z)}{2\Delta Z} - f_1}\right) \tag{A3}$$

Also, information about the height h at which the principal beams reach the sensor lens can be found using basic geometry for the setup sketched in Figure A2

$$\frac{h}{a_1' - l_1} = \frac{w}{a_1' - f_1} \tag{A4}$$

In combination with equation (A2) the expression for the height h can be determined

$$h = \frac{w(f_1 \frac{(f_1 + 2\Delta Z)}{2\Delta Z} - l_1)}{f_1 \frac{(f_1 + 2\Delta Z)}{2\Delta Z} - f_1} \tag{A5}$$

II) In the second step the influence of the parameter h and α in conjunction with the focal length f_2 of the sensor lens and the distance l_2 between the sensor lens and the detector plane to the light spot diameter D will be investigated. Using geometrical laws, the following equation can be found:

$$\frac{r}{l_2 - a_2'} = \frac{h}{a_2'} \quad (\text{A6})$$

where r indicates the semi-diameter of the light spot at the focal plane.

As illustrated in Figure A3, the incident beam contacts the surface of the sensor lens at the height h and under the angle α so that the point that will be imaged by the lens is apparently located at

$$a_2 = \frac{h}{\tan(\alpha)} \quad (\text{A7})$$

To find the location of the image of this point, the lens equation can be used

$$a_2' = \frac{a_2 f_2}{a_2 - f_2} \quad (\text{A8})$$

substituting equation (A8) into equation (A6), and using equation (A7) the desired function for the semi-diameter of the light spot is found.

$$r = \frac{h(l_2 - f_2)}{f_2} - l_2 \tan(\alpha) \quad (\text{A9})$$

III) In the final step the results of the above calculations will be combined to yield the mathematical sensor model. This can be done by substituting the equations (A3) and (A5) into equation (A9) which leads to

$$r = w \left\{ \frac{l_2 - f_2}{f_2} + 2 \frac{(f_1 l_2 - f_1 f_2 - l_1 l_2 + l_1 f_2 - l_2 f_2) \Delta Z}{f_1^2 f_2} \right\} \quad (\text{A10})$$

This leads to the diameter of the light spot

$$D = 2r = D_0 + K \Delta Z \quad (\text{A15})$$

with the initial diameter D_0 in equation (3) and the sensitivity constant K given by equation (4).



Optics & Laser Technology, Vol. 28, No. 6, pp. 423-429, 1996
 Copyright © 1996 Elsevier Science Ltd
 Printed in Great Britain. All rights reserved
 0030-3992/96 \$15.00 + 0.00

PII: S0030-3992(96)00004-7

Precise wavelength tuning of a dye laser using an active diffractive optical element

U. SAMUELS, H. KREITLOW, S. C. WRIGHT, CH. BUDZINSKI, H. J. TIZIANI

In this work, an active, reflecting diffraction grating was developed and characterized. A grating was holographically imposed onto the surface of a ceramic which could be deformed via the transverse, inverse piezoelectric effect, thus allowing active fine tuning of the grating constant. The tuning characteristics of this novel optical element were studied and the results compared with the linear theory of the piezoelectric effect. To demonstrate its applicability, the grating was installed in a dye laser and used to effect precise tuning of the output wavelength of the laser within a range of 220 pm. The possibility of quasi-static to high frequency operation of the system will allow this element to find use in a wide variety of applications. Copyright © 1996 Elsevier Science Ltd.

KEYWORDS: active diffractive optical elements, piezo-tuned gratings, lasers (dye)

Principles of Operation

The principles to be described in this work have been suggested previously¹⁻³. An area or volume change as a result of a uniform elastic deformation of a plane grating substrate (for example, a piezoelectric ceramic), results in a change in the line spacing and the profile of the surface structure of a straight, equidistant groove system (classical plane grating).

From the grating equation

$$k\lambda = g(\sin \alpha + \sin \beta) \quad (1)$$

it follows that, for a given optical geometry (that is, angles of incidence, α , and diffraction, β), the corresponding wavelength is dependent upon the grating constant

$$\frac{d\lambda}{dg} = \frac{1}{k}(\sin \alpha + \sin \beta) \quad (2)$$

whereby g is the grating constant and k the diffraction order.

From the linearity of the grating, equation (1) also follows the direct relationship between the relative expansion of the grating substrate along the direction of

dispersion and the relative variation of the wavelength into a given diffraction angle

$$\frac{dI}{I} = \frac{dg}{g} = \frac{d\lambda}{\lambda} \quad (3)$$

By use of a plane, polished piezoelectric ceramic grating substrate (1 in Fig. 1) onto which a diffracting structure (2) and electrodes covering the major surfaces (3, 4) have been imposed, it is possible to use the transverse, inverse piezoelectric effect to vary the grating line spacing via an imposed electric voltage, as depicted.

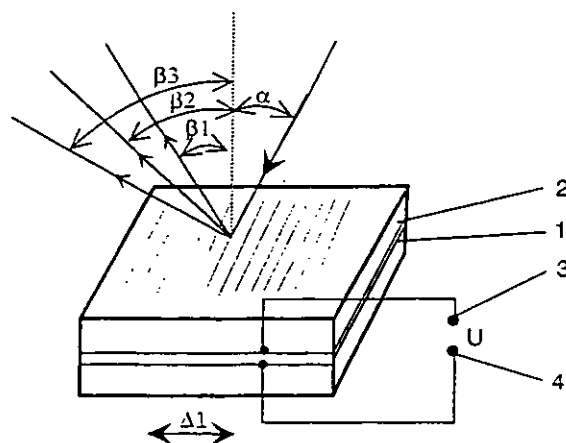


Fig. 1 Schematic representation of the reflection grating depicting various diffraction angles as a result of voltage tuning of the grating line spacing. The variation in β has been grossly exaggerated for clarity

US, HK and SCW are in Fachhochschule Ostfriesland, Institut für Lasertechnik, Constantiaplatz 4, 26723 Emden, Germany. ChB and HJT are at Universität Stuttgart, Institut für Technische Optik, Pfaffenwaldring 9, 70569 Stuttgart, Germany. Received 25 July 1995. Accepted 6 December 1995.

Substrate materials by which a length change may be caused via other effects (for example, electrostrictive or magnetostrictive materials) are also suitable for this purpose. The suitability of materials is, however, somewhat restricted in that it must be possible to polish the surface to optical quality. Regarding the choice of piezoelectric material, all ferroelectrics with a non-negligible transverse coefficient in their deformation matrix may also be considered suitable. In addition to the industrially produced solid solutions, in which certain characteristics may be especially cultivated, most natural substances also show piezoelectric and/or ferroelectric qualities. An important example is quartz which, owing to its high transparency in the visible and near ultraviolet spectral regions, is particularly interesting. However, the piezoelectric strain constant of quartz is small, thus limiting its use to very specialized applications.

Manufacture of the grating

Figure 2 shows a detailed cross-section of the piezo grating with its glass substrate (1), piezo-ceramic (2) and the various bonding layers (3 to 5). In this work, the ceramic PK51 from the company Marco in Hermsdorf, Germany, was chosen. This lead-zirconate-titanate ceramic (PZT) sample was 50 mm long, 20 mm wide and 1 mm thick. The upper surface of the ceramic was coated and polished to optical quality followed by the deposition of electrodes (6) and (7) onto the upper and lower surfaces. Photoresist (8) was then brought onto the optically polished surface and formed a sine grating with a grating constant of $g = 0.476 \mu\text{m}$ (2100 lines per mm) through holographic exposure in a laser interferometer. The surface of the grating was then coated with a highly reflective aluminium layer in order to achieve a high diffraction efficiency in the first order. Following electrical contacting, the piezo-ceramic was polarized.

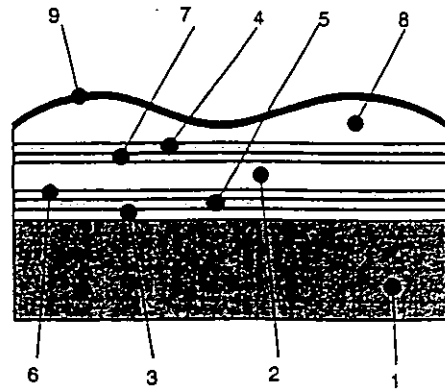
Tuning characteristics of the active diffraction grating

The principle of operation of piezo-ceramic actuators is based on the deformation of the piezoelectric material under the influence of an applied electric field (reciprocal piezoelectric effect). A positive (negative) voltage with respect to the direction of polarization results in an expansion (contraction) of the material in this direction and a contraction (expansion) in the perpendicular direction. Depending on the material employed and, thus, its piezoelectric strain constants, relative expansions of 0.15% may be attained. In the linear approximation, within the region of validity of Hooke's law, the relative change in length may be calculated as

$$\frac{\Delta l}{l} = d_{ij}E = d_{ij} \frac{U}{h} \tag{4}$$

where

- l = undeformed length of the piezo-ceramic;
- Δl = change of length of the piezo-ceramic;
- h = distance between the electrodes;
- d_{ij} = relevant piezoelectric strain constant;
- E = electric field strength;
- U = applied electric voltage.



1: Substrate	6: Electrode
2: Piezo Ceramic	7: "
3: Bonding Layer	8: Photoresist
4: Intermediate Bonding Layer	9: Aluminium
5: "	

Fig. 2 Cross-section of the piezo grating

Linear expansion and contraction as described by (4) (deformation proportional to the applied field strength and to the undeformed length of the element), is valid only for small applied voltages with electric field strengths less than 50 V mm^{-1} . Above this value, deviations from linear behaviour and hysteresis are readily observed. For the material employed here the range of applicable electric field strengths is limited by electrical breakdown of the material to about 2 kV mm^{-1} in the direction of polarization of the ceramic and to about one-third of this value for the opposite poling of the voltage source in order to avoid repolarization of the ceramic. The manufacturer's specifications for the piezoelectric strain constants, valid for small electric field strengths, were given as⁴

$$d_{31} = -1.7 \times 10^{-10} \text{ mV}^{-1} \quad (\text{deformation perpendicular to the electric field})$$

$$d_{33} = 4.5 \times 10^{-10} \text{ mV}^{-1} \quad (\text{deformation parallel to the electric field})$$

Using the apparatus depicted in Fig. 3, the validity of the linear deformation approximation for small signals and the non-linear response for larger signals was investigated.

The HeNe laser beam ($\lambda = 632.8 \text{ nm}$) was arranged to fall on the grating with an angle of incidence near the autocollimation angle which is calculated

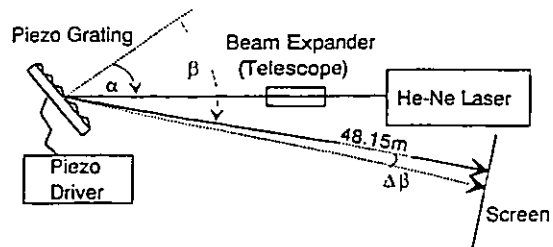


Fig. 3 Experimental set-up for the investigation of the tuning characteristics of the grating

as $\alpha = \beta = 41.6^\circ$ for this case. The change in the diffraction angle in first order as a result of tuning the grating with an applied voltage was determined by measuring the displacement of the beam at a great distance (48.15 m). To ensure a high precision during these measurements of extremely small angles (the largest angle measured was 1.2 mrad), the laser beam was expanded with a telescope to reduce the beam divergence over the long path length.

From the known geometry, the diffraction angles were determined as a function of the applied voltage and the corresponding grating constants calculated. The results of this experiment are depicted in Fig. 4 along with the calculated variation of the grating constant under the linear approximation from (3) and (4)

$$g = g_0 \left(1 + d_{31} \frac{U}{h} \right) \quad (5)$$

using the strain constant specified above and $g_0 = 1/2100 \text{ mm}^{-1}$.

With the voltage applied in the polarization direction ($U > 0 \text{ V}$), agreement with the linear theory was observed up to values of roughly 100 V, whereas for larger voltages, a strong deviation from linearity was found. With the opposite polarity ($U < 0 \text{ V}$), the observed dependence was found to be approximately linear down to -300 V followed by a lesser deviation from non-linearity than was the case for positive voltages. At a voltage of -700 V , the measured change in the grating constant was $105 \pm 4 \text{ pm}$, roughly 100% larger than the value expected from the linear theory.

A computer simulation was performed to test the insensitivity of the results with respect to small deviations from the assumed angle of incidence, which was found indeed to be the case for the geometry chosen with the beam incident near the autocollimation angle.

Fine tuning of dye lasers

Many applications of tunable lasers require extremely precise tuning of the laser wavelength to within 1 pm or less and/or stabilization of the laser in the resonant mode. These requirements are difficult, if not impossible, to satisfy with mechanical actuators. The piezo-grating described here is predestined for such applications, as fast wavelength tuning with a resolution less than 1 pm may be readily realized.

Design of the dye laser

Figure 5 shows the design of the dye laser used in this work, which was a modified FL 2000 system from Lambda Physik. Rhodamine 6G dye was chosen (tuning range 570–610 nm) which was continually recirculated through the cuvette via a pump system. The active diffraction grating was arranged with the high reflecting mirror in a Littmann/Metcalf (grazing incidence) configuration. This design has the advantage over the original Littrow configuration of this dye laser (in which the beam is diffracted directly back into the resonator without the use of a separate high reflector mirror), that the beam expander is obviated, resulting in a system that

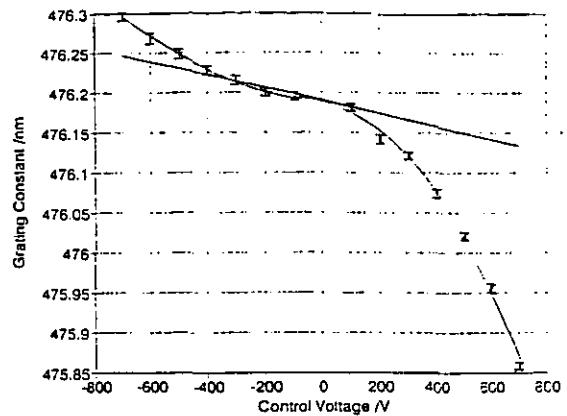


Fig. 4 Theoretically and experimentally determined grating constants as a function of the applied voltage. The curve drawn through the experimental data is to guide the reader's eye only and is not intended to represent any particular functional dependence

is simpler to adjust while using less expensive components. Furthermore, since the grating acts twice per pass, the dispersion is effectively increased, resulting in a narrowing of the wavelength bandwidth. The piezo-grating was supported on a cardanic mount to allow coarse mechanical tuning to the desired centre wavelength. An XeCl excimer laser was used as the pump source.

Tuning characteristics of the dye laser

For the purpose of tuning the dye laser, the control voltage was poled opposite to the polarization direction of the piezo-ceramic. The tuning characteristic of the dye laser according to the linear approximation to the transverse piezoelectric effect is obtained from (3) and (4) since variation of the grating constant, g , results in a variation in the wavelength of the light resonant within the laser cavity. Thus, the theoretical tunability of the dye laser is given by

$$\frac{d\lambda}{dU} = d_{31} \frac{\lambda_0}{h} \quad (6)$$

For the chosen wavelength of 595.3 nm, a tuning sensitivity of 0.10 pm V^{-1} is predicted for small signals.

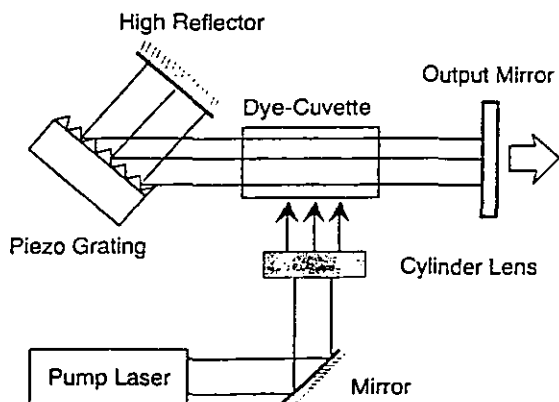


Fig. 5 Principle design of the dye laser with the piezo grating installed in a Littmann/Metcalf configuration

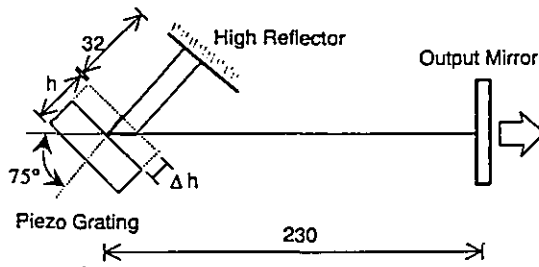


Fig. 6 Geometry of the dye laser resonator showing the effect of an expansion of the piezo ceramic parallel to the applied electric field

In order to demonstrate the size of the effect to be expected from the linear theory, values of the absolute wavelength change in first order are given in Table 1 for various pertinent wavelengths, using the parameters and typical voltages relevant for the present work.

Table 1. Tuning ranges for various pertinent wavelengths and voltages

λ (nm)	$\Delta\lambda$ (pm) ($U = -50$ V)	$\Delta\lambda$ (pm) ($U = -700$ V)
308	2.6	37
595	5.1	71
800	6.8	96

Following application of the control voltage, the piezo substrate is, in addition to the transverse effect described above, also expected to contract along the direction of polarization due to the longitudinal inverse piezoelectric effect. This results in a change of the length of the resonator which will, in principle, also result in a change in the wavelength of the light emitted from a given longitudinal mode. The change in thickness, Δh , of the substrate is determined by (4). Specifically

$$\frac{\Delta h}{h} = d_{33}E \tag{7}$$

Considering the geometrical details of the laser, as given in Fig. 6, this results in a change in the length, ΔL , of the resonator as follows

$$\Delta L = \Delta h \frac{[1 + \cos(\alpha + \beta)]}{\cos \alpha} \tag{8}$$

The tuning sensitivity due to this effect is, thus, given by

$$\begin{aligned} \frac{d\lambda}{dU} &= \frac{dL}{dU} \frac{\lambda}{L} = \frac{dh}{dU} \frac{\lambda}{L} \frac{[1 + \cos(\alpha + \beta)]}{\cos \alpha} \\ &= d_{33} \frac{\lambda}{L} \frac{[1 + \cos(\alpha + \beta)]}{\cos \alpha} \end{aligned} \tag{9}$$

Thus, for the geometry employed here, this effect leads to a 4% contribution to the tuning of the laser wavelength (4 fm V^{-1}) as compared with the contribution due to the variation of the grating constant and may, therefore, be neglected. Only for very grazing-incidence configurations will this effect come into play, contributing 10% at $\alpha = 85^\circ$ and still only 50% at $\alpha = 89^\circ$.

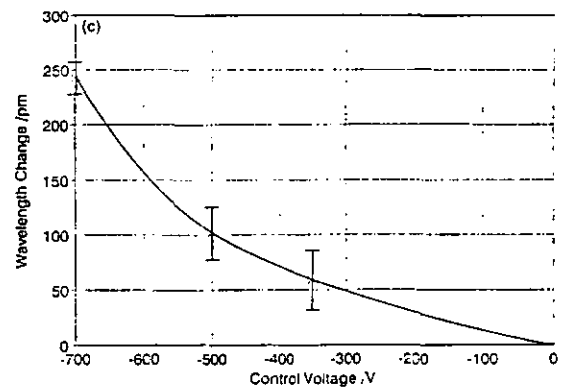
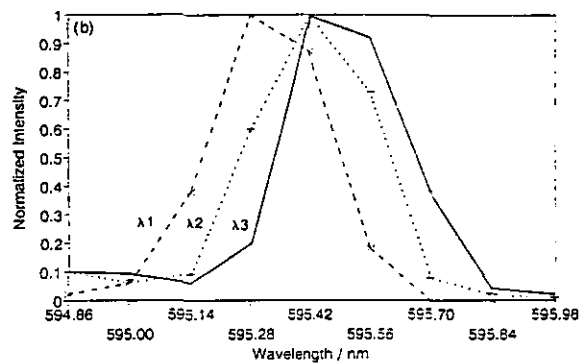
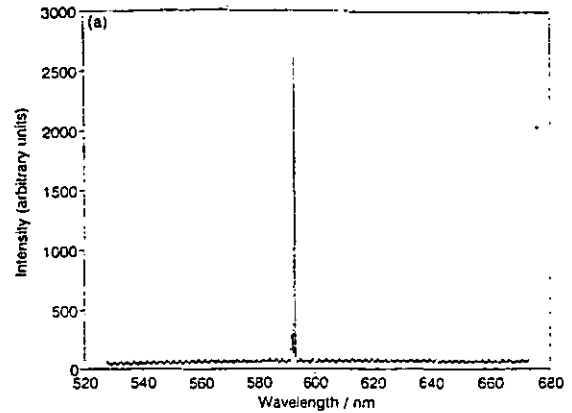


Fig. 7 Dye laser wavelength measurements. (a) Spectrum of the dye laser with zero applied voltage on the piezo grating; (b) detailed overlay of the dye laser spectrum for applied voltages of 0 V (---), -500 V (.....) and -700 V (—); (c) wavelength shifts as a function of the applied voltage as determined via the variation in the angle of diffraction from an external grating. The wavelength shift at -700 V was measured to be 234 ± 12 pm (curve: see note to Fig. 4)

Measurements of the wavelength tunability

The unshifted wavelength was measured and rough measurements of the wavelength shift for tuning voltages $U < -500$ V were made using a commercial spectrometer fitted with a diode array detector (see Figs 7(a) and 7(b)). These measurements were

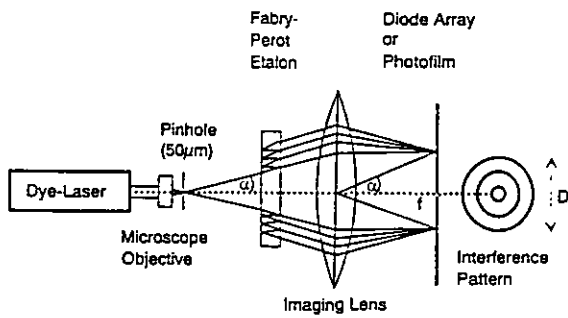


Fig. 8 Experimental set-up for the recording of FPE ring patterns

overly limited by the resolution of the spectrometer (1 pixel $\hat{=}$ 140 pm) and so can give only an estimate of the order of magnitude of the wavelength shifts to be expected. Measurements of the wavelength shift were also made by measuring the changes in the diffraction angle of the dye laser beam allowed to fall onto an external grating (1200 lines per mm) in an arrangement similar to that depicted in Fig. 3. These results are displayed in Fig. 7(c).

A more accurate and detailed analysis was undertaken by recording the characteristic ring pattern generated by a Fabry-Perot etalon (FPE) for each wavelength as a function of the voltage applied to the piezo-grating (see Fig. 8).

Recordings of the interference rings were made alternatively on photographic film and with a photodiode array in the focal plane of the lens for applied voltages from 0 to -700 V in steps of 100 V. As an example, Fig. 9 shows a typical interference pattern

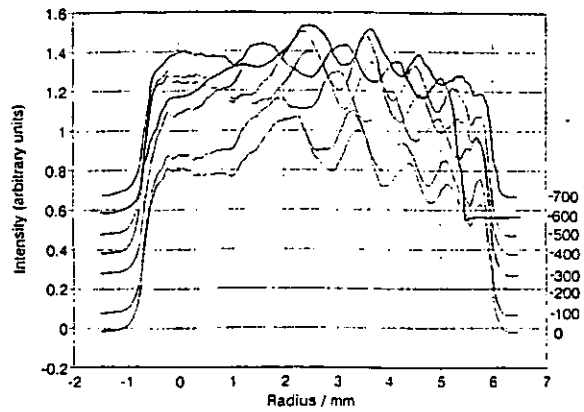


Fig. 10 Interference fringe structure from the FPE recorded with the photodiode array as a function of the distance from the centre of the ring pattern for each applied voltage

as recorded photographically for an applied voltage of -700 V. Through use of a CCD camera and a computer-based image analysis system, the contrast of the photographs was increased and the equivalent of a densitometric analysis was made along one diameter of each by assigning each pixel to one of 256 grey scales. These results were graphically overlaid onto the photographs and the ring diameters were then determined by measuring the distances between the corresponding optical density maxima.

In Fig. 10, the intensity distributions as a function of the distance from the centre of the pattern of interference fringes, as recorded with the photodiode array, are displayed for the various voltages applied. The intensity

-700 Volt

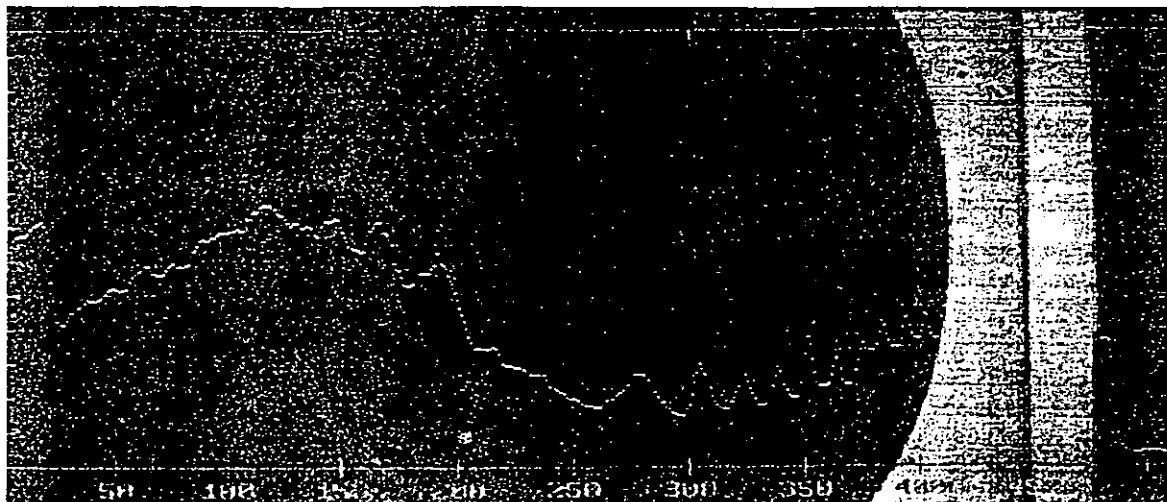


Fig. 9 Graphical output from the image analysis system of the interference structure generated by the FPE as recorded on photographic film for an applied voltage of -700 V (see insert)

maxima of the different interference orders wander toward the centre of the pattern for decreasing voltages (that is, for increasing absolute values of the voltage, as a negative polarity was employed here).

The analysis of the interference patterns involved the use of two methods as detailed below.

- (1) Under the approximation of paraxial geometry, one obtains for the diameter D_p of a ring of given interference order in the focal plane of the imaging lens (see Fig. 9)

$$\lambda = \frac{d}{4pnf_2^2} D_p^2(U_j) = kD_p^2(U_j) \tag{10}$$

whereby n is the index of refraction of the FPE (1.5 for BK7 glass at 595 nm), d its thickness (0.9 mm), f_2 is the focal length of the imaging lens (600 mm) and p is the ring number, counted from the centre of the interference pattern. Since the images used for the analysis were not the original photographs, a magnification factor would have to be taken into account. Thus, the factor k (including the unknown magnification factor) was determined through the measurement of a single ring diameter for the known absolute wavelength as determined through the measurements with the spectrometer. It then follows that

$$\Delta\lambda = k[D_p^2(U_j) - D_p^2(U_k)] \tag{11}$$

- (2) A procedure analogous to method 1 was employed, with the ring systems scaled according to the free spectral range of the FPE used, which for $\Delta\lambda \ll \lambda$ and $\alpha \ll 1$ is given by

$$\Delta\lambda = \frac{\lambda^2}{2nd} \tag{12}$$

Although these methods are, in principle, equivalent, they involve measurements of different parameters, which is useful as a means of control of the results. Both methods were used for the analyses of the photographic and diode array measurements and gave equivalent results within the limits of experimental error. For an unshifted wavelength of 595.2 nm and an applied voltage of -700 V, wavelength shifts of 210 ± 6 and 220 ± 6 pm were obtained from the photographic and diode array recordings respectively. The complete set of results is displayed graphically in Fig. 11.

In the region from 0 to -300 V, all measurements, including those using the external grating (see Fig. 7(c)) gave results in good agreement with the linear theory (curve 1 of Fig. 11). For larger applied voltages, the wavelength shifts calculated from the data from the measurements of the variation of the grating constant, diverge from the linear theory (compare with the equivalent results displayed in Fig. 4). The results of the measurements employing the FPE (curve 3 of Fig. 11) show the same characteristic dependence as displayed in Fig. 7(c) and give an averaged value of 215 ± 9 pm for the wavelength shift at an unshifted wavelength of 598.2 nm and applied voltage of -700 V.

Determination of the output energy stability of the dye laser during wavelength tuning

In order to determine the stability of the energy of the laser output during wavelength tuning, the pulse energy was measured using a fast photodiode and continually averaged over roughly 100 pulses using a boxcar averager since the shot-to-shot stability of this particular laser was quite poor. The results of this measurement are displayed in Fig. 12, whereby each of the regions shown corresponds to the results of one minute of measurement data, during which time the applied voltage was held constant at the values indicated.

Despite the large fluctuations in output energy, the results indicate a definite trend towards decreasing energy with decreasing applied voltage. Thus, at an applied voltage of -700 V, the output energy was reduced to 85% of the starting value. The fact that the output energy did not return to the original value following removal of the applied voltage (last region in Fig. 12) is an indication of hysteresis in the

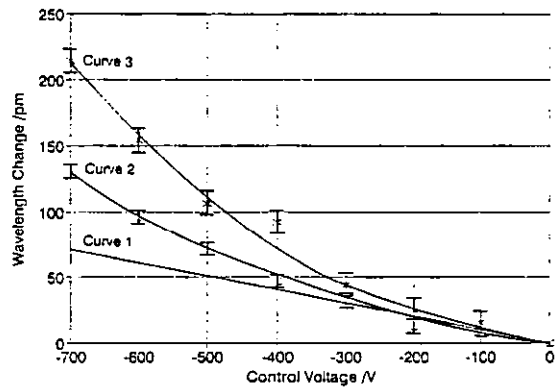


Fig. 11 Wavelength shift of the dye laser as a function of the voltage applied to the piezo grating. Curve 1: linear theory according to equation (6); Curve 2: calculated wavelength shifts, as expected from the experimentally determined grating constant data displayed in Fig. 4; Curve 3: average of the data obtained from the FPE measurements using photographic film and the diode array. (Curve: see note to Fig. 4)

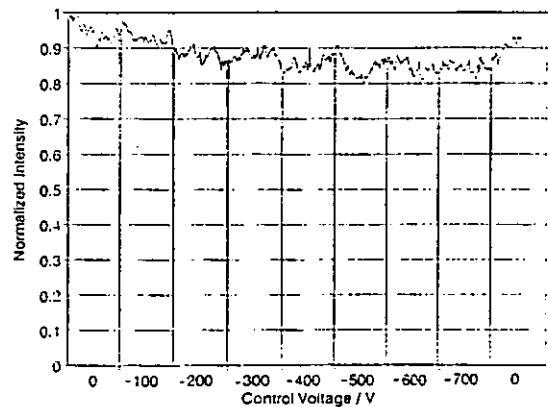


Fig. 12 Normalized pulse energy of the dye laser as a function of the applied voltage (each discrete voltage (0 V, -100 V, ..., -700 V) was held constant for a period of 1 minute during the regions indicated)

piezo-ceramic⁴. Similar indications of hysteresis were observed during the measurements of the grating constant. The energy fluctuations within each region of Fig. 12 are, for the most part, due to fluctuations in the energy and beam quality of the excimer pump laser used.

Applications of the active diffraction grating

The active diffraction grating described here is suitable for very sensitive tuning of laser wavelengths and diffraction angles, suggesting its use in a wide range of applications:

- fine tuning and stabilization of narrow bandwidth lasers (for example, dye and diode lasers), also in connection with coarse tuning (for example, by mechanically turning the piezo grating);
- distance measurements;
- heterodyne measurement techniques;
- two-wavelength contour measurements of large objects;
- differential spectroscopy (for example, DIAL);
- atomic absorption spectroscopy;

- Doppler free spectroscopy;
- optical switches.

Conclusions

An active, diffracting optical element was manufactured and its optical characteristics and function were investigated both theoretically and experimentally. This active diffraction grating was installed in a dye laser and used for precise tuning of the output wavelength. At a wavelength of ca. 600 nm, a wavelength shift of 215 ± 9 pm was recorded for an applied control voltage of -700 V.

References

- 1 Samuels, U., Kreittlow, H., Wild, St., Budzinski, Ch., Tiziani, H.J. Feindurchstimmung von Farbstofflasern mit einem aktiven diffraktiven optischen Element. *1994 Conference of the German Society for Applied Optics (Deutsche Gesellschaft für angewandte Optik, DGaO)*, Berchtesgaden (1994)
- 2 Fenske, G. Steuerbares Beugungsgitter. DD279077 A1 WPG02B/3244294 (1990)
- 3 Mory, S., Fenske, G. *Beitr Opt Quantenel.* 14 (1989) 148
- 4 Data sheets, Marco Systemanalyse und Entwicklung GmbH, Hermsdorf, Germany

AUTOMATED PLANT PROPAGATION BY USE OF IMAGE PROCESSING AND LASER BEAM CUTTING

U. Samuels, M.Phil., Dipl.-Ing., MVDI, MDGaO

Institut für Lasertechnik, Fachhochschule Ostfriesland, Emden, Germany

e-mail: n_samuel@perseus.fho-emden.de

Prof. Dr. H. Kreitlow, Dipl.-Phys., MDPG, MVDI, MDGaO, MEOS, MSPIE

Institut für Lasertechnik Ostfriesland, Fachhochschule Ostfriesland, Emden, Germany

Prof. R.M. Parkin, BSc, PhD, FRSA, CEng, MIEEE, MIEE, FIMechE

Mechanical Engineering Department, Loughborough University of Technology,

Loughborough, England

e-mail: r.m.parkin@lut.ac.uk

ABSTRACT

For many years, tree nurseries use cuttings as a successful method of propagation. Specific parts of plants are cut off from the mother plant and set in a special seed compost. This process requires a high personell effort and must be done under sterilised conditions. In order to avoid plant contamination, which would reduce the output of new plants, all cutting tools must be carefully and continuously sterilised. This process was automated by introducing an image processing system which is capable of finding optimised separation positions for laser cutting. A laser is the best tool to achieve a contamination free and sterile cut off from parts of plants. The necessary automated movement of the plants is controlled by a computer steered handling system. On the one hand the introduction of this technique will drastically reduce personell effort, and on the other hand the process output will be increased and improved, by contactless cutting using a laser beam. This process is not bound to a sterile environment of a laboratory and also the otherwise necessary sterilisation of cutting tools is not relevant. This will improve the economy of plant propagation by cutting decisively.

1 INTRODUCTION

Besides propagation of plants by seeds (generative or sexual propagation), they may also be propagated by planting of leaves, sprouts, roots, or parts of plants (vegetative or asexual propagation) [1]. The plant breeders choice of method depends very much on the characteristics and peculiarities of the plant to be propagated. For the vegetative or asexual propagation, a stock of healthy mother plants is an important requirement. Cuttings from a mother plant will grow up to new and independent replicas of this plant. In tree nurseries, gardeners take the plant to be propagated, cut off the necessary part with a

sterile knife and plant the cuttings in a special seed compost. This process requires a high personell effort, continuous and costly sterilisation of the cutting tools, while the process output is significantly reduced by contamination. For this reason, this method of propagation is only used with superior and expensive plants.

For investgating the sterile and automatic propagation of outdoor rhododendra and outdoor azalea, the system shown in Figure 1 was developed.

A computer-based handling system guides the mother plant into the observation range of the

CCD-camera which transmits the signals to an image processing system consisting of a computer with an image processing card and image processing software. The image evaluation circuitry delivers the coordinates to the handling control system in order to position the previously selected optimal separation spot of the plant exactly under the laser beam. After the cut has been performed by the laser beam, the cutting will be guided to an appropriate-sized pot with seed compost and planted into that pot.

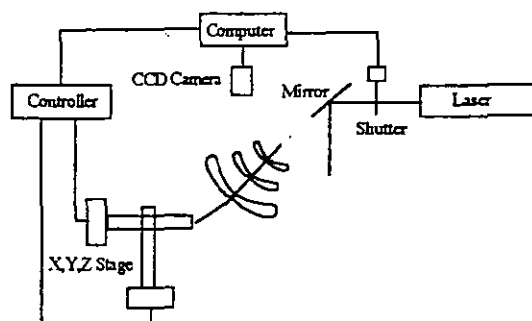


Figure 1: A complete laser cutting system for automatic plant propagation

In the following detailed description of the system developed, first the traditional process of propagation by cuttings will be explained. Then the image processing system with the necessary hardware and software components as well as theoretical and experimental results for the selection of the cutting laser, suitable for special types of plants, will be presented and discussed.

2 TRADITIONAL PROPAGATION

This method is based upon plants ability to reform missing organs under certain conditions, which means parts of sprouts can reform advanced roots. Sprouts of 3 - 8 cm length, called head cuttings, are separated from the mother plant without bruising them using a sterile cutting tool. In order to keep the wound as small as possible, the cuts should be placed perpendicular to the stem [2]. Through this wound, bacterial and viral diseases can attack the cutting caused by a contaminated cutting tool or rooting medium which leads to deterioration.

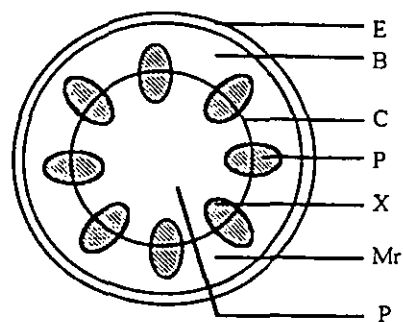


Figure 2: Cross section of a sprout stem

Figure 2 shows the cross section of a sprout stem with the cambrian ring (C) and the conducting bundles with xylem (X) and phloem (P). Between the bundles, one finds the martian rays (Mr) which connect the bark (B) with the pith (P) located in the centre of the stem. The stem is covered by the epidermis (E).

Rooting is a premise for successful growth of plants and can differ for various plants. Outdoor rhododendra starts rooting at the cambrian ring, whereas outdoor azalea starts at the sides through bark and epidermis.

Tree nurseries plant the cuttings in a special prepared rooting medium with a planting depth of 0.5cm under high manual effort. The rooting medium must be capable of holding sufficient moisture, permit free passage of air and be sterile. These conditions are fulfilled by a mixture of peat and coarse sand.

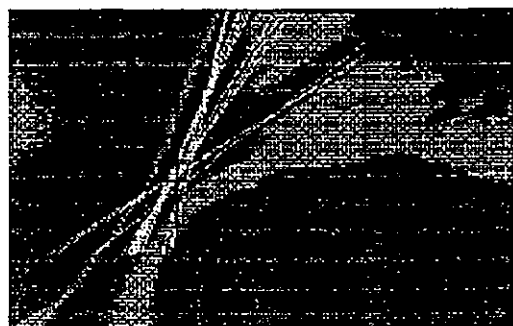
Cuttings tend to exhaust their food reserves until roots are formed. This is due to the fact that because of the ratio between leaf surface and roots, more moisture is exhausted through the leaves than can be absorbed by the roots. Therefore the moisture must be kept at an adequate level. This can be done by covering the cuttings with a PE-sheet or by spraying a moisture film over the leaves. Following sufficient rooting, ventilation and hardening of the cutting may begin.

3 IMAGE PROCESSING UNIT

The hardware of the system consists of a personal computer with an 80486 CPU, an image processing card and a CCD-camera. All image data will be processed by a special image processing algorithm which determines the optimal position of the laser cut. The algorithm is based upon the Hough transformation of the image. Observing the scene in a first approximation, one can find sprout stems of the plant which can be considered to be a straight line. Therefore the problem of recognising the spatially extended pattern of the sprouts can be transferred to the much simpler recognition of a local pattern in the parameter plane of the Hough-transformed image [4].



a)



b)

Figure 3: Photo of the plant and the reverse Hough-transformation

Figure 3a shows an image of the plant, while Figure 3b shows the plant with the intersection point found by the reverse Hough-transformation of Figure 3a.

4 LASER BEAM CUTTING OF PLANTS

In order to perform the cutting, the laser beam must penetrate into the plant and interact with its material. The required beam absorption rate for a given plant material depends on the laser wavelength. Plants have a very complex structure, are very heterogeneous with respect to their composition and are mainly composed of water, cellulose, and pectin [1]. Green parts of the plants, such as leaves, have a very pronounced concentration of chlorophyll. This imparts a very characteristic absorption maximum in the range of blue wavelengths at about 440nm. Because of the high portion of water, there are further high absorption values in the range of UV and IR, but not in the visible range of wavelengths.

Propagation by cuttings for different plants has different requirements to the cut surface. Some plants, such as outdoor rhododendra, will root through the front face of the cut. Thus, charring is not to be permitted. Other plants, such as outdoor azalea, root through the bark and epidermis. These plants can be protected by a charred front face against infection by viruses and bacteria. Therefore, an optimised cutting of special kinds of plants results in the following parameters:

- Laser operation mode
- Wavelength
- Focusing
- Focal position
- Intensity
- Duration of exposure

Table 1: Laser beam parameters for the cutting process

A systematic determination of optimised parameters for the cutting of outdoor rhododendra and azalea on an experimental basis was performed with various laser types having parameters listed in Table 2. The absorption of all laser types was determined by comparing their intensity in front of and behind the plant. These results are also listed in Table 2.

Laser	Wavelength[micron]	Power [W]	Absorption[%]	Quality of the cut
Excimer(Xe-Cl)	0.31	4.9	96	clean cut surface
Ar ⁺	0.49	1.2	81	sooty charring
Nd-YAG	1.06	2.1	60	sooty charring
Tm-YAG	2.01	5.1	90	slightly charring
CO ₂	10.60	1.0	98	sooty charring

Table 2: Parameter and results of investigated lasers

The experimentally determined absorption values of Table 2 approximately fit to the absorption response for *OPUNTIA ACICULATA*, as stated in the literature [5]. There is no significant difference in the absorption response between outdoor rhododendra and azalea.

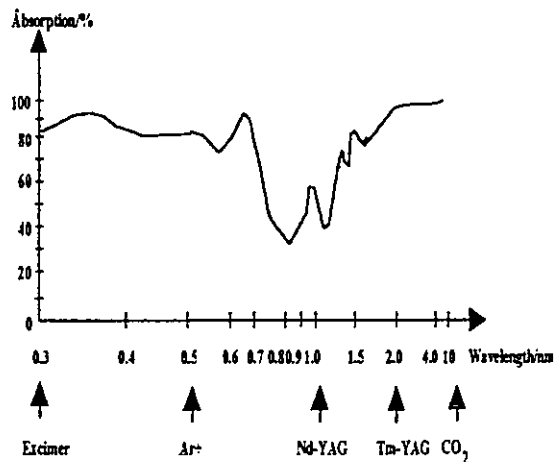


Figure 4: Absorption response of *OPUNTIA ACICULATA* [5]

The wavelengths of the investigated lasers are marked on the horizontal axis of the diagram shown in Figure 4. The absorption response of the Nd-YAG laser beam amounts to 60% and is the lowest value. All other lasers have an absorption response of more than 80%.

The parameters of Table 1 were experimentally optimised for cutting of plants with a stem diameter of 3 mm. The cut surface was visually examined. Those results are also shown in Table 2.

Pulsed lasers produce cut surfaces with no (Tm-YAG) or almost no charring (Excimer with Xe-Cl). This is due to the short pulse duration with high high power density which results in abrupt evaporation of the material. The material removal per pulse may be very small and even after many pulses a sprout stem of 3 mm may not be cut off completely. In order to reach a high quality of cut, good focusing is necessary. Experiments with continuous wave lasers (CO₂, Ar⁺, Nd-YAG) always resulted in burning instead of cutting of the material. Higher power densities result in less charring of cuts.

5 SUMMARY

An automatic plant propagation system for cutting production was described. This system combines an image processing system for computer-aided determination of the cutting points and a laser for contactless cutting of the stems. Compared to the classic method of plant propagation, the intrinsic contactless cutting as well as sealing of the cut surface by charring, results in cutting propagation with less contamination and higher process outputs. System adjustments will make it possible to propagate other plants, as well however, the expensive equipment will make it only profitable for large cutting quantities and/or expensive plants.

REFERENCES

- [1] Mohr, Schopfer, Lehrbuch der Pflanzenphysiologie, Springer Verlag, Berlin
- [2] Sachweh, U., Grundlagen des Gartenbaus, Ulmer Verlag
- [3] Welle, E. F., Kleines Repetitorium der Botanik, Privatdruck
- [4] Zamperoni, P., Methoden der digitalen Bildverarbeitung, Vieweg Verlag, Braunschweig (1989)
- [5] David, M., et al., Spectral properties of Plants, Applied Optics, 1965

COMBINED COMMUNICATION AND NAVIGATION SYSTEM FOR AUTOMATED GUIDED VEHICLES (AGV)

Prof. R.M. Parkin, BSc, PhD, FRSA, CEng, MIEEE, MIEE, FIMechE
Mechanical Engineering Department, Loughborough University of Technology, Loughborough, UK
e-mail: r.m.parkin@lut.ac.uk

J. Miesner, Dipl.-Ing., MVDI
Institut für Lasertechnik Ostfriesland, Fachhochschule Ostfriesland, Emden, Germany
e-mail: miesner@perseus.fho-emden.de

U. Samuels, M.Phil., Dipl.-Ing., MVDI, MDGaO
Mechanical Engineering Department, Loughborough University of Technology, Loughborough, UK
e-mail: n_samuel@perseus.fho-emden.de

ABSTRACT

Driverless transport systems are often used in an industrial environment to manage automatic material handling. For a sophisticated system, an information exchange between the AGVs and their environment for process management is required. To this end a new concept of a combined communication and navigation system will be presented. The basic principle of the concept is that the intelligent part of navigation of the system will be placed within the environment rather than on the vehicles. For this reason the optical device for sending the data from the AGV to the host computer also represents the specific AGVs location and orientation as an active beacon which will be detected and ranged by special sensors situated in the environment. The realisation of the concept leads to a more flexible and efficient AGV system.

1 INTRODUCTION

Flexible production plants need transport systems which execute transportation tasks automatically by taking goods from a loading station and then transferring them to their destination. In this case, it is important to place all components and modules at the correct time and at the correct location with a minimum of transport and handling [1]. The advantages of an optimised materials handling are reduced intermediate storage of the components and modules at the workstations and an efficient utilisation of production machines.

In the past, such, automated guided vehicles, like tractors, unit load carriers or fork lift trucks, have proved a success in fulfilling the requirements in actual practice [2]. A particular disadvantage of those systems is their inflexibility, since they are bound to structural installations such as buried wires, tapers and other guidance devices for finding their correct

path. Automatic guided vehicles which find their path without fixed guiding devices, as mentioned before, are much more flexible [3]. For this reason, an overall system consisting of vehicles and an environment with communication, navigation and auxiliary devices, will be controlled and monitored by a host computer system. In this way, the service of an automated guided vehicle system will be integrated in the production process of a flexible manufacturing plant efficiently.

In this study, the combined communication and navigation system for automated guided vehicles will be introduced. The system is set out under the following premises:

- From the totality of necessary functions and equipment installations which the system always needs for its operation, as few as possible shall be installed in vehicles [Goodhead], because on the one hand the investigation effort proportionally increases

with increasing numbers of vehicles and on the other hand the reliability would be reduced. For this reason, all information concerning position and orientation of all AGVs in operation will be generated from the environment with its sensors and navigational computers and not from measurement systems, such as gyroscope or a receiver for global positioning system signals, which would be situated on the AGVs [4]. An additional advantage of such a system is that computing and data transmission capacities will be saved and specific components on the AGVs will be avoided.

- Radio communication within industrial installations is with respect to data integrity in principle very difficult [5] and also very susceptible. For this reason, the connection between AGVs and environment should be realised using an optical communication system.
- In order to increase reliability, availability, and velocity, the operation of moving parts and the introduction of procedures for digitised image processing should be avoided [4].
- The system should be integrateable with other system components for the detection of obstacles, avoidance of accidents, particularly with persons, or secure handling of loads.
- The AGV system shall be comprised of a fleet of vehicles. For this reason the host computer needs to identify each AGV.
- Sophisticated decision and evaluation algorithms should be used for determining the best AGV of the fleet and the best associated detection combination for its optimal navigation to fulfil a concrete task. This will increase the efficiency and the performance of the system. For this reason all process parameters must exist and managed in the host computer system.

2 TECHNICAL REALISATION

Figure 1 shows the schematic of the combined communication and navigation system. The mobile robot is moving in the industrial environment. Receivers are linked to the host computer which are able to detect signals representing the position, orientation and identity from the AGV.

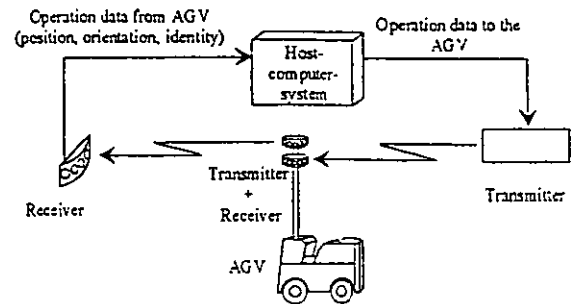


Figure 1: Schematic of a combined communication and navigation system

To this end, the beacon will have two functions [4]. First the beacon representing the AGV position is active, that is, it emits light which will be detected by receivers. For the second function the light is modulated to perform the transmission of the communication link. In the other direction, a transmitter in the environment is controlled by the host computer sending operation data to the AGV.

The computer installed on the AGV and the host computer installed in the environment are connected with the transmitting and receiving units via high performance interfaces.

2.1 Data transmission from host computer to AGV

The implementation of the communication system from the host computer to the AGV is shown in Figure 2.

The beam of a semiconductor laser which is mounted above the working area of the AGV follows the actual position of the AGV by use of a mirror mounted on a galvanometer driven cardanic mirror holder. The axes of the mirror holder are controlled in a closed-loop system.

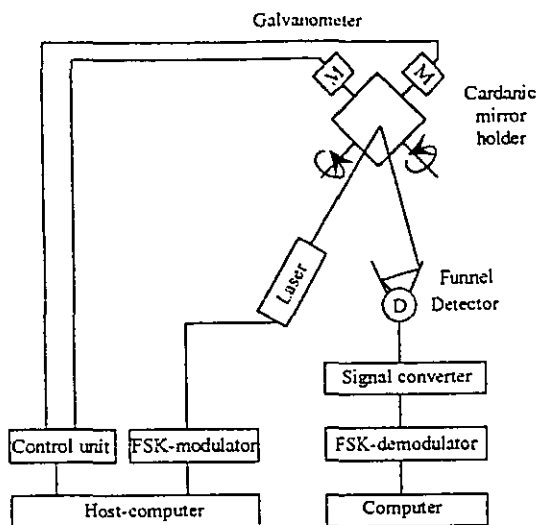


Figure 2: Data transmission system from host computer to AGV

The information is transferred by the laser with a simple laser intensity modulation as a result of current modulation. For data integrity purposes, the procedure of frequency-shift-keying (FSK) is used, whereby the binary signals are represented by different frequencies of the sinusoidal laser intensity modulation [6]. At the detector the laser beam is channelled to a linear working photodetector using a funnel (see Figure 2). Then the output signal is converted and amplified by an electronic system. After this, an FSK demodulator circuit transfers the signals of discrete frequencies into corresponding voltage levels which are passed onto the host computer. As a result of the relatively high transmission rates, the simple laser intensity modulation, and the simple signal detection and conversion by use of FSK, this is a very reliable system [6]. The disadvantage is the use of moving components for beam steering which, however, has to be accepted because of the required high signal directionality and the lack of alternatives for large angle beam deflection.

2.2 Data transmission from AGV to host computer

The system for data transmission from the AGV to the host computer is shown in Figure 3. The binary computer signals are processed by a FSK-modulator and passed on to a transmitting unit. This unit consists of circularly mounted LEDs whose cone of emitted

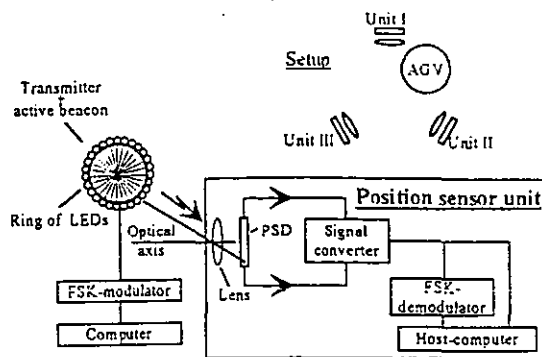


Figure 3: Data transmission system from AGV to host computer

light is horizontally directed by faceted cylinder lenses. This unit is mounted on top of the AGV and permits signal propagation in all directions horizontally. For the evaluation of the transmitted signals, three detector and evaluation units are installed for example in the environment in a systematic manner as shown in Figure 3 as well. These detectors are position sensitive detectors (PSD) [6] in combination with a lens were chosen. The lens images the beacon onto the PSD surface. With a moving AGV, the spot also changes its position on the PSD and, therefore, the PSD-signal represents a measure of the actual AGV position. The LEDs of the transmitting unit are modulated in their intensity with respect to the FSK-control and, therefore, also the PSD-signal is modulated with this digital information. Through inverse conversion of the PSD output signals by an FSK-demodulator, the host computer has not only access to the position signals of the AGV, but also to the operation data. In order to determine the AGV orientation it is assumed at the beginning of the operation that the position of the AGV is known and the position changes only due to AGV-actions following control commands. The transmission of the orientation is, therefore, only necessary when unforeseen and unwanted displacements have taken place. For this reason, a permanent measurement system, such as gyroscope or global positioning system (GPS), can be replaced by direct called test routines which determine the AGV orientation. For this, the single LEDs of the

transmitting unit will be controlled in consecutive order. Through synchronisation of the start and determination of the run-time until the LED in opposition to the detector is radiating, the measured time difference is a function of the actual orientation of the AGV. In a known industrial environment, this off-line orientation should be necessary only in very few instances.

3 SUMMARY

In this study a new optically based combined communication and navigation system for free automated guided vehicle transport systems was introduced. Ideal system requirements were formulated and a set-up, based on these requirements was suggested through which position and orientation of the AGV exclusively will be determined by system components installed within the environment. This new set-up reduces the coordinating data flow between the AGV and host computer and also the system effort necessary for controlling large AGV fleets.

REFERENCES

- [1] Groover, M.P. Automation, Production Systems and Computer Integrated Manufacturing, Prentice Hall Inc.,
- [2] Waltken, U., *Experience with a large AGV System in a distribution plant*, Proc. of an Executive Briefing on Automated Guided Vehicles, Nov. 6. - 7. 1986, Stratford - upon - Avon
- [3] Baptiste, P., Bideaux, E., Harwood, D., *Design and operation of multiple trackless automatically guided vehicle*, IEE, Innovations in Manufacturing Control Through Mechatronics, Newport, Gwent, 22. Nov. 1995
- [4] Miesner, J., *Navigational Systems for Automated Guided Vehicles*, Final year project at Leicester Polytechnic, Leicester, UK, 1990
- [5] McGillem, C.D., Callison, J.D., Rappaport, T.S., *Autonomous roving vehicles navigation, control and communication*, Proc. 6th Int. Conf. on Automated Guided Vehicle Systems, Nov. 25. - 26. 1986, Brussels, Belgium
- [6] Samuels, U., *Laser Communication System for Mobile Robots*, Final year project at De Montford University, Leicester, UK, 1993

OPTIMISED AUTOFOCUS SENSOR FOR FLEXIBLE DISTANCE AND PROFILE MEASUREMENT WITHOUT MOVING SENSOR PARTS

U. Samuels, M.Phil., Dipl.-Ing., MVDI, MDGaO
Mechanical Engineering Department, Loughborough University of Technology,
Loughborough, England
e-mail: n_samuel@perseus.fho-emden.de

Prof. R.M. Parkin, BSc, PhD, FRSA, CEng, MIEEE, MIEE, FIMechE
Mechanical Engineering Department, Loughborough University of Technology,
Loughborough, England
e-mail: r.m.parkin@lut.ac.uk

Prof. Dr. H. Kreitlow, Dipl.-Phys., MDPG, MVDI, MDGaO, MEOS, MSPIE
Institut für Lasertechnik Ostfriesland, Fachhochschule Ostfriesland, Emden, Germany

ABSTRACT

In modern production and inspection processes a very precise distance measurement is required in many applications. The tolerances in these working areas are narrowing and therefore require much more correct measuring procedures in course of which higher requirements are made in the fields of measurement characteristics, particularly with respect to their dynamic characteristics. This study is introducing an optimised autofocus sensor with an modified sensor configuration which can be adjusted to fulfil different applications with excellent dynamic characteristics. These characteristics of the sensor will be proved in representative applications. Because of its low instrumental effort a new, flexible, and profitable distance measuring system using a modified autofocus sensor is available.

1 INTRODUCTION

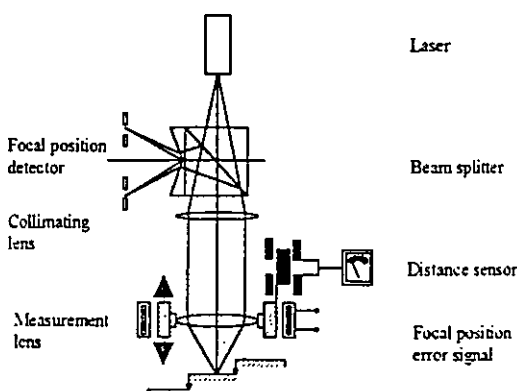


Figure 1: Autofocus sensor

The class of one-dimensional measuring optical distance sensors has captured new application fields in today's engineering,

particularly by its contactless measuring procedure useable on very sensitive and moving components. The autofocus sensor which measurement technique is based on the principle of a CD record player, is one of the well known representatives of this sensor class. Figure 1 shows a typical setup of an autofocus sensor [1,2,3,4] which operates on the principle of dynamic focussing. The beam of the measuring laser is collimated by the first lens and focused on the surface to be measured by the measurement lens. The reflected part of the measuring beam passes through the measurement lens in opposite direction and is decoupled from the main path by use of a beam splitter. After the beam splitting, done by two prism components fixed to the beam splitter, photodetectors are measuring the intensity of both parts of the beam. By means of mechanical autotracking of the measurement lens the focal position will be

kept dynamically on the measuring surface in order to enable both photodetectors to deliver the same signal. An asymmetric photodetector illumination causes the sensor to displace the measurement lens. Distance measurement will be achieved by determining the displacement of the measurement lens using a secondary sensor. This measuring principle will result in following disadvantageous measurement characteristics:

- in using moving parts the dynamic range is kept relatively small
- the secondary measurement system requires an additional effort in instrumentation

Thus the development of a modified autofocus system with a well aimed optimisation in measuring range and resolution and for use in different applications was mathematically modelled. After theoretical considerations, using raytracing simulation and experimental determination of the measurement characteristics, two representative applications will be shown.

2 SENSOR CONFIGURATION

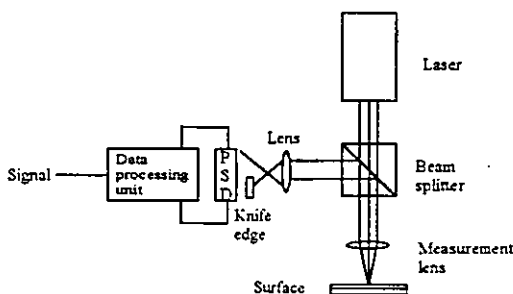


Figure 2: Modified autofocus sensor

Figure 2 shows the setup of the modified autofocus sensor [5]. As elucidated in the previous sensor principle, the parallel measuring beam of a laser is passing through the measurement lens and is focused on the surface. The reflected light from the surface to be measured passes the measurement lens in opposite direction and is then diverted from the main beam by a beam splitter. Instead of splitting, as shown in the example of Figure 1, the beam is manipulated by another sensor lens and a knife edge inserted in beam path and is

detected by a position sensitive detector (PSD), which passes its resulting signals to an analysing unit.

Half of the beam is blocked by the knife edge. In that way only a semicircle can be monitored in the detector plane. This semicircle is changing its size depending on the measured value ΔZ which, in turn, results from the distance between the surface and the focal position. The PSD is detecting this change in size. In response to the illumination with a real spot of the size H and the position of the spot on the PSD-surface, described by the distances A and B or the reduced distances A' and B' , the PSD is generating the characteristic currents I_A and I_B which are shaped to an output signal S by the data processing circuitry (see Figure 3).

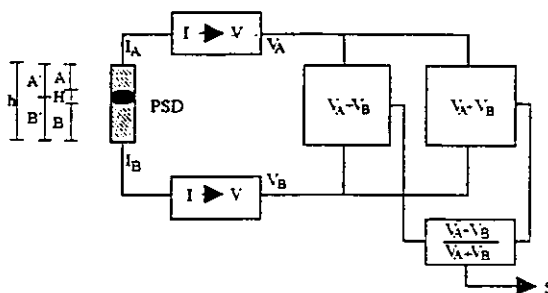


Figure 3: Illumination with a real light spot on the PSD with the signal evaluation circuitry

In case of the illumination, shown in Figure 3, the following analytical expression is given for the output signal S resulting from the electronic signal processing:

$$S_{(A,h,H)} = \frac{I_A - I_B}{I_A + I_B} = \frac{h - 2A}{h - H} \tag{1}$$

- I_A : 1. output current of the PSD
- I_B : 2. output current of the PSD
- h : Length of the PSD
- A : 1. coordinate of the spot on PSD
- A' : 1. reduced coordinate of the spot on PSD
- B : 2. coordinate of the spot on PSD
- B' : 2. reduced coordinate of the spot on PSD
- H : Spot diameter

3 MATHEMATICAL SENSOR MODELLING

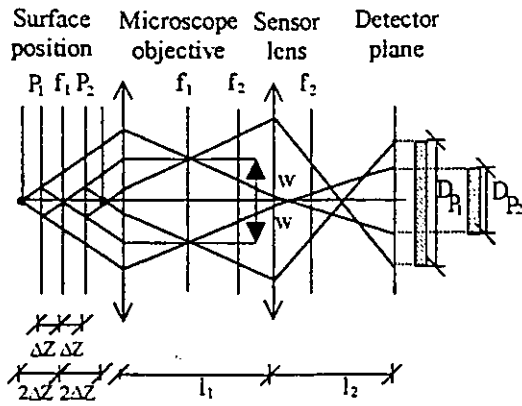


Figure 4: Beam path of the sensor

Figure 4 shows the beam path constructed under the laws of geometric optic. The parallel measuring beam of the radius w is passing through the microscope objective which the focal length f_1 and hits the surface under measurement located in a distance ΔZ to the focal plane of the microscope objective. The light reflected from the surface passes the microscope objective in opposite direction and is focused by the sensor lens which has a distance l_1 to the microscope objective and a focal length f_2 . This results in a spot of diameter D in the detector plane located in a distance l_2 to the sensor lens. The diameter of this spot can be calculated by the following equation:

$$D = D_0 + K\Delta Z \tag{2}$$

with the initial diameter

$$D_0 = 2w \frac{(l_2 - f_2)}{f_2} \tag{3}$$

and the sensibility constant

$$K = 4w \frac{(f_1 l_2 - f_1 f_2 - l_1 l_2 + l_1 f_2 - l_2 f_2)}{f_1^2 f_2} \tag{4}$$

with:

- w : Radius of the measuring beam
- f_1 : Focal length of the microscope objective
- f_2 : Focal length of the sensor lens

- l_1 : Distance between microscope objective and sensor lens
- l_2 : Distance between sensor lens and detector plane

Equation (2) shows that the diameter D is composed of the initial diameter D_0 and a term $K\Delta Z$ which is linearly dependent on the measured distance. Considering equation (3) it is proven that the initial diameter D_0 depends only on the ratio of the focal length f_2 of the sensor lens and the distance l_2 between sensor lens and detector plane. Equation (4) shows the linear relationship between sensibility constant k and the distances l_1 and l_2 and the non-linear relationship between k and the focal length f_1 and f_2 .

Using the relations described in equation (1) to (4) the adaption of the sensors measuring range and resolution to different applications will be possible. The case where the sensitivity constant k has the value zero ($k = 0$) has to be prevented, because in this case the sensor will not work. With an increasing sensitivity constant k , the sensitivity increases but the measuring range reduces, and vice-versa. This sensor modelling, derived from the laws of geometric optics is only valid for lenses with infinite diameter.

4 TESTING THE SENSOR LINEARITY BY RAYTRACING SIMULATION

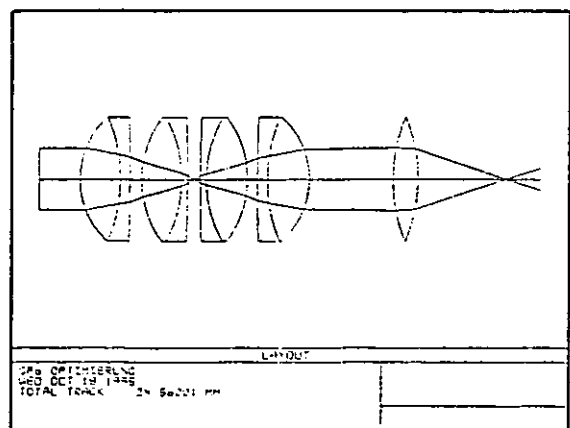


Figure 5: Raytracing model of the autofocus sensor

Figure 5 shows the autofocus sensor without knife edge which is reproduced by raytracing. The incident laser beam coming from the left is passing through and focused by a microscope objective with the focal length f_1 based on two doublets. Instead of a beam reflection from the surface at the distance ΔZ and instead of passing the same microscope objective in the reversed direction for the raytracing simulation the beam passes a second microscope objective in the reversed orientation which is located in a distance $2 \cdot \Delta Z$ (forward configuration).

This construction is including also a sensor lens with a focal length f_2 and located in a distance l_1 which focuses the laser beam and causes the reproduction of a spot with a diameter D in the detector plane located in a distance l_2 . This raytracing model allows the determination of the spot diameter for different setups to be monitored by observing the spot diagram in the output plane.

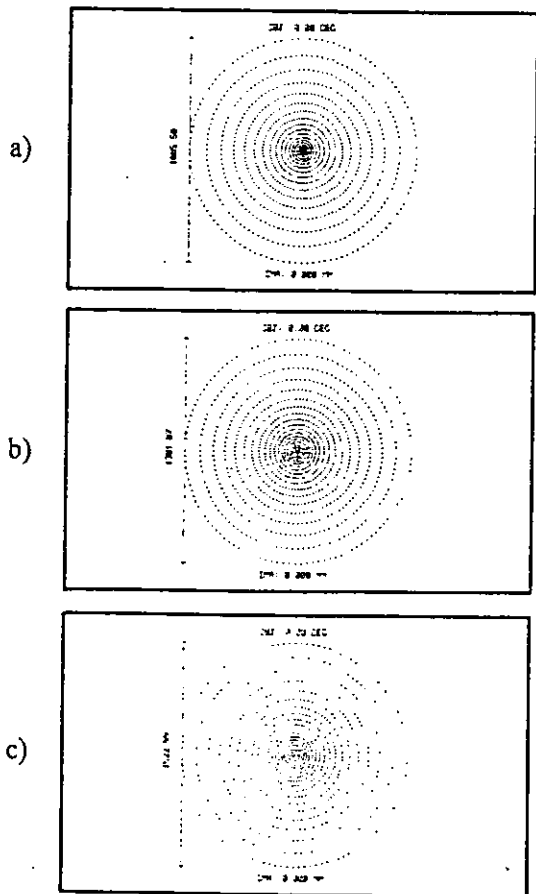


Figure 6: Spot diagram for three different measuring values

Figure 6 shows three representative spot diagrams for different distances. For $\Delta Z = -100 \mu\text{m}$ (see Figure 6a) the diameter D has a value $D = 1085 \mu\text{m}$, for $\Delta Z = 0 \mu\text{m}$ (see Figure 6b) a value $D = 1302 \mu\text{m}$, and for $\Delta Z = +100 \mu\text{m}$ (see Figure 6c) a value $D = 1522 \mu\text{m}$. This demonstrated that the changes in diameter depends almost linear on the changes of the measured distances and conform the predictions of the mathematical sensor model.

5 PSD ADJUSTMENT

The distance l_2 defines the detector plane with respect to the sensor lens. A detector has to detect the illumination spot in this plane or as a result of the knife edge the semicircle of this spot, respectively. The PSD, being the detector, is placed in a perpendicular position to the optical axis which leads to the illumination as sketched in Figure 3 and to the signal represented by equation (1).

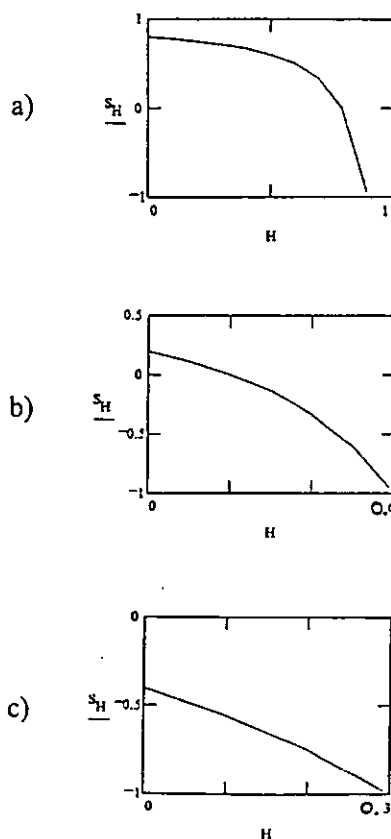


Figure 7: PSD output signal for three different PSD adjustments

A mathematical model of the measuring signal described by equation (1) can be used to optimise the measuring signal with respect to linearity and amplitude by introducing different PSD positions described by the distance B and keeping the changes of the spot radius in a linear range.

For this simulation the length of the PSD is normalised to 1 and for each curve value B is different. Figure 7 illustrates three different signal curves simulated in the described manner.

As shown in Figure 7a, the PSD is positioned off-axis at $B = 0.1h$, in Figure 7b at $B = 0.4h$, and in Figure 7c at $B = 0.7h$. In Figure 7a it can be seen that the curve has a large amplitude and is strongly non-linear. In Figure 7c the linearity is good but the signal amplitude is relatively small. Figure 7b shows an acceptable compromise between linearity and amplitude, so that can be used for the sensor adjustment.

6 EXPERIMENTAL SENSOR TESTING

For the experimental testing of the sensor a setup with the parameters of Table 1 was used. A positioning system was used for defined and accurate object movements of four different surfaces as there were cardboard, photo resist, copper, and mirror.

Microscope objective (Spindler&Hoyer)	
Focal length f_1	2.93mm
Numerical aperture NA	0.85
Entrance aperture	5mm
Sensor lens	
Focal length f_2	20mm
Type	singlet
Setup, geometry, distances	
Microscope objective- sensor lens	70mm
Sensor lens-knife edge	40mm
Knife edge-PSD	25mm
Adjustable parameter	
Beam diameter is adjustable by a variable aperture	3mm, 4mm 5mm, 6mm

Table 1: Sensor characteristics

In Figure 8, the sensor voltages as a function of the measured distances are shown in the four coordinate systems. They correspond to four different laser beam radii of 1.5mm in Figure 8a, 2mm in Figure 8b, 2.5mm in Figure 8c, and 3mm in Figure 8d. Each of these sensor configurations was examined with the four different measured surfaces. It can be seen that, within the measured range, almost all characteristic curves have portions with an excellent linearity. Only the resist surface measured with a beam diameter of 1.5mm has no reproducible characteristics. The measuring sensitivity described by the signal slope depends on the parameters of the measured surface so that a certain homogeneous surface is needed for a successful sensor operation. Furthermore, before starting the operation of the sensor it needs to be calibrated with respect to the surface to be measured. Using different sensor adjustments a maximum linear measuring range of 100µm and a maximum resolution of 200nm was determined.

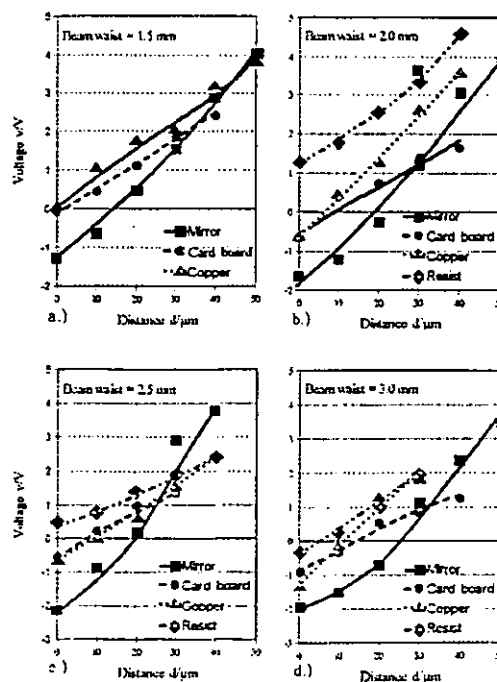


Figure 8: Measured curves of the sensor

7 APPLICATIONS

In order to demonstrate the operational characteristics of the sensor, it was coupled with a precision rotation axis. The sensor measures the distance to the rotation axis. In the first application the sensor was optimised due to high measuring resolution for measurement at low rotation speed. In this way it can be used to examine surfaces and roundness characteristics of the axis. Figure 9 shows a roundness curve measured this way. Using a measurement resolution of $112\text{mV}/\mu\text{m}$ a voltage of 0.53V represents a roughness depth $R_t = 4.73\mu\text{m}$.

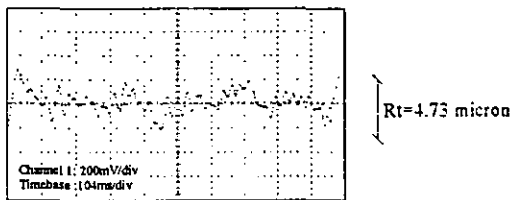
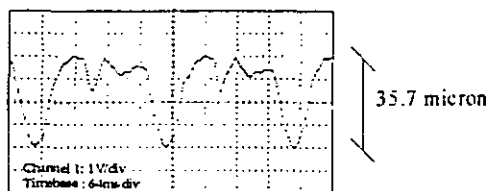
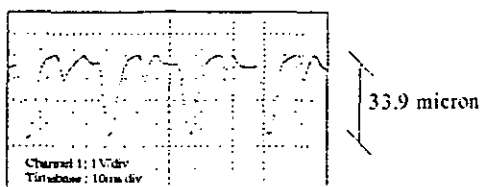


Figure 9: Roundness characteristics of a rotation axis

In the second application the sensor signal was additionally lowpass filtered to ensure that only signal portions with a maximum frequency, which is ten times the rotation frequency, can be monitored. In this manner the dynamic characteristics of the system are used to examine the true running characteristics of the axis in the range of high rotational speeds.



a)



b)

Figure 10: True running measurement

Figure 10 shows two measured curves for two different rotational speeds. Applying a rotational speed of 240rpm for the measurement sensitivity mentioned above the curve in Figure 10a shows a movement of the axis of $35.7\mu\text{m}$. Applying a rotational speed of 2400rpm the curve in Figure 10b shows a movement of the axis of $33.9\mu\text{m}$. The measurement reproducibility is illustrated by the periodicity of the signals in Figure 10.

8 SUMMARY

A modified autofocus sensor was developed which can operate in several measurement and resolution ranges to meet the requirements of various applications. This can be done with the aid of a mathematical sensor model. The linear measurement characteristics and the excellent dynamic range - gained by avoiding moving sensor parts - as well as the applicability for a wide range of surfaces are further advantages of the system. Compared to other autofocus sensors this one has the additional advantage of a relatively small investment costs.

REFERENCES

- [1] Brodmann, R., Messen in CD-Qualität, Laser 3/1989
- [2] Breitmeier, U., Lasermesstechnik zur Oberflächen-Qualitätskontrolle, Laser und Optoelektronik, 2/1992
- [3] Tönshoff, H.K., Heekenjann, P.B., Overmeyer, L., Autofocus sensor for micromachining, Laser und Optoelektronik, 25(6), 1993
- [4] Overmeyer, L., Dickmann, K., Dynamischer Autofokussensor zur dreidimensionalen Mikrostrukturerfassung, tm Technisches Messen 59/1992
- [5] Samuels, U., Focal position controlled processing haed for a laser pattern generator for flexible microstructuring, MPhil Thesis, Loughborough University of Technology, 1996

LASER PATTERN GENERATOR (LPG) FOR FLEXIBLE MICROSTRUCTURING

U. Samuels, M.Phil., Dipl.-Ing., MVDI, MDGaO

Mechanical Engineering Department, Loughborough University of Technology,
Loughborough, England

e-mail: n_samuel@perseus.fho-emden.de

Prof. R.M. Parkin, BSc, PhD, FRSA, CEng, MIEEE, MIEE, FIMechE

Mechanical Engineering Department, Loughborough University of Technology,
Loughborough, England

e-mail: r.m.parkin@lut.ac.uk

Prof. Dr. H. Kreitlow, Dipl.-Phys., MDPG, MVDI, MDGaO, MEOS, MSPIE

Institut für Lasertechnik Ostfriesland, Fachhochschule Ostfriesland, Emden, Germany

ABSTRACT

The microstructuring technology deals with the manufacturing of technical components in the (sub)micron range in the fields of electronics, optics, and mechanics. In the first production step the required substrate will be covered with a radiant sensitive resist and then exposed using serial writer like an electron beam - or a laser beam writer. In the second production step this resist structure will be transferred onto the real component using a different production technique like ion beam etching. This study will introduce a laser beam writer, which can be used for the generation of structures in the submicron range. The manufacturing results demonstrate the feasibility of the profitable manufacturing of binary, multi-level, and continuous structures at a relatively low cost.

1 INTRODUCTION

The resist structuring as a first processing step is common to all tasks of microstructuring. The substrate (e.g. silicon or silica glass) will be coated with a radiation sensitive layer - called resist - and exposed to a locally pointed focussed corpuscular or laser beam. After a subsequent photochemical development the required structure can be found on the resist. A further processing step - called batch processing - will transfer the structure to the surface of the substrate which represents the final component. In this manner one can produce binary, multi-level or continuous structures which can be reproduced in high quantities and profitable using copying or replicating operations like mask projection or microgalvanic shaping treatment. Electron beam writers are the suitable serial writers mainly used to do the structuring in the sub-micron range [1]. Basic disadvantages of this

process are the relatively high equipment expenditure on the one hand and the relatively high processing effort in the writing process (e.g. vacuum chamber) on the other hand.

An alternative to this equipment which is in close relation to a raster electron microscope, the development entered into the optional construction of laser beam writers which either use deflection mirrors in guiding the focused laser beam over the substrate to be exposed (laser beam scanner) [2] or guide the resist layered substrate relative to the focused laser beam in using a positioning system (laser beam writer) [3]. Comparing both laser exposing systems it can be proved that the laser beam writer, equipped with almost identical effort in hardware technology, because of its principal applicability in using focusing optics with short focal distances leads to smaller structures [4]. In this study the developed sub-systems of the laser beam

writer will be examined and its applicability will be demonstrated by presenting various microstructures.

2 LASER PATTERN GENERATOR

Figure 1 shows the principle set-up of the Laser Pattern Generator.

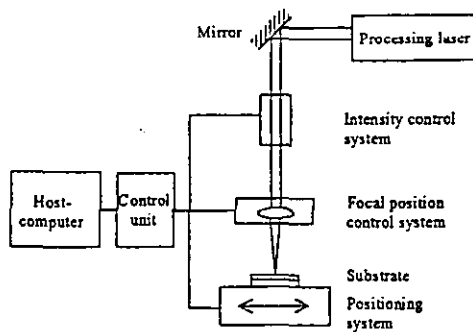


Figure 1: Principle set-up of the Laser Pattern Generator

The beam of the He-Cd processing laser passes through a closed-loop intensity control system and is focused to the surface of the substrate in using an exposure unit head. During the exposure process the intensity of the laser as well as the focal position will be controlled by closed-loop control systems. The movement of the substrate necessary for the structuring will be done by a positioning system of high-resolution. The total process will be controlled by an host computer in combination with an electronic control unit. In this chapter subsystems of the total system will be represented.

2.1 Beam path of the exposure laser

The exposure laser is a He-Cd laser operating in Gaussian mode with a wavelength of $\lambda = 441.6\text{nm}$ which lies within the sensitive wavelength range of the photo resist.

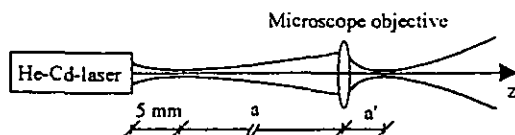


Figure 2: Beam path of the exposure laser

The beam focusing is performed by a microscope objective with a relatively short focal distance of $f = 2.9\text{mm}$. This leads to the optical system shows in Figure 2.

Following the laws of Gaussian beam transformation, equation (1) determines the radius w_o' of the beam in the working area

$$w_o' = \frac{f \cdot w_o}{\sqrt{(a-f)^2 + Z_r^2}} \quad (1)$$

and

$$Z_r = \frac{\pi \cdot w_o^2}{\lambda} \quad (2)$$

with:

- w_o : Beam radius at the waist before focusing
- w_o' : Beam radius at the waist after focusing
- f : Focal distance of the focusing lens
- a : Distance of the input beam at the waist to the focusing lens
- λ : Wavelength of the laser beam
- Z_r : Rayleigh length

The Rayleigh length Z_r is the length over which the beam cross-section is doubled. Therefore, the Rayleigh length describes the divergence of the beam.

According to the construction geometry shown in Figure 2 and introducing $a = 1\text{m}$ and $w_o = 0.5\text{mm}$ equation (1) will yield a focal point radius of $w_o' = 0.7\mu\text{m}$. With this value equation (2) will deliver a Rayleigh length of $Z_r = 3.5\mu\text{m}$.

2.2 Focal position closed-loop control system

Due to the short Rayleigh length Z_r the focal position must be controlled during the exposure process in order to establish a correct exposure result. In doing this an accuracy of half of the Rayleigh length Z_r is aimed for [4]. Controlling the focal positioning can be established with the closed-loop control system shown in Figure 3.

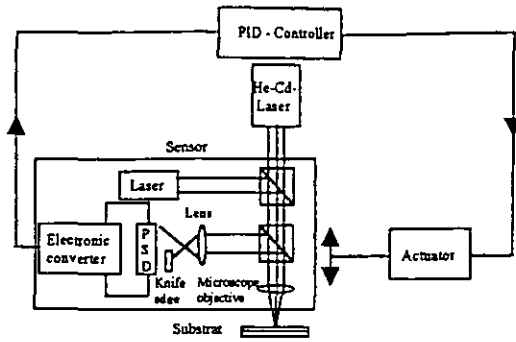


Figure 3: Closed-loop control system for the focal positioning

The microscope objective used for beam focusing is coupled to a distance measuring system and to put it into the correct position it is mounted on an actuator (piezo translator). The actual distance between the microscope objective and the surface of the substrate will be registered in using a modified auto focusing principle. This will be done by overlaying the exposure beam with a second beam from a semiconductor laser that is focused on the surface by the same microscope objective. The reflection of the measuring laser will be decoupled from the main beam using a beam splitter cube, then manipulated with a lens and knife edge (Foucault's cutting principle) and then transformed to a distance signal using a PSD in conjunction with an electronic transformation unit. Figure 4 shows the resulting characteristic curve of the focal position adjustment and measurement system.

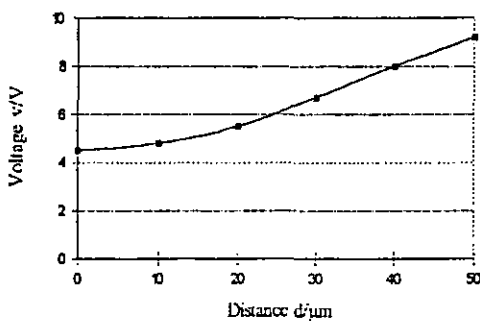


Figure 4: Characteristic curve of the focal position adjustment and measurement system

The characteristic curve in Figure 4 shows the sensor signal as a function of the distance between the measured surface and the microscope objective. The displacement is

realised by the electronic control of the piezo translator.

The linear portion of the characteristic curve is between $20\mu\text{m}$ and $50\mu\text{m}$ where the measurement resolution is better than 500nm despite the presence of signal noise. The piezo translator has a positioning dynamics which limits the dynamics of the system and in the course of which the piezo driver electronics limits the cut-off frequency of the piezo translator to 50Hz . The controlling is realised by a digital software controller housed in the LPG host computer, operating within the linear portion of the characteristic curve. The response of the closed-loop control system to a step of the set point is shown in Figure 5.

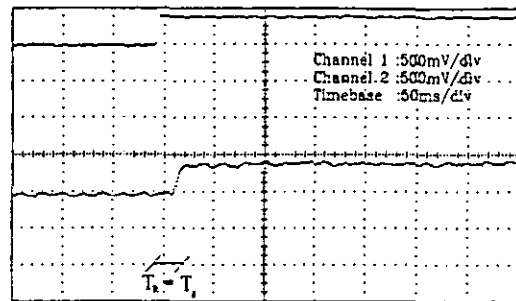


Figure 5: Response of the closed-loop system to a step of the set point

The upper part of the Figure 5 shows the step of the set point and in the lower part the resulting reaction of the controlled parameter is shown. It can be seen that the settling time T_g equals the rise time $T_R = 30\text{ms}$. The control accuracy is $\pm 1.5\mu\text{m}$ and therefore better than half of the Rayleigh length Z_r .

2.3 Exposure beam intensity closed-loop system

The monitoring of the correct irradiance during the exposure process is realised by a closed-loop system shown in Figure 6. An acousto-optic modulator (AOM or Bragg-Cell) with a bandwidth of 20MHz is manipulating the intensity digitally and analogously. This is done using the first diffraction order for the exposure while all other diffraction orders are blocked by an iris aperture positioned in the beam path.

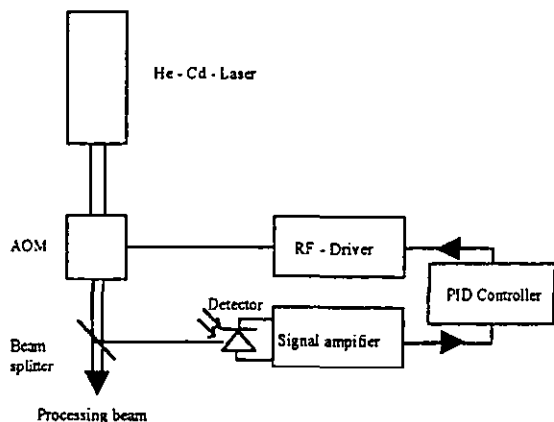


Figure 6: Closed-loop system for intensity control

The intensity of this diffraction order is monitored by a PIN-photodetector with signal amplifier whose response signal is a linear function of the laser intensity. Figure 7 shows the characteristic curve of the intensity adjustment and measurement system.

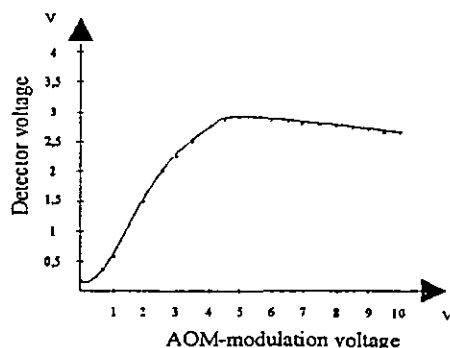


Figure 7: Characteristic curve of the intensity adjustment and measurement system

The curve shows the detector output voltage as a function of the analogous AOM-modulation voltage. Within the range from 1V to 3V of the modulation voltage the detector output has a pronounced linear response. This corresponds to an intensity modulation within a range of 5mW to 25mW, taking into account that the measurement resolution is limited by signal noise and is better than 80µW. The response time of the photodetector limits the dynamics of the system described by the cut-off frequency of 4kHz of the photodetector. The controlling is realised by putting another

digital software controller in the LPG host computer, operating within the linear portion of the characteristic curve. The response of the closed-loop system to a step of the set point is shown in Figure 8.

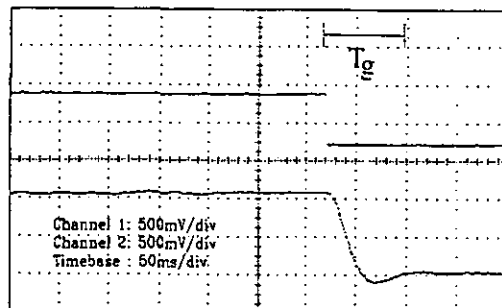


Figure 8: Response of the closed-loop system to a step of the set point

The upper part of Figure 8 shows the step of the set point while the lower part shows the output of the closed-loop system as a reaction to the step of the set point. It can be seen that the settling time equals $T_g = 80ms$. The controlling accuracy of the system is around $\pm 200\mu W$.

2.4 Positioning unit

In order to position the substrate a positioning system based on two crossing linear axes in combination with a rotation axis normal to this plane. This is advantageous in giving details of movements in both controlling the two linear axes using cartesian coordinates and combining a linear and a rotation stage using polar coordinates. The rotation axis enables a rotation of the substrate with a high rotation accuracy and an angular resolution of 1/1000°. The linear axes enable movements within a control range of 1" and a step resolution of 25nm. The monitoring of the actions of the linear axes is implemented using laser interferometers having a resolution of 16nm and being connected to a host computer using fibre optical links. In order to synchronise the positioning of the substrate with switch-on and switch-off of the laser a so-called Direct-Axis-Interface (DAI) being part of the positioning system and delivering TTL-Pulses with a positioning accuracy of 250nm is used. These pulses are used to determine the correct laser turn-on and turn-off points while the

probe is moving along the linear axes. This enables the switch-on of the laser after a certain number of pulses in order to prevent an exposure of the probe during the acceleration phase of the stages. According to the same principle the laser can be switched-off in order to prevent an exposure during the deceleration phase so that a homogenous exposure during the movement of the substrate can be realised.

2.5 Control unit

The coordination of all LPG-actions is established through a PC-80386 host computer with different I/O interface modules. One I/O interface module establishes the connections of the closed-loop systems for intensity control and focal positioning through A/D and D/A channels. Another I/O interface module is registering through 24 bit counting inputs the signals of the interferometers which are of quadrature nature. A serial RS-232 port is being used to address the controller of the three-axis-positioning system. Furthermore a 48 bit TTL -output signal card is programming the evaluation circuit of the Direct-Axis-Interface.

The information representation and user intervention for LPG set-up and during the exposure process is realised through a control desk where all process parameters can be controlled and adjusted. This control desk establishes the connection between host computer and all other components of LPG and consists of 23 printed circuit boards which are connected through a bus system. These cards enable different operating voltages, as well as signal amplification, - filtering, and - shaping. A counting card is registering signals from the Direct-Axis-Interface, and in order to switch-on and -off the laser is comparing those signals with two counter presets. In order to establish a very efficient processing the software of the host computer continuously controls all actions of the control desk and its integrated circuitry.

2.6 Process parameters of the system

For the exposure using the LPG the following parameters can be used:

- Exposure energy
- Focal position

Having the correct focal positioning and considering a static exposure condition of the substrate (the substrate is not moving), the exposure is controlled by switch-on with a predetermined duration and intensity. Considering the dynamic condition (the substrate is being exposed while moving), the exposure intensity is controlled in defining the moving velocity in dependence of the laser intensity. The necessary parameters for laser intensity, focal-, and substrate positioning have to be introduced into the host computer using a macro-editor. In order to meet the required exposure these parameter have to be optimised in an experimental manner.

3 MANUFACTURE OF SELECTED MICROSTRUCTURES

Demonstrating the capabilities of LPG microstructuring Figure 9 shows three different micro lenses.

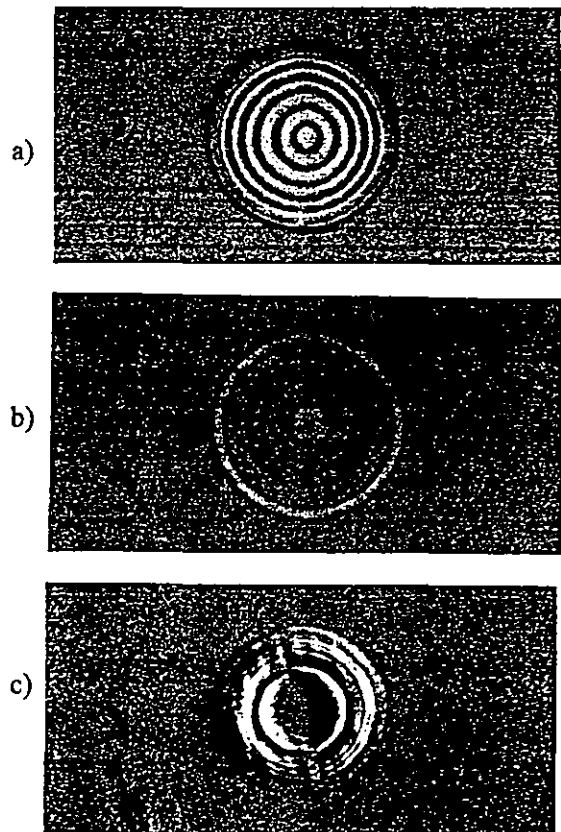


Figure 9: Manufactured micro lenses
 a: binary profile;
 b: multi-level profile;
 c: continuous profile

The structures shown in Figure 9 were manufactured using a combination of numerous discrete exposures with the same distance to each other while the substrate was not moving (static exposure). The smallest resulting structures have a diameter of $0.5\mu\text{m}$. During the total writing process the focal position was directly positioned on the surface. For highest precision the rotation of the substrate was established interpolating the circular movement on the linear axes.

Figure 9a shows a binary micro lens with exposed zones established by numerous discrete exposures leading to a closed ring structure with an outside diameter of $200\mu\text{m}$. The intensity of all exposures had the same value.

Figure 9b shows a multi-level structure generated by selecting different exposure times for zones of different depths. This led to a complete resist removal in two zones and a zone between showing a profile with three steps with an outside diameter of $200\mu\text{m}$.

The continuous structure shown in Figure 9c was manufactured by varying the exposure time for numerous discrete exposures. Exposure time being a function of the radius creates an analogous profile with an outside diameter of $80\mu\text{m}$.

4 SUMMARY

The development of a Laser Pattern Generator for surface microstructuring was described. Systematic examination and optimisation of all system components controlling automatically the intensity of the exposure beam, the focal positioning of the exposure laser and substrate movement as well as the synchronisation of all actions using an host computer and a control desk results in a highly efficient exposure system for binary, multi-level and continuous structures which was demonstrated by the manufacturing examples of three micro lenses.

REFERENCES

- [1] Menz, W., Bley, P., *Mikrosystemtechnik für Ingenieure*, VCH Verlag, Weinheim, 1993
- [2] Jäger, E., et. al., Design of a laser scanner for kinoform fabrication, *Proc. SPIE*, vol. 1136, pp. 228-235, 1989
- [3] Haselbeck, S., et. al., Synthetic phase holograms written by laser lithography, *Proc. SPIE*, vol. 1718, pp. 117-128, 1992
- [4] Samuels, U., Focal position controlled processing head for a laser pattern generator for flexible microstructuring, M.Phil. Thesis, Loughborough University of Technology, January 1996

